ISSN NO. 0737-5352-59

THE IONIC COMPOSITION OF AEROSOL IN BIG BEND NATIONAL PARK

Taehyoung Lee and Jeffrey L. Collett, Jr.

Department of Atmospheric Science
Colorado State University
Fort Collins, CO 80523

Funding Agency:
National Park Service
CA238099001

July, 2002

CIRA Cooperative Institute for Research in the Atmosphere

Colorado State University

THE IONIC COMPOSITION OF AEROSOL IN BIG BEND NATIONAL PARK

Taehyoung Lee and Jeffrey L. Collett, Jr.

Department of Atmospheric Science
Colorado State University
Fort Collins, CO 80523

Funding Agency:
National Park Service
CA238099001

July, 2002

ABSTRACT

THE IONIC COMPOSITION OF AEROSOL IN BIG BEND NATIONAL PARK

The chemical compositions of $PM_{2.5}$ and size-resolved aerosol particles were measured from July to October, 1999 in Big Bend National Park, Texas, during the Big Bend Regional Aerosol and Visibility Observational (BRAVO) Study. Daily $PM_{2.5}$ samples were collected using a URG cyclone/annular denuder/filter pack sampling system consisting of a $PM_{2.5}$ cyclone inlet, two coated annular denuders in series (for nitric acid and ammonia), and a filter pack. Aerosol particles collected on a Teflon filter were analyzed for major ions and a backup nylon filter was used to capture nitric acid volatilized from the collected particles.

A Micro Orifice Uniform Deposition Impactor (MOUDI) was used to collect 24 hr size-resolved aerosol particle samples in 9 size categories (D_{50} = 18, 10, 5.6, 3.2, 1.8, 1.0, 0.56, 0.32 and 0.18 μm). 41 MOUDI sample days were selected for analysis of the ionic chemical composition as a function of particle size.

$PM_{2.5}$ and size-resolved aerosol concentrations of Cl^-, SO_4^{2-}, NO_3^-, Na^+, NH_4^+, K^+, Mg^{2+}, and Ca^{2+} were obtained through ion chromatographic analysis of the filter and impactor samples. Aerosol acidity was measured on-site in the daily $PM_{2.5}$ filter samples.

The composition of the BRAVO $PM_{2.5}$ aerosol was dominated by sulfate and ammonium. Daily average sulfate and ammonium concentrations were strongly correlated (R^2=0.97). The ratio of ammonium to sulfate averaged 1.54 with standard deviation of 0.30. This ratio is consistent with the direct pH measurements of aerosol

acidity. The highest concentrations of sulfate were observed from August to October, reaching as high as 8.5 $\mu g/m^3$. Back-trajectories suggested long-range transport from regions along the Texas/Mexico border and east Texas was associated with peak sulfate concentrations in the park.

The particle composition as a function of size obtained from the MOUDI samples suggests that most of the particulate nitrate is associated with coarse mode particles in the range of 4 – 5 µm diameter. Aerosol nitrate concentrations were correlated with the sum of aerosol Na^+ and Ca^{2+} concentrations ($R^2 = 0.70$ and 0.60 for MOUDI and URG, respectively), demonstrating the importance of sea salt and soil dust particles in providing non-acidic surfaces for the condensation of nitric acid. The MOUDI samples indicate that nitrate and sulfate are separated into supermicron (mode diameter 4 – 5 µm) and submicron (mode diameter 0.4 – 0.5 µm) particles, respectively. The MOUDI samples show that a 1 µm size cut would have provided a better division between the fine mode and the coarse mode aerosol during the BRAVO study.

Comparison of ISORROPIA and SCAPE2 thermodynamic model predictions of solid phase sulfate species shows reasonable agreement between the models, although ISORROPIA sometime predicts higher concentrations of some species. ISORROPIA often predicts the presence of solid phase Na_2SO_4, while SCAPE2 seldom does. The difference between solid phase sulfate concentrations predicted by the two models largely reflects differences in predicted aerosol water content.

Both models reasonably predict the observed phase partitioning of N(-III) but poorly predict the observed phase partitioning of N(V). The underprediction of aerosol

nitrate by these bulk aerosol models reflects the fact that the $PM_{2.5}$ aerosol is externally mixed, containing acidic submicron sulfate particles and supermicron nitrate particles.

ACKNOWLEDGMENTS

So many people have helped me in some way from the beginning of the field campaigns to completion of my work. Special thanks are given to Dr. Sonia Kreidenweis for allowing me to use several models for this study and spending her time to help me understand the models and to review this work. Also I would like to thank Prof. Jerry F. Magloughlin in Earth Resources, for his time and energy spent reviewing this report and providing helpful comments.

I cannot forget the help from D. Eli Sherman. Without his efforts, the successful BRAVO study could not be completed. Also I wish to thank to Dr. Mike Hannigan, Dr Jenny L. Hand and Jill E. Reilly for their excellent contributions to the success of the field campaign. I thank Derek J. Straub for proofreading my writing as well. Thanks for logistical support in the field to Air Resources Specialists.

This study was funded by the National Park Service, grant # CA238099001 TO01-52 and CA238099001 TO 01-54.

TABLE OF CONTENTS

LIST OF FIGURES

LIST OF TABLES

Chapter 1. Introduction

The Big Bend Regional Aerosol and Visibility Observational (BRAVO) study was conducted in the region surrounding Big Bend National Park during four months from July to October, 1999. In spite of its remote location, Big Bend National Park frequently experiences poor visibility due to long range pollutant transport (Gebhart et al., 2000). Goals of the CSU component of the BRAVO study included a determination of the particle size distribution, the characterization of the molecular composition of the organic aerosol, and a detailed investigation of aerosol inorganic chemical composition in Big Bend National Park. The impact of these aerosol physical and chemical properties on visibility degradation was also studied.

The first component of this study, regarding particle size distributions and their impact on visibility degradation, was presented in detail by Hand (2001). The chemical characterization of the organic aerosol, the second component of this study, has been discussed in Brown (2001). The components of the study discussed in this thesis include the detailed ionic chemical composition of daily $PM_{2.5}$ aerosol present in Big Bend National Park, the ionic composition as a function of particle size, and the application of thermodynamic equilibrium models.

1.1 BRAVO project motivation and objectives

Big Bend National Park, located on the Rio Grande River on the Texas – Mexico border, is designated a Class I area . The Interagency Monitoring of Protected Visual Environments (IMPROVE) network has included Big Bend as part of its network since

1982. A 1996 study found that sulfate was the major contributor to fine particle mass and the largest contributor to visibility degradation in Big Bend National Park (Gebhart et al., 2001). The highest fine particulate sulfate concentrations were observed in summer and autumn when air masses were predominantly influenced by industrial regions of Mexico, other Mexican cities, and the cities of east Texas.

Organic carbon and soil derived aerosol particles contribute to visibility degradation in Big Bend National Park as well. The highest contribution of organic carbon has been observed during the spring when agriculture related biomass burning in Mexico is suspected to be a primary source. The presence of soil and dust particles was associated with suspected Saharan dust episodes in July and August and local sources as well (Gebhart et al., 2001).

Based on fine particulate aerosol and optical data obtained since 1982 as part of the IMPROVE network at Big Bend (Gebhart et al., 2000) and the 1996 study (Big Bend Air Quality Working Group, 1999; (Gebhart et al., 2001), a more detailed field study was recommended to provide an in depth investigation of aerosol physico-chemical characteristics and their contributions to visibility degradation in the park. The 1999 BRAVO study was organized to provide this information by measuring particle size distributions, inorganic particle chemical composition, and organic aerosol species in Big Bend National Park. Other non-CSU investigators also looked at regional variability in aerosol concentrations and tracer transport in order to help identify important source regions for the haze that plagues the park.

1.2 Aerosol sources and formation mechanisms

Particles in the atmosphere can be directly emitted from natural sources (e.g. soil dust, sea salt, fire smoke, volcanoes) and anthropogenic activities, or they can be formed in the atmosphere through gas to particle conversion. Aerosols can then evolve in size and composition through condensation, evaporation, and coagulation. Table 1.1 and Figure 1.1 summarize the formation of particles, global emission rates of particles into the atmosphere, and chemical characteristics of particles.

Table 1.1 The chemical characteristic and global emission rates of particles

	Fine particles	Coarse particles
Formation pathways	Chemical reactions Nucleation Condensation Coagulation Cloud/fog processing	Mechanical disruption Suspension of dusts Gas reaction with sea salt and soil dust Sea spray generation
Composition	Sulfate Nitrate Ammonium Hydrogen ion Elemental Carbon Organic compounds Water vapor Metals	Soil dust and crustal compounds (Na^+, Mg^{2+}, Ca^{2+}, $CaCO_3$, and Si, Al, Ti, and Fe oxides) Sea salt (NaCl) Biogenic compounds (Pollen, spores plant) Tire wear debris
Atmospheric lifetime	Days - weeks	Minutes - days
Species	**Primary emission strength (Tg/yr)**	
Sulfate(as H_2SO_4)	Natural (32) and Anthropogenic (111)	
Nitrate	11.3	
Ammonium	33.6	
Black carbon	Biomass burning (5.6) and Fossil fuel (6.6)	
Organic carbon	Biomass burning (54.3), Fossil fuel (28.8), and Terpene (18.5)	
Soil dust	<1 μm (250) and 1 – 20 μm (6125)	
Sea salt	< 2μm (82.1) and 2 – 20 μm (2460)	

source : (Seinfeld and Pandis, 1998; EPA, 1999; Raes et al., 2000)

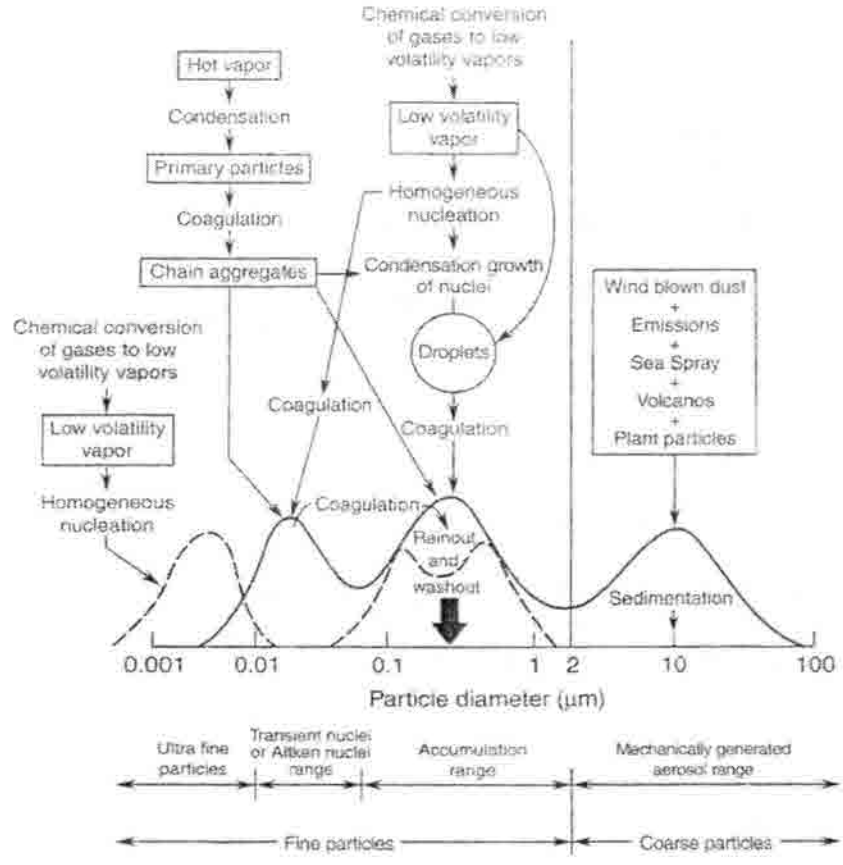

Figure 1.1 The formation of an atmospheric aerosol and its size distribution source : (Finlayson-Pitts and Pitts, 2000)

Figure 1.1 depicts the many processes that influence the size distribution and chemical composition of the atmospheric aerosol. It illustrates the wide range of sizes that are involved in the formation and evolution of aerosol particles and the existence of primary particles and secondary particles. Generally, atmospheric aerosol particles have been divided into two main size classes: coarse ($D_p > 1$ μm (or 2 μm)) and fine ($D_p < 1$ μm (or 2 μm)), indicating the two major particle formation process: mechanical generation for coarse mode particles and combustion/secondary processes for fine mode

particles. The category of fine mode particles is further divided into three size classes: the accumulation mode, the Aitken mode (condensation mode), and the Ultra fine mode.

Aerosol particles are removed from the atmosphere by dry and wet deposition processes. For Aitken nuclei mode (condensation mode) particles, the dominant removal mechanisms involve diffusion to surfaces, which becomes less efficient as particle size increases, or coagulation to form larger, accumulation mode particles. For accumulation mode particles, the removal process is very slow, and particles of this size tend to accumulate in the atmosphere due to their long residence times. Accumulation mode particles are removed mainly through activation and growth into cloud drops followed by removal in precipitation. Coarse particles settle gravitationally, a process which becomes less efficient as particle size decreases.

1.2.1 Primary emission of aerosols and precursors to secondary aerosols

Mineral particles from soil and dust

Mineral particles raised by wind blowing over soils or transported dust, containing mostly coarse particles of 2 – 10 μm, have received much attention due to their important influence on earth's radiation balance and atmospheric chemical reactions. The surfaces of dust particles are subject to heterogeneous chemical reactions with sulfur dioxide, nitric acid, and other species (Dentener et al., 1996; Tabazadeh et al., 1998). Mineral particles often have significantly different chemical compositions as results of interacting with various anthropogenic emissions during transport (Choi et al., 2001; Chun et al., 2001). It has been estimated that global emissions are in the range of

1000 – 3000 Tg/yr (Dentener et al., 1996). The shape, chemical composition, size and regional distribution of mineral dust particles are variable.

Sea salt

The formation of sea-salt particles is associated with the generation of sea spray, including formation of so-called film and jet drops associated with bursting of air bubbles at the ocean's surface. High winds tear drops from the wave crests and emit larger sea-salt drops into the atmosphere directly. As a result, sea-salt drop sizes range from submicron (~ 0.1 μm) to several hundred microns (> 100 μm). The smaller drops remain suspended in the air long enough to evaporate and produce sea-salt particles. These particles may initially have compositions similar to sea water, but can be altered significantly as a result of various chemical reactions with species such as HNO_3, H_2SO_4, NO_3 and others (Finlayson-Pitts and Pitts, 2000) whereas the large drops fall back into the sea.

Sulfur dioxide

Coal combustion and industrial utilities are important anthropogenic sources of sulfur dioxide, which is an important precursor to fine particle sulfate. Volcanic activity is a major natural emitter of SO_2 as well as H_2O, CO_2, H_2S, SO_4^{2-}, and primary particles (ash). Explosive eruptions can inject large amounts of material into the upper atmosphere, where volcanic pollution may remain for several years. The total mass of volcanic sulfur emissions has been estimated at 14±6 Tg(s) per year (Graf et al., 1997; Andres and Kasgnoc, 1998).

Table 1.2 shows an estimate of the total sulfur emitted into the atmosphere from various natural and anthropogenic sources in the northern and southern hemispheres. As shown in Table 1.2 anthropogenic emissions account for about 75 % of total sulfur emissions and 90 % in the Northern hemisphere.

Table 1.2 Global sulfur emission estimates for different sources (unit :Tg(s)/yr)

Source	H_2S	DMS	CS_2	OCS	SO_2	SO_4	Total
Combustion + industry					70	2.2	71 – 77
Biomass burning	< 0.01		< 0.01	0.075	2.8	0.1	2.2 – 3.0
Oceans	< 0.3	15 - 25	0.08	0.08		40 - 320	15 – 25[a]
Wetlands	0.006 – 1.1	0.003 – 0.68	0.0003-0.06				0.01 – 2
Plants and Soil	0.17 – 0.53	0.05 – 0.16	0.02 – 0.05				0.25 – 0.78[b]
Volcanoes	0.5 – 1.5			0.01	7 - 8	2 - 4	9.3 – 11.8
Total Anthropogenic							**73 - 80**
Total Natural (without sea salt and soil dust)							**25 - 40**
Total							**98 - 120**

Source : (Berresheim et al., 1995; Seinfeld and Pandis, 1998)
[a] : Excluding sea-salt contributions
[b] : Excluding soil dust contributions

SO_2 can also be formed in the atmosphere through the oxidation of CS_2, DMS, and H_2S by $OH\cdot$ and NO_3 in the troposphere, and photolysis of transported OCS (carbonyl sulfide) or reaction with O atoms in the stratosphere. Stratospheric sulfur species may then sink to the troposphere in the form of SO_2 or sulfate. Figure 1.2 shows the general pathways of sulfur compounds in the atmosphere after their emission from either anthropogenic or natural sources.

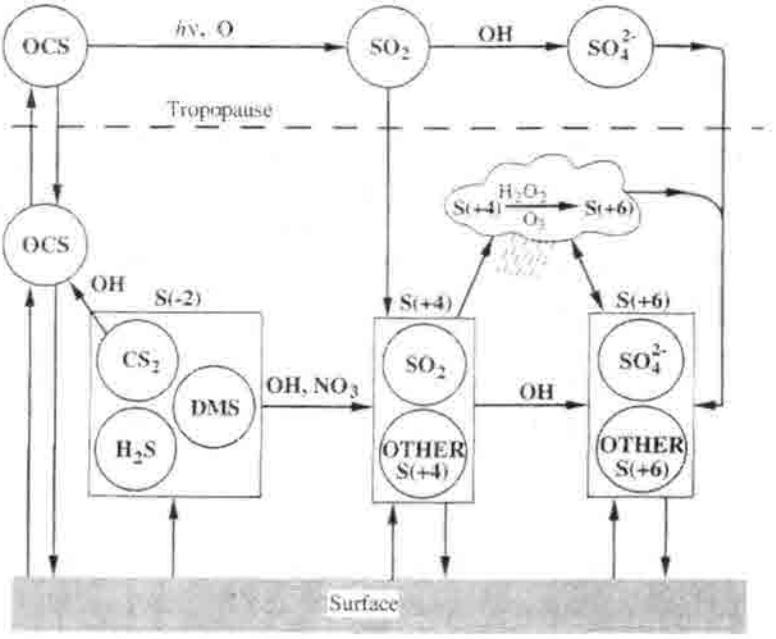

Figure 1.2 Major pathways of sulfur compounds in the atmosphere
Source : (Seinfeld and Pandis, 1998)

Ammonia

Ammonia is the most prevalent gas phase base in the atmosphere. It has received much attention due to its influence on a range of atmospheric processes including excess nitrogen removal which can affect sensitive ecosystems, the neutralization of acidic precipitation, and the formation of atmospheric aerosols (Warneck, 1988; Bouwman et al., 1995). Emissions of NH_3 originate from animal waste, fertilizers, biomass burning, soils, vegetation and other minor sources (Bouwman et al., 1995). Data presented in Figure 1.3 from Battye et al.(1994) reveal that cattle and calves, poultry, hog operations, and fertilizer are the major ammonia sources of ammonia in the atmosphere in the US. Global estimates of the magnitude of NH_3 sources and sinks are presented in Table 1.3.

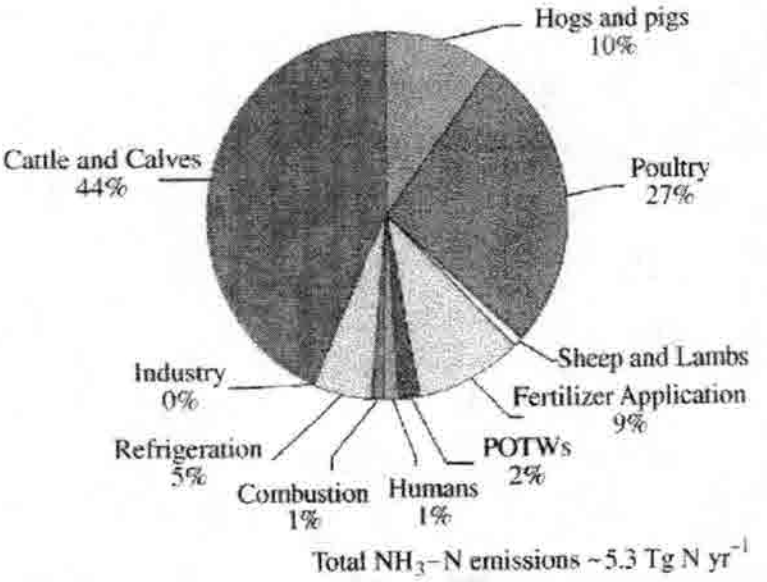

Figure 1.3 Contribution of ammonia emission in the US from different sources (Source : (Battye et al., 1994))

Table 1.3 Global atmospheric budget for NO_x, N_2O, and NH_3

Source or Sink	NO_x (Tg N yr^{-1})	N_2O (Tg N yr^{-1})	NH_3 (Tg N yr^{-1})
Fossil fuel combustion	21	0.5	2
Biomass burning	8.0	0.4	5
Sea Surface	< 1.0	5.7	13
Domestic animal waste		1.6	32
Human excrement			4
Lightning	8		
NH_3 oxidation by OH	1	0.6	
Stratospheric input	0.5		
Soil emissions	20.2	10.7	19
Other		6.3	
Total sources	**59**	**26**	**75**
Wet deposition	12 - 42		46
Dry deposition	12 - 22		10
Stratospheric sink		19.3	
NH_3 oxidation by OH			1
Atmospheric accumulation		3.5	
Total sinks	**59**	**19.3**	**57**

Note : The apparent difference between total NH_3 sources and sinks represents uncertainties in identified budget terms, not atmospheric accumulation.

Source : (Aneja et al., 2001)

Nitrogen-containing compounds

Important nitrogen-containing trace species in the atmosphere include nitrous oxide (N_2O), nitric oxide (NO), nitrogen dioxide (NO_2), and nitric acid (HNO_3). N_2O is mostly emitted by soil and water-based biological sources, and is considered a greenhouse gas. The major atmospheric sink of N_2O is photodissociation in the stratosphere, where it can be transported due to its long tropospheric lifetime. In addition to photodissociation, N_2O can be oxidized in the stratosphere by $O(^1D)$ to produce NO. The oxides of nitrogen, NO and NO_2, are important as precursor trace gases in secondary aerosol formation.

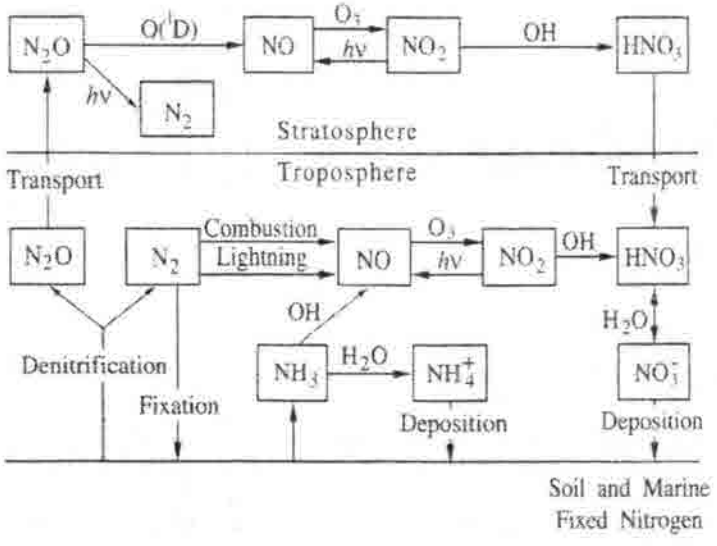

Figure 1.4 Processes in the atmospheric cycle of nitrogen-containing compounds
Source : (Seinfeld and Pandis, 1998)

Table 1.4 Formation of NO, NO_2, NO_3, NO_2^-, NO_3^-, N_2O_5, N_2O, HNO_3, and HONO

Species	Reaction
NO	$NO_2 + h\nu \rightarrow NO$
	$NO_2 + NO_3 \rightarrow NO + NO_2 + O_2$
	$HONO + h\nu \rightarrow OH + NO$
NO_2	$2NO + O_2 \rightarrow 2NO_2$
	$NO + HO_2 (RO_2) \rightarrow NO_2 + OH (RO)$
	$NO + O_3 \rightarrow NO_2$
	$NO_2 + NO_3 \rightarrow NO + NO_2 + O_2$
	$HONO + OH \rightarrow H_2O + NO_2$
NO_3	$NO_2 + O_3 \rightarrow NO_3 + O_2$ **(Night Time)**
NO_2^-	$2NO_2 + H_2O \rightarrow 2H^+ + NO_3^- + NO_2^-$
	$NO + NO_2 + H_2O \rightarrow 2H^+ + 2NO_2^-$
NO_3^-	$2NO_2 + H_2O \rightarrow 2H^+ + NO_3^- + NO_2^-$
N_2O_5	$NO_2 + NO_3 \rightarrow N_2O_5$ **(Night time)**
N_2O	$4HONO \rightarrow N_2O + 2HNO_3 + H_2O$
HNO_3	$NO_2 + OH \rightarrow HNO_3$
	$2NO_2 + H_2O$ **(water vapor)** $\rightarrow HONO + HNO_3$
	$2NO_2 + CH_3OH \rightarrow CH_3ONO + HNO_3$
	$4HONO \rightarrow N_2O + 2HNO_3 + H_2O$
HONO	$NO + NO_2 + H_2O$ **(Water vapor)** $\rightarrow 2HONO$
	$HO_2 + NO_2 \rightarrow HO_2NO_2 \rightarrow HONO + O_2$

Source : (Seinfeld and Pandis, 1998; Finlayson-Pitts and Pitts, 2000)

Major emissions of NO_x($NO + NO_2$) are associated with fossil-fuel combustion and natural release from soils. As indicated in Table 1.3, fossil fuel combustion produces 21 Tg(N) yr^{-1} and soils release 20 Tg(N) yr^{-1}. Nitric acid (HNO_3) is the major oxidation product of NO_x in the atmosphere. HNO_3 is rapidly removed from the atmosphere by deposition to surfaces or dissolution in fog or cloud drops due to its high water solubility, followed by wet deposition processes. Figure 1.4 schematically illustrates the major

processes in the atmospheric cycling of nitrogen-containing compounds. Reactions that form key nitrogen-containing compounds are shown Table 1.4.

1.2.2 Secondary aerosol formation

Secondary aerosol particles are formed through 1) reactions between gas phase species and primary particles, 2) gas to particle conversion reactions, and 3) reactions in the aqueous phase following transfer of trace species (SO_2 and NO_x) from the gas phase. Key reactions include:

$$\mathbf{SO_2 + OH \rightarrow H_2SO_4} \qquad \mathbf{(1.1)}$$

$$\mathbf{NO_2 + OH \rightarrow HNO_3} \qquad \mathbf{(1.2)}$$

In the presence of NH_3, H_2SO_4 and HNO_3 can form particulate ammonium sulfate ($(NH_4)_2SO_4$) and particulate ammonium nitrate (NH_4NO_3) through gas to particle conversion reactions. In the presence of sea salt (NaCl) or soil dust ($CaCO_3$), H_2SO_4 can react to form particulate sulfate (e.g. Na_2SO_4 or $CaSO_4$) and HNO_3 can react to form particulate nitrate (e.g. $NaNO_3$ or $Ca(NO_3)_2$), illustrating the creation of aerosol mass through the reaction of gas phase species with primary particles.

Clouds also play an important role in converting gaseous species, such as SO_2, to non volatile forms (e.g., sulfate). When the water droplets evaporate, the non-volatile residuals form more aerosol particles, mostly in the droplet size mode. Table 1.5 summarizes the reactions that contribute to the formation of condensation, droplet, and coarse mode aerosols in atmosphere.

Table 1.5 Summary of particle formation reaction and its size distribution

species	Fine Particle		Coarse particle
	Condensation mode (Aitken mode)	Droplet mode (accumulation mode)	
Sulfate	$H_2SO_4 + NH_3 \rightarrow (NH_4)_2SO_4$	$SO_2 + (H_2O_2/O_3) \rightarrow SO_4^{2-}$	$H_2SO_4 + 2NaCl \rightarrow Na_2SO_4 + 2HCl$
		Growth out of condensation mode (Aitken mode)	$H_2SO_4 + CaCO_3 \rightarrow CaSO_4 + H_2O + CO_2$
Nitrate	$HNO_3 + NH_3 \rightarrow NH_4NO_3$	$NO_3^- + NH_4^+ \rightarrow NH_4NO_3$	$2HNO_3 + NaCl \rightarrow NaNO_3 + HCl$
		Growth out of condensation mode (Aitken mode)	$2HNO_3 + CaCO_3 \rightarrow Ca(NO_3)_2 + CO_2 + H_2O$
			$2NO_2 + NaCl \rightarrow NaNO_3 + NOCl$
Ammonia	$H_2SO_4 + NH_3 \rightarrow (NH_4)_2SO_4$	$SO_4^{2-} + 2(NH_4^+) \rightarrow (NH_4)_2SO_4$	$NaNO_3 + NH_4^+ \rightarrow NH_4NO_3$
	$HNO_3 + NH_3 \rightarrow NH_4NO_3$	$NO_3^- + NH_4^+ \rightarrow NH_4NO_3$	$Ca(NO_3)_2 + 2NH_4^+ \rightarrow 2NH_4NO_3$
		$NH_4^+ + Cl^- \rightarrow NH_4Cl$	
		Growth out of condensation mode (Aitken mode)	
Chloride*			Sea salt
Potassium*			Soil dust
Magnesium*			Soil dust
Calcium*			Soil dust

*** : sea salt and soil dust source**

Chapter 2. Experiment

During the 4-month study from July to October, 1999 in Big Bend National Park, Texas, Colorado State University (CSU) collected daily $PM_{2.5}$ samples using a URG Cyclone /Annular Denuder/Filter pack sampling system; a Micro Orifice Uniform Deposition Impactor (MOUDI) was used to collect daily particle samples in 9 size categories (D_{50} = 18, 10, 5.6, 3.2, 1.8, 1.0, 0.56, 0.32 and 0.18 μm). Gas phase concentrations of HNO_3 and NH_3 and $PM_{2.5}$ concentrations of Cl^-, SO_4^{2-}, NO_3^-, Na^+, NH_4^+, K^+, Mg^{2+}, Ca^{2+} and acidity were measured on-site for all study days (EPA, 1999). Selected MOUDI samples (41 days) were analyzed for inorganic ions later at CSU.

2.1 Description of site

The Big Bend National Park (29.30° N, 103.12° W, 1075 m of elevation) sampling site is located in the west of Texas close to Mexico (Figure 2.1). In spite of its remote location Big Bend National Park (BBNP) frequently experiences poor visibility due to long range pollutant

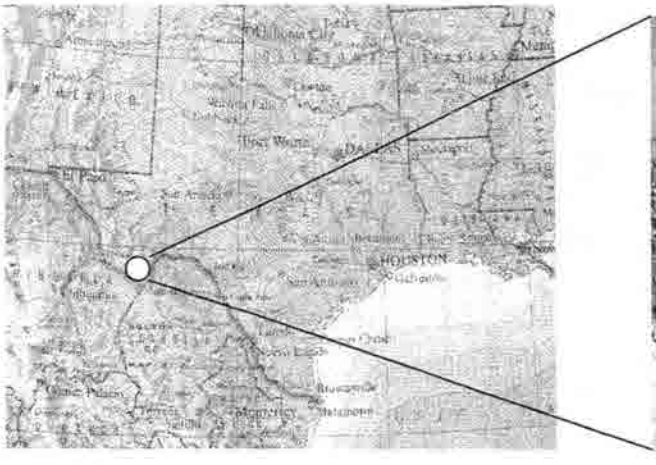

Figure 2.1 Big Bend National Park, Texas

Figure 2.2 K-Bar Study Site

transport. The Big Bend Regional Aerosol and Visibility Observational (BRAVO) study was conducted from July through October 1999 to determine the sources of aerosol present in park, the physico-chemical characteristics of the aerosol, and its effects on visibility degradation. Samples were collected at the K-Bar study site (Figure 2.2) of Big Bend National Park.

2.2 Sampling and Analysis

2.2.1 URG cyclone/annular denuder/filter pack sampling system

Filter techniques have commonly been used to collect gases and particulate matter of interest in the past. However, an important disadvantage of such a collection procedure is the potential interaction of gases and aerosols on the filter. To overcome this problem, annular denuder techniques have been developed, which selectively remove gases of interest before the particles are deposited (Figure 2.3). All detailed procedures are described in appendix B.

Ambient air was drawn through a cyclone ($D_{50} = 2.5$ μm) (Figure 2.4), and along etched glass denuder walls (air passes through two denuders in series) (Figure 2.5) which have been coated with chemicals that absorb the gaseous species of interest. NaCl (0.1 %) coated the first denuder for collection of HNO_3 and the second denuder was coated with 0.5 g citric acid in 50 mL of methanol to collect ambient NH_3. Pre-filter collection of NH_3 helps preserve acidic aerosol samples (Perrino et al., 1990). The remaining air stream was then filtered through 47 mm diameter Teflon, nylon, and coated glass fiber filters in series

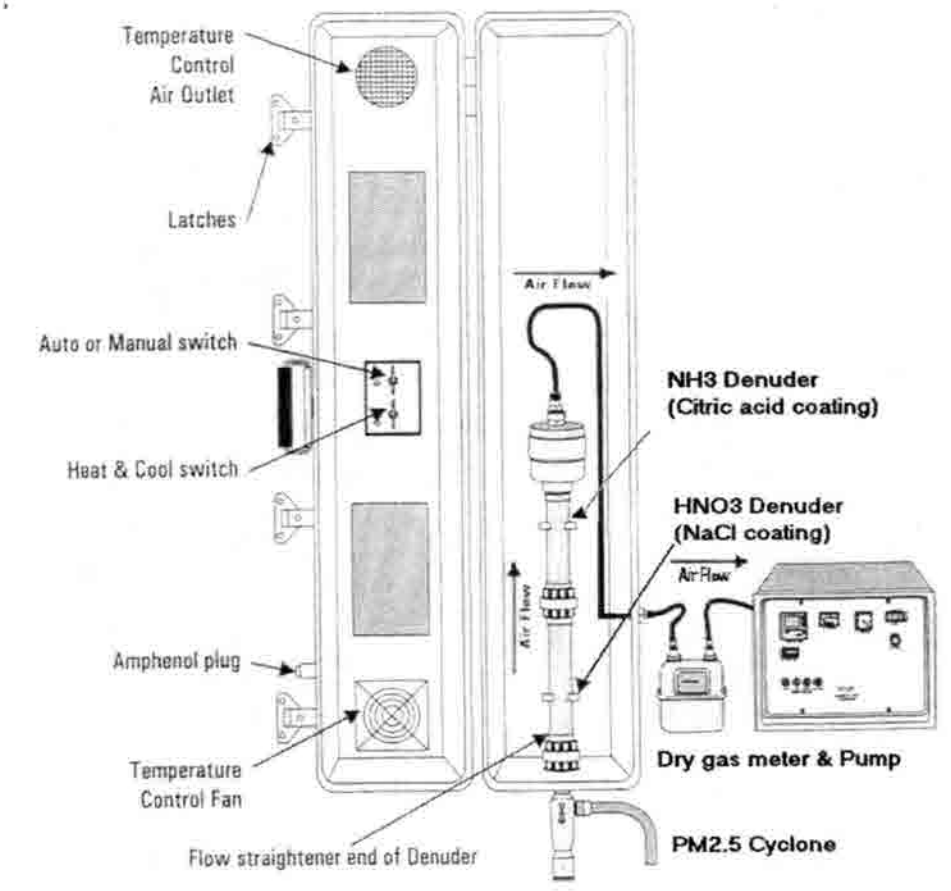

Figure 2.3 URG cyclone/annular denuder/filter pack sampler (Source : URG catalog)

Figure 2.4 $PM_{2.5}$ Cyclone (Source : URG catalog)

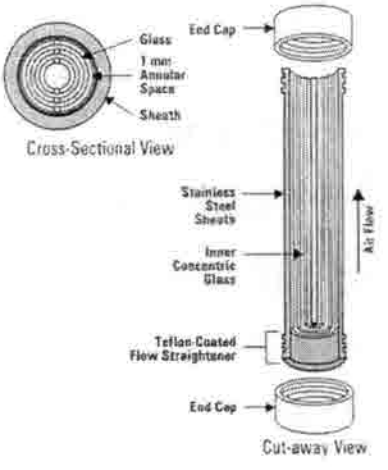

Figure 2.5 Annular denuder (Source : URG catalog)

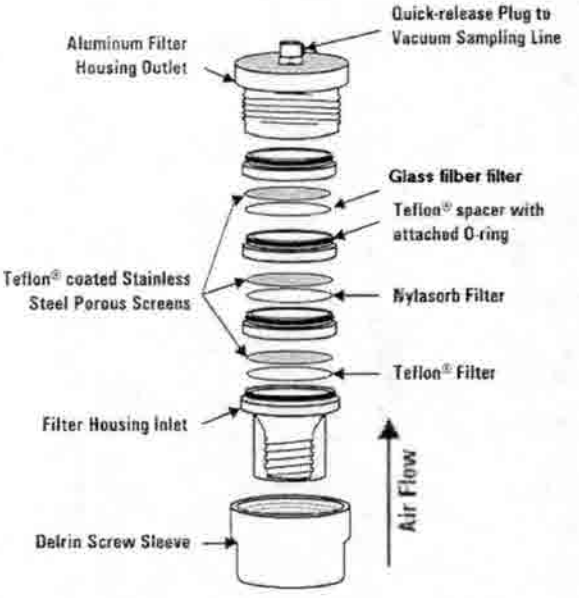

Figure 2.6 3-stage filter pack
(Source : URG catalog)

(Figure 2.6). The Teflon filter (Gelman Teflo, 2 μm pore size) was used to collect particulate matter.

The nylon membrane filter (Gelman Nylasorb) and citric acid impregnated glass fiber filter were used to capture nitric acid and ammonia, respectively, which may be volatilized from particulate matter on the Teflon filter (Figure 2.6).

The URG denuder/filter-pack assembly was used to collect daily, 24-hour samples. Samples were run from 08:00 (CDT) - 08:00(CDT). Two parallel sampling trains were used to facilitate a rapid change between samples. Air was drawn through the sample train at a nominal value of 10 lpm (actual volumetric flow) in order to provide the desired

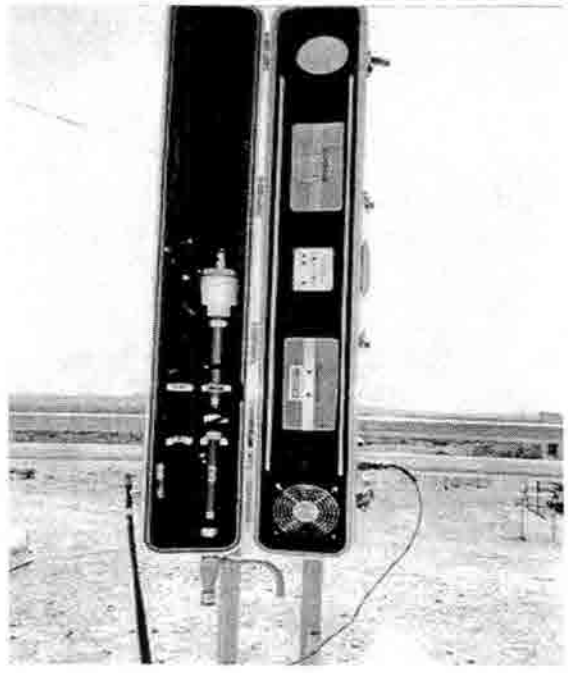

Figure 2.7 URG sampler

2.5 μm aerodynamic diameter size cut in the URG cyclone. Flow was provided by a vacuum pump and controlled by a mass flow controller. A dry gas meter was installed in-line between the filter pack and mass flow controller in order to provide an integrated measure of total sample flow. The sample flow read by the dry gas meter was corrected to ambient conditions by correcting for the pressure drop through the denuders and filters. An inline pressure measurement was used to make this correction. Figures 2.7 and 2.8 depict the URG sampler and the overall sampling arrangement at the site.The URG samplers were mounted on the top of the scaffolding with the pumps located on the ground below.

The primary $PM_{2.5}$ ionic species, Cl^-, SO_4^{2-}, NO_3^-, Na^+, NH_4^+, K^+, Mg^{2+} and Ca^{2+} and gas phase concentrations of HNO_3 and NH_3 were measured. Also $PM_{2.5}$ aerosol acidity was measured on-site for all study days.

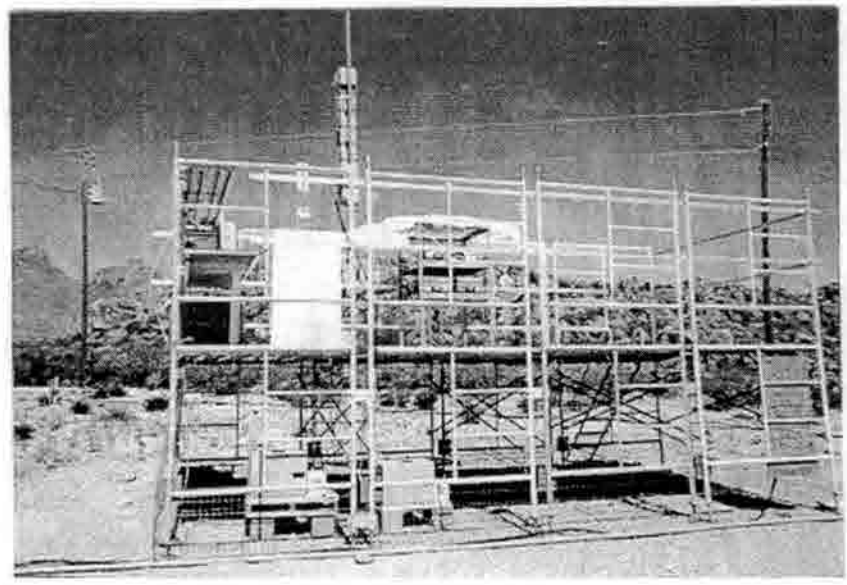

Figure 2.8 Field setup at Big Bend National Park , Texas

2.2.2 Micro Orifice Uniform Deposition Impactor (MOUDI)

The principle of operation of the MOUDI (Figure 2.9), with stage cut-sizes ranging from 0.18 to 18 μm at a flow rate of 30 L/min, is inertial cascade impaction with

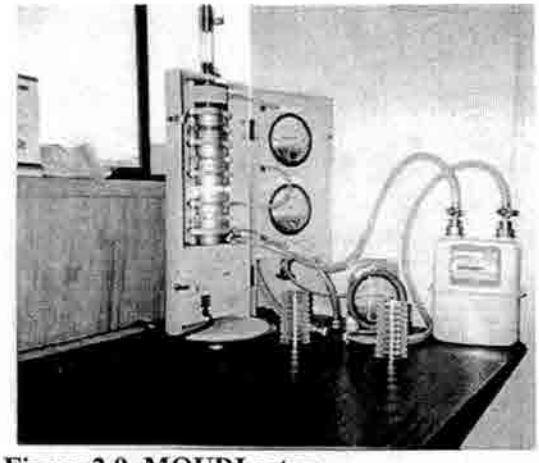

Figure 2.9 MOUDI setup

multiple nozzles. At each stage, jets of particle laden air impinge upon an impaction plate and particles larger than the cut size of that stage cross the air streamlines and are collected upon the impaction plate. The smaller particles with less inertia do not cross the streamlines and proceed onto the next stage where the nozzles are smaller, the velocity through the nozzles is higher and a smaller cut size of particles is achieved. A pump pulled the ambient air through an inlet which was located on the roof of the CSU BRAVO chemistry trailer. This inlet was covered with a rain shield and some aluminum bug screen. 24 hour samples were collected at Big Bend National Park, Texas beginning at approximately 08:00 local time. Grease coated aluminum foil was used for the impaction substrate (Marple et al., 1991). The largest 8 stages of the MOUDI were used, corresponding to the following aerodynamic diameter size ranges: (Stage 1A) 18–10 μm, (stage2A) 10–5.6 μm, (Stage 3A) 5.6–3.2 μm, (Stage 4A) 3.2–1.8 μm, (Stage 5A) 1.8–1.0 μm, (Stage 6A) 1.0–0.56 μm, (Stage 7A) 0.56–0.32 μm, (Stage 8A) 0.32–0.18 μm. Additionally, there was an initial stage that collected particles with aerodynamic diameter > 18 μm. The after-filter was not used in this field campaign.

Analysis of the collected size-resolved particulate matter focused on quantification of the primary ionic species, e.g. Cl^-, SO_4^{2-}, NO_3^-, Na^+, NH_4^+, K^+, Mg^{2+}, and Ca^{2+}. MOUDI samples from 41 days were analyzed. The subset of periods was selected based on interesting $PM_{2.5}$ aerosol chemistry measurements (e.g. high sulfate, sodium, nitrate days and suspected sea-salt days) and other study results (particle size distributions and thermodynamic modeling studies).

2.2.3 Sample Analysis

The inorganic ion analysis was completed using two DIONEX DX-500 series ion chromatographs. The inorganic ion concentrations and acidity of all URG annular denuder/filter samples were quantified in the CSU chemistry trailer on site in Big Bend National Park (Figure 2.10).

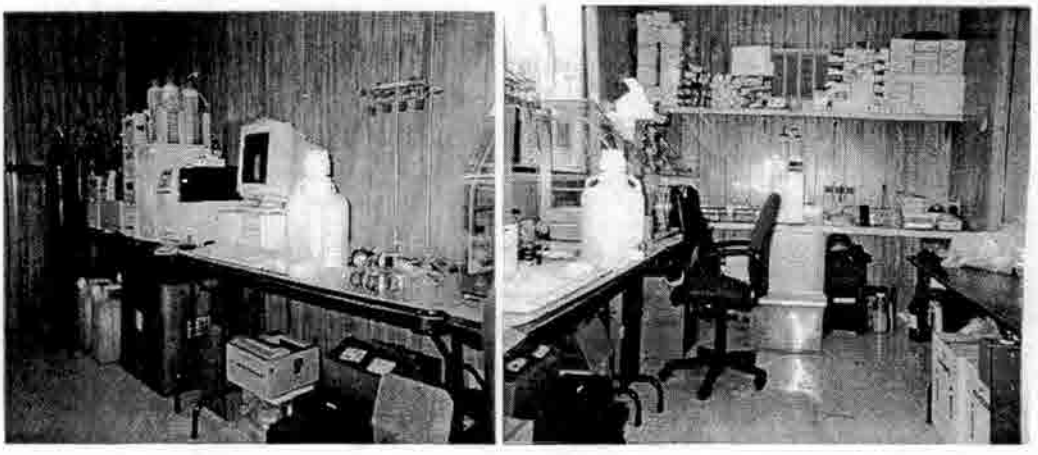

Figure 2.10 CSU Chemistry trailer inside setup

A Dionex AG4A-SC guard column, AS4A-SC separation column and a self-regenerating anion suppressor were used to quantify concentrations of major anions (Cl^-, SO_4^{2-}, and NO_3^-). The cation setup used to find concentrations of major cations (Na^+, NH_4^+, K^+, Mg^{2+}, and Ca^{2+}) was a CG12A guard column and a CS12A separation column and a self-regenerating cation suppressor was also used. Table 2.1 summarizes the conditions for ion chromatograph operation.

Table 2.1 The conditions of IC operation

System	Anion	Cation
Sample Injected volume	25 μL	100 μL
Auto sampler	AS3500*	AS3500**
Guard column*	AG4A-SC	CG12A
Separation column*	AS4A-SC	CS12A
Eluent	1.8mM Na2CO3/ 1.7mM NaHCO3	Methanesulfonic Acid 20mM
Eluent flow rate	2 mL/min	1 mL/min
Detector*	Conductivity (Dionex CD20)	Conductivity (Dionex CD20)
IC pump*	Gradient pump*** (GP40)	Isocratic pump (IP20)
Suppressor*	Self-regenerating Anion Suppressor (ASRS-ULTRA)	Self-regenerating Cation Suppressor (CSRS-UTRA)

*** : Dionex**
**** : TSP (Thermal Separation Products)**
***** : Used in isocratic mode for anion analysis**

2.3 Methodology

Ambient 24-hour average samples were collected for 4 months from July 1, through October 31, 1999 in Big Bend National Park, Texas. Standard operating procedures for aerosol and trace gas sampling are provided in appendices B and C. A brief summary of sampling methodology is presented below.

The Annular Denuder System (ADS) was composed of (1) a Teflon-coated aluminum cyclone (D_{50} = 2.5 μm, University Research Glassware, URG-2000-30EN): followed by (2) two annular denuders (URG-200-30X242-3CSS, 242mm stainless steel), (3) a filter pack (URG-2000-30F, 3 stage) with Teflo® (47 mm diameter with 2 μm pore size, Gelman Science), and Nylon (47mm diameter Nylasorb with 1 μm pore size,

Gelman Science) filter and citric acid impregnated glass fiber filter, (4) a flow controller (URG-3000-02BA) with timer, pump, and mass flow meter, (5) dry gas meter (Gallus 2000, URG-3000-02C) and (6) a housing box (URG-2000-01A) to protect the annular denuder and filter pack and maintain internal temperature at 2 °C above ambient. The denuders, filter pack and cyclone are coupled to each other with a hard plastic inert coupler fitted with "O" rings. The denuder consists of concentric glass cylinders. The cylinders define a 1mm annular orifice which allows the air stream to pass through.

The first denuder is coated with 10mL of 0.1 % (W/V) sodium chloride (NaCl) in 1:9 methanol/water solution to collect nitric acid (HNO_3). The second denuder is coated with 10mL of 1 % (W/V) citric acid in methanol to collect ammonia (NH_3). Ammonia must be removed prior to the filter pack to prevent artifact neutralization of any acidic sulfate particles collected on the Teflo filter. Particulate Cl^-, SO_4^{2-}, NO_3^-, Na^+, NH_4^+, K^+, Mg^{2+}, Ca^{2+}, and H^+ are collected on the Teflo filter. The nylon membrane filter, chosen for low SO_4^{2-}, NO_3^- and NO_2^- background levels, is used to collect any particulate nitrate which evaporates from the Teflo filter. A $PM_{2.5}$ cyclone was used to exclude coarse particles.

The ADS, which is composed of glass, plastic and Teflon pieces, must be handled with great care. The annular denuders and filter pack were in a heated insulated housing box (100 cm × 10 cm × 8 cm) during sampling. The housing box, which minimizes condensation of moisture within the denuder and on the filters, was heated or cooled to 1 to 2 °C above ambient temperature.

After coating, the denuders were dried by contact with clean N_2 gas for about 10 minutes. The denuders were capped until sampling. After sampling, the annular denuders

were extracted with 10 mL of deionized water. The extracts were stored in 5 mL cryovials and 600 μL polypropylene IC vials in a clean refrigerator at 5 °C until weekly anion and cation analyses on site.

Preparation and extraction of Teflo filters and denuders for NH_3 were performed in a clean, ammonia-free glove box to protect from contamination by NH_3. The Teflo filter was extracted with 5.85 mL of 10^{-4} N perchloric acid ($HClO_4$) solution with 150 μL of ethanol added first to wet the filter. The $HClO_4$ acidity inhibits dissolution of CO_2 and other weak acids. The nylon membrane filter was extracted using 6mL of ion chromatographic anion eluent (1.8 mM Na_2CO_3 and 1.7 mM $NaHCO_3$). Filters were extracted in screw-top polypropylene bottles (Nalgene, wide-mouth 125 mL) with the filters placed face-downwards and completely covered by extraction solution. Filter bottles were put in an ultrasonic bath for 20 minutes. Two 1mL aliquots of Teflo filter extract were transferred to 1.2 mL cryovials for acidity analysis and 600 μL of extract was refrigered in an IC vial at 5 °C until weekly anion and cation analyses on site. Residual extract was refrigerated in a 5 mL cryovial for possible future use.

20 μL of 0.04 M KCl, which increases the ionic strength, was added to each 1.2mL cryovial slated for acidity measurement. 1N H_2SO_4 was used to prepare different acidity standards in a range corresponding to the concentration of 0 – 444 nmole/m^3. The pH determinations were made right away after extraction of Teflo filters using an Orion Model 250A portable pH meter and a Ross Sure-Flow combination pH electrode. The H^+ ion concentration of each filter blank was subtracted from the filter extract concentration to measure the aerosol strong acidity contribution.

A Micro Orifice Uniform Deposit Impactor (MOUDI) was used to collect daily samples in 9 size fractioned stages with nominal cut-sizes (D_{50}) of 18, 10, 5.6, 3.2, 1.8, 1.0, 0.56, 0.32 and 0.18 μm. The substrate used in the MOUDI was a grease coated aluminum foil. The oil (No. 11025 silicon spray) was sprayed onto the substrate. After the oil is applied, it is necessary to bake the substrate in an oven at 65 °C for 90 minutes. Grease coated and baked substrates were placed in individual plastic Petri dishes in the laboratory. 24-hr daily samples were stored in plastic Petri dishes in a freezer during the field study and later in the laboratory prior to anion and cation analyses.

The extraction of selected MOUDI samples was later performed at CSU in a clean, ammonia-free glove box to avoid contamination by NH_3. Substrates were extracted in 125 mL screw-top polypropylene bottle (Nalgene bottle) with 6 mL of deionized water

Table 2.2 Solutions for coating, extracting, and H^+ measurement

	Coating solution		Extracting solution				pH
	Denuder 1	Denuder 2	Teflo filter	Nylon filter	Denuder 1 and 2	MOUDI	
DI water	90mL				10mL	6mL	
Methanol	10mL	50mL					
Ethanol			150μL				
NaCl	0.1 g						
Citric Acid		0.5 g					
Glycerol							
$HClO_4$ $10^{-4}N$			5.85mL				
Anion IC Eluent				6mL			
KCl 2M							20 μL
Volume of extracting or coating solution used	10mL	10mL	6mL	6mL	10mL	6mL	Two 1mL from Teflo filter extract were used for pH measurment

using an ultrasonic bath for 20 minutes. Two 600 μL aliquots of extract were transferred to IC vials for anion and cation analysis. Remaining extract in a 5 mL cryovial was stored in a refrigerator at 5 °C.

Table 2.2 shows the summary of each chemical coating and extract solution used in this study and the volume needed for coating and extracting each denuder and filter type. All procedures are described in detail in appendix B.

The concentrations of all species were calculated using the procedures described in the following sections.

2.3.1 HNO_3 concentration

$$C_g\ (HNO_3, \mu g/m^3) = (\ 1.016 \times C_{NO3\text{-}}(\mu N) \times V_{ext}(L) \times MW_{NO3\text{-}}) / V_{act.\ air}(m^3) \quad (2.1)$$

$$V_{act.\ air} = V_{air} \times (26.6\ _{\text{inch of Hg(ambient)}} - (\text{Final Vac}\ _{\text{inch of Hg}} + \text{Initial Vac}\ _{\text{inch of Hg}})/2)/26.6_{\text{inch of Hg(Ambient)}} \quad (2.2)$$

In equations 2.1 and 2.2, C_g (HNO_3, $\mu g/m^3$) is the concentration of nitric acid gas expressed in $\mu g/m^3$. The basic assumption is that the first denuder stage collects 100 % of sampled HNO_3 as nitrate. Since the diffusivity of HNO_3 is high, diffusion to the side walls is assumed to be very quick (sickles et al., 1988; Perrino et al., 1990; Brauer et al., 1991). Subscript "g" denotes "gas". $C_{NO3\text{-}}(\mu N)$ is the measured amount of nitrate in the first denuder extract. V_{ext} (0.01 L) is the extract solution volume and $MW_{NO3\text{-}}$ represents the molecular weight of NO_3^-. The factor 1.016 reflects the ratio of molecular weights of HNO_3 and NO_3^-. $V_{act.\ air}$ stands for the actual sampled ambient air volume considering the pressure drop during sampling. V_{air} represents the sampled air volume measured by the dry gas meter.

2.3.2 NH_3 concentration

$$C_g\,(NH_3, \mu g/m^3) = (\,0.994 \times C_{NH4+}(\mu N) \times V_{ext}\,(L) \times MW_{NH4}\,) / V_{act.\ air}\,(m^3) \quad (2.3)$$

In this equation, C_g (NH_3) is the concentration of ammonia in $\mu g/m^3$. $C_{NH4+}(\mu N)$ is the measured amount of ammonium in the second denuder extract. The extraction volume (V_{ext}) was 0.01 L and MW_{NH4} represents the molecular weight of NH_4. The ratio of molecular weights NH_3 and NH_4^+, 0.994, was used.

2.3.3 Cl^-, SO_4^{-2}, NH_4^+, Na^+, K^+, Mg^{2+} and Ca^{2+} concentration

$$C_p\,(\mu g/m^3) = (C(\mu N) \times V_{ext}\,(L) \times EW\,) / V_{act.\ air}\,(m^3) \quad (2.4)$$

In Equation 2.4, C_p is the concentration of each $PM_{2.5}$ particulate species Cl^-, SO_4^{2-}, NH_4^+, Na^+, K^+, Mg^{2+} or Ca^{2+} in $\mu g/m^3$. C (μN) is the measured concentration of each species (micronormal) in the Teflo filter extract. The assumption is that the Teflo filter collects all of these species with 100 % efficiency. The extract volume was 0.006 L. EW is the equivalent weight of each species and $V_{act.air}$ is determined as outlined above.

2.3.4 NO_3^- concentration

$$C_p\,(NO_3^-, \mu g/m^3) = (C_{NO3-,F1}\,(\mu N) \times V_{F1} + C_{NO3-,F2}\,(\mu N) \times V_{F2}) \times MW_{N03-}\,) / V_{act.\ air}\,(m^3) \quad (2.5)$$

$C_{NO3-,F1}(\mu N)$ is the measured concentration of nitrate in the Teflo filter extract and $C_{NO3-,F2}(\mu N)$ is the measured nitrate concentration in the nylon filter extract. V_{F1}(0.006 L) and V_{F2} (0.006 L) are the Teflo filter and nylon filter extract solution volumes,

respectively, and C_p (NO_3^-, $\mu g/m^3$) is the concentration of particulate nitrate in $\mu g/m^3$. The assumption is that the Teflo filter (F1) collects 100% of particulate nitrate and the nylon filter (F2) collects any nitrate that evaporates from the Teflo filter (Appel et al., 1980b; Appel and Tokiwa, 1981).

2.3.5 Calculations of H^+

For each standard and each filter extract, the apparent hydrogen ion concentration, $[H^+]$, is calculated as follows:

$$[H^+]\ (\mu N) = (10^{-pHs} - 10^{-pHb}) \times 10^6 \qquad (2.6)$$

Where pHs and pHb represent the pH of the extracted Teflo filter samples and corresponding blank. To determine the airborne concentration of hydrogen ion, $[H^+]$ is divided by the actual air sampling volume and multiplied by the volume of the filter extract solution (V_{ext} = 0.006 L). The equation for the airborne concentration of hydrogen ion is :

$$[H^+]\ (\mu eq/m^3) = ([H^+] \times V_{ext}) / V_{act.\ air} \qquad (2.7)$$

$V_{act.\ air}$ represents the actual sampled ambient air volume calculated as shown in Equation 2.2 considering the pressure drop during sampling.

2.3.6 Determination of the equivalent concentration of H_2SO_4

Calibration curves are also available to determine the aerosol strong acidity as the equivalent concentration of H_2SO_4. Table 2.3 shows the corresponding equivalent

concentration of H_2SO_4 for each working standard and approximate pH. All calibration values and calculations and the measured pH data are described in detail in appendix D.

Table 2.3 Equivalent concentration of H_2SO_4 for working standards

Standard number	Volume of 1.0 N H_2SO_4 added each Flask, µL	Equivalent Strong Acid Mass as H_2SO_4, µg	Approximate pH*
Standard 1	0	0	4.11
Standard 2	25	2.45	4.07
Standard 3	50	4.9	4.03
Standard 4	100	9.8	3.97
Standard 5	200	19.6	3.88
Standard 6	400	39.2	3.73
Standard 7	800	78.4	3.53
Standard 8	1600	156.8	3.29

*** Average of 33 calibrations for standards**

The equivalent concentration of H_2SO_4 in µg/m$_3$ is calculated by using the actual sample air volume, $V_{act.\ air}$, in m^3 as follows:

$$C_s = (10^{-pH_S} - 10^{-pH_B}) \times 10^6 \qquad (2.8)$$

$$M_s = C_s \times \text{Slope} + \text{Intercept} \qquad (2.9)$$

$$C_{H2SO4}\ (\text{as } H_2SO_4, \mu g/m3) = \frac{M_s}{V_{act.air}} \qquad (2.10)$$

where C_s is the apparent net strong acid concentration of each Teflo filter extract, which is calculated as with the Teflo filter blank. M_s represents the H_2SO_4 mass concentration (µg) corresponding to the Teflo filter extract pH. The equivalent concentration of H_2SO_4 in µg/m^3 is calculated by dividing by the actual sample air volume, $V_{act.\ air}$.

2.4 Quality Assurance and Control

A variety of types of quality control procedures were undertaken throughout both the field campaign and the chemical analysis to ensure the samples collected were not contaminated and were accurately and precisely analyzed. These included cleaning the sampler, taking blanks, measuring sample replicates and duplicates, and checking flow rate and sampling pressure drop during the field study.

2.4.1 The flow rate of the pump for the URG annular denuder and MOUDI

URG annular denuder sampler

Adjusting the set point on the mass flow controller set the flow rate. An estimate of typical ambient temperature and pressure at the sampling site (Big Bend National Park, Texas) was used to choose the mass flow set point. The following equation was used to determine the " Corrected Flow Rate" that should be set on the pump for these atmospheric conditions to achieve nominal actual volumetric flow rate of 10 lpm.

$$Q_V = Q_S \cdot \left(P_S / P_I \right) \cdot \left(T_I / T_S \right) \qquad \textbf{(2.11)}$$

where
Q_S = the flow rate at standard conditions in SLPM
Q_V = the desired ambient volumetric flow rate (LPM) at a given temperature, and barometric pressure
P_S = the standard condition barometric pressure (760 mm Hg)
P_I = the indicated (ambient) barometric pressure reading (in mm Hg)
T_S = the standard condition temperature (294.18 K)
T_I = the indicated temperature reading in Kelvin at the time of the calibrator flow reading

Table 2.4 shows the mass flow set point determined for the conditions typical of operation at Big Bend National Park. Pressure differences from standard conditions due to differences in sampling altitude exert the greatest influence on the ratio of standard to actual flow rate.

Table 2.4 Calculation of standard flow for ambient flow of 10 lpm

	Q_V (LPM)	P_S (mmHg)	P_I (mmHg)	T_S (K)	T_I (K)	Q_S (LPM)
Standard	10	760	760	294.18	294.18	10
Big Bend	10	760	675.2	294.18	300.18	8.71

For the BRAVO field campaign at Big Bend National Park, 8.71 slpm was applied for the mass flow controller set point to set a nominal actual flow rate of 10 lpm. Also the actual sampling volume and time were determined from readings made with an in-line dry gas meter, measured pressure drop, and an elapsed time meter on the URG pump assembly. Equation 2.12 shows the actual sampling volume calculation.

$$\text{Actual sampling volume } (m^3) = (\text{Final}_{\text{dry gas meter}} - \text{Initial}_{\text{dry gas meter}})(m^3) \times \frac{26.6 - (\text{Final vaccum} + \text{Initial vaccum})/2}{26.6} \quad \textbf{(2.12)}$$

where
$\text{Initial}_{\text{dry gas meter}}$ = Dry gas meter reading at the start sampling (m^3)
$\text{Final}_{\text{dry gas meter}}$ = Dry gas meter reading at the end sampling (m^3)
$\text{Initial}_{\text{vaccum}}$ = pressure drop reading at the start sampling (inches of Hg)
$\text{Final}_{\text{vaccum}}$ = pressure drop reading at the end sampling (inches of Hg)

All calculated actual sampling volumes during BRAVO are presented in appendix D.

Micro Orifice Uniform Deposit Impactor (MOUDI)

Three magnehelics in the MOUDI sampler housing were used in order to achieve and check the manufacturer's 30 lpm flow rate and pressure drop. The upper magnehelic (magnehelic1) setting of 20.7 inches of water was used to set a 30 lpm nominal flow rate through the MOUDI. The lower magnehelic (magnehelic2) should read 21 inches of water when magnehelic1 is set to 20.7 inches of water. Magnehelic2 was included to determine if there was a clogging or leaking problem in the MOUDI sampler. A third magnehelic and dry gas meter were used to determine the total actual air sampling volume pulled through the MOUDI. An elapsed time meter was used to verify the sample duration. Equation 2.13 presents an actual sampling volume calculation.

$$\text{Actual sampling volume}(m^3) = (\text{Final}_{\text{dry gas meter}} - \text{Initial}_{\text{dry gas meter}})\,(m^3) \times \frac{13.06 - (\text{Final magnehelic3} + \text{Initial magnehelic3})/2}{13.06} \qquad \textbf{(2.13)}$$

where
$\text{Initial}_{\text{dry gas meter}}$ = Dry gas meter reading at the start sampling (m^3)
$\text{Final}_{\text{dry gas meter}}$ = Dry gas meter reading at the end sampling (m^3)
$\text{Initial}_{\text{magnehelic3}}$ = Mgnehelic3 reading at the start sampling (psi)
$\text{Final}_{\text{magnehelic3}}$ = Mgnehelic3 reading at the end sampling (psi)

All calculated actual sampling volumes during BRAVO are presented in appendix D.

2.4.2 Sampler cleaning and blanks

High purity deionized water taken from a Barnstead EasyPure System (> 18 MΩ-cm) was used for cleaning all samplers. Clean aluminum foil was routinely used to provide a "clean" surface to handle samplers and sampler components. All cleaning blank collection procedures were performed regularly.

Denuder cleaning was done right away after extracting the denuder by running deionized water through the denuder. Filter packs, cyclones, tweezer and the ammonia-free glove box were cleaned with deionized water every week. Blanks were taken for all filters and denuders on each Tuesday and Friday. Blanks were taken by loading denuders and filters into one channel in the URG housing box without airflow, leaving them in place for ~24 hours, and then retrieving and processing them the same way samples were processed. Duplicate filter and denuder samples were collected every Sunday by using both URG channels.

A MOUDI cleaning procedure was performed after blanks were taken each Monday. Each MOUDI stage was scrubbed with Triton X-100 aqueous solution and a Q-tip, and then the soapy water was rinsed off completely with deionized water. Blanks were taken for all stages of the MOUDI. Blanks were collected by loading impaction surfaces on each stage, leaving them for 30-40 minutes without airflow, and then processing them the same way MOUDI samples were processed. Table 2.5 summarizes URG and MOUDI sampling, handling and analysis schedules.

Fresh solutions were prepared daily for pH measurement. pH meter calibration was done using pH 7 and 4 buffers and the slope recorded in the log book. Most pH meter calibration slopes were in the range of 98 – 100%. Two 1.2 mL cryovials, each containing 1mL extract, were used to rinse the electrode and to determine the pH of the Teflo filter aerosol extract. All calibration slopes and pH measurements are presented in appendix D.

2.4.3 Quality control of analysis for major anions and cations

Accuracy, precision, and detection limit checks were performed for analyzed ions throughout the field study. Dilutions of NIST traceable ion standards from Dionex were used to monitor calibration accuracy for each IC run. The duplicate URG denuder and filter samples and the replicate MOUDI sample analyses were used to determine measurement precision. To determine the minimum detection limit for each species, low level standards and blanks were analyzed, respectively.

Accuracy, Precision and Quality Control Chart

The Dionex NIST traceable standards were combined five anion and combined six cation standards. Dilutions (1:100 and 1:20) for anions and dilutions (0.075:100, 0.15:100 and 1:100) for cations of the Dionex standards were prepared and used as check standards periodically. Table 2.6 summarizes the manufacturer-standard concentrations of ions in the Dionex standards and the corresponding dilutions.

Figure 2.11 compares the measured ion concentrations to the nominal values of the Dionex standards for each IC run on site during the study. Most ion concentrations were within 5 % of the nominal concentrations except for Ca^{2+} and Mg^{2+} which were within 10 % of the nominal values.

Table 2.7 presents more information about the accuracy and precision of IC analyses from Dionex calibration checks and internal calibration checks. Ca^{2+} and Mg^{2+} were difficult to measure accurately at concentrations below 5 μN. Results for the other species show good accuracy even at concentration levels below 5 μN.

Table 2.5 Sampling and analysis schedule

		Monday	Tuesday	Wednesday	Thursday	Friday	Saturday	Sunday
Sampler in use		URG channel 1	URG Channel 1 and 2 MOUDI	URG Channel 1 MOUDI	URG Channel 2 MOUDI	URG Channel 1 and 2 MOUDI	URG Channel 2 MOUDI	URG Channel 1 and 2 MOUDI
Comments	URG	24 hr sample: C1	24 hr sample: C2 Blank sample: C1	24 hr sample: C1	24 hr sample: C2	24 hr sample: C1 Blank sample: C2	24 hr sample: C2	(Duplicate sample) 24 hr sample: C1 24 hr sample: C2
	MOUDI	Blank and cleaning	24 hr sample	24 hr sample	24 hr sample	24 hr sample	24 hr sample	24 hr sample
Preparation (Solution)			Analysis Solution (Cation, pH)			Analysis Solution (Anion, pH)		Coating Glass filter Coating solution Extract solution MOUDI
Analysis			IC (Cation) pH			IC (Anion) pH		

Table 2.6 Concentrations of Dionex check standards

Anion	Stock (μN)*	1:100 (μN)	1:20 (μN)
Chloride	846.19	8.46	42.30
Nitrate	1611.21	16.11	80.56
Sulfate	3123.13	31.21	156.15

Cation	Stock (μN)*	0.075:100(μN)	0.15:100 (μN)	1:100 (μN)
Sodium	8699.51	6.52	13.05	86.99
Ammonium	13859.28	10.39	20.79	138.59
Potassium	12788.28	9.59	19.18	127.88
Magnesium	20571.90	15.43	30.86	205.72
Calcium	24950.10	18.71	37.43	249.50

*** : Dionex provides the concentrations as ppm**

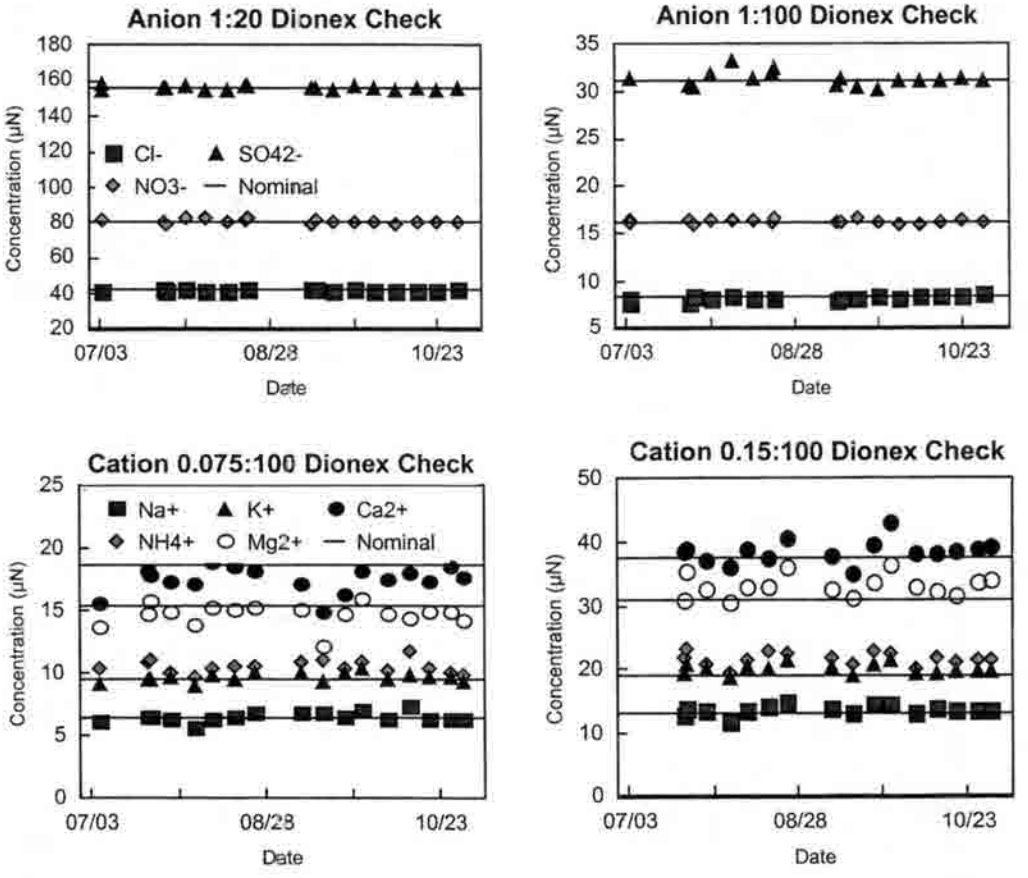

Figure 2.11 Quality Control Chart of CSU analyses of accuracy check standards made from Dionex NIST-traceable solutions

Uncertainties of URG annular denuder/filter and MOUDI

Analytical uncertainties are expressed as a Relative Standard Deviation (RSD) calculated using replicate concentration analyses or duplicate samples. Replicate IC concentration measurements were made every 10^{th} sample, followed by injection of a standard (anion standard 5 or cation standard 7) and then DI water. Duplicate samples , representing two paired filter/denuder samples, were collected every Sunday by using both URG channels.

To calculate the precision of URG annular denuder/filter and pH measurements, the duplicate sample concentrations were used. Replicate concentration measurements were used for MOUDI sample precision determination, because no simultaneous duplicate MOUDI measurements were possible.

The formulas for RSD calculation are shown in Equations 2.14 and 2.15. The results for species measured by ion chromatography and pH meter are reported in

$$\mathrm{RSD} = \frac{S_{pooled}}{\overline{X}} \times 100\% \qquad \textbf{(2.14)}$$

$$S_{pooled} = \sqrt{\frac{\sum_{i=1}^{N1}\left(X_i - \overline{X_1}\right)^2 + \sum_{j=1}^{N2}\left(X_j - \overline{X_2}\right)^2 + \sum_{k=1}^{N3}\left(X_k - \overline{X_3}\right)^2 + \bullet\bullet\bullet}{N_1 + N_2 + N_3 + \bullet\bullet\bullet - Ns}} \qquad \textbf{(2.15)}$$

Table 2.8. For the above equations, S_{pooled} is the pooled standard deviation and N_i represents the number of replicate or duplicate data points in set "i". The term Ns represents the total number of data sets pooled. $\overline{X_1}$ is the average concentration of

Table 2.7 Accuracy and precision of standard analyses

Species		Nominal (μN)	$\overline{X}$ (μN)	Accuracy* (μN)	Accuracy** (%)	Std. Dev.	Precision*** CV(%)	# of analyses
Cl^-	Standard 1	1	1.03	-0.03	3.0	0.195	18.99	20
	Standard 3	10	10.17	-0.17	1.7	0.245	2.41	18
	Standard 5	50	50.18	-0.18	0.4	1.507	3.00	98
	Dionex 1:20 check	42.3	41.86	0.44	-1.0	0.540	1.29	20
	Dionex 1:100 check	8.46	8.17	0.29	-3.4	0.247	3.02	20
NO_3^-	Standard 1	2	1.98	0.02	-1.0	0.362	18.28	20
	Standard 3	20	20.12	-0.12	0.6	0.334	1.66	18
	Standard 5	100	100.55	-0.55	0.5	1.912	1.90	98
	Dionex 1:20 check	80.56	80.92	-0.36	0.4	1.073	1.33	20
	Dionex 1:100 check	16.11	16.25	-0.14	0.9	0.217	1.34	20
SO_4^{2-}	Standard 1	2	2.12	-0.12	6.0	0.423	2.01	20
	Standard 3	20	20.06	-0.06	0.3	0.569	2.84	18
	Standard 5	100	100.31	-0.31	0.3	1.887	1.88	98
	Dionex 1:20 check	156.15	156.27	-0.12	0.1	1.186	0.76	20
	Dionex 1:100 check	31.21	31.41	-0.2	0.6	0.731	2.33	20
Na^+	Standard 1	1	1.12	-0.12	12.0	0.341	3.51	16
	Standard 3	4	3.87	0.13	-3.3	0.247	6.36	19
	Standard 5	15	14.8	0.02	-1.3	0.515	3.48	19
	Standard 7	40	39.6	0.4	-1.0	1.466	3.70	52
	Dionex 0.075:100 check	6.52	6.48	0.04	-0.6	0.361	5.56	20
	Dionex 0.15:100 check	13.05	13.64	-0.59	4.5	0.756	5.54	20
	Dionex 1:100 check	86.99	87.28	-0.29	0.3	4.093	4.69	20
NH_4^+	Standard 1	2	1.87	0.13	-6.5	0.657	3.52	16
	Standard 3	8	7.59	0.41	-5.1	0.432	5.69	19
	Standard 5	30	29.37	0.63	-2.1	0.556	1.89	19
	Standard 7	80	79.26	0.74	-0.9	2.525	3.18	52
	Dionex 0.075:100 check	10.39	10.57	-0.14	1.7	0.513	4.84	20
	Dionex 0.15:100 check	20.79	21.7	-0.91	4.4	1.022	4.71	20
	Dionex 1:100 check	138.59	142.39	-3.8	2.7	5.469	3.84	20
Mg^{2+}	Standard 1	1	2.83	-1.83	1.8	0.537	18.96	16
	Standard 3	4	3.8	0.2	-5.0	0.426	11.18	19
	Standard 5	15	12.9	2.1	-14.0	1.174	9.11	19
	Standard 7	40	40.01	-0.01	0.0	1.753	4.38	52
	Dionex 0.075:100 check	15.43	14.64	0.79	-5.1	0.840	5.74	20
	Dionex 0.15:100 check	30.86	33.14	-2.28	7.4	1.693	5.11	20
K^+	Standard 1	1	1.16	-0.16	16.0	0.270	23.25	16
	Standard 3	4	3.79	0.21	-5.3	0.178	4.68	19
	Standard 5	15	14.75	0.25	-1.7	0.579	3.92	19
	Standard 7	40	39.79	0.21	-0.5	1.252	3.14	52
	Dionex 0.075:100 check	9.59	9.68	-0.09	0.9	0.364	3.75	20
	Dionex 0.15:100 check	19.18	20.07	-0.89	4.6	0.762	3.79	20
	Dionex 1:100 check	127.88	124.03	3.85	-3.0	8.892	7.16	20
Ca^{2+}	Standard 1	1	3.09	-2.09	2.1	0.568	18.38	16
	Standard 3	4	4.35	-0.35	8.7	0.471	10.84	19
	Standard 5	15	13	2	-13.3	1.100	8.81	19
	Standard 7	40	39.67	-0.33	-0.8	1.961	4.94	52
	Dionex 0.075:100 check	18.71	17.5	1.21	-6.5	1.019	5.82	20
	Dionex 0.15:100 check	37.43	38.57	-1.14	3.0	1.755	4.55	20

*** : Abolute Error, $E = X_i - X_t$ (where X_i is the measurement of a quantity and X_t is true value)**

**** : Relative Error, $E_r(\%) = ((X_i - X_t)/X_t) \times 100\%$**

***** : Precision, CV(Coefficient of Variation) = (Standard Deviation/ $\overline{X}$) × 100%**

replicates or duplicates in set 1, $\overline{X_2}$ is the average concentration of replicates or duplicates in set 2 and so forth. $\overline{X}$ represents the average of all sample replicates or duplicates.

Precisions for the major measured aerosol species (NO_3^-, SO_4^{2-}, NH_4^+, and H^+) were good with RSD's in the range of 3-5 %. RSD's for trace aerosol species were higher, ranging from 12 – 23 %. RSD's for duplicate denuder measurements of HNO_3 and NH_3 were each 9 %. RSD's for replicate analyses of MOUDI ion concentrations were all below 6 %.

Table 2.8 Precision [RSD (%)] of measured aerosol species concentrations

URG denuder/filter and pH measurement					
Species	$\overline{X}$ ($\mu g/m^3$)	Std. Deviation Pooled ($\mu g/m^3$)	# of data set (Ns)	# of samples (N)	RSD (%)
Cl^-	0.03	0.006	17	34	20.6
NO_3^-	0.14	0.008	17	34	5.2
SO_4^{2-}	1.83	0.086	17	34	4.7
Na^+	0.05	0.006	17	34	11.7
NH_4^+	0.54	0.018	17	34	3.3
K^+	0.02	0.004	17	34	20.5
Mg^{2+}	0.01	0.002	17	34	18.1
Ca^{2+}	0.09	0.020	17	34	22.9
$[H^+]$ (μeq/m3)	0.01	0.0004	17	34	4.8
HNO_3	0.70	0.06	17	34	8.6
NH_3	0.44	0.038	17	34	8.7
MOUDI					
Species	$\overline{X}$ ($\mu g/m^3$)	Std. Deviation Pooled ($\mu g/m^3$)	# of data set (Ns)	# of samples (N)	RSD (%)
Cl^-	2.01	0.088	5	10	4.4
NO_3^-	1.27	0.075	15	30	5.9
SO_4^{2-}	6.25	0.343	13	26	5.5
Na^+	10.99	0.354	6	12	3.2
NH_4^+	1.76	0.085	8	16	4.8
K^+	0.75	0.033	9	18	4.4
Mg^{2+}	2.91	0.154	14	28	5.3
Ca^{2+}	5.93	0.206	14	28	3.4

Determination of Detection Limit

To determine the minimum detection limit (MDL) for each species blank samples were used. The MDL (@ 95% confidence limit) was calculated for URG and MOUDI samples separately. The equation used to calculate the MDL is shown as Equation 2.16:

$$MDL \geq t \times S_b \times \sqrt{\frac{N_1 + N_2}{N_1 \times N_2}} \qquad \textbf{(2.16)}$$

where t is the t value given at the 95% confidence level for the appropriate number of degrees of freedom, S_b is the blank standard deviation, N_1 is the number of sample measurements (single measurement, $N_1 = 1$), and N_2 is the number of analyzed blanks.

Table 2.9 Minimum Detection Limit (MDL) for URG and MOUDI sampler

URG annular denuder/filter and pH measurement						
	S_b (μN)	N_1	N_2	Degrees of Freedom	t (95% CL)	MDL μN([a]μg/m^3)
Cl^-	0.42	1	32	31	1.96	0.83 (0.011)
NO_3^-	0.55	1	32	31	1.96	1.10 (0.015)
SO_4^{2-}	0.59	1	32	31	1.96	1.18 (0.016)
Na^+	0.80	1	32	31	1.96	0.80 (0.011)
NH_4^+	0.49	1	32	31	1.96	0.97 (0.013)
K^+	0.29	1	32	31	1.96	0.58 (0.008)
Mg^{2+}	0.57	1	32	31	1.96	1.12 (0.015)
Ca^{2+}	1.54	1	32	31	1.96	3.07 (0.041)
$[H^+]$ (μeq/m3)	0.028	1	30	29	1.96	1.70 (0.0006)
HNO_3	0.47	1	32	31	1.96	0.94 (0.012)
NH_3	1.85	1	32	31	1.96	3.68 (0.049)
MOUDI						
	S_b (μN)	N_1	N_2	Degrees of Freedom	t (95% CL)	MDL μN([a]ng/m^3)
Cl^-	0.770	1	36	35	1.96	1.53 (8.2)
NO_3^-	0.356	1	36	35	1.96	0.71 (6.6)
SO_4^{2-}	0.277	1	36	35	1.96	0.55 (4.0)
Na^+	1.152	1	36	35	1.96	2.29 (8.0)
NH_4^+	0.263	1	36	35	1.96	0.52 (1.4)
K^+	0.173	1	36	35	1.96	0.34 (1.2)
Mg^{2+}	0.735	1	36	35	1.96	1.46 (5.1)
Ca^{2+}	1.779	1	36	35	1.96	3.54 (12.3)

a : To express MDL as μg/m^3, the average 24 hr sampling volume set was used.

Table 2.9 shows the MDL of each species for URG and MOUDI samples. In general their detection limits are quite low compared to observed aerosol ion concentrations. Table 2.10 shows the blank concentrations used for MDL calculation of URG and MOUDI samples. It should be noted that all sample values reported here are blank-corrected values.

Table 2.10 Blank concentration for $PM_{2.5}$ URG and MOUDI (Units : μN)

$PM_{2.5}$ URG										
Date	Cl^-	SO_4^{2-}	NO_3^-	HNO_3	Na^+	NH_4^+	K^+	Mg^{2+}	Ca^{2+}	NH_3
7/2/1999	0.87	5.08	0	0	0	1.8	0.9	4.5	5.9	3.3
7/6/1999	0	5.86	0	0.99	0.54	0.92	0.57	4	4.38	8.93
7/9/1999	0.36	5.32	0	0	1.54	1.39	1.01	2.7	4.26	7.41
7/13/1999	0.03	5.15	1.19	0	0.57	1.1	0.94	3.21	6.64	7.38
7/16/1999	0.3	5.15	0	0	0.86	0	1.04	2.7	8.83	6.99
7/20/1999	0.1	5.1	0	0	0.36	0.8	1.08	2.97	6.35	4.59
7/23/1999	0	3.73	0.02	0	0.34	1.13	0.86	2.67	3.92	4.63
7/27/1999	0	3.85	0.04	0	0	1.03	0.62	3.46	5.55	4.59
7/30/1999	0.24	4.74	0.01	0	0.26	1.12	0.69	3.11	6.21	5.64
8/3/1999	0.96	4.95	0	0	0.35	0.18	0.78	2.73	5.02	5.54
8/6/1999	0	4.97	0	0	0.13	0	0.41	2.26	4.35	5.3
8/10/1999	1.04	5.67	0	1.03	0.28	0.39	0.76	3.08	5.32	3.94
8/17/1999	0	5.81	0	0.15	0	0	0	2.8	4.79	2.14
8/20/1999	0	5.38	0	0	0	0	0	2.06	4.94	2.08
8/24/1999	0.3	5.7	0	1.27	0.87	0.21	0.96	3.24	4.74	2.67
8/27/1999	1.06	5.95	0	0	1.16	0.12	1.14	2.66	4.57	4.45
8/31/1999	0.55	6.77	1.42	0.99	0.34	0.2	0.73	3.34	5.38	5.55
9/3/1999	0	6.25	1.54	0	0.52	0.6	0.66	2.59	7.04	4.97
9/10/1999	0.52	5.59	1.09	0	1.04	1.57	1.23	3.13	4.98	6.48
9/17/1999	0.86	5.62	1	0	0.68	0.7	0.93	3.01	5.92	4.36
9/21/1999	0	5.06	1.26	0	0.06	0.06	0.42	3.32	6.12	3.93
9/24/1999	0.95	6.04	0	0	0.29	0.26	0.46	2.24	10.65	3.1
9/28/1999	0	5.62	0	0	0.14	0.45	0.42	3.46	7.59	4.88
10/1/1999	0	5.16	0	0	0.18	0.73	0.47	2.65	4.76	1.7
10/5/1999	0.81	5.36	0	1.06	0.55	0.82	0.9	3.18	5.09	4.35
10/8/1999	0	5.82	1.17	0	0.16	0.52	0.47	2.73	4.62	2.17
10/12/1999	0	5.6	0	1.06	0.45	0.78	0.72	4.32	5.59	2.36
10/15/1999	0.97	5.38	0	1.43	1.11	1.25	0.88	3.85	5.45	3.05
10/19/1999	1.1	5.08	1.3	0	1.16	0.38	0.74	3.37	5.47	2.48
10/22/1999	0.64	5.25	0	0	0.46	0.42	0.5	2.42	9.19	1.86
10/26/1999	0.73	5.67	0	0	0.78	0.71	0.64	3.29	7.09	2.48
10/29/1999	0.67	5.4	0	0	0.82	0.75	0.95	2.82	7.38	2.8
Average	0.41	5.38	0.31	0.25	0.50	0.64	0.72	3.06	5.88	4.25
MOUDI										
7/19/1999	0.096[a]	0.116	0.041		0.022	0.002	0.002	1.962	3.143	
8/2/1999	0.691[a]	0.524	0.000		1.347	0.000	0.000	2.253	3.768	
9/6/1999	0.226[a]	0.505	0.317		0.105	0.341	0.341	3.252	5.867	
10/4/1999	0.678[a]	0.402	0.000		0.764	0.589	0.589	2.528	4.458	
Average	0.423	0.387	0.090		0.559	0.233	0.114	2.499	4.309	

a : This value presents the average of all 9 stages, which is applied all species.

Chapter 3. Ionic composition of $PM_{2.5}$

Chemical properties of $PM_{2.5}$ aerosol were measured from July to October, 1999 in Big Bend National Park, Texas, during the Big Bend Regional Aerosol and Visibility Observational (BRAVO) Study. A URG cyclone/annular denuder/filter pack sampling system was used to collect 24-hr daily $PM_{2.5}$ (Cl^-, SO_4^{2-}, NO_3^-, NH_4^+, K^+, Mg^{2+}, and Ca^{2+}) and trace gas (HNO_3 and NH_3) samples. Aerosol acidity was also measured.

Sulfate and ammonium were the dominant ionic species in daily $PM_{2.5}$, with smaller contributions from NO_3^- and Na^+. Daily average sulfate and ammonium concentrations had a strong correlation of $R^2 = 0.97$. $PM_{2.5}$ nitrate concentrations showed a correlation of $R^2 = 0.70$ with the sum of $PM_{2.5}$ Na^+ and Ca^{2+}, indicating the possibility that sea salt and soil dust particles provide non-acidic surfaces for condensation of nitric acid. $PM_{2.5}$ nitrate and sulfate concentrations showed little correlation ($R^2 = 0.05$).

The aerosol was usually acidic, with an average $PM_{2.5}$ ammonium to sulfate ratio of 1.54 (standard deviation of 0.30). The most acidic aerosol was observed during August, September and the beginning of October, with 24hr concentrations that exceeded 70 neq/m^3 of H^+ concentration on some days. The ratios of ammonium to sulfate showed a trend consistent with the aerosol acidity measurements.

N(V) and N(-III) were found to be distributed between the particle and gas phases. The average ratio for HNO_3(g)/N(V) was 0.73 and for NH_3(g)/N(-III) was 0.22. These ratios do not reflect any aerosol nitrate or ammonium contained in particles with aerodynamic diameters larger than 2.5 μm.

3.1 Daily variation of $PM_{2.5}$ chemical composition and trace gas concentrations

Figure 3.1 shows the daily $PM_{2.5}$ sulfate concentration measured from July to October, 1999 in Big Bend National Park (BBNP). Lower concentrations of sulfate were observed in July and the end of October. Periods of higher sulfate concentrations started in the beginning of August with the highest concentrations on 8/21/99, 9/1/99, 9/14/99, 10/5/99, and 10/12/99 with 6.6 $\mu g/m^3$, 8.5 $\mu g/m^3$, 7.7 $\mu g/m^3$, 5.3 $\mu g/m^3$ and 8.0 $\mu g/m^3$, respectively.

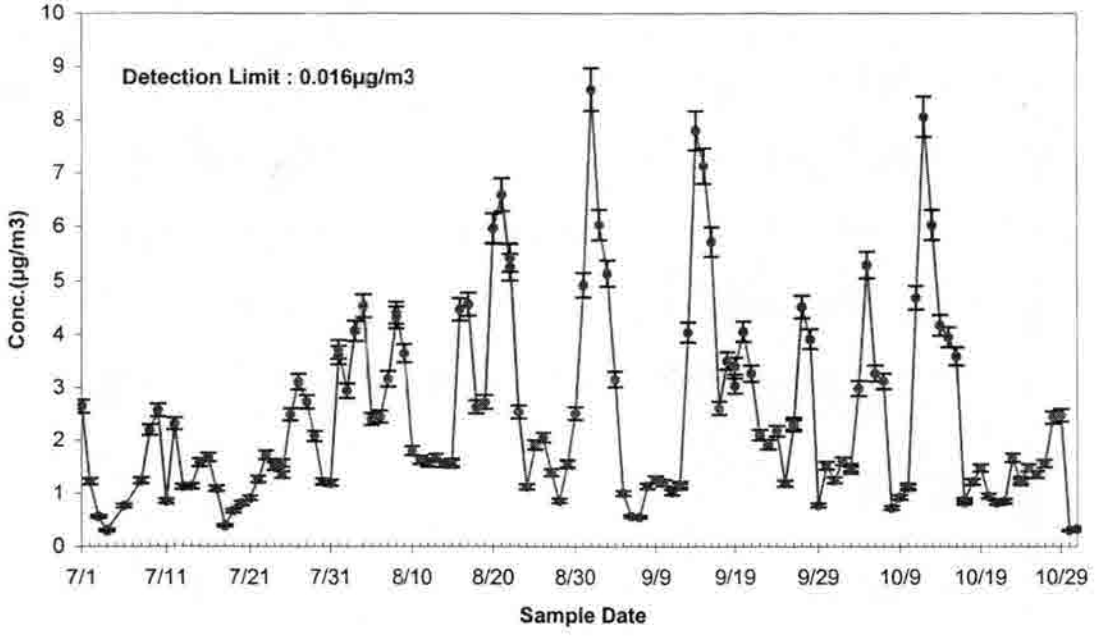

Figure 3.1 Timeline of $PM_{2.5}$ sulfate concentration. Results of duplicate measurements are included where available (Error bars represent RSD for duplicate analyses)

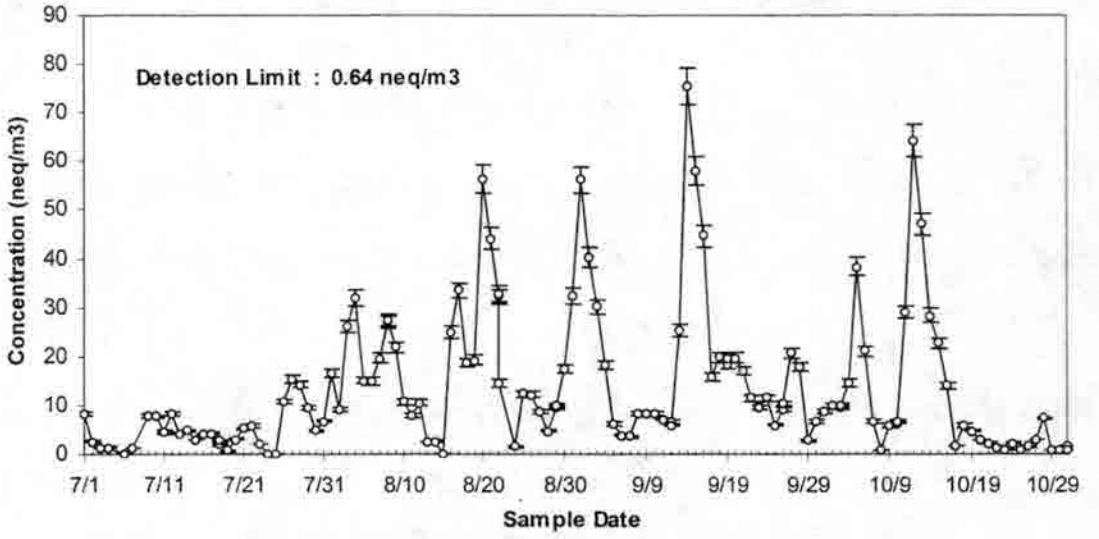

Figure 3.2 Timeline of $PM_{2.5}$ $[H^+]$ concentration (Error bars represent RSD for duplicate analyses)

Aerosol acidity was also measured in daily $PM_{2.5}$ samples. Figures 3.2 and 3.3 show the concentration of H^+ and the strong aerosol acidity expressed as the equivalent concentration of H_2SO_4 ($\mu g/m^3$). The equivalent H_2SO_4 concentration ranged from 0.0 to 4.4 $\mu g/m^3$. Figure 3.4 shows a comparison between the net hydrogen ion concentrations from each sample filter extract (Equations 2.6 and 2.7) and the H^+ concentrations

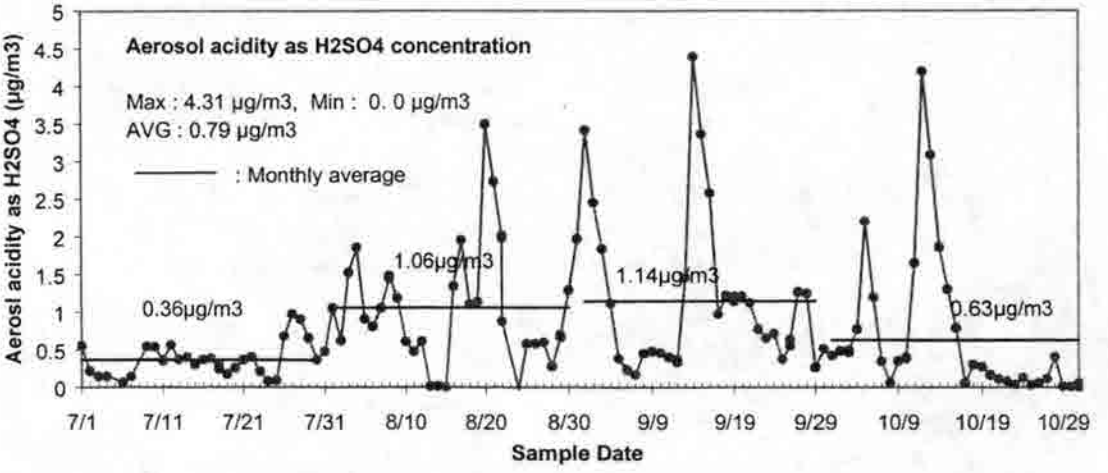

Figure 3.3 Timeline of the strong aerosol acidity as H_2SO_4 concentration

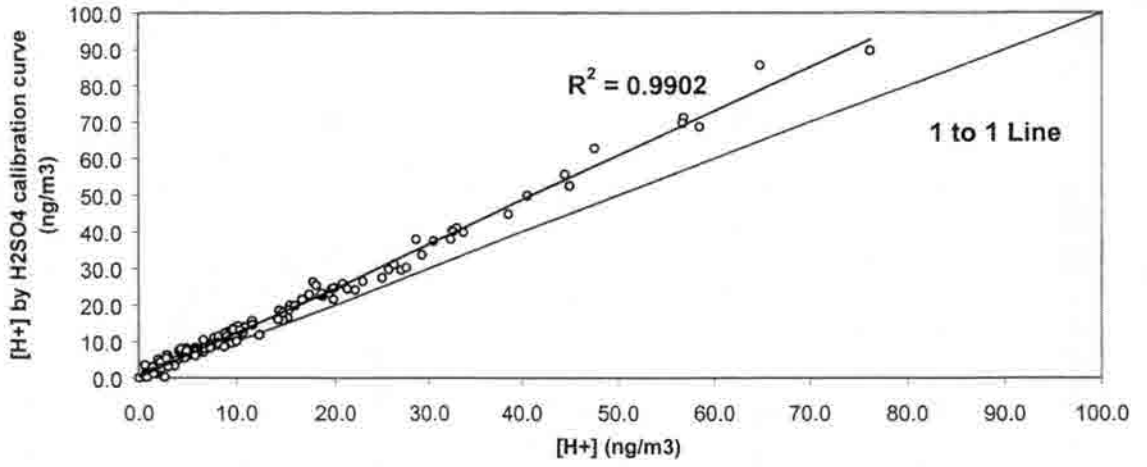

Figure 3.4 A comparison between the H^+ concentration from each Sample filter extract and the H^+ concentration calculated with the H_2SO_4 calibration curve.

obtained from the H_2SO_4 standard curves. Both methods produce similar H^+ concentrations and are well correlated with $R^2 = 0.99$. A comparison between H^+ and sulfate concentrations is shown in Figure 3.5. The highest H^+ concentration was measured as 75.5 neq/m^3. Figure 3.5 shows that the aerosol was generally acidic during periods of high sulfate concentration. Hydrogen and sulfate ions have been

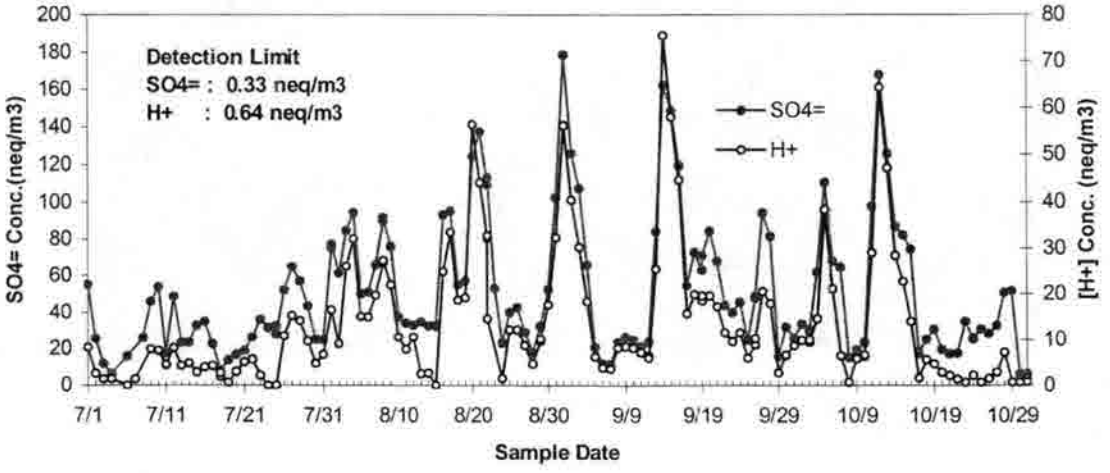

Figure 3.5 Timelines of $PM_{2.5}$ SO_4^{2-} and H^+ concentrations

reported to show similar size distributions (mostly between 0.18 and 0.6 μm (Koutrakis et al., 1989); sulfate concentrations peaked at 0.4 - 0.5 μm in this study (see chapter 4 for details). The difference between the sulfate and H^+ concentrations in Figure 3.5 primarily represents the extent of sulfate neutralization by NH_4^+. Periods of low H^+ concentration, which also represent more fully neutralized sulfate, are found in July and the end of October. The aerosol acidity trends are consistent with the molar ratios of $[NH_4^+]/[SO_4^{2-}]$ associated with compositions of ammonium sulfate ($[NH_4]_2SO_4$), letovicite ($[NH_4]_3H[SO_4]_2$), ammonium bisulfate(NH_4HSO_4), and sulfuric acid(H_2SO_4) (see chapter 3.2.1 for details).

Figure 3.6 presents timelines of $PM_{2.5}$ NO_3^- and Cl^- concentrations and gaseous nitric acid concentrations. Most Cl^- concentrations were close to the detection limit, 0.011 μg/m^3, except for a few days in July. NO_3^- and HNO_3 concentrations ranged from 0.015 to 0.45 μg/m^3 and from 0.084 to 1.555 μg/m^3, respectively. In July, NO_3^- and

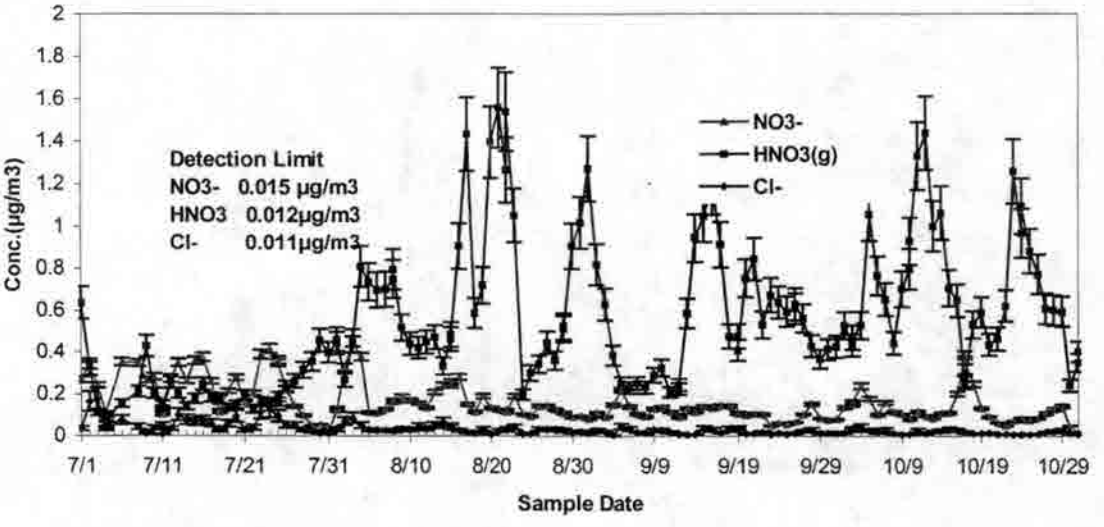

Figure 3.6 Timelines of NO_3^-, Cl^- and HNO_3(g) concentrations (Error bars represent RSD for duplicate analyses)

HNO_3 were found to have similar concentrations in the particle and gas phases. Otherwise, larger N(V) concentrations were found present as gaseous nitric acid. This finding is consistent with the presence of acidic sulfate in the fine particles. In general, ammonium nitrate is not formed until aerosol sulfate is fully neutralized (Seinfeld and Pandis, 1998).

The variation of NH_3 and NH_4^+ concentrations is shown in Figure 3.7. Ammonium was the dominant cation species measured in the $PM_{2.5}$ samples. Generally, the ammonium concentration trends were similar to sulfate, suggesting that the most of the ammonium is associated with sulfate, forming species that contain various combinations of ammonium and sulfate.

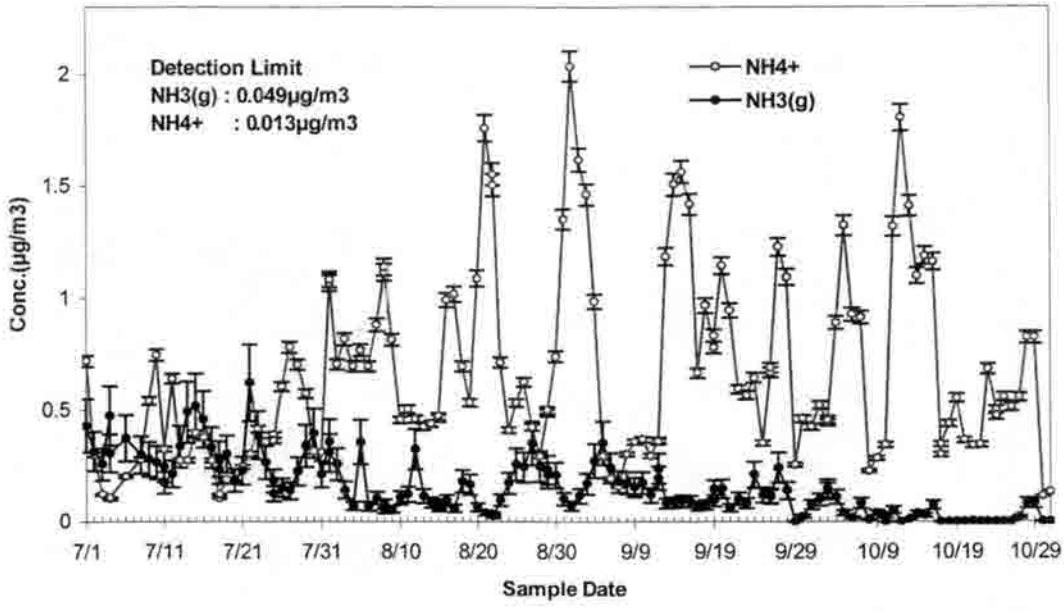

Figure 3.7 Timelines of NH_3(g) and NH_4^+ concentrations (Error bars represent RSD for duplicate analyses)

The maximum concentration of ammonium was 2.0 $\mu g/m^3$ on 9/1/99. Concentrations ranged from 0.18 to 2.0 $\mu g/m^3$ during the 4-month study. Most N(-III) was present as particulate ammonium rather than ammonia gas.

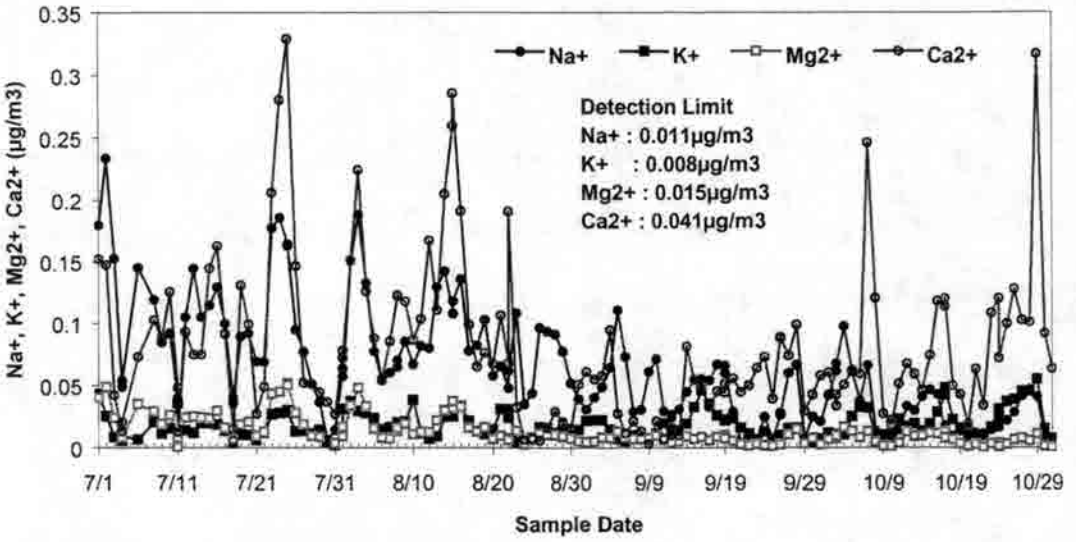

Figure 3.8 Timelines of Na^+, K^+, Mg^{2+} and Ca^{2+} concentrations

Mg^{2+} and K^+ were found to be minor contributors to total cation concentrations in the $PM_{2.5}$ samples (Figure 3.8). The highest concentrations of Mg^{2+} were approximately 0.05 $\mu g/m^3$ on 7/2/99, 7/25/99, and 8/4/99 with concentrations of Mg^{2+} close to the detection limit on many other days. The highest concentrations of Na^+ and Ca^{2+} were measured in July and August. Some of these high concentrations were associated with suspected Sahara dust episodes (Hand, 2001). Presence of sea salt aerosol could also contribute to high concentrations of Na^+ and Ca^{2+} in July and August and Na^+ in October. The crustal ions were observed in both the coarse and accumulation modes on many

days, providing a non-acidic surface for nitric acid condensation (see chapter 4 for details).

3.2 Relationship between chemical species

If all ionic species in a sample are measured accurately, the ion balance should sum to zero or, alternatively, produce a 1:1 anion to cation ratio. A charge balance for all measured ionic species including hydrogen ion is shown in Figure 3.9. The slope of 0.63 (cation/anion) when hydrogen ion concentrations are neglected indicates the importance of measuring H^+ for a complete understanding of ionic species contributions in acidic environments. When H+ is included the charge balance values are close to the expected value of 1.0, indicating most major anion and cation species were probably included.

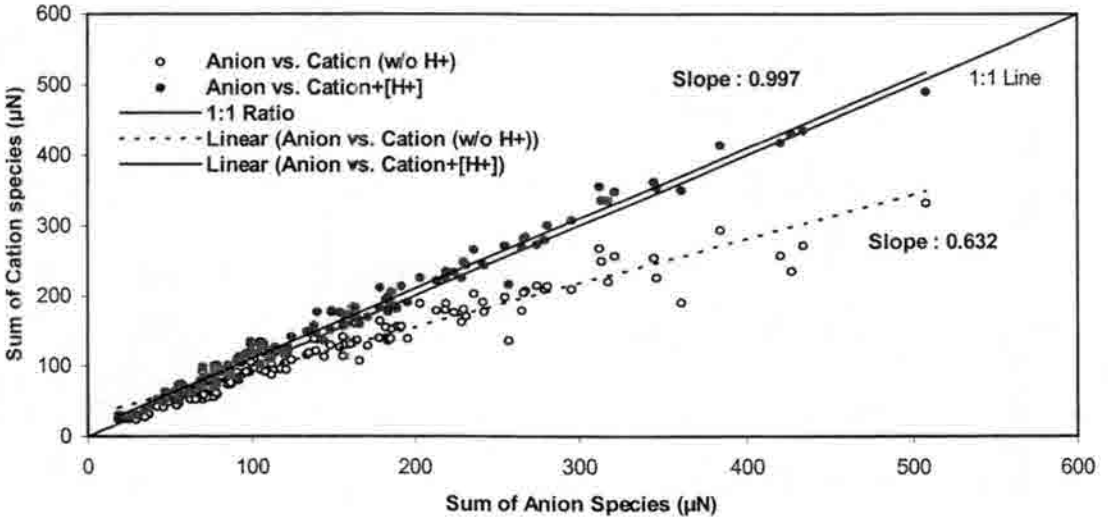

Figure 3.9 Ion charge balance for $PM_{2.5}$ samples

3.2.1 Hydrogen ion (H^+), Ammonium (NH_4^+) and Sulfate (SO_4^{2-})

Since a methodology for the measurement of particle acidity has been developed (Appel et al., 1980a) and reviewed (Koutrakis et al., 1988b; Lodge, 1989; EPA, 1999), it has seldom been used (Koutrakis et al., 1988a; Spengler et al., 1989; Brauer et al., 1991; Lee et al., 1993; Tsai et al., 2000) because of difficulties that include (1) neutralization by NH_3 if present during extraction and sample treatment, (2) neutralization by other alkaline gases, and (3) measurement of H^+ concentration must be completed on the same day as the sample extraction. Average aerosol acidities in previous studies were measured at 8 nmol/m^3 (Koutrakis et al., 1988a; Koutrakis et al., 1988b) and 10 nmol/m^3 (Spengler et al., 1989) with ranges of 0-78 nmol/m^3 and 0-122 nmol/m^3 in Portage, WI and St. Louis, MO, respectively. The mean hydrogen ion concentrations in Kingston, TN and Boston, MA were 36.1(range of 0-290) nmole/m^3 and 17.9 (range of 1.3-84) nmole/m^3 (Spengler et al., 1990; Brauer et al., 1991), respectively. H^+ concentrations of 7.7 nmole/m^3 (0-78.0 nmol/m^3) were measured in Chicago, IL in 1992 (Lee et al., 1993) and 18.9 nmol/m^3 with a range of 0-337.3 nmol/m^3 in Hsinchu, Taiwan (Tsai et al., 2000). These values compare to an average H^+ concentration of 13.0 nmole/m^3 (range of 0-75.6 nmole/m^3) measured in BRAVO. Results from the cities of Kingston and St. Louis reveal that the Kingston sulfate composition was usually in the range between $[NH_4]_2SO_4$ (ammonium sulfate) and NH_4HSO_4 (ammonium bisulfate), and in St. Louis sulfates were mostly in the composition range of $[NH_4]_2SO_4$ (ammonium sulfate) to $[NH_4]_3H[SO_4]_2$ (letovicite). The acidity in St. Louis was lower than that for Kingston due to aerosol neutralization by more NH_3 present in the urban area.

If we limit our consideration to only the sulfate anion and the ammonium cation, various molar ratios of $[NH_4^+]/[SO_4^{2-}]$ can be compared to specific compounds. Molar ratios of $[NH_4^+]/[SO_4^{2-}]$ of 0.0, 1.0, 1.5 and 2.0 correspond to H_2SO_4 (sulfuric acid), NH_4HSO_4 (ammonium bisulfate), $[NH_4]_3H[SO_4]_2$ (letovicite) and $[NH_4]_2SO_4$ (ammonium sulfate). As shown in Figure 3.10, the BRAVO $PM_{2.5}$ ratio of ammonium to sulfate averaged 1.54, with a standard deviation of 0.3, roughly consistent with the molar ratio of $[NH_4]_3H[SO_4]_2$ (letovicite). Variations in the ratio of $[NH_4^+]/[SO_4^{2-}]$ suggest that

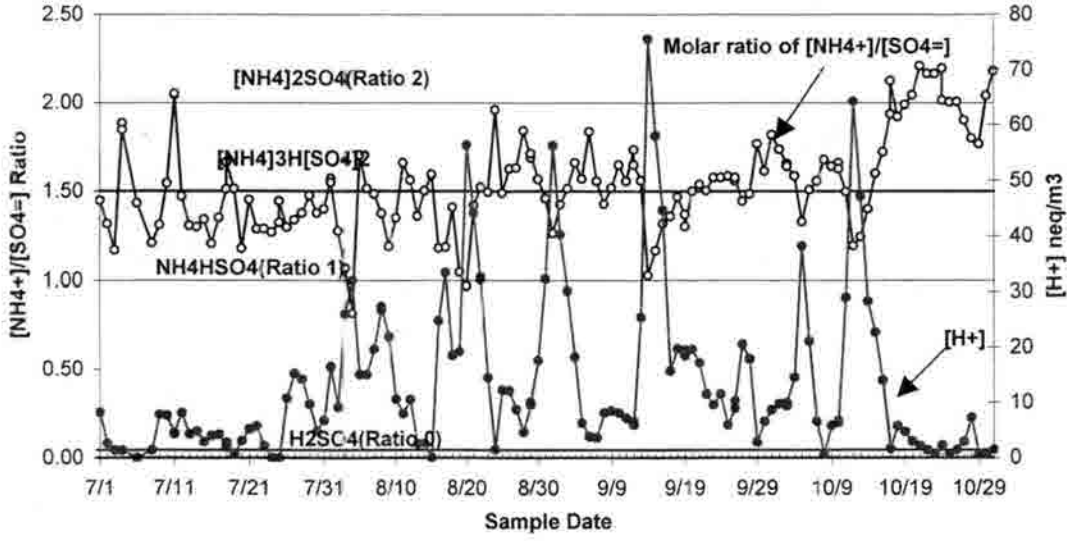

Figure 3.10 Timeline of molar ratio of $[NH_4^+]/[SO_4^{2-}]$ and H^+ concentration

in Big Bend National Park sulfates usually correspond to a composition range between NH_4HSO_4 (ammonium bisulfate) and $[NH_4]_2SO_4$ (ammonium sulfate).

Atmospheric sulfates are most often associated with submicron particles (Meszaros et al., 1997; Zhuang et al., 1999). A sulfate mode diameter of 0.4-0.5 μm is typically observed (see chapter 5 for details). Hydrogen ion has been reported to have similar size distributions as sulfate ion (Koutrakis et al., 1989; Tsai et al., 2000). Figure

3.11 shows H^+ concentrations plotted against sulfate concentrations in $PM_{2.5}$ during the entire 4-month BRAVO sampling period. A high correlation between SO_4^{2-} and H^+ was observed ($R^2 = 0.895$). Strong correlations ($R^2 = 0.94$) between sulfate and ammonium were observed as well (Figure 3.12)

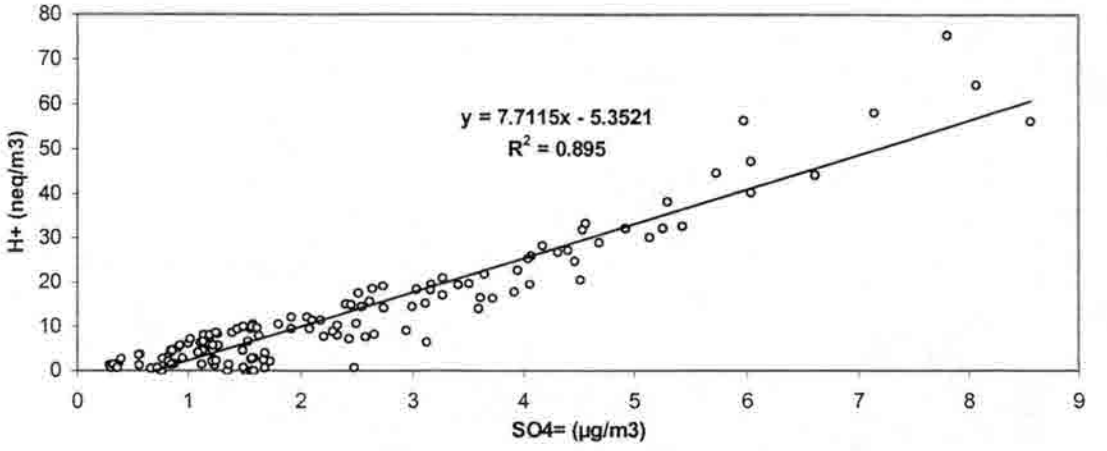

Figure 3.11 Relationship between SO_4^{2-} and H^+ concentrations

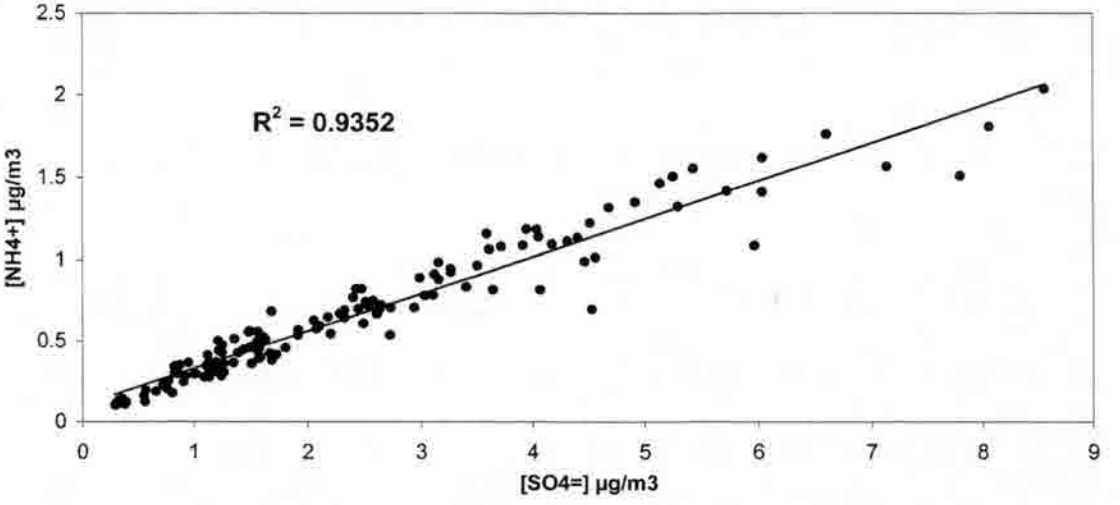

Figure 3.12 Relationship between SO_4^{2-} and NH_4^+ concentrations

Atmospheric sulfur dioxide can be oxidized to form sulfate by photochemical reaction in the gas phase, oxidation processes in the liquid phase, or heterogeneous reaction on the surface of existing particles (Seinfeld and Pandis, 1998; Finlayson-Pitts and Pitts, 2000). If sea salt particles are present in the atmosphere, sulfuric acid may condense on these particles, displacing HCl to the gas phase as shown in Equation 3.1.

$$\mathbf{H_2SO_4\,(g) + 2NaCl \rightarrow Na_2SO_4 + 2HCl} \qquad \mathbf{(3.1)}$$

Since seawater itself contains some sulfate, the amount of non sea salt-$[SO_4^{2-}]$ (nss-$[SO_4^{2-}]$) was calculated by subtracting the SO_4^{2-} amount associated with sea water from total measured particulate sulfate in $PM_{2.5}$ samples using the ratio of SO_4^{2-}/Na^+ (ratio = 0.252) for sea water as shown in Equation 3.2 (Ohta and Okita, 1990; Carmichael et al., 1997; Finlayson-Pitts and Pitts, 2000). The sea salt fraction (SSF) of sulfate was calculated by dividing the amount of SO_4^{2-} associated with sea salt by the total measured particulate sulfate. The timeline of SSF (%) and nss-$[SO_4^{2-}]$ is shown in Figure 3.13.

$$\mathbf{nss\text{-}[SO_4^{2-}] = [SO_4^{2-}]_{air} - ([SO_4^{2-}]/[Na^+])_{sea} \times [Na^+]_{air} = [SO_4^{2-}]_{air} - 0.252[Na^+]_{air}} \quad \mathbf{(3.2)}$$

The highest $PM_{2.5}$ SSF observed was 6.8 % on 7/3/99 and the monthly averages of SSF were calculated to be 2.3 %, 0.9 %, 0.6 % and 0.4 % in July, August, September and October, respectively. Overall, fine particulate sulfates at BBNP have little influence from sea salt particles, suggesting fine particle sulfate has mainly an anthropogenic

source. Long-range transport of an anthropogenic source is likely, because the concentration of particulate sulfate is much higher than the observed concentration of

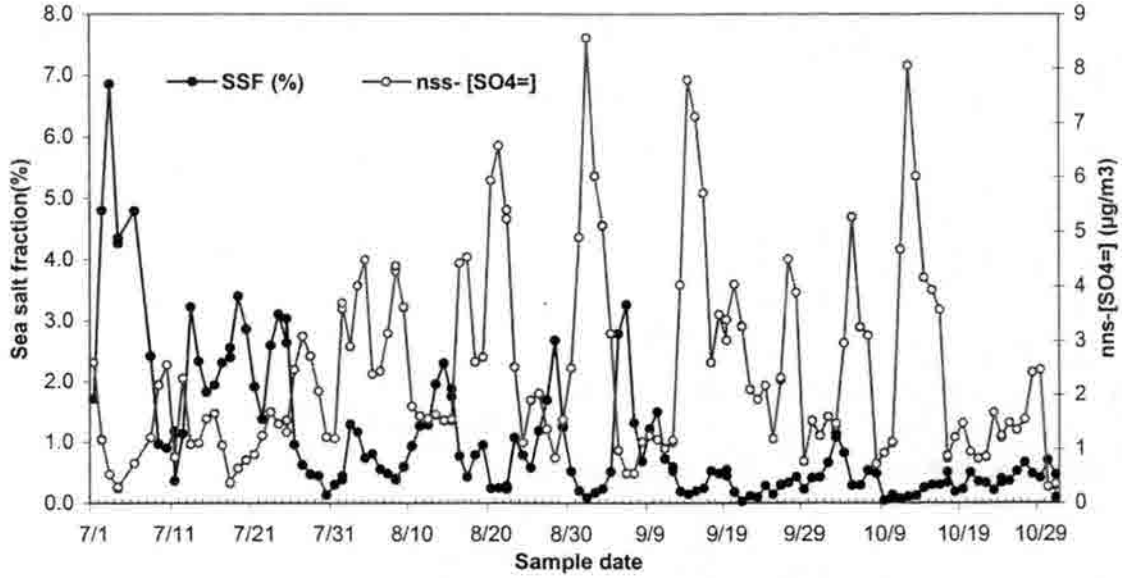

Figure 3.13 $PM_{2.5}$ timelines of sea salt fraction (SSF) and non sea salt-$[SO_4^{2-}]$

gaseous SO_2 (measured by Air Resources Specialist (ARS))(Figure 3.15) indicating sufficient time and/or cloud processing for substantial SO_2 oxidation (Cooke and Wadden, 1981; Scheff et al., 1984; Lee et al., 1993). Figure 3.14 shows that many air mass back-trajectories (NOAA Hysplit_4, Hybrid single-Particle Lagrangian Integrated Trajectory) pass over industrial or power-generating regions in northern Mexico and eastern Texas. Most air masses in July and August pass over only Mexico, along the Mexico-Texas border, or through Mexico and eastern Texas. Figure 3.15 presents a comparison between the concentrations of SO_4^{2-} and SO_2 (measured by Air Resource Specialists (ARS)). The 50 SO_2 data points included represent days that have a daily average comprised of at least 20 hourly average data points.

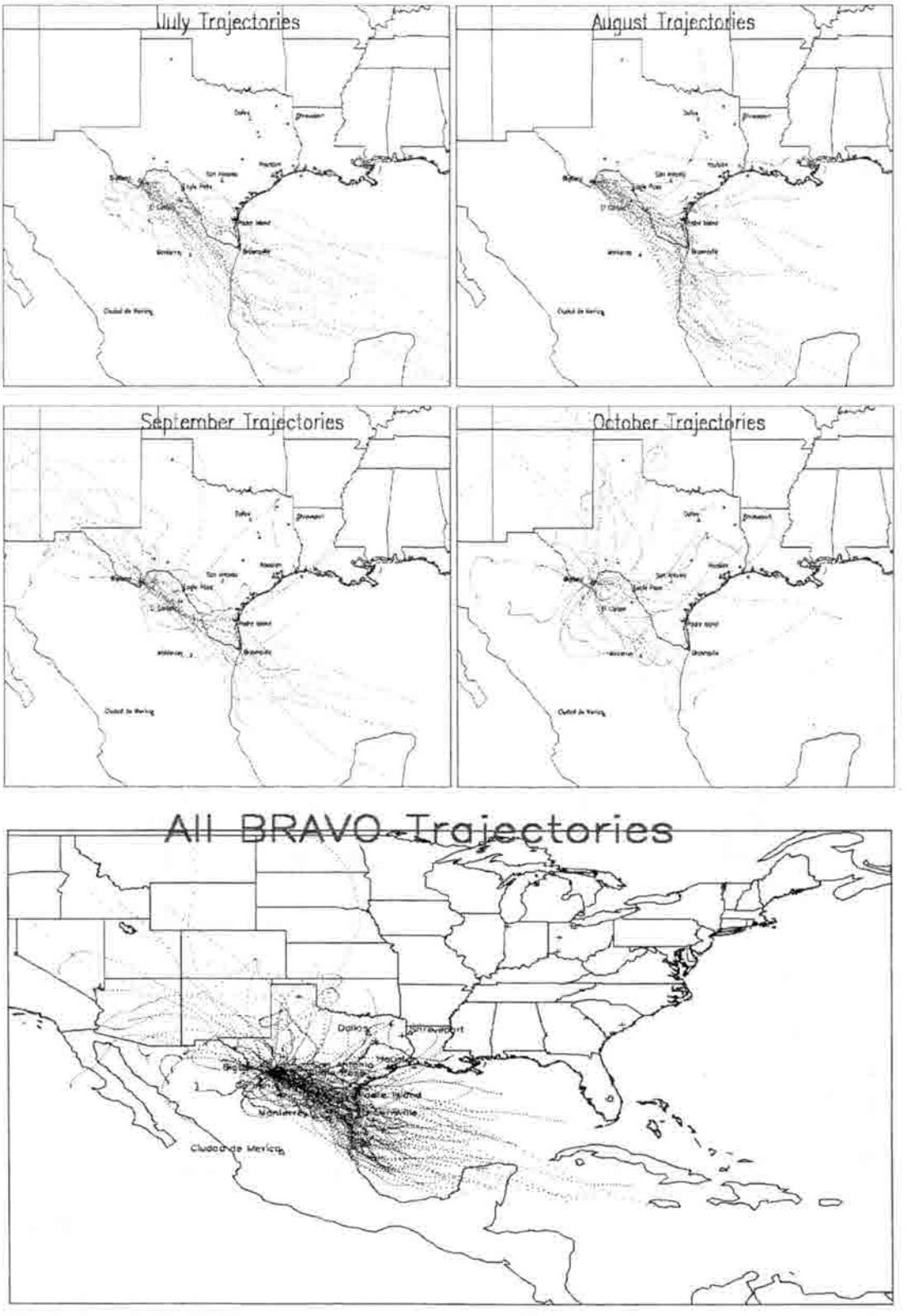

Figure 3.14 Daily HYSPLIT trajectories during the BRAVO study (July, August, September, October, and all BRAVO trajectories) (Note : some major cities are labeled and the locations of several power plants are indicated by "+")

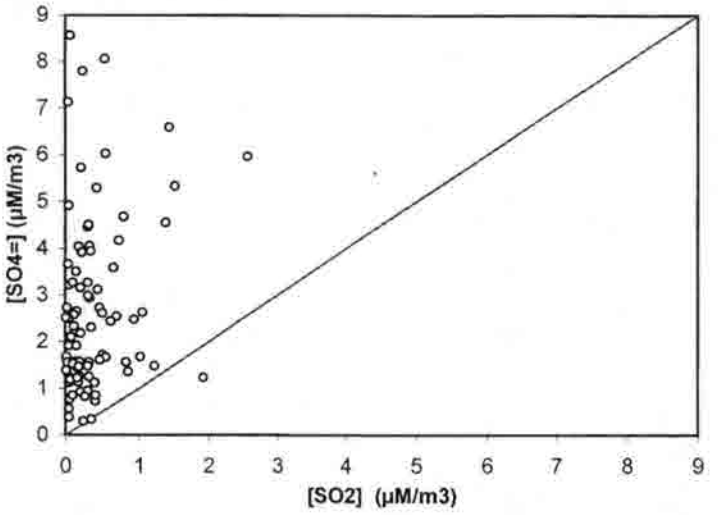

Figure 3.15 Comparison of SO_4^{2-}(p) and SO_2(g)

3.2.2 Nitrate(NO_3^-), ammonium(NH_4^+), sulfate(SO_4^{2-}) and trace gases (HNO_3, NH_3)

Reactions 3.3 to 3.6 show possible particulate nitrate formation pathways : 1) gaseous HNO_3 reaction with NH_3 gas to form particulate NH_4NO_3, 2) gaseous HNO_3 reaction with NaCl aerosol, the major component in sea salt particles, 3) nitric acid condensation on calcium carbonate particles, and 4) gaseous NO_2 reaction with NaCl aerosol.

$HNO_3(g) + NH_3(g) \leftrightarrow NH_4NO_3(p)$ **(3.3)** (Seinfeld and Pandis, 1998)

$HNO_3(g) + NaCl(Sea\ salt) \rightarrow NaNO_3 + HCl(g)$ **(3.4)** (Finlayson-Pitts and Pitts, 2000)

$2HNO_3(g) + CaCO_3(Mineral\ aerosol) \rightarrow Ca(NO_3)_2 + CO_2(g) + H_2O(aq)$ (3.5)

(Prospero and Savoie, 1989; Dentener et al., 1996)

$2NO_2\ (gas) + NaCl(aerosol) \rightarrow NaNO_3(aerosol) + NOCl(g)$ **(3.6)** (Spurny, 2000)

Figure 3.16 shows the correlation between $PM_{2.5}$ nitrate and $PM_{2.5}$ ammonium (left panel, $R^2 = 0.03$) and between N(V) (the sum of gaseous nitric acid and $PM_{2.5}$ nitrate) and $PM_{2.5}$ ammonium (right panel, $R^2 = 0.55$). The higher correlation between

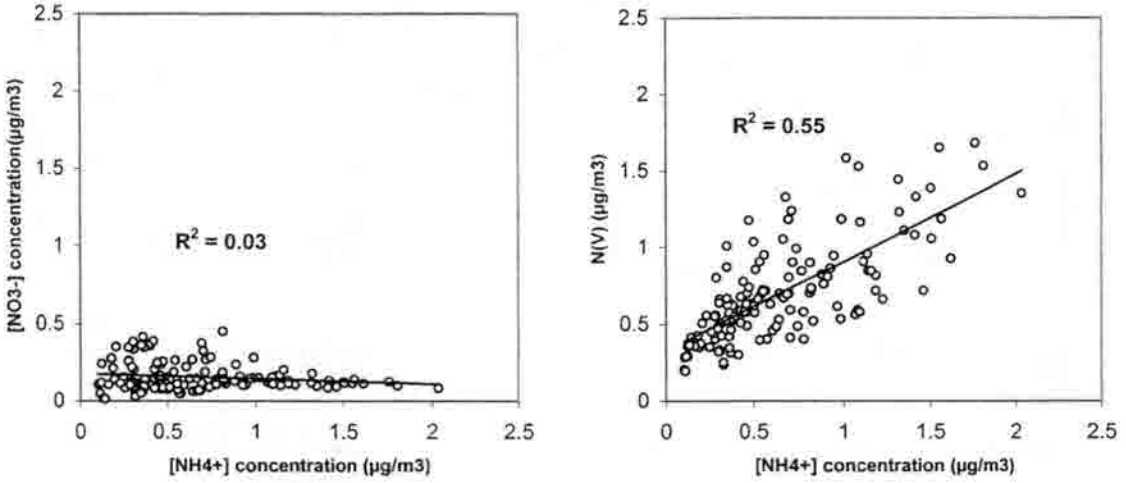

Figure 3.16 Correlation of $[NO_3^-]$ and $[NH_4^+]$ and [N(V)] and $[NH_4^+]$

N(V) and $PM_{2.5}$ ammonium suggests that there is probably some similarity in the source regions for these species. The extremely low correlation between $PM_{2.5}$ nitrate and ammonium is consistent with the significant aerosol acidity discussed previously. In the absence of sufficient ammonia to fully neutralize sulfuric acid, formation of particulate ammonium nitrate is not favored thermodynamically (Seinfeld and Pandis, 1998). The high temperatures and relatively low humidities observed during BRAVO also do not favor particulate ammonium nitrate formation. A timeline of the ratio of gaseous nitric acid to total N(V) is shown in Figure 3.17. While approximately half of the N(V) was found, on average, as gaseous HNO_3 in July, the averages for the subsequent three months show more than three-fourths of the N(V) was present as HNO_3. As will be discussed in more detail below, the main factor controlling formation of particulate

nitrate in this environment appears to be the availability of sea salt and/or soil dust particles that act as sites for gaseous nitric acid condensation.

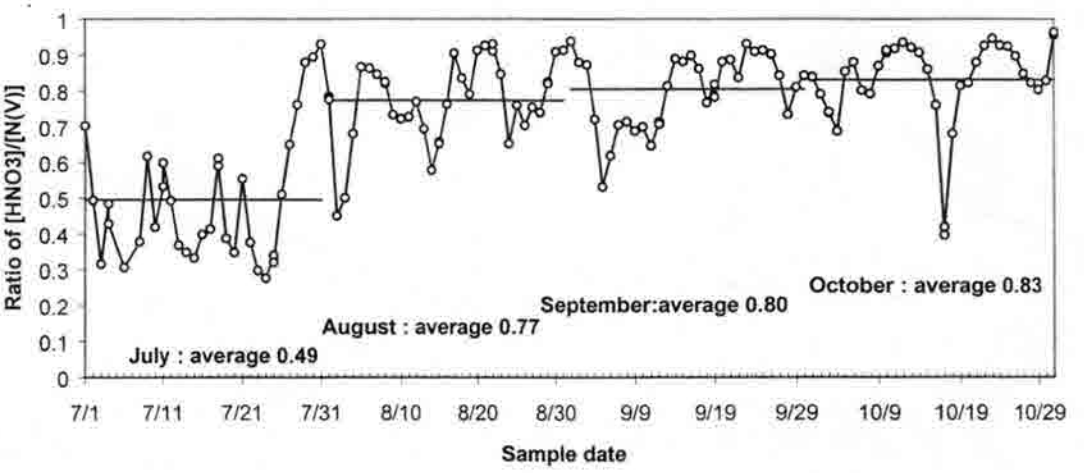

Figure 3.17 Timeline of ratio of $[HNO_3]/[N(V)]$, $N(V) = HNO_3 + [NO_3^-]$

Unlike N(V), total N(-III) (the sum of gaseous ammonia and $PM_{2.5}$ ammonium) tended to be associated mainly with particles (see. Figure 3.18). While the monthly average for July showed similar amounts of $PM_{2.5}$ ammonium and gaseous ammonia, only 5 to 19 % of the total N(-III), on average, during the subsequent three months was present as $NH_{3(g)}$. This is also consistent with the observed aerosol acidity: the lowest average aerosol acidity was observed during July.

Figure 3.19 shows $PM_{2.5}$ NO_3^- and N(V) concentrations plotted against SO_4^{2-} concentrations. The modest correlation ($R^2 = 0.55$) between N(V) and sulfate, along with the back trajectories shown in Figures 3.20 and 3.21, suggest similar source regions for their precursor emissions : NO_x and SO_2. Air mass trajectories in Figure 3.20 show that

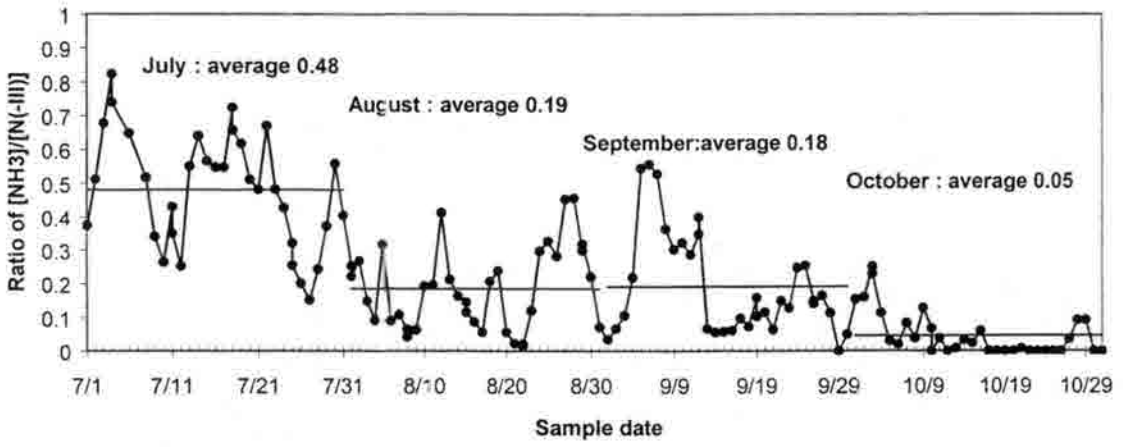

Figure 3.18 Timeline of ratio of $[NH_3]/[N(-III)]$

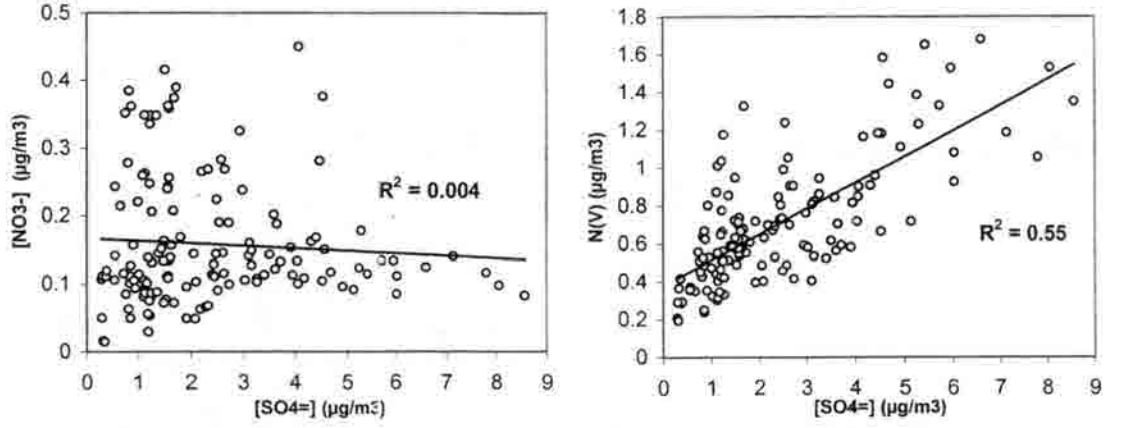

Figure 3.19 Correlation of $[NO_3^-]$ and $[SO_4^{2-}]$ and [N(V)] and $[SO_4^{2-}]$

most of the air masses for 10 highest sulfate concentration days spent time over eastern Texas or Louisiana before arriving at BBNP. Similar patterns are seen for the 10 days with the highest N(V) concentrations. On the other hand, air masses travel mostly through Mexico from the Gulf of Mexico into Big Bend for the 10 days with highest $PM_{2.5}$ NO_3^- (Figure 3.21), indicating that high particle nitrate concentrations do not

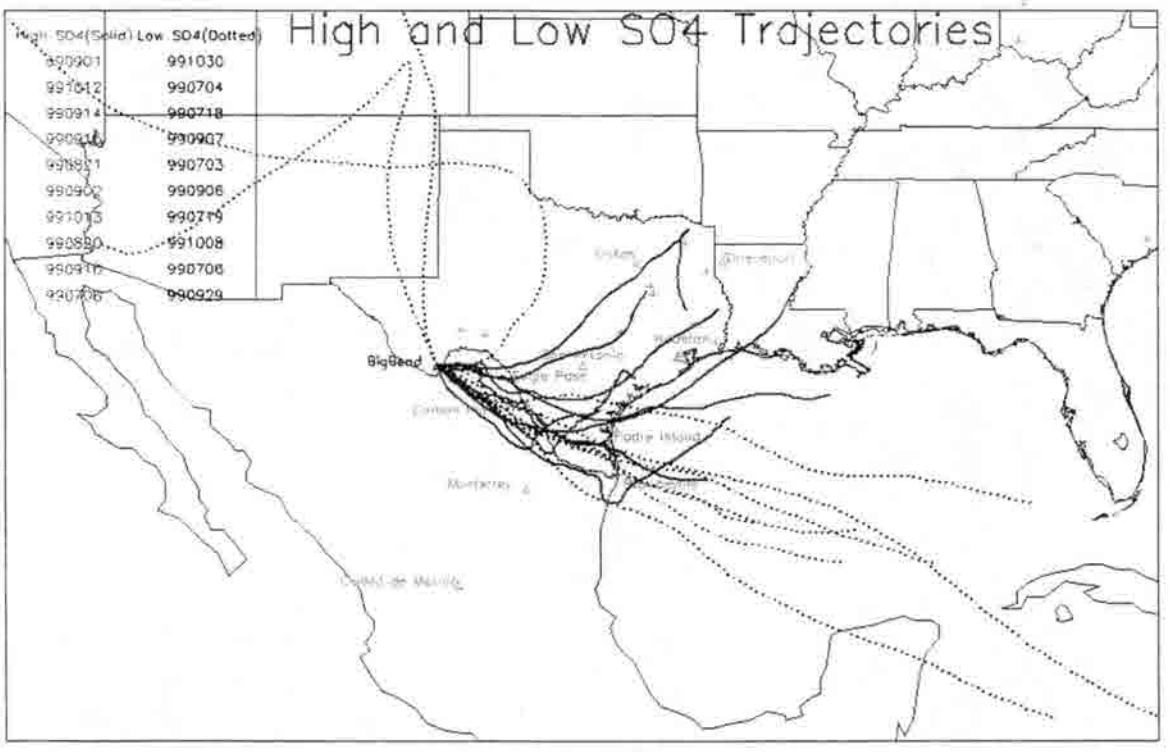

Figure 3.20 Air mass trajectories for the 10 day with highest and lowest $PM_{2.5}$ sulfate concentrations

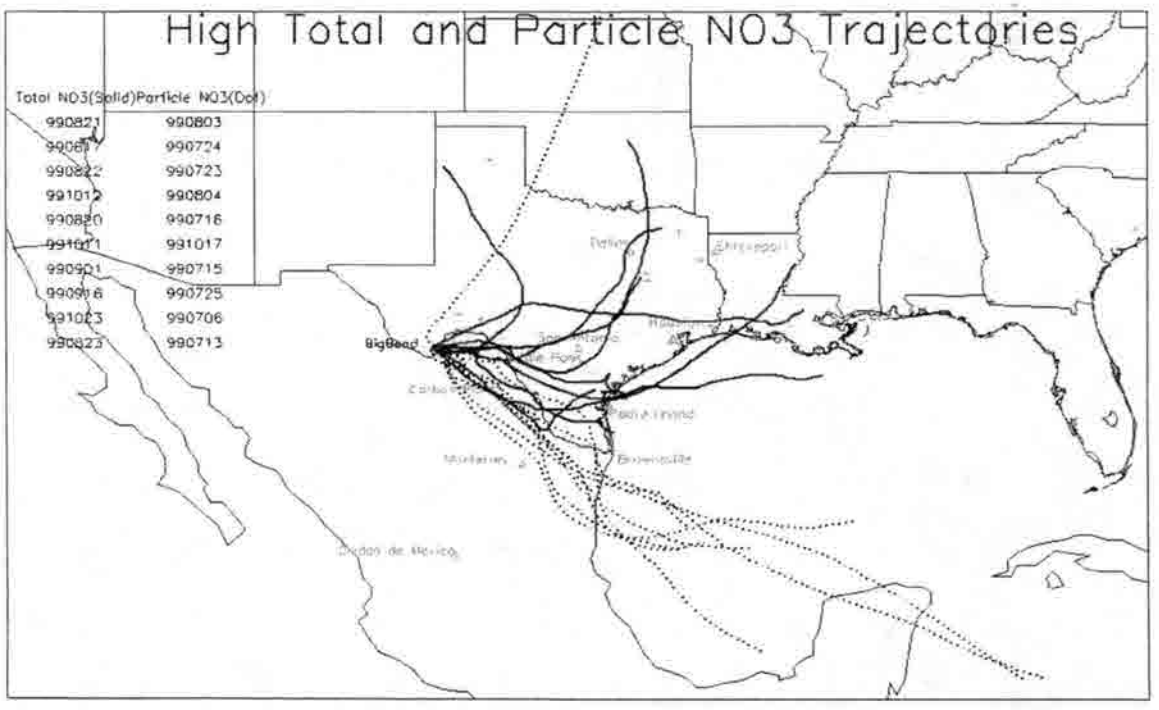

Figure 3.21 Air mass trajectories for 10 days with highest [N(V)](Total NO_3^-) and $PM_{2.5}$ NO_3^- concentrations

generally occur just due to elevated N(V) levels. The high $PM_{2.5}$ nitrate trajectories pass over likely sea salt and soil dust source areas, suggesting nitric acid reaction with these particles (Equation 3.4 and 3.5, (Padgett and Bytnerowicz, 2001)) may be an important mechanism for particulate nitrate formation. Further evidence for this hypothesis will be seen in chapter 4 when the MOUDI results are discussed.

If sulfate concentrations at Big Bend were substantially reduced, for example due to upwind reductions in SO_2 emission, it is possible that the aerosol could move toward neutralization. Further sulfate reductions beyond the neutral point could release ammonia providing the potential for ammonium nitrate formation. Because two ammonia molecules are required to neutralize one sulfate molecule, and two nitrate molecules

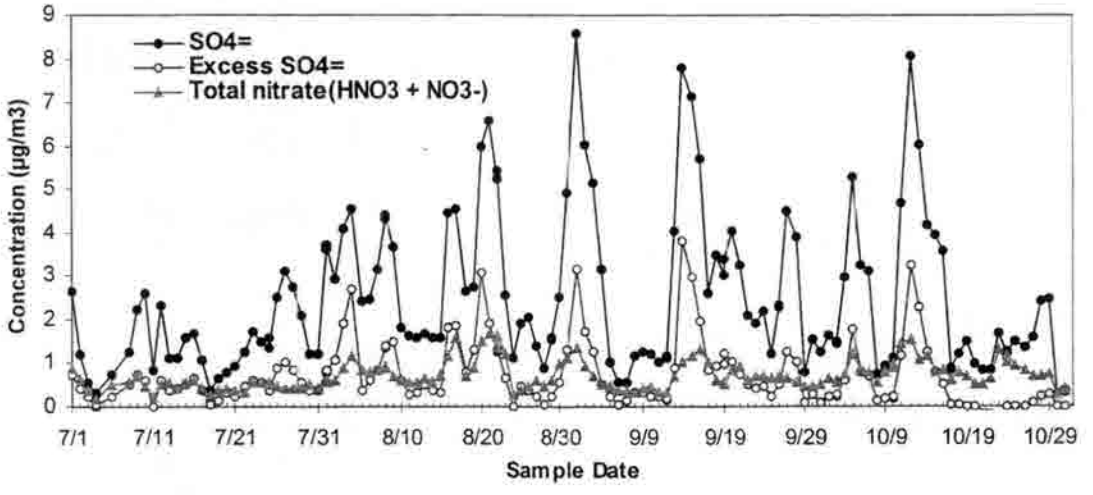

Figure 3.22 Timelines of sulfate, excess sulfate, and total nitrate $PM_{2.5}$ aerosol

have greater mass than one sulfate molecule, replacement of $(NH_4)_2SO_4$ by NH_4NO_3 has the potential to actually produce an increase in the $PM_{2.5}$ mass concentration. Figure 3.22 shows timelines of sulfate, N(V) and "excess" sulfate, where the latter refers to the amount of sulfate required to be removed to bring the aerosol to the neutral point. During

most periods of high sulfate there is also considerable excess sulfate, indicating that significant sulfate reductions are possible before replacement by ammonium nitrate becomes a concern.

3.2.3 NO_3^-, Cl^-, Na^+, Ca^{2+}, Mg^{2+}, and K^+ (Chlorine loss and sea salt and soil dust effect)

$PM_{2.5}$ nitrate showed almost no correlation with $PM_{2.5}$ sulfate and ammonium, although N(V) has a modest correlation with both species. Occurrence of high particle nitrate concentrations in air masses coming off the Gulf Mexico suggested nitric acid condensation on sea salt particles may be an important process for particulate nitrate formation. Condensation of nitric acid on sea salt and dust has been reported by several investigators (Prospero and Savoie, 1989; Dentener et al., 1996; Spurny, 2000; Padgett and Bytnerowicz, 2001). Figures 3.23 and 3.24 show the correlation of particle nitrate with Na^+ and Ca^{2+}, which typically are associated with sea salt and soil dust. $PM_{2.5}$ nitrate concentrations were correlated with Na^+ concentrations ($R^2 = 0.65$) and Ca^{2+} concentrations ($R^2 = 0.33$), and the sums of Na^+ and Ca^{2+} concentrations ($R^2 = 0.57$).

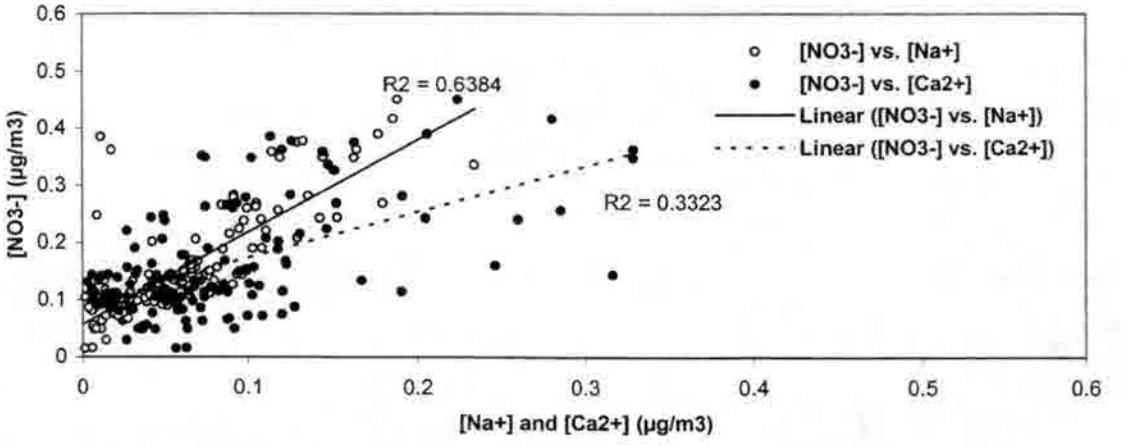

Figure 3.23 Relationship of [NO_3^-] vs. [Na^+] and [NO_3^-] vs. [Ca^{2+}]

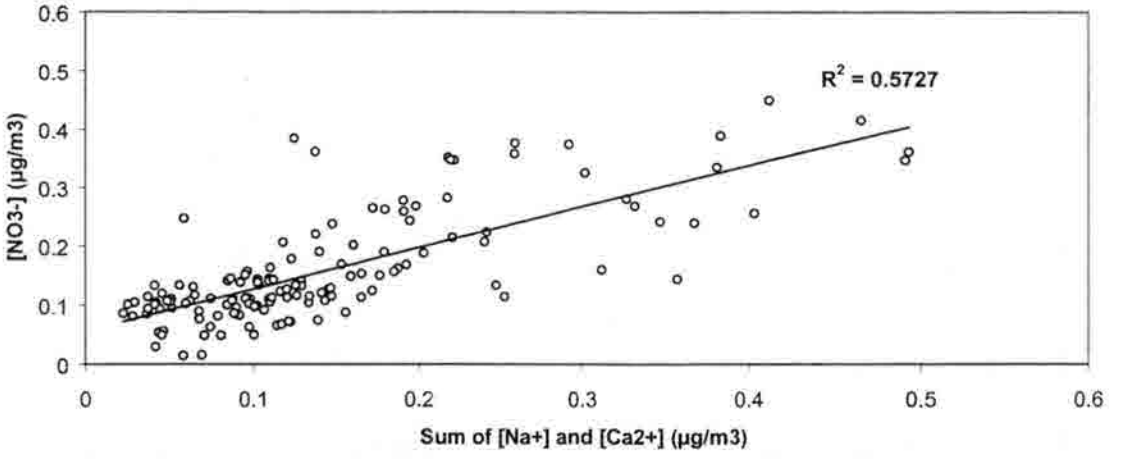

Figure 3.24 Relationship of $[NO_3^-]$ and sum of $[Na^+]$ and $[Ca^{2+}]$

The strong correlation of $[NO_3^-]$ and $[Na^+]$ and apparent loss of Cl^- from sea salt aerosol (Figure 3.25) suggest NO_3^- reacts with sea salt to form $NaNO_3$ particles, simultaneously displacing chlorine. To quantitatively determine the amount of chlorine loss (neq/m^3) and evaluate the relationship between particulate $NaNO_3$ and chlorine loss, the theoretical chlorine loss was calculated from Equation 3.8, with an equivalence-based $[Cl^-]/[Na^+]$ ratio of 1.164

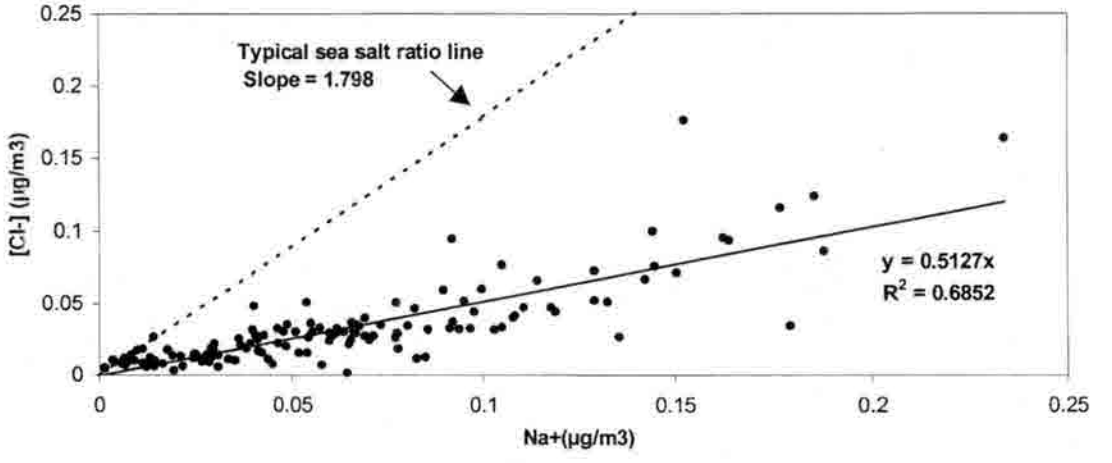

Figure 3.25 Relationship between Na^+ and Cl^- concentrations

in sea water (1.798 based on weight). The amount of chlorine loss was estimated as shown in Equation 3.9 assuming that the observed Na^+ concentration derived only

$$Cl^-_{(Theoretical\ chlorine)} = 1.164 \times Na^+_{(Observed)} \quad (3.8)$$

$$Cl^-_{(Chlorine\ loss)} = Cl^-_{(Theoretical\ chlorine)} - Cl^-_{(Observed)} \quad (3.9)$$

from sea salt particles. Figure 3.26 shows Na^+ concentrations plotted against $[Cl^-]_{obs}$ as well as the sum of $[NO_3^-]$ and $[Cl^-]_{obs}$. If Cl^- in sea salt particles (NaCl) is replaced with NO_3^- by the reaction between nitric acid (HNO_3) and sea salt as shown in Equation 3.4, the ratio of $([Cl^-_{obs}]+[NO_3^-])$ to $[Na^+]$ should be close to the typical ratio of $[Cl^-]$ to $[Na^+]$ in sea water. The average ratio for $[Cl^-]_{obs}$ to Na^+ concentration was calculated to be 0.33, while the ratio of the sum of $[Cl^-]_{obs}$ and $[NO_3^-]$ to $[Na^+]$ was calculated as 1.14, which is close to the ratio of $[Cl^-]$ to $[Na^+]$ in sea water (Figure 3.26).

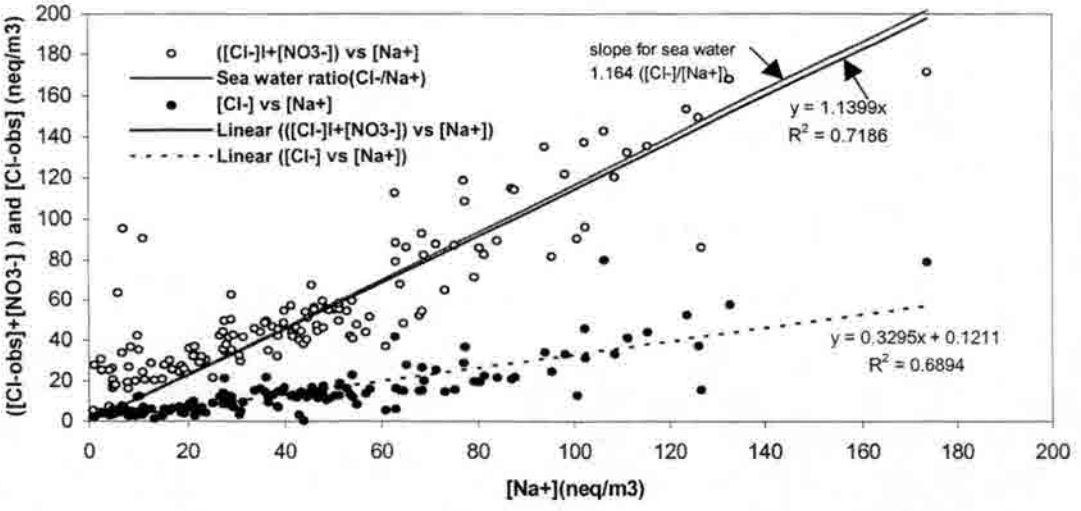

Figure 3.26 Relationship between $[Na^+]$ and the sum of $[NO_3^-]$ and $[Cl^-]_{obs}$, and between $[Na^+]$ and $[Cl^-]_{obs}$

The weekly and monthly averaged computed chlorine loss concentrations are presented in Table 3.1. NO_3^- concentration is plotted against the calculated chlorine loss concentration in Figure 3.27. The greatest chlorine loss was observed in July and August. October showed the least chlorine loss. The close relationship between $PM_{2.5}$ nitrate and chlorine loss supports the hypothesis that $PM_{2.5}$ NO_3^- is mostly formed through the reaction between gaseous nitric acid and sea salt.

Table 3.1 Monthly and weekly average concentrations of chlorine loss

Period	Average	Cl^- Theoretical neq/m3	Cl^- Observed neq/m3	Cl^- Loss neq/m3
7/1/99 – 7/31/99	July	80.2	27.6	52.6
8/1/99- 8/31/99	August	70.7	15.4	55.3
9/1/99 – 9/30/99	September	33.9	9.1	24.7
10/1/99 – 10/31/99	October	22.7	7.7	15.0
7/1/99 - 7/3/99	1st week	157.1	58.3	98.8
7/4/99 – 7/10/99	2nd week	73.7	19.3	54.4
7/11/99 – 7/17/99	3rd week	76.7	26.6	50.1
7/18/99- 7/24/99	4th week	77.4	29.7	47.7
7/25/99- 7/31/99	5th week	62.3	21.2	41.2
8/1/99 – 8/7/99	6th week	79.1	20.1	58.9
8/8/99 – 8/14/99	7th week	74.8	18.0	56.8
8/15/99 – 8/21/99	8th week	78.8	12.3	66.4
8/22/99 – 8/28/99	9th week	59.9	13.1	46.8
8/29/99 – 9/4/99	10th week	44.6	9.3	35.3
9/5/99 – 9/11/99	11th week	46.7	12.2	34.5
9/12/99 – 9/18/99	12th week	36.7	9.0	27.8
9/19/99 – 9/25/99	13th week	21.4	8.1	13.3
9/26/99 – 10/2/99	14th week	28.2	7.8	20.3
10/3/99 – 10/9/99	15th week	41.2	11.5	29.7
10/10/99 – 10/16/99	16th week	21.7	9.3	12.3
10/17/99 – 10/23/99	17th week	10.1	5.2	4.9
10/24/99 – 10/31/99	18th week	18.2	5.4	12.8

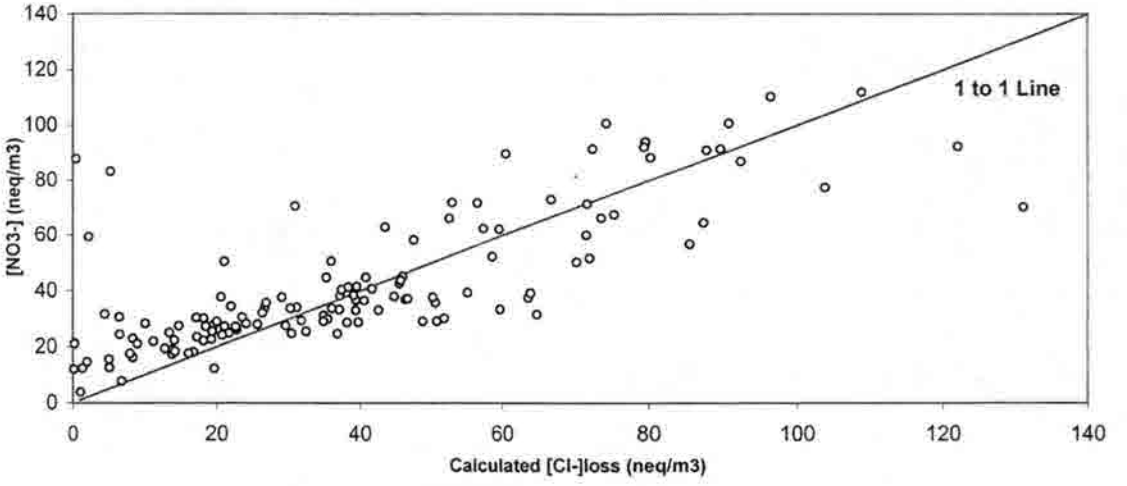

Figure 3.27 Relationship between the calculated chlorine loss and $[NO_3^-]$

Ratios of individual species concentrations (Cl^-, K^+, Mg^{2+} and Ca^{2+}) with Na^+ were calculated to determine possible sources. Table 3.2 presents the ratios for sea water as reported by (Wilson, 1975; Cheng et al., 2000; Cheng et al., 2001). Ratios of each

Table 3.2 Ionic concentration ratios in sea water

Combination $(\mu eq/m^3)/(\mu eq/m^3)$	Ratio (Cheng et al., 2000)	Ratio (Wilson, 1975)
Cl^- / Na^+	1.164	1.16
K^+ / Na^+	0.0218	0.0218
Mg^{2+} / Na^+	0.223	0.227
Ca^{2+} / Na^+	0.0415	0.0439
SO_4^{2-} / Na^+	0.121	0.121

species (Cl^-, K^+, Mg^{2+}, Ca^{2+} and SO_4^{2-}) with Na^+ were calculated for the BRAVO $PM_{2.5}$ data along with estimates of non sea salt SO_4^{2-} using Equation 3.10.

$$\text{nss-}[SO_4^{2-}] = [SO_4^{2-}]_{air} - ([SO_4^{2-}]/[Na^+])_{sea} \times [Na^+]_{air} = [SO_4^{2-}]_{air} - 0.121[Na^+]_{air} \quad (3.10)$$

(Note the ratio of 0.121 for SO_4^{2-}/Na^+ is based on $\mu eq/m^3$ unit in equation 3.10, otherwise, the ratio of 0.252 for SO_4^{2-}/Na^+ in Equation 3.2 is for $\mu g/m^3$ unit)

Figure 3.28 and Table 3.3 represent the timeline and monthly average species ratios, respectively. Soluble K^+ is sometimes regarded as a good tracer for biomass burning when it is correlated with black carbon and when the K^+ concentration is observed to have a very high enrichment factor (EF values > 10) (Arimoto et al., 1995; Echalar et al., 1995). However, a poor correlation between K^+ and black carbon suggests that biomass burning did not significantly influence aerosol composition during the BRAVO study (see (Brown, 2001)). Ca^{2+}/Na^+ and Mg^{2+}/Na^+ ratios were generally higher than sea water (0.0439 and 0.227) (Table 3.3). This suggests that the $PM_{2.5}$ aerosol composition during BRAVO was likely influenced both by sea salt and soil dust. The SO_4^{2-}/Na^+ ratio was much higher than the sea water ratio, indicating that SO_4^{2-} is predominantly of anthropogenic origin.

Table 3.3 Monthly ionic concentration ratios in BRAVO BBNP $PM_{2.5}$ samples

Period	Average	Cl^-/Na^+	K^+/Na^+	Ca^{2+}/Na^+	Mg^{2+}/Na^+	SO_4^{2-}/Na^+
Typical ratio in sea water[a]						
(μeq/m³)/(μeq/m³)		***1.16***	***0.0218***	***0.0439***	***0.227***	***0.121***
Typical ratio in Earth's crustal elements[b]			***K/Na***	***Ca/Na***	***Mg/Na***	
(μeq/μeq)			***0.54***	***1.47***	***1.42***	
7/1/99 – 7/31/99	July	0.48	0.13	1.284	0.37	12.01
8/1/99- 8/31/99	August	0.35	0.14	1.301	0.33	20.29
9/1/99 – 9/30/99	September	0.32	0.34	2.391	0.36	55.84
10/1/99 – 10/31/99	October	0.29	0.76	6.424	0.46	53.95

a : source (Wilson, 1975; Cheng et al., 2000)
b : source (Finalyson-Pitts et al., 2000)

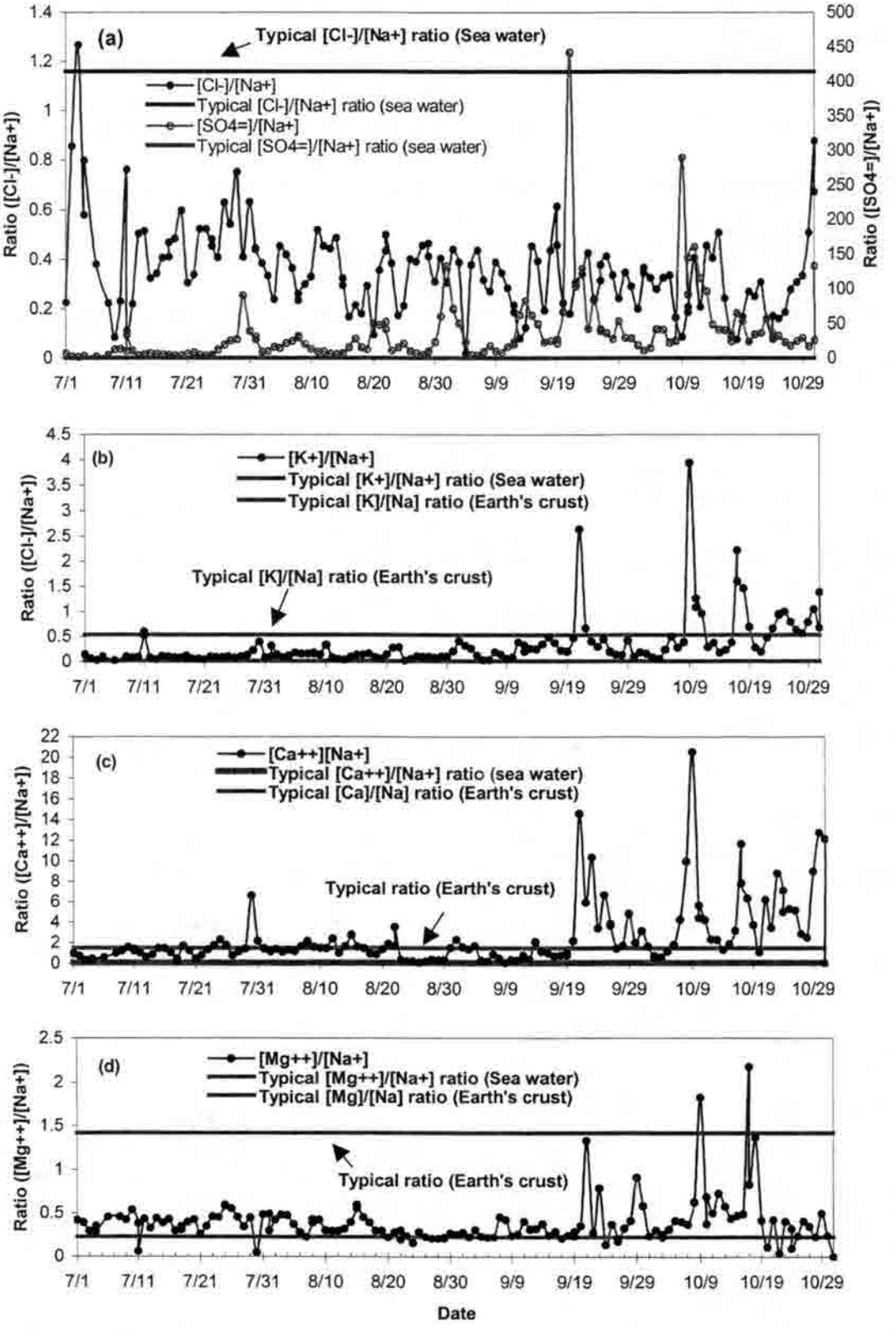

Figure 3.28 Timeline of species ratios; (a) $[Cl^-]/[Na^+]$ and $[SO_4^{2-}]/[Na^+]$, (b) $[K^+]/[Na^+]$, (c) $[Ca^{2+}]/[Na^+]$, and (d) $[Mg^{2+}]/[Na^+]$

3.3 Statistical analysis (factor analysis and correlation matrix)

Multivariate statistical analysis has been previously used to identify likely sources of particulate matter in aerosol studies (Kaiser, 1958; Lee, 1992; Cheng et al., 2000; Herckes et al., 2002). Several factor analysis techniques (Kaiser, 1958; Currie et al., 1984; Hopke, 1988) were developed to suggest likely source concentration profiles using the assumption that the observed concentrations were linearly correlated with a number of independent sources. In this study correlation matrix and factor analysis were performed to identify potential sources of major $PM_{2.5}$ ions.

In a multiple component variable system, it is common to have groups of variables that follow similar trends. Factor analysis is one way to assess multivariate information. As an eigenvector method, factor analysis compresses data into fewer dimensions. This makes the interrelationships between the variables in a system easier to evaluate.

Factor analysis assumes that the variables are linearly related to some number of underlying factors that govern the values of the measured data. For this study, the variance of each sample was assumed to be determined by several distinct source types, which are represented by factors. Simply, each variable, X_{ij}, can be expressed by a linear combination of several factors, f_{pj}. A simple expression can be written as shown in Equations 3.11 and 3.12.

$$\mathbf{X_{ij} = a_{i1}f_{1j} + a_{j2}f_{2j} + \ldots + a_{ip}f_{pj} + d_iU_{ij}} \qquad \mathbf{(3.11)}$$

$$\mathbf{f_{pj} = w_{p1}X_{1j} + w_{p1}X_{1j} + \ldots + w_{pi}X_{ij}} \qquad \mathbf{(3.12)}$$

where X_{ij} is the mixing ratio of species i in sample j and f_{pj} is the factor score for factor p in sample j. d_iU_{ij} represents the residual error in the theoretical representation of the observed measurement X_{ij}, which is a unique factor for each variable in sample j. The coefficients, a_{ip} and w_{pi} in Equations 3.11 and 3.12 are the factor loading and the factor score coefficient for the i^{th} variable in factor p, respectively.

An initial correlation matrix, R, is established as shown in Equation 3.13, and then the correlation matrix is diagonalized by an eigenvalue-eigenvector analysis as expressed in Equation 3.14

$$\mathbf{R} = \frac{1}{nDD'} \qquad \textbf{(3.13)}$$

$$\mathbf{U\text{-}1} \times \mathbf{R} \times \mathbf{U} = \mathbf{L} \qquad \textbf{(3.14)}$$

where n is the number of observations, D is the observed data matrix standardized to a mean of 0 and variance of 1 for every row in the initial data set, and D' is the transpose of matrix D. L is a diagonal matrix whose diagonal elements are eigenvalues. The corresponding eigenvectors are the column vectors of matrix U.

The number of underlying factors is determined next. The objective is to find the minimum number of factors while still retaining the maximum variance. In factor analysis, algorithms are usually designed to keep as much of the variance as possible in the first factor. Then, the maximum amount of the remaining variance is retained in the second factor. This process continues, with each successive factor explaining less of the total system variance.

After the number of factors is determined, a new factor loading and factor score matrix (f_{pj}) is calculated. The new factor loadings must then be related to the controlling

processes in the system because the new calculated factors are no longer related to the original variables. This makes an interpretation of the physical meaning of the new factors difficult. A rotation of the data is needed to achieve maximum overlap with the original variables.

For the factor analysis calculation, the statistical package SPSS 8.0 for Windows was used. The factors were rotated by the VARIMAX method (Kaiser, 1958), which has been widely used because it produces reasonably unique source compositions that have a maximum amount of inter-species variability. The principal component factoring (PCF) method was applied for the factors analyzed. Days with concentrations below MDL (μN concentration) were excluded from the statistical analysis. Analysis of the distributions of concentration values in the analyzed data set indicated ion concentrations approximated a normal distribution.

Table 3.4 shows the statistical summary of the variables used in the BRAVO study factor analysis. The results of the factor analysis are presented in Table 3.5. Table 3.5 presents computed $PM_{2.5}$ factor loadings. The first factor, with an eigenvalue greater than 1 (i.e. 4.63) and 42 % of the variance, has a high loading in Cl^-, NO_3^-, Na^+, and Mg^{2+} indicating that the source may be sea salt from the marine environment that also contains condensed nitric acid. The second factor has a high loading in SO_4^{2-}, NH_4^+, HNO_3, and H^+ and an eigenvalue of 3.45, accounting for 31 % of the variance. The second factor may represent anthropogenic sources, which include the by-products of oxidation of SO_2 and NO_x originating from fossil fuel combustion, including vehicle and power plant emissions. The third factor, with an eigenvalue of 1.23 and explaining 11 % of the variance, contains K^+ and Ca^{2+} consistent with a crustal or soil component source.

Table 3.4 Statistical summary of the variables used in the BRAVO study factor analysis

unit : μg/m3

Variables	Minimum	Maximum	Mean	Std. Dev.	Used data points*
Cl^-	0.013	0.177	0.031	0.028	112
SO_4^{2-}	0.289	8.568	2.371	1.751	112
NO_3^-	0.015	0.450	0.139	0.093	112
Na^+	0.011	0.234	0.061	0.037	112
NH_4^+	0.102	2.037	0.651	0.405	112
K^+	0.010	0.055	0.015	0.011	112
Mg^{2+}	0.014	0.052	0.029	0.011	112
Ca^{2+}	0.042	0.329	0.082	0.058	112
NH_3	0.050	0.624	0.156	0.131	112
HNO_3	0.084	1.555	0.645	0.341	112
H^+	0.00063	0.076	0.013	0.014	112

*** The days having values below MDL(based on μN concentration) were not used for statistical analysis (Original data points including duplicate samples : 140)**

Table 3.5 Factor loading of the different species of the BRAVO study

Variables	Factor				
	1	2	3	4	5
Cl^-	**.909**	-.151	.112	-3.75E-03	-4.55E-2
SO_4^{2-}	1.761E-02	**.984**	-4.04E-2	.101	3.95E-02
NO_3^-	**.865**	-.120	9.33E-2	.240	.125
Na^+	**.922**	5.144E-3	.220	1.77E-02	.157
NH_4^+	-9.09E-02	**.951**	-5.21E-02	.158	6.96E-02
K^+	.177	.219	**.757**	.929	.187
Mg^{2+}	**.903**	-2.99E-02	.234	8.039E-02	.337
Ca^{2+}	.492	3.484E-02	**.707**	.300	.796
NH_3	.318	-.204	-.573	-.108	-6.31E-02
HNO_3	-.256	**.757**	.295	9.27E-02	7.08E-2
H^+	-3.996E-02	**.958**	-5.208E-02	-1.14E-02	1.137
Eigenvalue	4.63	3.45	1.23	0.55	0.36
% of Variance	42.06	31.36	11.19	4.95	3.23

Sampling adequacy, Kaiser-Meyer-Olkin (KMO) : 0.73

Table 3.6 Spearman's correlation matrix of ionic species for the entire BRAVO

	Cl^-	NO_3^-	SO_4^{2-}	Na^+	NH_4^+	K^+	Mg^{2+}	Ca^{2+}	H^+
Cl^-	**1.00**								
NO_3^-	**.767****	**1.00**							
SO_4^{2-}	-.066	-.003	**1.00**						
Na^+	**.517****	.470**	.141	**1.00**					
NH_4^+	-.244**	-.189*	**.937****	-.110	**1.00**				
K^+	.094	.290**	.317**	.003	.350**	**1.00**			
Mg^{2+}	**.622****	**.730****	-.009	-.046	-.078	.281**	**1.00**		
Ca^{2+}	.298**	.459**	.071	-.089	.083	**.525****	**.700****	**1.00**	
H^+	-.243**	-.181**	**.915****	-.061	**.859****	.169*	-.119	-.094	**1.00**

*** : Correlation is significant at the 0.01 level (2-tailed)**
**** : Correlation is significant at the 0.05 level (2-tailed)**

Tables 3.6 and 3.7 present the statistical correlation matrices between chemical species. The correlation matrix for the entire study presented in Table 3.6 shows that H^+ has strong positive correlations with SO_4^{2-} and NH_4^+. This indicates that most of the acidity is associated with partially neutralized sulfate and not with nitrate.

Correlation matrices based on each month are presented in Table 3.7. While H^+ has a modest positive correlation with SO_4^{2-} (and NH_4^+) in July there is a stronger correlation in August, September, and October. Correlation between nitrate and chloride are strongest in July and August as are nitrate and calcium correlations.

Table 3.7 Spearman's correlation matrices of ionic species for each month

	Cl^-	NO_3^-	SO_4^{2-}	Na^+	NH_4^+	K^+	Mg^{2+}	Ca^{2+}	H^+	
Cl^-	**1.00**									
NO_3^-	.747**	**1.00**								July
	.801**									Aug.
	.606**									Sep.
	.455**									Oct.
SO_4^{2-}	.246	.474**	**1.00**							July
	-.151	.081								Aug.
	.050	.070								Sep.
	.460**	.057								Oct.
Na^+	.555**	.587**	.680**	**1.00**						July
	.844**	.895**	-.143							Aug.
	.754**	.818**	.115							Sep.
	.853**	.301	.442**							Oct.
NH_4^+	-.293	-.044	.595**	-.163	**1.00**					July
	-.229	-.156	.924**	-.330*						Aug.
	.025	.054	.978**	.100						Sep.
	.509**	.087	..980**	.490**						Oct.
K^+	.291	.437**	.274	.053	.348*	**1.00**				July
	.403*	.504**	.398**	.363*	.347*					Aug.
	.271	.297	.647**	.262	.639**					Sep.
	.162	.450**	.124	.170	.214					Oct.
Mg^{2+}	.394*	.539**	.027	-.234	.241	.634**	**1.00**			July
	.775**	.933**	-.014	.900**	-.197	.492**				Aug.
	.637**	.721**	.140	.853**	.117	.204				Sep.
	.771**	.615**	.626**	.780**	.649**	.381*				Oct.
Ca^{2+}	.250	.467**	.076	-.198	.266	.636**	.879**	**1.00**		July
	.569**	.647**	.151	.577**	.076	.572**	.768**			Aug.
	-.151	-.194	.497**	-.001	.529**	.162	.026			Sep.
	.186	.197	.045	.206	.118	.678**	.363*			Oct.
H^+	-.354*	-.207	.420*	.013	.458**	-.086	-.172	-.127	**1.00**	July
	-.303	-.038	.933**	-.231	.805**	.216	.324	-.050		Aug.
	.057	.125	.953**	.134	.879**	.625**	.156	.377*		Sep.
	.344*	.002	.944**	.319	.872**	-.088	.503**	-.208		Oct.

***: Correlation is significant at the 0.01 level (2-tailed)**

**** : Correlation is significant at the 0.05 level (2-tailed)**

Chapter 4. Ionic composition of size-resolved aerosol

It is well known that the environmental effects of aerosol particles depend on their size and ionic composition. Fine particles (e.g. $D_p < 1$ μm) are usually associated with anthropogenic activities such as smelting of metals, combustion of fossil fuels, and gas phase reactions. On the other hand, most coarse particles are mechanically produced by natural or anthropogenic processes

Daily Micro Orifice Uniform Deposit Impactor (MOUDI) samples were collected in 9 size categories (D_{50} = 18, 10, 5.6, 3.2, 1.8, 1.0, 0.56, 0.32 and 0.18 μm) during the BRAVO study. Selected MOUDI samples (41 days) were analyzed to provide information about chemical composition as a function of aerosol size. The 41 MOUDI samples selected for chemical analysis are listed in Table 4.1. All MOUDI samples are listed in appendix A.

The following topics regarding size-resolved aerosol properties will be discussed in this chapter:

1) In order to validate the MOUDI aerosol data, inorganic water soluble ionic concentrations from appropriate stages of the MOUDI sampler were compared to the ionic concentrations obtained from the $PM_{2.5}$ URG samples.
2) The daily and monthly average ionic compositions of the size-resolved aerosol are used to provide more information about the source and behavior of each ion species.
3) The ion balance (ratio of cation to anion) of the size-resolved aerosol is used to estimate aerosol acidity vs. particle size.

Table 4.1 MOUDI Sample dates selected for analysis

July	August	September	October
7/2, 7/3, 7/6, 7/8, 7/11,7/16, 7/18, 7/19*, 7/20, 7/23, 7/24, 7/30,	8/2*, 8/3, 8/14, 8/15, 8/20, 8/21, 8/24, 8/27, 8/28,	9/1, 9/2, 9/6*, 9/8, 9/14, 9/15, 9/21, 9/29	10/4*, 10/5, 10/7, 10/8, 10/9, 10/10, 10/12, 10/13, 10/14, 10/15, 10/16, 10/17, 10/21, 10/27, 10/28, 10/29

*** : Blank sample**

4.1 Comparison between MOUDI and URG data

The aerosol chemical concentrations measured with URG (D_{50} = 2.5 μm) filter samples were compared to the sum of the aerosol concentrations obtained from stage 4 (1.8 – 3.2 μm) to stage 8 (0.18 – 0.32 μm) of the MOUDI sampler. This was done in order to validate the MOUDI chemical analysis results. Figures 4.1 and 4.2 show daily average concentrations of ionic species measured with the URG sampler vs. those obtained using the MOUDI sampler.

As can be seen in Figure 4.1, concentrations of NO_3^- and SO_4^{2-} are similar for the URG and MOUDI samplers with most points closely following the 1:1 ratio line with R^2 = 0.89 and 0.98, respectively. Cl^- concentrations (R^2 = 0.68), on the other hand, do not exhibit as good a correlation. The poor relationship for the measurement of chloride using the URG and MOUDI samplers may be due to difficulties in accurately measuring very low concentrations of Cl^-. For the cation species, good relationships between the URG and MOUDI samples were observed for ammonium, sodium, and potassium with R^2 = 0.95, 0.94, and 0.72, respectively. The greater scatter in the K^+ results is not surprising given the low concentrations seen on the MOUDI stages. The correlations for magnesium

and calcium had $R^2 = 0.66$ and 0.21 due to higher uncertainties in measuring very low concentration of those species and, perhaps, the difference between the URG and MOUDI size cut.

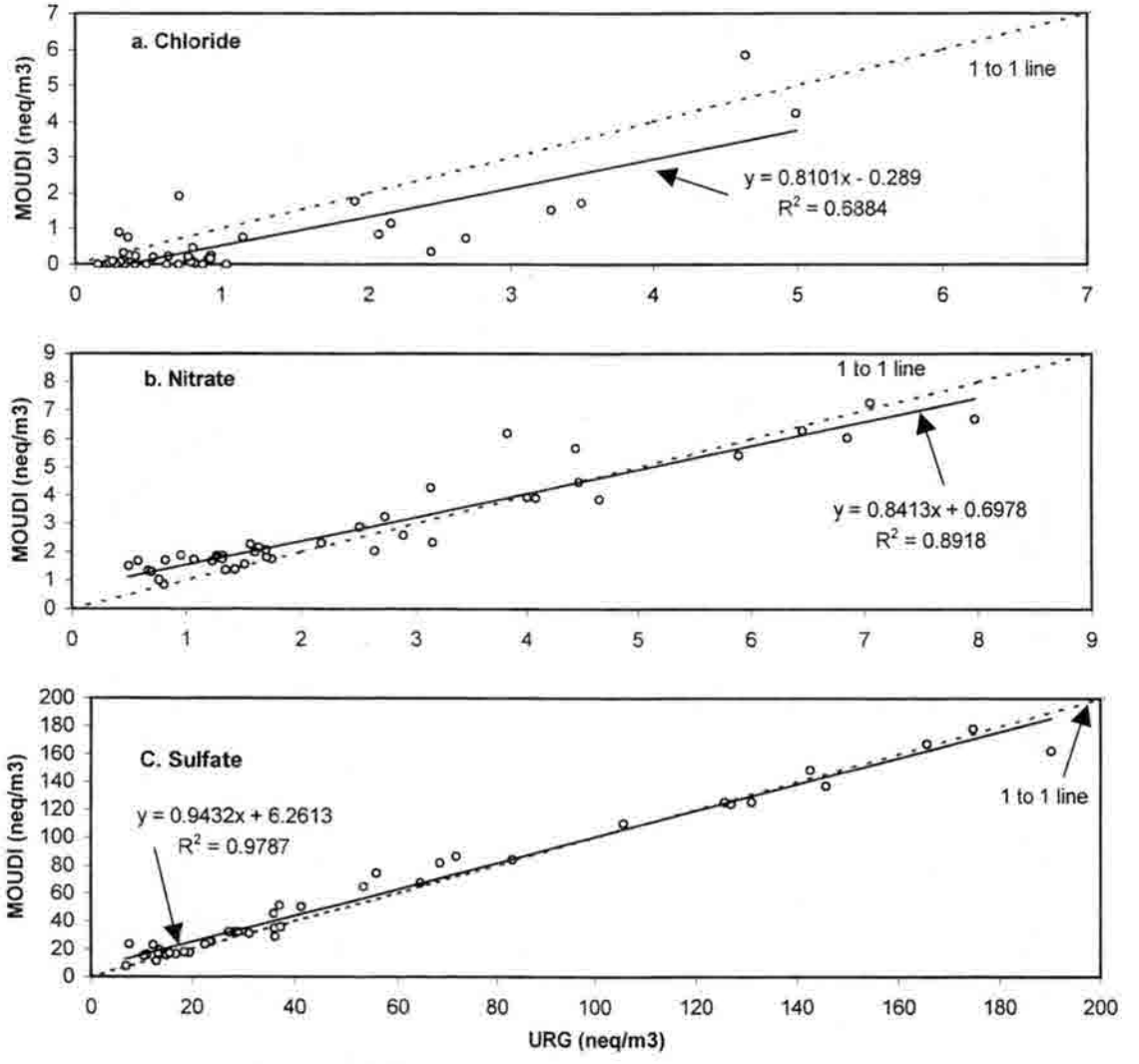

Figure 4.1 The comparison of anion concentrations of (a) chloride, (b) nitrate, and (c) sulfate between the URG and MOUDI samplers. The dot and solid lines show the 1:1 ratio and regression, respectively

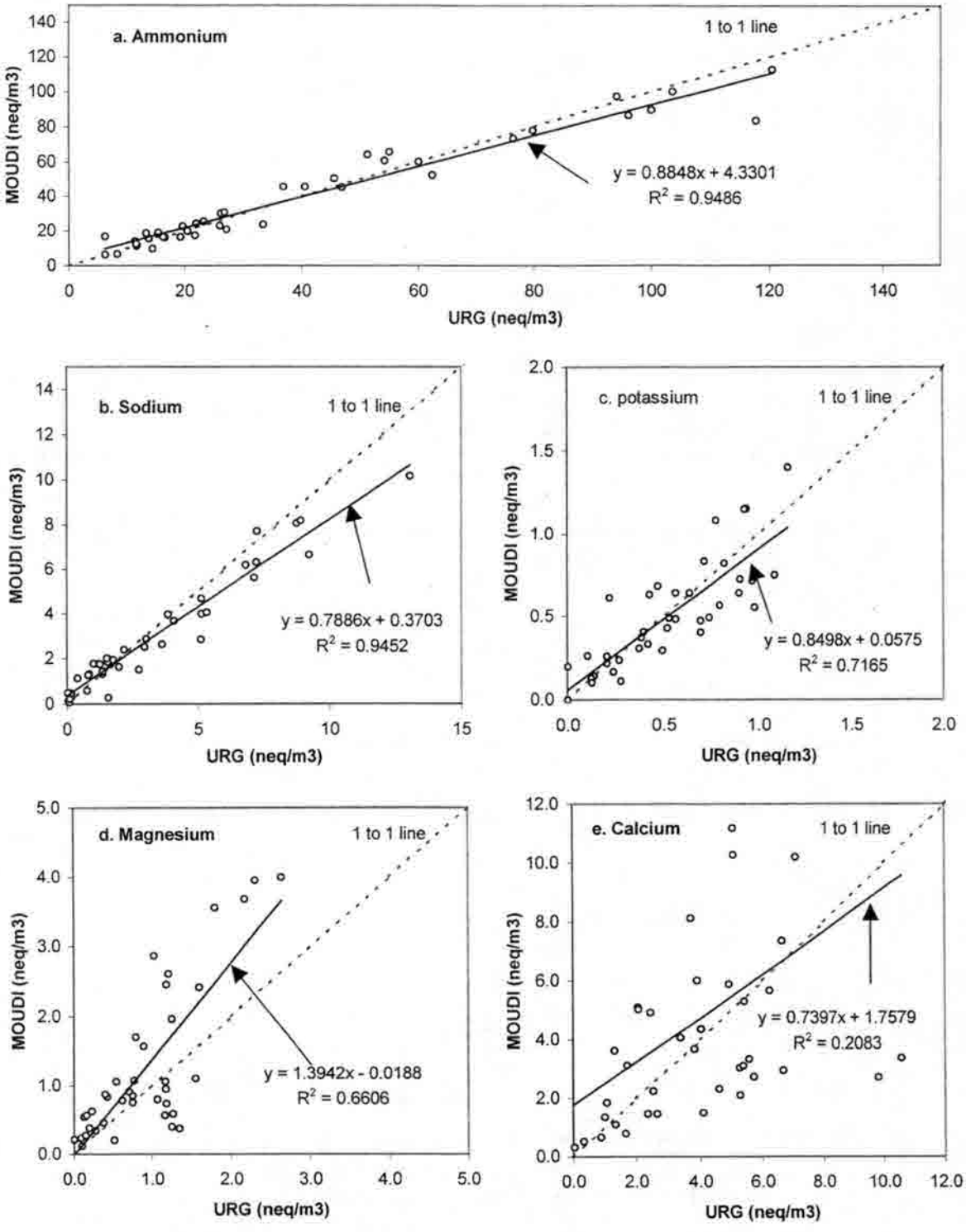

Figure 4.2 The comparison of cation concentrations of (a) ammonium, (b) sodium, (c) potassium, (d) magnesium, and (e) calcium between the URG and MOUDI samplers. The dot and solid lines show the 1:1 ratio and regression, respectively

4.2 Size-resolved aerosol chemical composition

The major inorganic ion species in the sub-micron aerosol size range are secondary compounds such as sulfate, nitrate and ammonium. Researchers have shown that the mass size distribution of inorganic aerosols needs to be described with three modes. Two modes (the condensation and droplet mode) contain fine particles (e.g. diameter less than 2 μm) and one mode (the coarse mode) contains particles larger than 2 μm (John et al., 1990; Sloane et al., 1991; Hering et al., 1997; Zhuang et al., 1999). The smallest mode, typically having a mass median aerodynamic diameter between 0.1 - 0.2 μm, is called the condensation mode. It is comprised primarily of particles formed through the condensation of gas phase species and nucleation processes. The formation of the droplet mode, with a mass median aerodynamic diameter between 0.5 and 0.7 μm, has been linked to processes related to aqueous sulfate production in the atmosphere (Meng and Seinfeld, 1994) and transfer from the condensation mode by addition of sulfate (John et al., 1990; Kerminen and Wexler, 1995). The coarse mode mass median aerodynamic diameter is often observed at 3 – 6 μm.

Size distributions of inorganic ions were determined from the concentrations measured on each stage of the 41 selected 24-hour MOUDI samples. The MOUDI aerosol concentrations were inverted using the Twomey Inversion (Winklmayr et al., 1990). The Twomey algorithm for the inversion of size distributions includes continuous and smooth kernel functions and weighting functions.

Most of the resulting distributions are unimodal or bimodal over the 0.18 – 10 μm size range. The MOUDI samples indicate that nitrate and sulfate are separated into

supermicron (mode diameter ~ 4-5 μm) and submicron (mode diameter ~ 0.4–0.5 μm) modes, respectively.

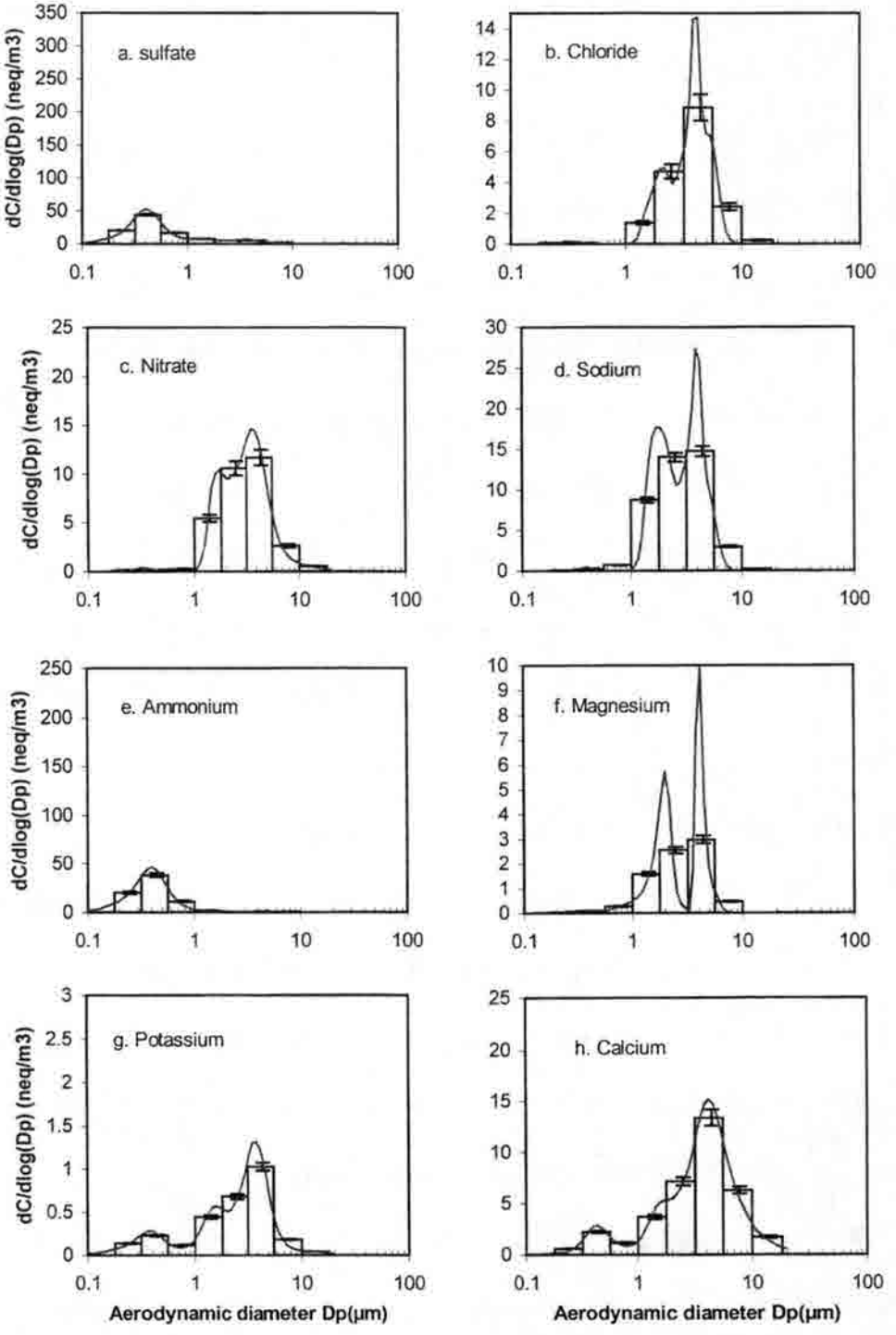

Figure 4.3 The size distribution of monthly averaged inorganic concentrations in July (Error bar and curve represent uncertainties based on RSD(%) of MOUDI and the Twomey inversion, respectively)

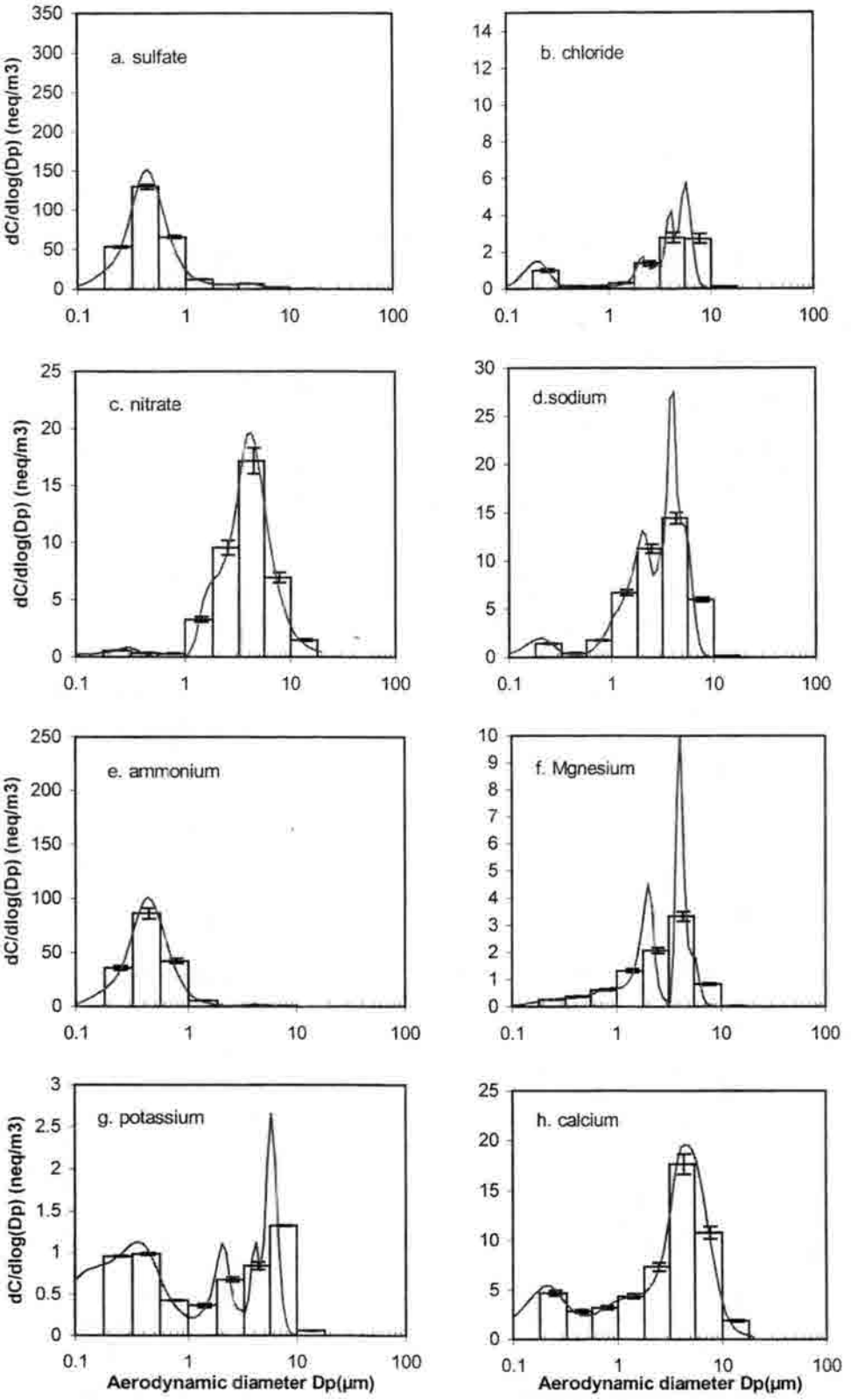

Figure 4.4 The size distribution of monthly averaged inorganic concentrations in August (Error bar and curve represent uncertainties based on RSD(%) of MOUDI and the Twomey inversion, respectively)

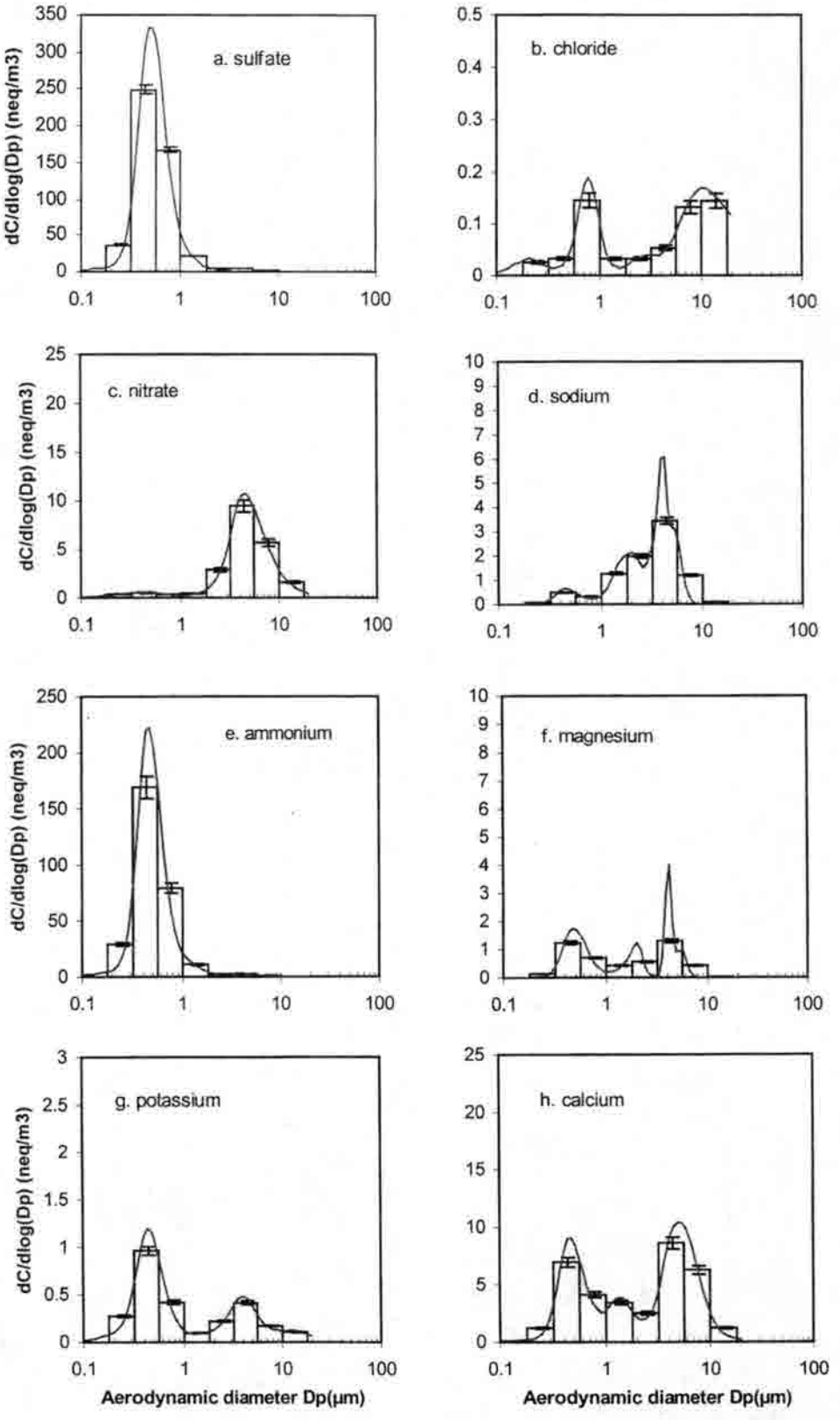

Figure 4.5 The size distribution of monthly averaged inorganic concentrations in September (Error bar and curve represent uncertainties based on RSD(%) of MOUDI and the Twomey inversion, respectively)

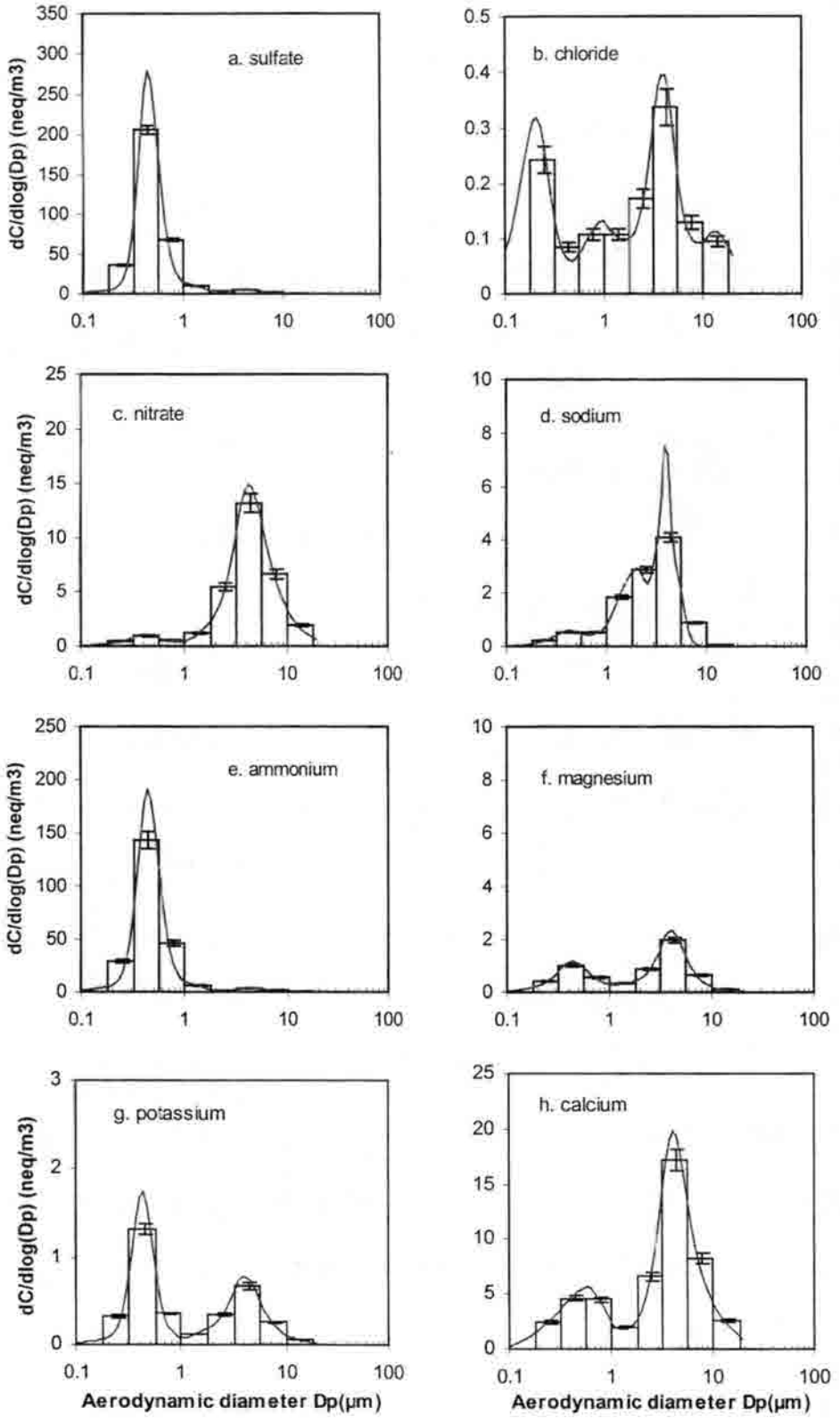

Figure 4.6 The size distribution of monthly averaged inorganic concentrations in October(Error bar and curve represent uncertainties based on RSD(%) of MOUDI and the Twomey inversion, respectively)

A small fine mode was sometimes observed for nitrate while a small coarse mode was sometimes observed for sulfate. K^+, Mg^{2+}, and Ca^{2+} were observed to have bimodal size distributions with fine and coarse modes. Figures 4.3, 4.4, 4.5, and 4.6 show the size distributions of the monthly averaged inorganic ion concentrations. Included in these figures is the measured size distribution histogram and the Twomey Inversion curve. Daily size distributions obtained from the MOUDI samples are provided in Appendix E.

4.2.1 Sulfate size distribution

Table 4.2 shows a comparison of mode diameters for sulfate, ammonium and nitrate calculated for the BRAVO study and previous studies at different locations.

The maximum concentration of sulfate was associated with particles in the 0.4 – 0.5 μm diameter range (Figures 4.3, 4.4, 4.5, and 4.6), similar to measurements made during past studies. Sulfate aerosol observed in the study likely was produced by a combination of gas and aqueous phase oxidation processes. The acidic nature of the aerosol suggests that regional clouds were probably also acidic. Under these conditions, hydrogen peroxide was probably the dominant aqueous phase S(IV) oxidant. Hydrogen peroxide concentrations measured during BRAVO were high, with a study average value of 1.09 ppb (monthly average : 0.96 ppb in July, 1.40 ppb in August, 1.03 ppb in September and 0.96 ppb in October). Oxidation of anthropogenically emitted SO_2 followed by partial neutralization by ammonia and long-range transport as ammoniated sulfate appears to be the major source of sulfate aerosols in Big Bend National Park. This assumption is supported by URG $PM_{2.5}$ ionic concentrations and air mass back trajectories (Figure 3.20).

Table 4.2 Mass median aerodynamic diameter of sulfate, ammonium, and nitrate in different studies

Compound		Fine mode (μm)		Coarse mode (μm)	Location time/season
		Condensation mode	Droplet mode		
SO_4^{2-}	John et al. (1990)	0.17- 0.25	0.6.– 0.65	3 –5	Southern California, 1987 11days from June to Sep. 6 days from Nov. to Dec.
	Meszaros et al. (1997)	-	0.5 - 1	-	Veszprem in western part of Hungry Between Sep./1995 and Aug./1996
	Zhuang et al. (1999)	0.2 ± 0.15	0.58 ± 0.11	4.2 ± 2	Hong Kong Nov/Jan, 1996/1997
	This study (1999)	-	0.4 – 0.5 (average)	4 – 5* (average)	Texas (Big Bend) From July to Oct., 1999
NH_4^+	Meszaros et al. (1997)	-	0.5 - 1	-	
	Zhuang et al. (1999)	0.21 ± 0.10	0.56 ± 0.10	5.7 ± 2	Same as SO_4^{2-}
	This study (1999)	-	0.4 – 0.5 (average)	4 – 5* (average)	
NO_3^-	John et al. (1990)	0.1 – 0.3	0.5 – 0.7	4.40 ± 0.64	
	Meszaros et al. (1997)	-	1 – 2	-	
	Zhuang et al. (1999)	0.14 ± 0.22	0.46 ± 0.33	3.95 ± 0.69	Same as SO_4^{2-}
	This study (1999)	-	0.4 – 0.5* (average)	4 – 5 (average)	

*** : concentrations were very low**

The formation of particles in the size range of 0.4 – 1 μm by fog/cloud processing has been studied by (Meng and Seinfeld, 1994) and (Kerminen and Wexler, 1995).

Sea salt and soil particles may contribute to the presence of sulfate in the coarse mode. While coarse mode sulfate may be derived from soil and sea salt in July when low nss-SO_4^{-2} concentrations were calculated (Figure 3.13), coarse mode sulfate may be formed through the reaction of gas-phase SO_2 or H_2SO_4 on the surface of sea salt and soil particles in August, September and the beginning of October (Figure 3.13). Coarse mode sulfate, however, was observed as a very low fraction of total sulfate in this study.

4.2.2 Ammonium size distribution

The presence of fine mode ammonium is likely the result of condensation of ammonia gas on the surface of acidic particles or the direct involvement of ammonia in nucleation of fine particles. Ammonia in the atmosphere mostly reacts with acidic species such as sulfuric acid, nitric acid and hydrochloric acid. The formation of ammonium sulfate aerosol is thermodynamically favored over the formation of ammonium nitrate. Also, while ammonium sulfate is stable, the dissociation of ammonium nitrate is very sensitive to temperature and humidity (Figure 3.17) and ammonium chloride is too volatile to form particles under some conditions. For these reasons, nearly the same mode diameter is observed for ammonium and sulfate (Figures 4.3, 4.4, 4.5 and 4.6). Overall, the ammonium and sulfate size distributions were very similar, primarily in the droplet mode (0.4 – 0.5 μm aerodynamic diameter). The correlation of $R^2 = 0.97$ between sulfate and ammonium in all size ranges suggests that they mostly co-exist in particles (Figure 4.7).

4.2.3 Nitrate size distribution

While ammonium and sulfate size distributions mainly cover the fine mode, nitrate can be found in coarse modes. The nitrate size distribution depends on the season, location, and weather conditions. Most coarse mode nitrate has been observed in coastal regions where sea salt particles provide a surface for gaseous HNO_3 to react with NaCl (sea salt), resulting in the loss of chlorine from sea salt particles (John et al., 1990; Pakkanen, 1996; Pakkanen et al., 1996; Spurny, 2000). John et al.(1990) reported that

nitrate transitions from the coarse mode to the fine mode as one moves from the coastal area to an inland area. A few researchers found a seasonal change in the nitrate size

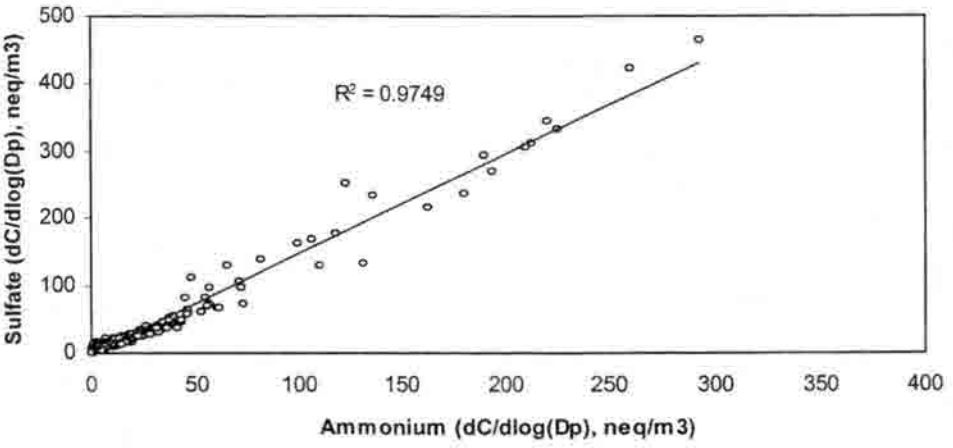

Figure 4.7 The comparison between NH_4^+ and SO_4^{2-} concentrations for all MOUDI stages

distribution due to humidity and temperature effects, which suggests that ammonium nitrate predominates in the winter and sodium nitrate in the summer (Yoshizumi and Hoshi, 1985). In addition, gaseous HNO_3 can deposit on and react with soil particles to form coarse mode nitrate (Wolff, 1984; Prospero and Savoie, 1989; Dentener et al., 1996).

Nitrate was found mainly in the coarse mode with a maximum concentration in the size range of 4-5 μm in this study, indicating that sea salt and soil dust particles provide non-acidic surfaces for the condensation of nitric acid (Figures 4.3, 4.4, 4.5 and 4.6). Figures 4.8 and 4.9 suggest the extent to which sea salt and soil dust contribute to the formation of coarse mode nitrate. Nitrate and calcium show a modest correlation ($R^2 = 0.46$), but nitrate shows a stronger correlation of $R^2 = 0.69$ with the sum of sodium and calcium, which suggests that both sea salt and soil dust contribute to the formation of

particle nitrate in this study. One does not expect a very high correlation as the formation of coarse mode $NaNO_3$ or $Ca(NO_3)_2$ requires the presence of coarse mode sea salt or soil dust aerosol as well as HNO_3. Figure 4.10 indicates that there is no correlation between ammonium and nitrate due to their different size distributions. All of the results from the MOUDI samples are consistent with the URG $PM_{2.5}$ sample data. Table 4.3 shows additional information regarding the correlation of coarse mode nitrate and the coarse mode cation species.

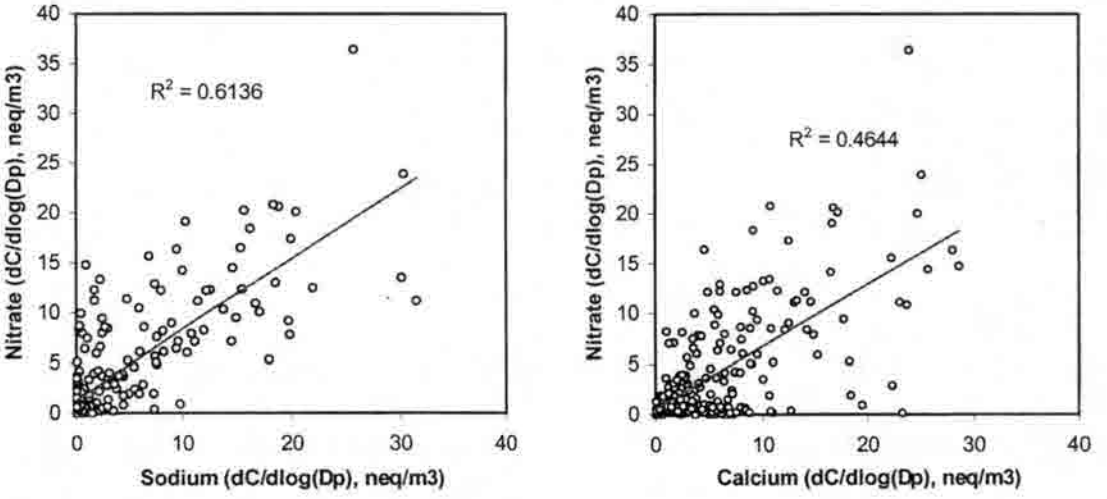

Figure 4.8 The correlation of $[NO_3^-]$ vs $[Na^+]$ and $[NO_3^-]$ vs $[Ca^{2+}]$ for all MOUDI stages

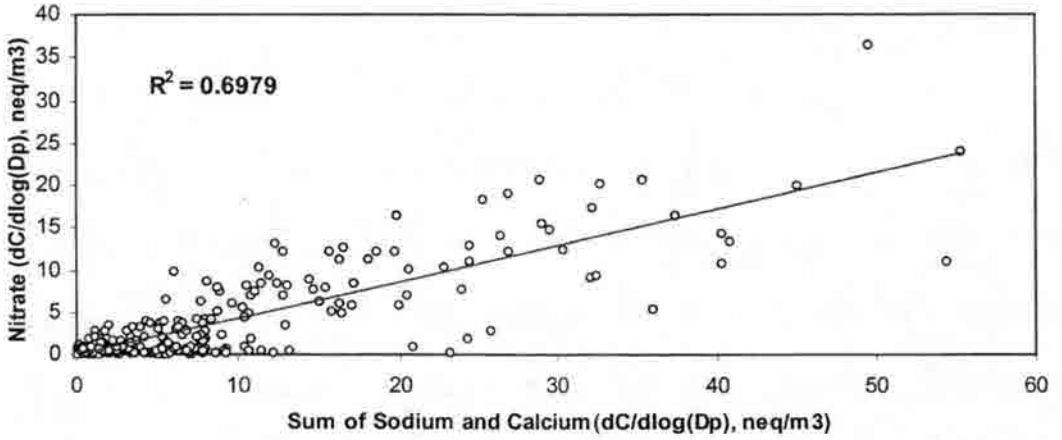

Figure 4.9 The correlation between $[NO_3^-]$ and sum of $[Na^+]$ and $[Ca^{2+}]$ for all MOUDI stages

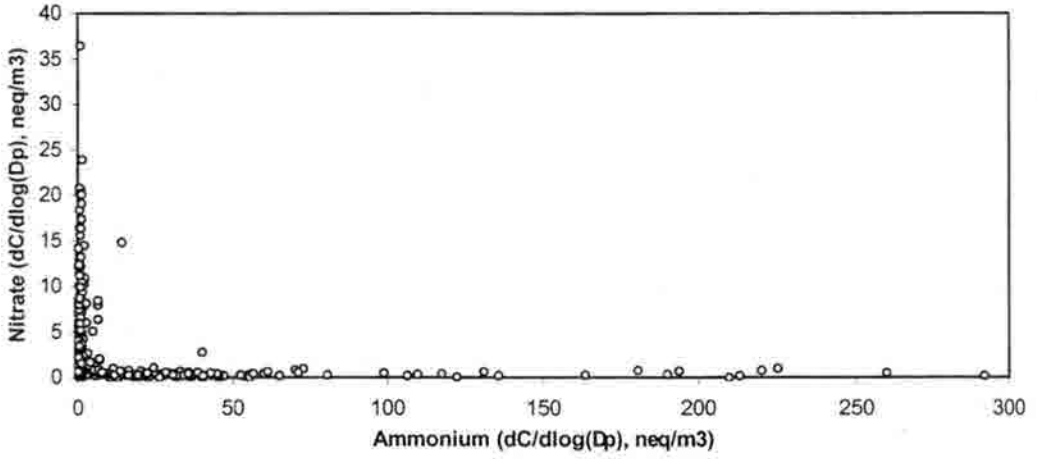

Figure 4.10 The relation between $[NO_3^-]$ and $[NH_4^+]$ for all MOUDI stages

Table 4.3 summary of correlations (R^2) between $[NO_3^-]$ and cation concentrations

	$[Na^+]$	$[Ca^{2+}]$	$[Mg^{2+}]$	$[K^+]$	$[Na^+]+[Ca^{2+}]$	$[Na^+]+[Ca^{2+}]+[Mg^{2+}]$
$[NO_3^-]$	0.61	0.46	0.66	0.13	0.69	0.71

4.2.4 Cl^-, K^+, Mg^{2+}, and Ca^{2-} size distributions

While sulfate, ammonium, and nitrate were mainly observed in unimodal size distributions exhibiting very low coarse mode concentrations of ammonium and sulfate and low fine mode nitrate concentrations, K^+, Mg^{2+}, and Ca^{2+} were clearly found to be bimodal in distribution, with fine mode peaks in the range of 0.3 – 0.4 μm and coarse mode peaks in the range of 4 – 5 μm.

The disintegration of soil and sea salt are well known contributors to the coarse mode for these species. Cl^-, K^+, Mg^{2+}, and Ca^{2+} (4 – 5 μm) in the coarse mode are typically of crustal and sea salt origin.

While potassium and calcium were found in the fine mode throughout BRAVO, chloride, magnesium and sodium were found in the fine mode only in September and October (Figures 4.3, 4.4, 4.5 and 4.6). The mechanism that generates these species in the fine mode is not well known. Soluble calcium and magnesium from fine mode soil particles may be associated with sulfate or nitrate as $CaSO_4/Ca(NO_3)_2$ or $MgSO_4/Mg(NO_3)_2$. Biomass burning and other anthropogenic sources are possible sources of fine mode potassium and chloride.

4.3 Ion balance of size-resolved aerosol

An ion balance was calculated as a cation to anion ratio for each of the size-resolved MOUDI samples. Figure 4.11 presents the monthly averaged ratios of some cation to anion species' concentrations as a function of particle size in this study. The number of MOUDI samples used for the monthly average is presented in Table 4.1. While the ratios of cation to anion over the 4-month study were less than unity for small particle sizes (less than 1 μm) suggesting that particles of this size were acidic, the cation to anion ratios were greater than unity for particles larger than 1μm.

In the fine mode particle size range (less than 1 μm), the minimum average cation to anion ratios were found in the size range of 0.3 – 0.8 μm, which corresponds to the size range of maximum sulfate concentration (0.4 – 0.5 μm). This result suggests that there is insufficient ammonia to fully neutralize the sulfate in this size range, consistent with the URG $PM_{2.5}$ ammonium/sulfate ratios and acidity.

In the coarse mode particle size range, the average cation to anion ratios over most of the 4-month study were greater than unity. The maximum ratio was observed in

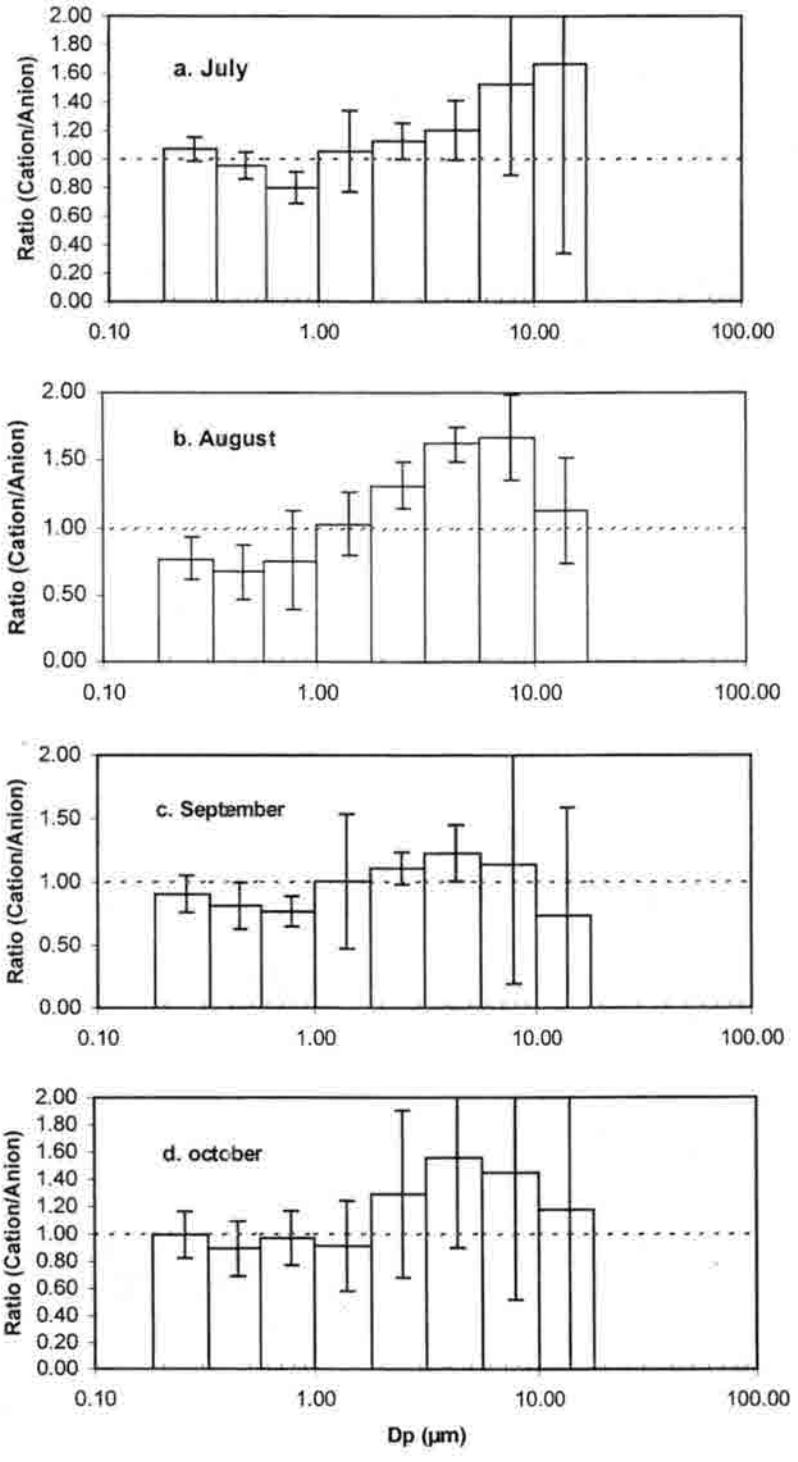

Figure 4. 11 The monthly ratio of cation to anion in a) July, b)August, c)September, and d)October as a function of size-resolved particle (Error bars represent one standard deviation)

the size range of 6 – 10 μm, then decreased for particles sizes larger than 10 μm, except for July. The high cation to anion ratio in the coarse mode may be due to the presence of mineral dust particles and unidentified anion species including oxides, hydroxides, carbonates or organic acids. The effect of mineral dust was most pronounced in July when the average ratio was higher for particles greater than 10μm compared to other months.

Chapter 5. Thermodynamic Model Study

A thermodynamic equilibrium aerosol model is a useful tool for analyzing ambient aerosol data and for predictive aerosol modeling studies. Such a model can calculate important equilibrium properties that are difficult to measure, such as water content, particle acidity, and the complex solid phase particle composition.

Several atmospheric aerosol models, based on thermodynamic equilibrium between the gas and particle phases, have been developed over the past decade. These are EQUIL (Bassett and Seinfeld, 1983), KEQUIL (Bassett and Seinfeld, 1984), MARS (Saxena et al., 1986), AIM (Wexler and Seinfeld, 1991), SCAPE (Kim and Seinfeld, 1993; Kim et al., 1993), SCAPE2 (Kim and Seinfeld, 1995; Meng et al., 1995a), EQUISOLV (Jacobson et al., 1996), ISORROPIA (Nenes et al., 1998; Nenes et al., 1999), and GFEMN (Ansari and Pandis, 1999) for bulk aerosol modeling in which size dependencies are not considered, and SEQUILIB (Pilinis and Seinfeld, 1987) and EQUISOLV-II (Jacobson, 1999) for size dependent aerosol studies where a sectional approach is used.

These models have been used for the analysis of ambient measurements and the investigation of chemical transport mechanisms (Pilinis et al., 1989; Watson et al., 1994; Meng et al., 1995b) and can be combined with air quality models to predict aerosol behavior. For example, ISORROPIA has a data interface designed for the air quality model.

Four properties are necessary to predict gas-aerosol equilibrium in a typical thermodynamic aerosol model.

(1) Inorganic chemical composition
(2) Solute activity coefficients (γ), which can be multicomponent and binary activity coefficients
(3) Water activity (a_w)
(4) Relative Humidity of Deliquescence (RHD), which is temperature and composition dependent.

It should be noted that treatment of thermodynamic effects of organic aerosol components is outside the scope of most current models.

Inorganic chemical composition

Table 5.1 shows the chemical species considered in various thermodynamic equilibrium models. EQUIL, KEQUIL, and MARS have been developed to predict inorganic aerosol composition based on the chemical species ammonium, sulfate, and nitrate (Table 5.1). These thermodynamic models are incomplete in representing the general composition of atmospheric aerosols because many key species are omitted. Marine aerosol , for example, can be 100% depleted in chloride due to reactions with strong acids (H_2SO_4 and HNO_3) (Hitchcock et al., 1980). The later models, SEQUILB, AIM, SCAPE, SCAPE2, ISORROPIA, and GFEMN were developed to include reactions involving NaCl (Table 5.1). The calculation routines are divided into several subdomains (except for GFEMN): 1) if the molar ratio of total ammonia (including ammonium and total sodium) to total sulfate is less than 2, the system is called sulfate-rich, 2) if the ratio is about 2, it will be sulfate-neutral 3) if larger than 2, the system will be sulfate-poor. Furthermore, SCAPE2 incorporates the effects of crustal species, Ca^{2+}, Mg^{2+}, and K^{+}.

Crustal species can influence the overall chemical characteristics of aerosol particles and provide an important sink for gas phase nitric acid (Tabazadeh et al., 1998).

Table 5.1 Comparison of chemical components in each model

	Gas phase	Liquid phase	Solid phase
EQUIL	NH_3, HNO_3, H_2SO_4 H_2O	H^+, NH_4^+, NO_3^-, HSO_4^-, SO_4^{2-}, H_2O	NH_4HSO_4, $(NH_4)_2SO_4$, NH_4NO_3, $(NH_4)_3H(SO_4)_2$, $(NH_4)_2SO_4$-$2NH_4NO_3$, $(NH_4)_2SO_4$-$3NH_4NO_3$
KEQUIL	NH_3, HNO_3, H_2SO_4 H_2O	H^+, NH_4^+, NO_3^-, HSO_4^-, SO_4^{2-}, H_2O	NH_4HSO_4, $(NH_4)_2SO_4$, NH_4NO_3, $(NH_4)_3H(SO_4)_2$, $(NH_4)_2SO_4$-$2NH_4NO_3$, $(NH_4)_2SO_4$-$3NH_4NO_3$
MARS	NH_3, HNO_3, H_2O	H^+, NH_4^+, NO_3^-, HSO_4^-, SO_4^{2-}, H_2O	NH_4HSO_4, $(NH_4)_2SO_4$, NH_4NO_3, $(NH_4)_3H(SO_4)_2$
SEQUILB	NH_3, HNO_3, HCl H_2O	H^+, NH_4^+, Na^+, NO_3^-, Cl^-, HSO_4^-, H_2SO_4, H_2O	NH_4HSO_4, $(NH_4)_2SO_4$, NH_4NO_3, NaCl, NH_4Cl, $NaNO_3$, $NaHSO_4$, Na_2SO_4, $(NH_4)_3H(SO_4)_2$
AIM	NH_3, HNO_3, HCl H_2O	H^+, NH_4^+, Na^+, NO_3^-, Cl^-,SO_4^{2-}, H_2O	NH_4HSO_4, $(NH_4)_2SO_4$, NH_4NO_3, NaCl, NH_4Cl, $NaNO_3$, $NaHSO_4$, Na_2SO_4, $(NH_4)_3H(SO_4)_2$
SCAPE	NH_3, HNO_3, HCl H_2O	H^+, NH_4^+, Na^+, OH^- ,NO_3^-, Cl^-, HSO_4^-, SO_4^{2-}, H_2O, H_2SO_4	NH_4HSO_4, $(NH_4)_2SO_4$, NH_4NO_3, NaCl, NH_4Cl, $NaNO_3$, $NaHSO_4$, Na_2SO_4, $(NH_4)_3H(SO_4)_2$
SCAPE2	NH_3, HNO_3, HCl H_2O	H^+, NH_4^+, Na^+, NO_3^-, Cl^-, HSO_4^-, H_2SO_4, H_2O, Ca^+, Mg^+, K^+	NH_4HSO_4, $(NH_4)_2SO_4$, NH_4NO_3, NaCl, NH_4Cl, $NaNO_3$, $NaHSO_4$, Na_2SO_4, $(NH_4)_3H(SO_4)_2$, KCl, K_2SO_4, $KHSO_4$, KNO_3, $CaCl_2$, $CaSO_4$, $Ca(NO_3)_2$, $MgCl_2$, $MgSO_4$, $Mg(NO_3)_2$
ISORROPIA	NH_3, HNO_3, HCl H_2O	H^+, NH_4^+, Na^+, NO_3^-, Cl^-, HSO_4^-, H_2SO_4, H_2O, OH^-	NH_4HSO_4, $(NH_4)_2SO_4$, NH_4NO_3, NaCl, NH_4Cl, $NaNO_3$, $NaHSO_4$, Na_2SO_4, $(NH_4)_3H(SO_4)_2$
GFEMN	NH_3, HNO_3, HCl H_2O	H^+, NH_4^+, Na^+, NO_3^-, Cl^-, HSO_4^-, H_2SO_4, H_2O	NH_4HSO_4, $(NH_4)_2SO_4$, NH_4NO_3, NaCl, NH_4Cl, $NaNO_3$, $NaHSO_4$, Na_2SO_4, $(NH_4)_3H(SO_4)_2$

Solute activity coefficients and water activity

The equilibrium constant is defined on the basis of species activities. For ionic species in the aqueous phases, the activity is defined as $a_i = \gamma_i m_i$ (where m_i is the molar concentration of species i and γ_i is its activity coefficient). Several methods for calculating a multicomponent activity coefficient for aerosol species have been developed. The Bromley, K-M (Kusik and Messner), and Pitzer methods are widely used. Table 5.2 presents a summary of the principal methods in existing routines for calculating gas-aerosol equilibrium for various models.

Table 5.2 Comparison of thermodynamic equilibrium aerosol models

	EQUIL	KEQUIL	MARS	SEQUILB	AIM	SCAPE	SCAPE2	ISORROPIA	GFEMN
Multicomponent Activity Coeffi.	K-M[a]	K-M	Bromley[b]	Bromley	K-M	K-M Pitzer	K-M Pitzer Bromley	Bromley	Clegg et al (1997)
Binary Activity Coefficient	K-M	K-M	Pitzer[c]	Pitzer	K-M	K-M	K-M	K-M	N/A
Water Activity	K-M	ZSR[d]							
Temperature Dependence of RHD	No				Yes				
Composition Dependence of RHD	No				No			Yes	
Kelvin Effect	No	Yes	No						

a : Kusik and Meissner method (Kusik and Meissner, 1978)
b : Bromley method (Bromley, 1973)
c : Pitzer method (Pitzer, 1973)
d : Zdanovskii, Stokes, and Robinson (ZSR) method (Stokes and Robinson, 1966)

Bromley (1973) proposed the following formula for the activity coefficient of an ion pair in a multicomponent solution.

$$\text{Log } \gamma_{12} = \text{-Ar } \frac{Z_1 Z_2 I^{(1/2)}}{1 + I^{(1/2)}} + \frac{Z_1 Z_2}{Z_1 + Z_2}\left[\frac{F_1}{Z_1} + \frac{F_2}{Z_2}\right] \quad \textbf{(5.1)}$$

(where Ar, the Debye-Huckel constant for activity coefficient, has a value of $0.511 kg^{1/2} mol^{-1/2}$ at 298K)

$$F_1 = Y_{21}\log\gamma^0_{12} + Y_{41}\log\gamma^0_{14} + \ldots. + \frac{A_r I^{(1/2)}}{1 + I^{(1/2)}}[Z_1 Z_2 Y_{21} + Z_1 Z_4 Y_{41} + \ldots] \quad \textbf{(5.2)}$$

$$F_2 = X_{12}\log\gamma^0_{12} + X_{32}\log\gamma^0_{32} + \ldots. + \frac{A_r I^{(1/2)}}{1 + I^{(1/2)}}[Z_1 Z_2 X_{12} + Z_3 Z_2 X_{32} + \ldots] \quad \textbf{(5.3)}$$

$$Y_{21} = \left(\frac{Z_1 + Z_2}{2}\right) \times \left(\frac{M_2}{I}\right), \quad X_{12} = \left(\frac{Z_1 + Z_2}{2}\right) \times \left(\frac{M_1}{I}\right), \quad I = \sum_i \left(\frac{1}{2}\right) \times m_i Z_i^2 \quad \textbf{(5.4)}$$

Z_i is the absolute number of unit charges on ionic species i, and γ^0_{ij} is the mean ionic activity coefficient for a single solute solution with the i-j ion pair.

The K-M method reduces to the same form as the Bromley method if all the ion species are singly charged. The Pitzer method is derived from the definition of the excess Gibbs free energy. For water activity, most models use the ZSR method. The EQUIL model, however, uses the K-M method for the calculation of water activity.

Relative Humidity of Deliquescence (RHD)

The deliquescence behavior of inorganic aerosols has been measured as a function of temperature and aerosol composition (Wexler and Seinfeld, 1991). AIM and SCAPE use data from Wexler and Seinfeld (1991) to calculate the RHD as a function of temperature, but the temperature dependence for Na_2SO_4 and $NaHSO_4$ are not available. SCAPE2 and ISORROPIA use additional data to calculate the RHD as a function of temperature. ISORROPIA calculates the RHD behavior as a function of composition using the phase diagrams determined by (Potukuchi and Wexler, 1995a; Potukuchi and

Wexler, 1995b). However, the diagrams do not include the compositional dependence of the RHD for all compounds, and in such a case, ISORROPIA tries to approximate the RHD behavior based on combinations of similar species.

5.1 Preparation for model calculation

ISORROPIA (v1.1) and SCAPE2 require a total (=gaseous + particulate) concentration of each inorganic soluble species (NH_3, H_2SO_4, HCl, and HNO_3) in $\mu g/m^3$, temperature in K, and relative humidity as inputs. Measured concentrations of crustal cations (Na^+, K^+, Ca^+, and Mg^+) in $\mu g/m^3$ were also an input for SCAPE2, but only the concentration of Na^+ was required as an input for ISORROPIA (v1.1). Daily average concentrations of ion species, temperature, and humidity during the BRAVO study

Table 5.3 Summaries of inputs for ISORROPIA and SCAPE2

	Inorganic species ($\mu g/m^3$)	Crustal species ($\mu g/m^3$)	Others	Calculations
SCAPE2	Total $[SO_4^{2-}]$ as $[H_2SO_4]$ Total concentration ammonium (gas+aerosol) as $[NH_3]$ Total concentration nitrate (gas+aerosol) as $[HNO_3]$ Total $[Cl^-]$ as [HCl]	Na^+ K^+ Ca^{2+} Mg^{2+}	Humidity (RH) Temperature (K)	Gas/aerosol equilibrium (gas + aerosol as input) Full rigorous calculation (Solid, liquid, or both as output) Calculating minor solids
ISORROPIA (v 1.1)	Total $[SO_4^{2-}]$ as $[H_2SO_4]$ Total concentration ammonium (gas+aerosol) as $[NH_3]$ Total concentration nitrate (gas+aerosol) as $[HNO_3]$ Total $[Cl^-]$ as [HCl]	Na^+	Humidity (RH) Temperature (K)	Forward problem (gas + aerosol as input) thermodynamically stable state (Solid, liquid, or both as output)

were used as input data for SCAPE2 and ISORROPIA.

The ISORROPIA model can be run to predict thermodynamically stable compositions (i.e., those along the deliquescence branch of the hygroscopic growth curve) or compositions corresponding to the metastable equilibrium state of the efflorescence branch. In the latter (metastable) case, solids formation is suppressed. All ISORROPIA simulations presented here were obtained by running the model in the thermodynamically stable modes (i.e. with solid formation). Table 5.3 summarizes the input requirements for each model. The chemical species provided as outputs from each model are shown in Table 5.1. Figure 5.1 shows the timeline of measured daily average BRAVO temperature and humidity used in this study.

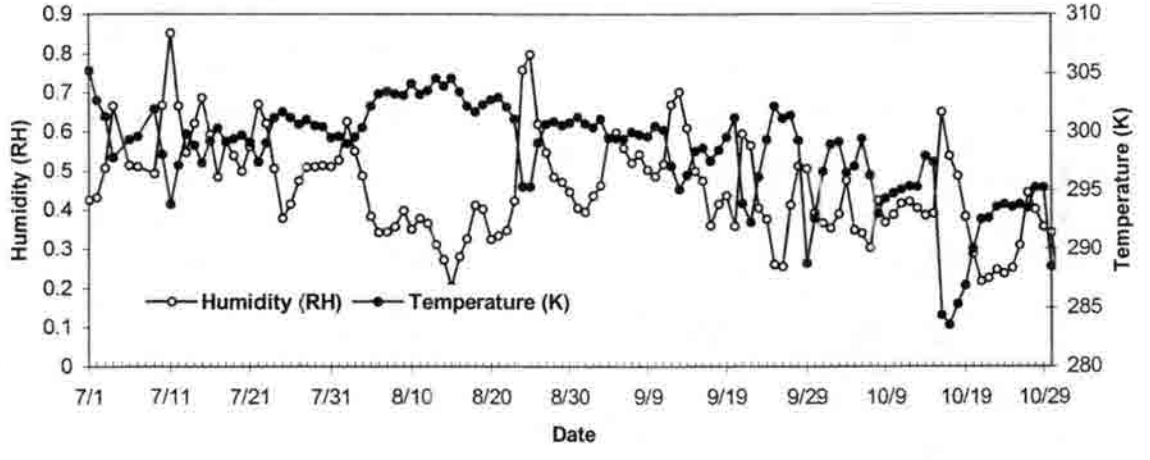

Figure 5.1 The timeline of daily average temperature and humidity during the BRAVO study

5.2 The Relative Humidity of Deliquescence (RHD) study

The water associated with an atmospheric aerosol is an important medium in which chemical processes can occur. At low humidities inorganic salts are typically

found in crystalline form. As relative humidity increases, these salts may take up water to form a saturated solution drop in a process referred to as deliquescence. The humidity at which deliquescence occurs is referred to as the relative humidity of deliquescence (RHD). RHD's for several important species are shown in Table 5.4. As humidity

Table 5.4 Relative humidity of deliquescence for inorganic salts (@298K)

Salt	RHD (%)
Na_2SO_4	84.2 ± 0.4
$(NH_4)_2SO_4$	79.9 ± 0.5
NaCl	75.3 ± 0.1
$NaNO_3$	74.3 ± 0.4
NH_4NO_3	61.8

Sources : Tang (1980) and Tang and Munkelwitz (1993)

increases above the RHD, the aerosol solution droplet takes up additional water (See Figure 5.2). If the humidity now begins to decrease, water is lost, but some water is maintained until the relative humidity of crystallization (RHC). As shown in Figure 5.2, the RHC is less than the RHD, leaving a "hysteresis" region where the water content of the particle is determined by the particles' previous relative humidity history. The bottom branch of the growth curve in Figure 5.2 is the deliquescence branch. The top branch is the crystallization branch.

The relative humidities of deliquescence in ISORROPIA and SCAPE2 were evaluated for the inorganic salts Na_2SO_4, $(NH_4)_2SO_4$, NaCl, $NaNO_3$, and NH_4NO_3. Water contents ($\mu g/m^3$) were calculated using ISORROPIA and SCAPE2 for humidities ranging from 0.05 to 0.95 for representative concentrations of Na_2SO_4, $(NH_4)_2SO_4$, NaCl, $NaNO_3$ and NH_4NO_3. To obtain consistent results, the Bromley method was used in both ISORROPIA and SCAPE2 for the calculation of multicomponent activity coefficients.

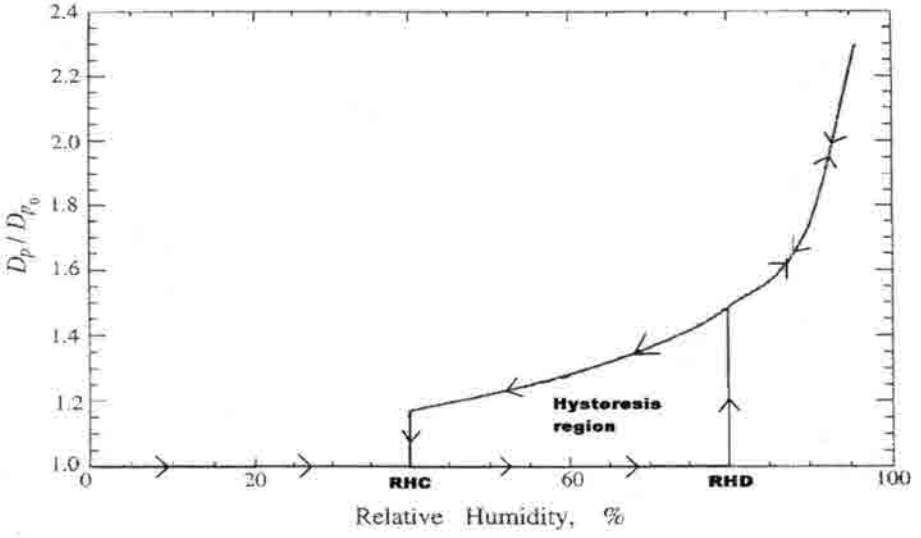

Figure 5.2 The wet-to-dry diameter ratio (D_p/D_0) for a hypothetical aerosol particle. Note the hysteresis region between the deliquescence and crystallization relative humidities

Figures 5.3 and 5.4 show the deliquescence branch liquid water content as a function of RH for inorganic salts as predicted by ISORROPIA and SCAPE2, respectively. The relative humidity of deliquescence for Na_2SO_4 is similar for the two models and agrees

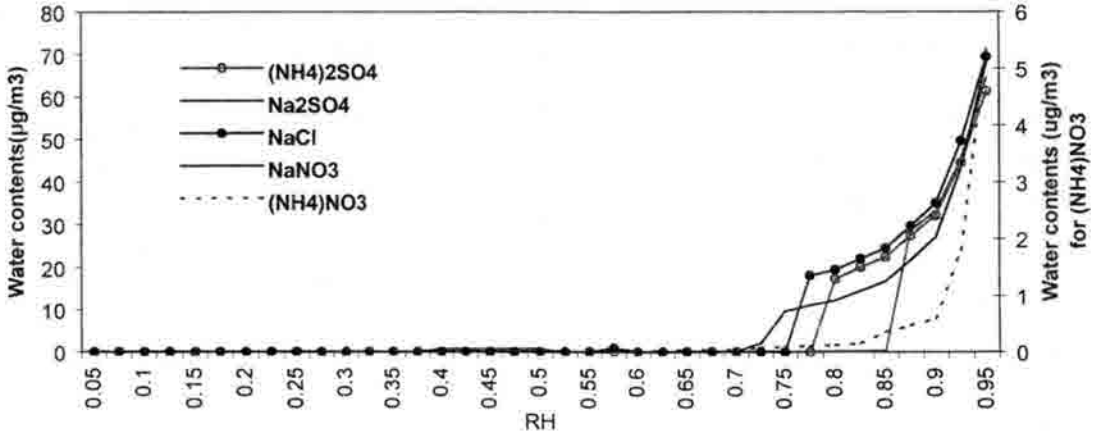

Figure 5.3 Deliquescence as function of RH for each inorganic salt from ISORROPIA

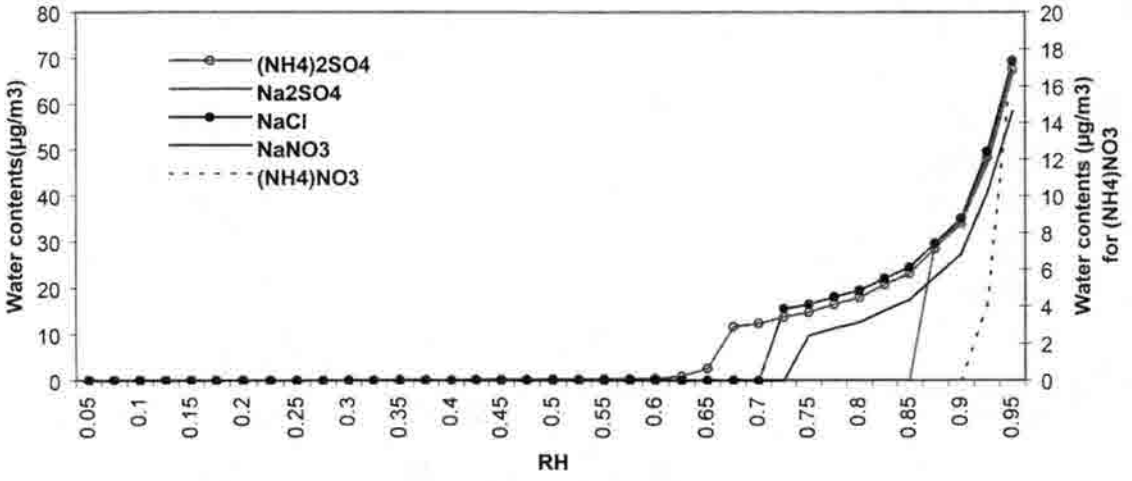

Figure 5.4 Deliquescence as a function of RH for each inorganic salt from SCAPE2

well with Table 5.4. The relative humidities of deliquescence predicted by ISORROPIA generally show good agreement with RHD values in Table 5.4, although ISORROPIA tends to predict a lower relative humidity of deliquescence for $NaNO_3$. On the other hand, SCAPE2 predicts a higher RHD for $(NH_4)NO_3$ and a lower RHD for $(NH_4)_2SO_4$ and NaCl.

5.3 ISORROPIA and SCAPE2 thermodynamic model study results

The thermodynamic model (ISORROPIA and SCAPE2) study using the $PM_{2.5}$ URG data as inputs provided predictions of solid phase concentrations of Na_2SO_4, $(NH_4)_2SO_4$, and $(NH_4)_3H(SO_4)_2$ and liquid phase concentrations of Na^+, SO_4^{2-}, NH_4^+, HSO_4^-, NO_3^-, Cl^- and H^+.

Gas-particle partitioning of the measured inorganic aerosol and gas phase species obtained from the $PM_{2.5}$ URG samples was compared to thermodynamic model predictions as well. While the models achieve good agreement with the observed phase

partitioning for N(-III), the prediction of phase partitioning for N(V) was much different from the observed phase partitioning.

5.3.1 Solid phase chemical composition

Figure 5.5 shows a comparison of ISORROPIA and SCAPE2 predictions of solid phase concentrations of Na_2SO_4, $(NH_4)_2SO_4$, and $(NH_4)_3(SO_4)_2$.

The comparison between ISORROPIA and SCAPE2 predicted $(NH_4)_2SO_4$, and $(NH_4)_3H(SO_4)_2$ concentrations shows reasonable agreement, although ISORROPIA predicts higher concentrations of these species at times. In contrast, predictions of Na_2SO_4 concentrations were quite different. ISORROPIA predicts the presence of solid phase Na_2SO_4, while SCAPE2 indicates that this species is not present. This discrepancy is due to differences in the predicted aerosol water content in in the models, as reflected in Figures 5.3 and 5.4 which show the differences in RHD between ISORROPIA and SCAPE2.

In addition, the variation in aerosol water content predicted by the models is further illustrated in Figure 5.6. Figure 5.6 shows the variation of water content as a function of the relative humidity using $PM_{2.5}$ URG inorganic data for several days as calculated by the ISORROPIA and SCAPE2 models. For the SCAPE2 model, three different methods (Bromley, K-M, and Pitzer) for calculating multicomponent activity coefficients were separately applied to predict aerosol water content. While ISORROPIA predicted the average deliquescence point (zero aerosol water content) at a relative humidity of 60 – 80 %, the start of water uptake predicted by SCAPE2 with the K-M and Bromley methods was in the relative humidity range of 20 – 30 %. However, predictions

made with the SCAPE2 model employing the Pitzer method clearly indicate a different deliquescence point that occurs at a relative humidity of 40 – 60 %, midway between the ISORROPIA and SCAPE2 (K-M and Bromley method) models. This indicates that the difference in predicted concentrations of the solid and liquid phase aerosol species is due to differences in water content predictions, which in turn are functions of RH in the two models (Figure 5.4). Different deliquescence points between SCAPE2 (K-M and Bromley) and SCAPE2 (Pitzer) yield additional solid phase aerosol formation (K_2SO_4, $CaSO_4$ and $MgSO_4$) in the SCAPE2 (Pitzer) case (see Figure 5.7). Figure 5.8 shows solid phase Na_2SO_4 and ammoniated sulfate concentrations predicted by SCAPE2 using K-M and Pitzer methods.

In summary, ISORROPIA and SCAPE2 often make similar predictions of solid phase ammoniated sulfate. However, discrepancies in solid phase Na_2SO_4 predictons exist between ISORROPIA and SCAPE2. In addition, significant differences were found for solid phase crustal sulfate species in SCAPE2 depending on the method used for calculating the multicomponent activity coefficients.

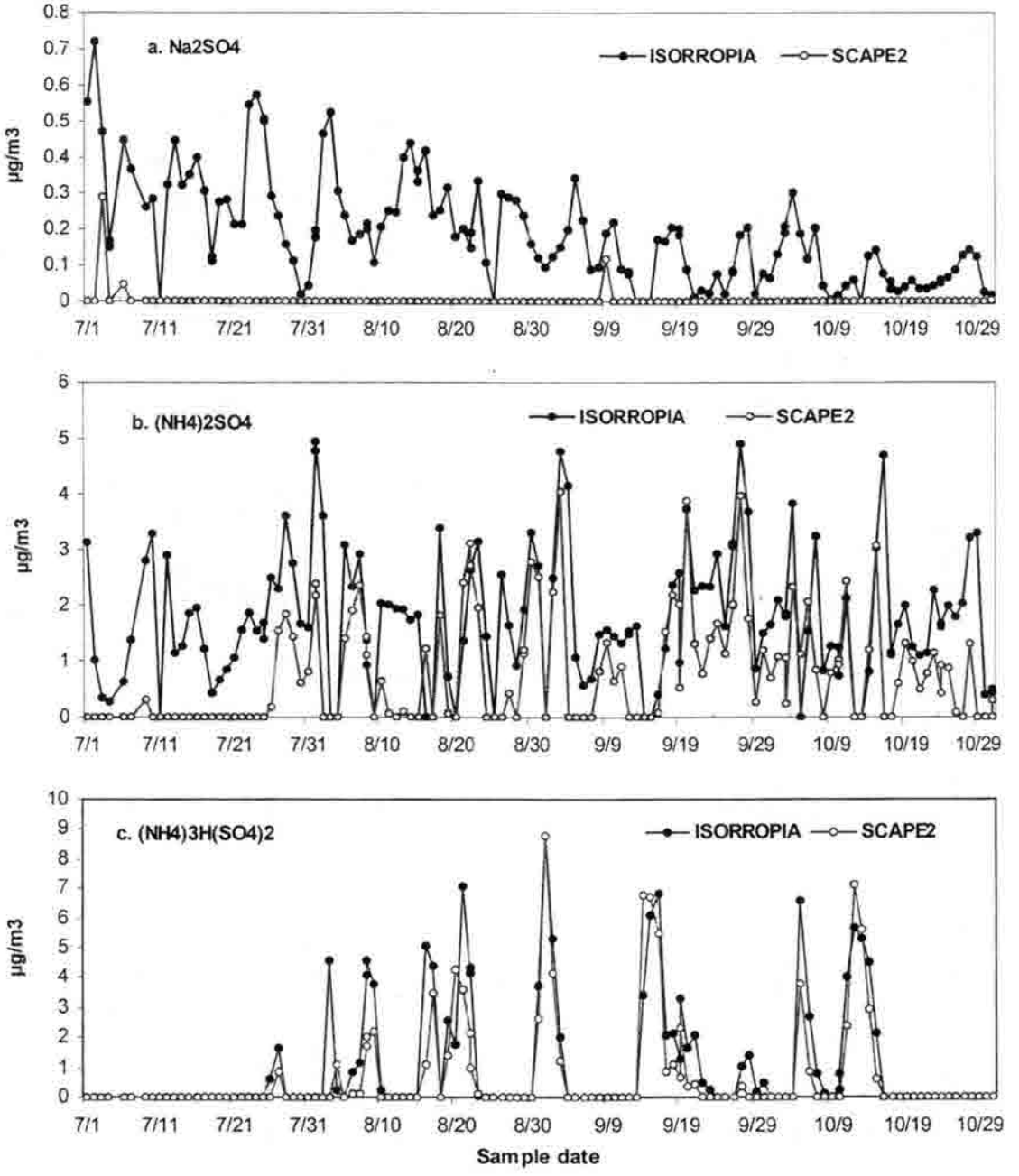

Figure 5.5 ISORROPIA and SCAPE2 predictions of solid phase chemical species, (a) Na_2SO_4, (b) $(NH_4)_2SO_4$, and (c) $(NH_4)_3H(SO_4)_2$

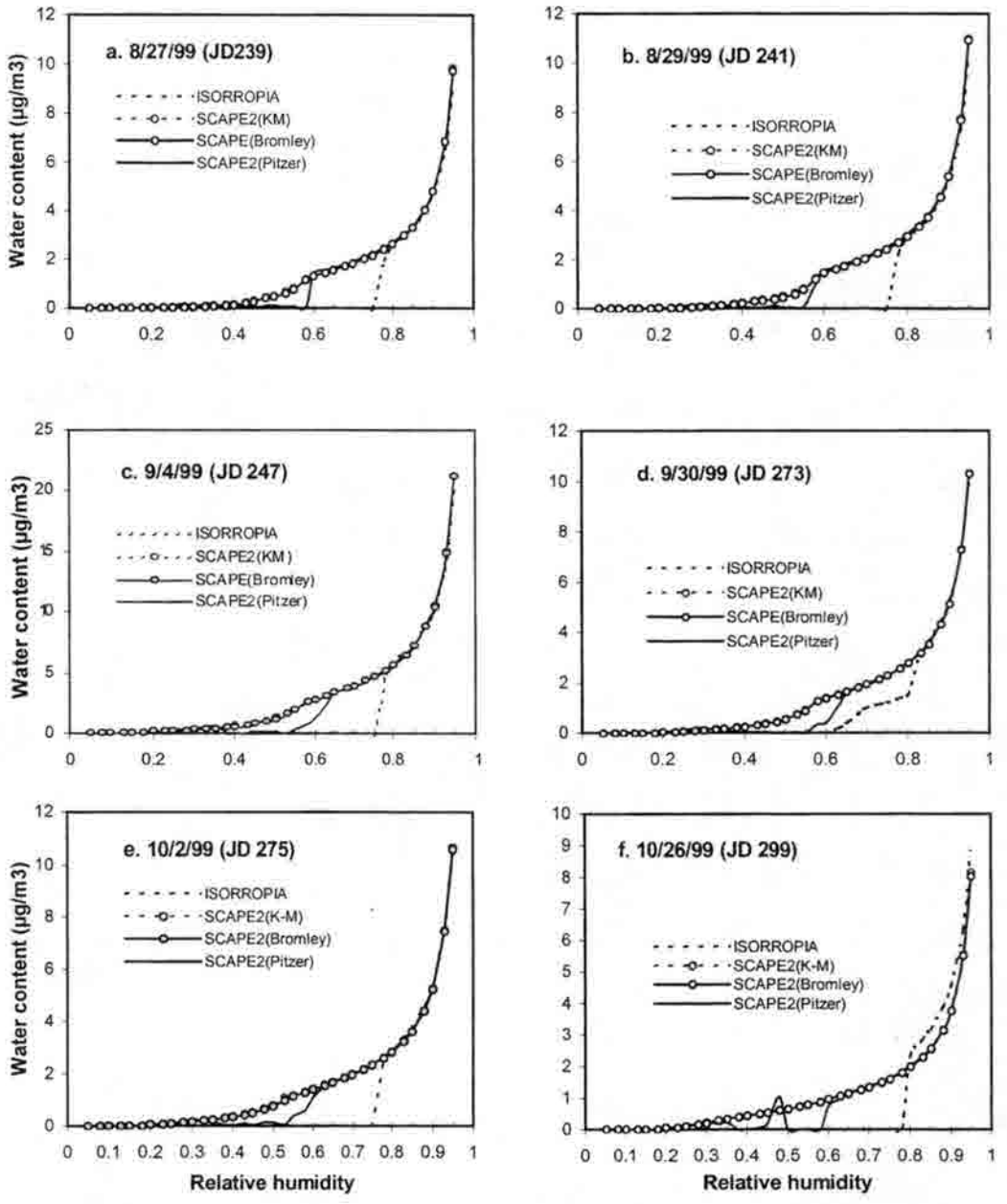

Figure 5.6 The variation of aerosol water content as function of increasing RH predicted by ISORROPIA and SCAPE2 (K-M, Bromley and Pitzer) using $PM_{2.5}$ URG data from several days

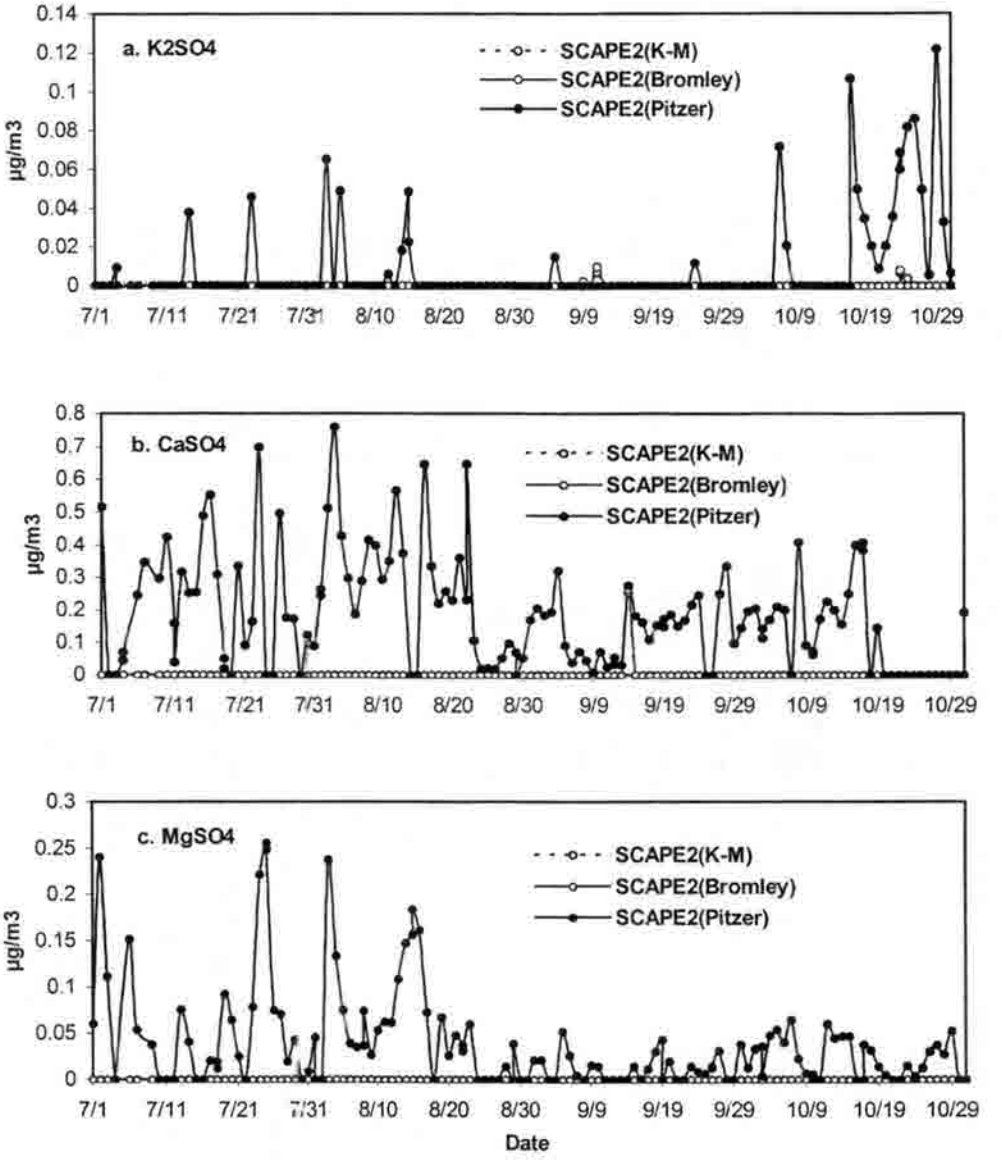

Figure 5.7 Additional solid phase sulfate concentrations predicted by SCAPE2 with different methods (Kusik and Meissner (K-M), Bromley, and Pitzer)

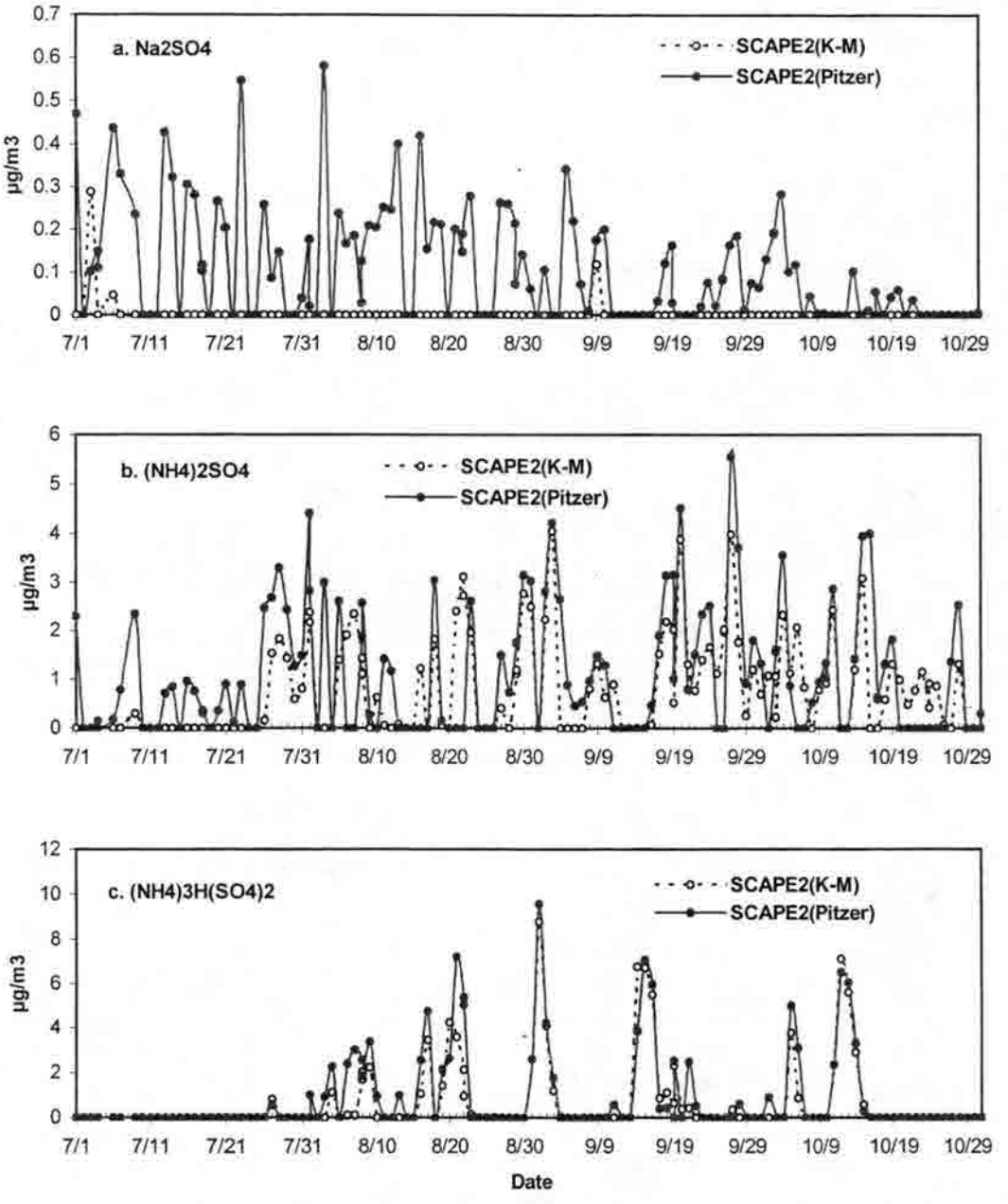

Figure 5.8 Comparison of key solid phase sulfate species concentrations Predicted by SCAPE2 with different methods (Kusik and Meissner (K-M) and Pitzer)

5.3.2 Liquid phase chemical composition

Figures 5.9 and 5.10 present a comparison of ISORROPIA and SCAPE2 (Bromley) predicted liquid phase chemical compositions, including Na^+, SO_4^{2-}, NH_4^+, HSO_4^-, Cl^-, NO_3^- and H^+. Figure 5.11 shows the additional liquid phase crustal species predicted by SCAPE2. Figure 5.12 shows a comparison of the concentrations of liquid phase species predicted by the K-M and Pitzer methods in SCAPE2.

ISORROPIA and SCAPE2 showed significant discrepancies in partitioning species between the solid and liquid phases. While SCAPE2 predicts average concentrations of 0.06 $\mu g/m^3$ (0 – 0.23 $\mu g/m^3$), 1.2 $\mu g/m^3$ (0 – 3.9 $\mu g/m^3$), 0.23 $\mu g/m^3$ (0 – 1.21 $\mu g/m^3$) and 0.98 $\mu g/m^3$ (0 – 3.98 $\mu g/m^3$) for Na^+, SO_4^{2-}, NH_4^+, and HSO_4^-, respectively, in the liquid phase, ISORROPIA suggests that most of the inorganic species are present in the solid phase rather than the liquid phase (Figure 5.9). ISORROPIA and SCAPE2 similarly predict very low concentrations of Cl^- (Figure 5.9), whereas SCAPE2 predicts higher H^+ concentrations than ISORROPIA (Figure 5.10). The differences in the concentrations of inorganic species predicted by both models are mainly due to differences in the treatment of deliquescence behavior in the models. In addition, as seen in Figure 5.10, there are significant discrepancies between model predictions and observations of H^+ concentration.

ISORROPIA and SCAPE2 both predict concentrations of NO_3^- that are close to zero. However, the observed particle NO_3^- concentrations show an average NO_3^- concentration of 0.12 $\mu g/m^3$ (Figure 5.10). This issue will be addressed further below. SCAPE2 predicted liquid phase concentrations of K^+ and Mg^{2+} to be less than 0.07 $\mu g/m^3$ and the average concentration of Ca^{2+} to be 0.11 $\mu g/m^3$, with a range of 0 – 0.33 $\mu g/m^3$.

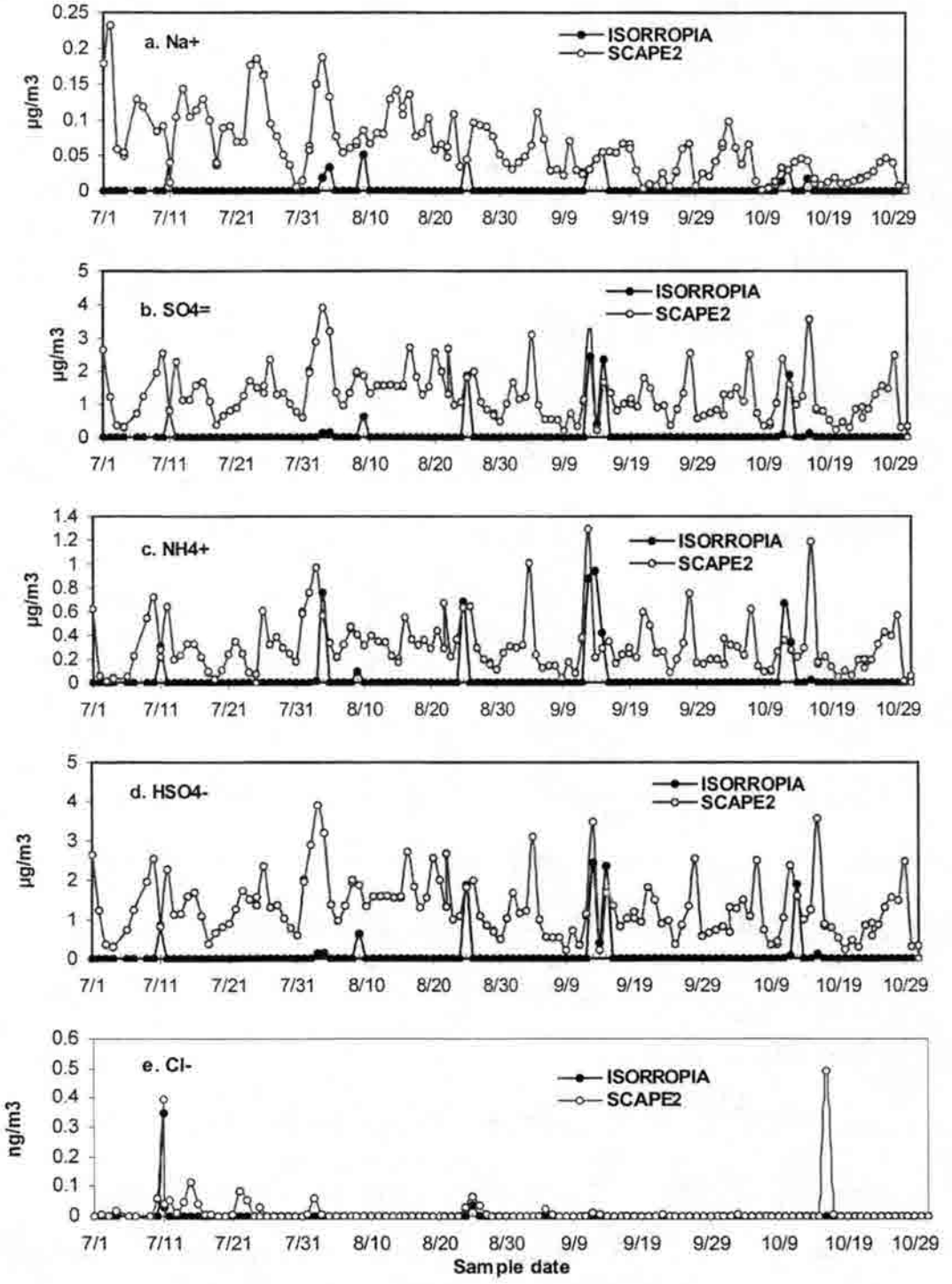

Figure 5.9 Comparison of concentrations of the liquid phase (a) Na^+, (b) SO_4^{2-} (c) NH_4^+, (d) HSO_4^-, and (e) Cl^- predicted by ISORROPIA and SCAPE2 (Bromley)
(note that (e) Cl- has different concentration scale units)

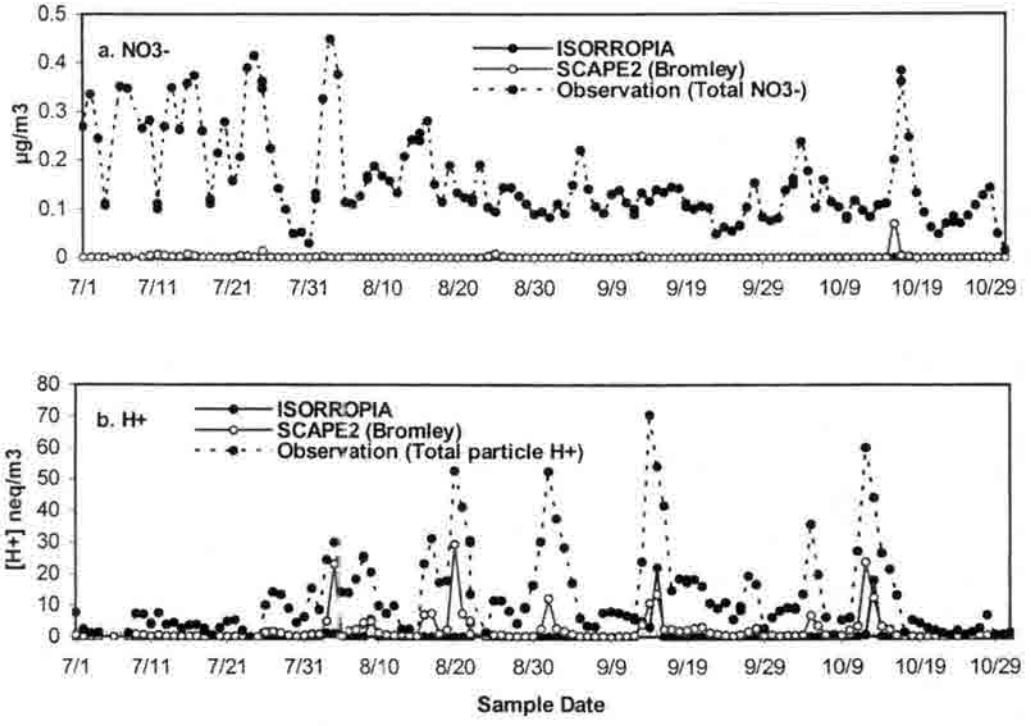

Figure 5.10 Comparison of concentrations of the liquid phase (a) NO_3^- and (b) H^+ predicted by ISORROPIA and SCAPE2 (Bromley) and observed in URG samples

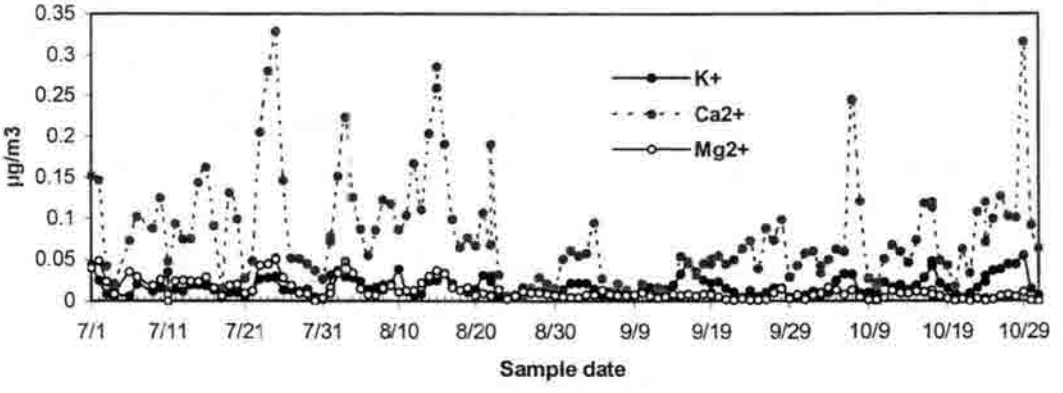

Figure 5.11 Timeline of the concentration of additional liquid phase crustal species predicted by SCAPE2(Bromley)

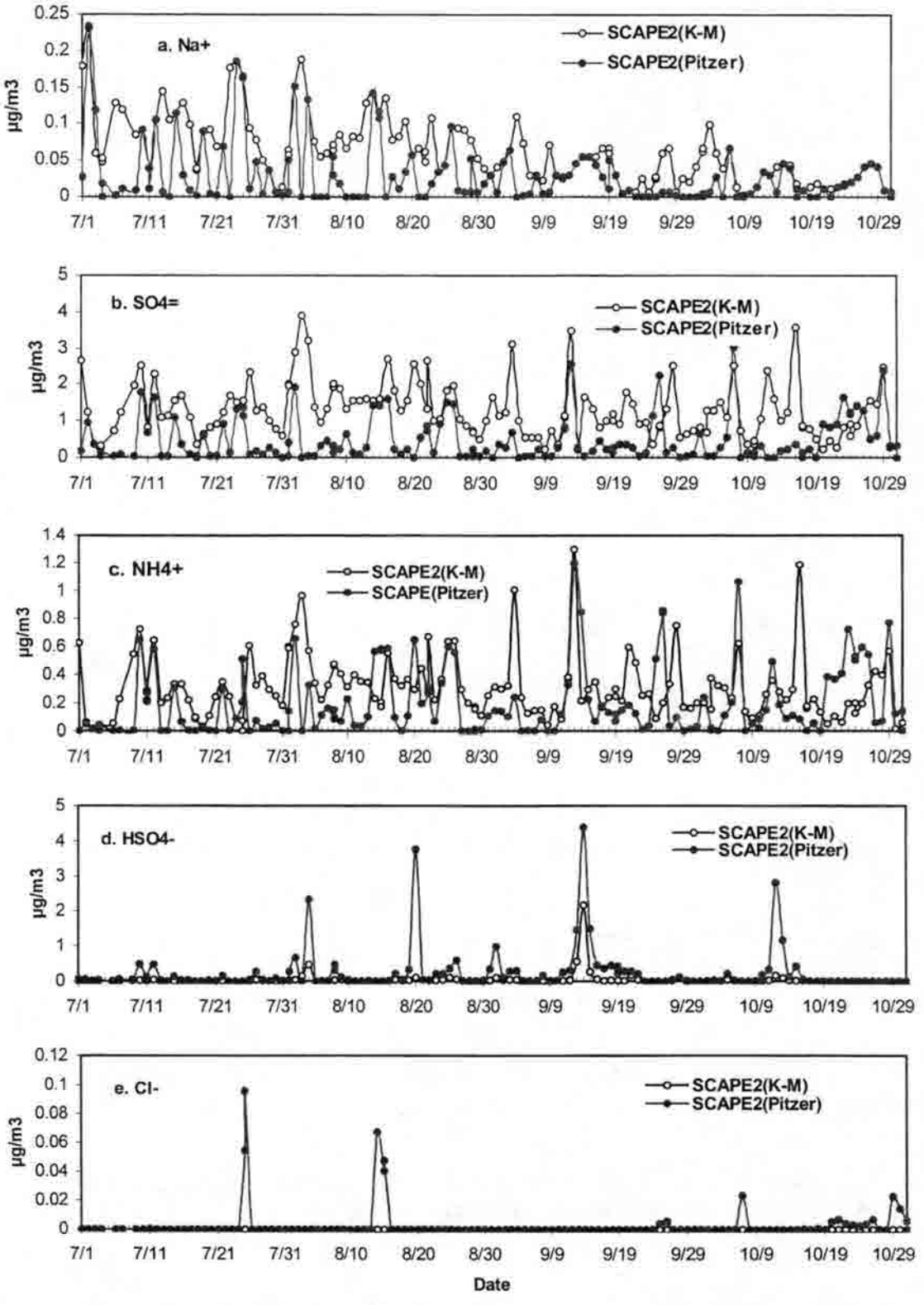

Figure 5.12 Comparison of liquid phase chemical species by SCAPE2 predicted with different methods (K-M and Pitzer)

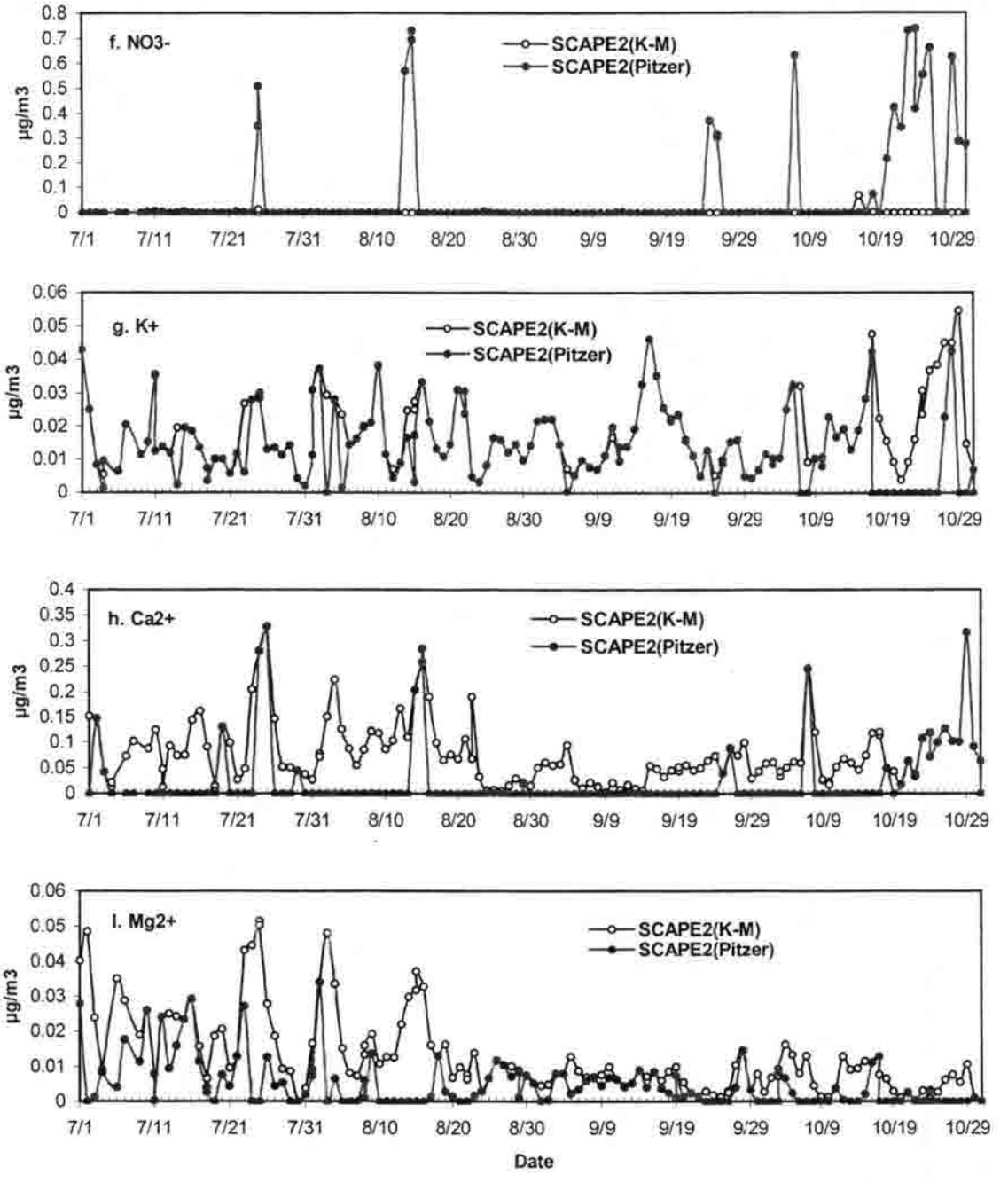

Figure 5.12 (Continued) Comparison of liquid phase chemical species predicted by SCAPE2 with different methods (K-M and Pitzer)

Figure 5.12 shows the liquid phase chemical compositions predicted by SCAPE2 using the K-M and Pitzer methods,. The SCAPE2 results using the K-M method are similar to the results of SCAPE2 using the Bromley method, which are shown in Figure 5.9.

However, SCAPE2 with the Pitzer method resulted in different inorganic ion species concentrations in the liquid phase. As seen in Figure 5.5, this difference can be attributed to a disparity in the calculation of water content as a function of RH between the Pitzer, K-M, and Bromley methods.

5.3.3 Gas phase chemical composition (partitioning N(V) and N(-III))

As mentioned in section 5.1, the total ambient measurements (gas + particle) of nitrate and ammonium were used as inputs for ISORROPIA and SCAPE2. The partitioning of nitrate and ammonium between gas and particle phases was predicted by the models. In Figure 5.13, the gas-particle partitioning ratios of nitrate and ammonium

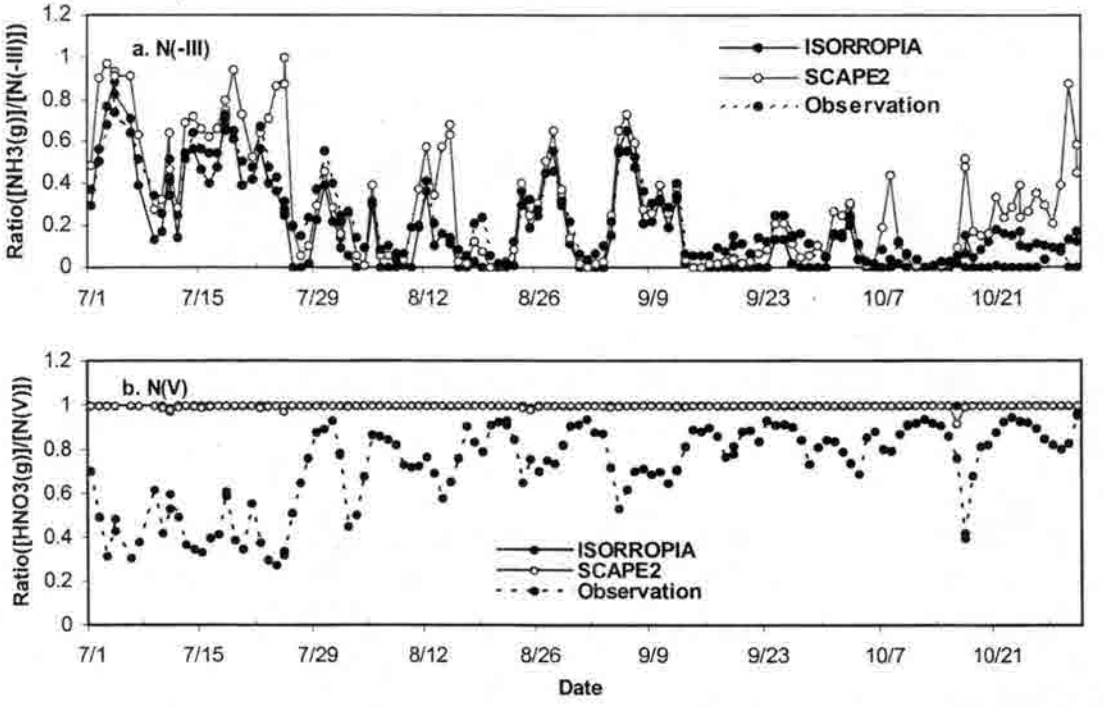

Figure 5.13 The comparison of partitioning of $PM_{2.5}$ nitrate and ammonium predicted by ISORROPIA and SCAPE2 and observations as ratios of $[NH_3(g)]/[N(-III)]$ for ammonium and ratios of $[HNO_3(g)]/[N(V)]$ for nitrate

as computed by ISORROPIA and SCAPE2 are compared to partitioning ratios calculated from measured values of the gas and particulate phases during the BRAVO study. Figure 5.13 shows the comparison between model predictions and observations as ratios of $[NH_3]/[N(-III)]$ and $[HNO_3]/[N(V)]$, where N(-III) is the sum of ammonia gas and $PM_{2.5}$ ammonium and N(V) is the sum of gaseous nitric acid and $PM_{2.5}$ nitrate.

In general, both models predict ammonium partioning that is in good agreement with the observed phase partitioning of N(-III). This result is consistent with the evaluation of the performance of other models (Ansari et al., 1999b; Moya et al., 2000). However, a significant difference in the partitioning of N(V) between gas and particulate phases was found between observation and model results. While ISORROPIA and SCAPE2 predicted that N(V) is clearly dominated by gas phase nitric acid during the 4-month study, observations show that N(V) was distributed fairly evenly between particulate nitrate and gaseous nitric acid in July and that particulate nitrate was still present in August, September, and October. This discrepancy between predictions and observations has been reported by Moya et al (2000) in which the authors found an over prediction of particulate nitrate during the morning sampling period and an under prediction during the afternoon sampling time. Prediction of N(V) partitioning between the gas and particulate phase in models is not easy due to the sensitivity of N(V) partitioning to temperature and RH. Tests were made of the sensitivity of N(-III) and N(V) phase partitioning to humidity. Phase partitioning was calculated using ISORROPIA for the following relative humidities: (1) the 24-hr average RH (base case, already described), (2) the 5^{th} percentile of RH observed for the 24 hr period, and (3) the 95^{th} percentile RH observed for the 24 hr period. Results of this comparison, presented in

Appendix F, show little dependence of predicted phase partitioning on relative humidity, within observed diurnal relative humidity variations. In our study, the significant difference in N(V) partitioning between ISORROPIA and SCAPE2 predictions and observations is probably mostly due to the external mixture of acidic submicron sulfate particles with supermicron nitrate particles mixed together in $PM_{2.5}$ samples used as the basis for the thermodynamic modeling studies. As shown earlier using the MOUDI results, a $PM_{2.5}$ size cut would include a fair portion of the nitrate-containing sea salt/soil dust coarse particle mode.

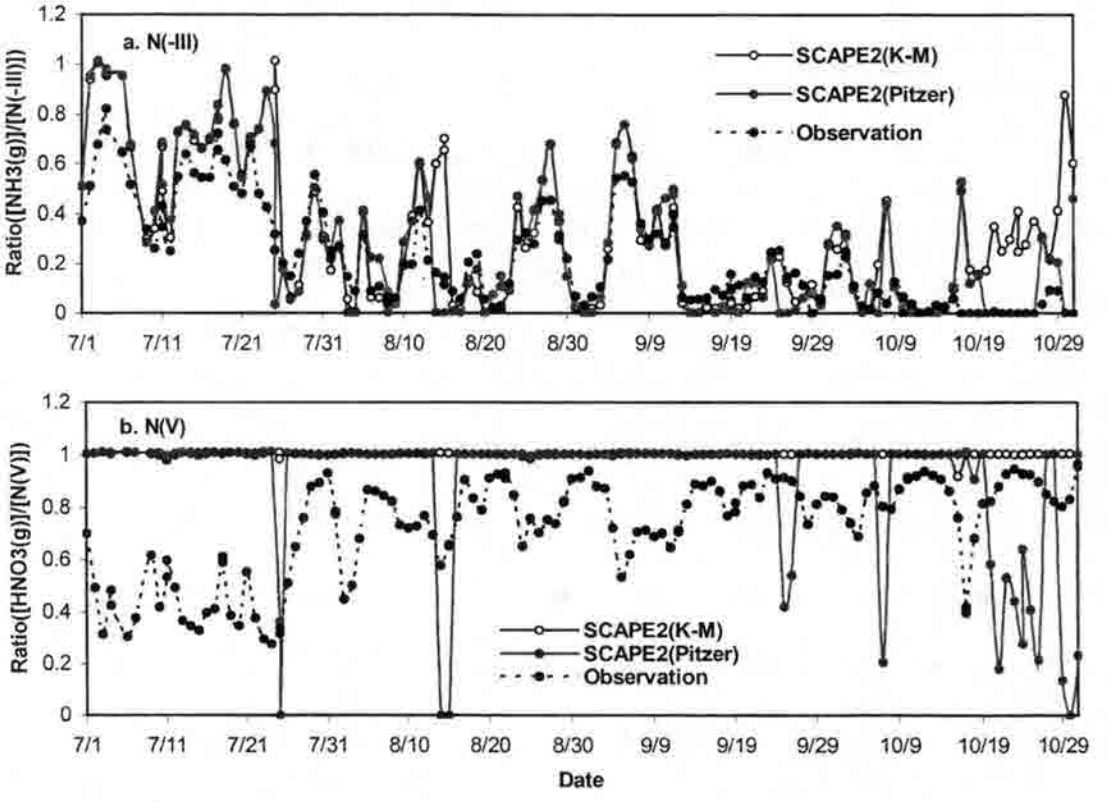

Figure 5.14 The comparison of partitioning of N(-III) and N(V) predicted by SCAPE2(K-M and Pitzer) and observations as ratios of $[NH_3]/[N(-III)]$ and $[HNO_3]/[N(V)]$

Figure 5.14 shows a comparison of N(-III) and N(V) partitioning predicted by SCAPE2 with the K-M (Kusik and Meissner) and Pitzer methods. The K-M method produces similar results to the Bromley method, which were reported in Figure 5.13. The Pitzer method generates fairly similar partitioning values except for an over prediction of particulate nitrate and gaseous ammonia at the end of October in comparison to results using the K-M method and observations.

Chapter 6 Summary and Conclusions

Chemical characterization of the inorganic ions in atmospheric aerosols was performed during the Big Bend Regional Aerosol and Visibility Observational (BRAVO) study with $PM_{2.5}$ particle (URG) samples and size-resolved particle (MOUDI) samples. Aerosol acidity was also measured in the $PM_{2.5}$ samples. Measured $PM_{2.5}$ sample compositions were compared with compositions predicted by the ISORROPIA (Nenes et al., 1998) and SCAPE2 (Kim et al., 1995; Meng et al., 1995) thermodynamic models.

Overall, aerosol particles sampled in Big Bend National Park from July to October 1999 were generally acidic with submicron particles comprised mainly of sulfate and ammonium. Nitrate was found primarily in coarse mode particles, indicating the importance of reactions with sodium and calcium in coarse mode sea salt and soil dust particles. The division between the fine and the coarse mode aerosol was typically located at an aerodynamic particle diameter of approximately 1 μm. Specific findings are detailed below.

$PM_{2.5}$ inorganic ions and trace gases

- Sulfate and ammonium were the dominant ionic species in the daily $PM_{2.5}$ samples, with smaller contributions from nitrate and sodium. Daily average sulfate and ammonium concentrations were strongly correlated ($R^2 = 0.97$).

- The highest concentrations of sulfate and ammonium were observed from August through October. Sulfate and ammonium concentrations were in the range of 0.03 – 8.5 $\mu g/m^3$ and 0.18 – 2.0 $\mu g/m^3$, respectively, for the whole study.

- The ratio of ammonium to sulfate averaged 1.54 with a standard deviation of 0.3, indicating that on average the aerosol was acidic. This is consistent with direct measurements of aerosol acidity which ranged from 0 to 75.5 neq/m^3.

- Concentrations of N(V) and aerosol sulfate showed a modest correlation ($R^2 = 0.55$), suggesting some similarity in the source regions for those species. Also, back-trajectory calculations performed for days with the highest concentrations of sulfate and N(V) showed that transport from source regions in east Texas and along the Texas/Mexico border may be significant.

- $PM_{2.5}$ nitrate concentrations were found to have little correlation ($R^2 = 0.004$) with $PM_{2.5}$ sulfate. However, $PM_{2.5}$ nitrate concentrations were correlated ($R^2 = 0.6$) with the sum of $PM_{2.5}$ sodium and calcium concentrations, suggesting nitric acid reaction with sea salt and soil dust. This is also supported by back trajectories performed for the high $PM_{2.5}$ nitrate days, in which air masses passed over likely sea salt and soil dust source areas.

- Total N(V) was present mostly as HNO_3. On the other hand, N(-III) tended to be associated mainly with particles. Although sulfate reductions could release ammonia and provide the potential for ammonium nitrate formation, the aerosol is acidic enough during peak pollution periods that the required sulfate reductions would be large. Ammonium nitrate formation would also be suppressed by the high summer temperatures characteristic of the region.

Size-resolved particle inorganic ions

- The inorganic ion concentration measurements as a function of particle size indicate that nitrate and sulfate are separated into supermicron (peak diameter of 4 – 5 μm) and submicron (peak of 0.4 – 0.5 μm) modes, respectively.

- Potassium, magnesium, calcium, and chloride were found to exhibit bimodal size distributions with both a fine mode (peaked at 0.4 – 0.5 μm) and a coarse mode (peaked at 4 – 5 μm) present.

- For aerosol samples from all of the MOUDI stages, particle nitrate concentrations were correlated with the sum of particle sodium and calcium ($R^2 = 0.70$), consistent with the correlation between $PM_{2.5}$ nitrate and the sum of $PM_{2.5}$ sodium and calcium. This again indicates the importance of sea salt and soil dust particles in providing non-acidic surfaces for reaction with nitric acid.

- A 1 μm size cut would have provided a better division between the fine mode and the coarse mode for atmospheric aerosols sampled during BRAVO study. The cut at 2.5 μm typically included a significant fraction of the coarse mode.

Thermodynamic model study

- Comparison of the ISORROPIA and SCAPE2 model predictions of solid phase sulfate species shows reasonable agreement for $(NH_4)_2SO_4$ and $(NH_4)_3H(SO_4)_2$ between the two models, although ISORROPIA often predicts higher concentrations of these species. ISORROPIA often predicts the presence of solid phase Na_2SO_4,

while SCAPE2 seldom does. Differences between solid phase sulfate concentrations predicted by the two models largely reflect differences in predicted aerosol water content and the existence of a liquid phase.

- Both models predict the observed phase partitioning of N(-III) well, but poorly predict observed phase partitioning of N(V). Underprediction of aerosol nitrate reflects the fact that the $PM_{2.5}$ aerosol composition is externally mixed, containing acidic submicron sulfate particles and supermicron nitrate particles, a condition not represented in the models, which are designed to model only internal mixtures.

Chapter 7 Recommendations for further study

Recommendations for further study include:

- Extending the period of study to other times of the year would provide interesting data for further study. Changes in the behavior of the $NO_3^-/HNO_3/NH_3/NH_4^+/SO_4^{2-}$ system could be discerned under different temperature and humidity conditions than those experienced during the summer study. Spring in Big Bend is often accompanied by intrusion of smoke plumes from Mexico that would also be interesting to examine.

- Additional simultaneous gas phase measurements such as O_3, SO_2, SO_x, NO, NO_2, and NO_x would provide a better understanding of the photochemical production of secondary pollutants and the potential formation of secondary aerosol.

- Additional measurements in the size resolved aerosol samples would be informative. pH measurement as a function of particle size would be helpful in confirming the variation of particle acidity with particle size. Those measurements would improve our understanding of particle/trace gases reactions that depend on particle acidity.

References

Andres, R.J. and Kasgnoc, A.D., 1998. A time-averaged inventory of subaerial volcanic sulfur emissions. Journal of Geophysical Research, 103: 25251-25261.

Aneja, V.P., Roelle, P.A., Murray, G.C., Southerland, J., Eristman, J.W., Fowler, D., Asman, W.A.H. and Patni, N., 2001. Atmospheric nitrogen compounds II: emissions, transport, transformation, deposition and assessment. Atmospheric Environment, 35: 1903-1911.

Ansari, A.S. and Pandis, S.N., 1999. Prediction of muticomponent inorganic atmospheric aerosol behavior. Atmospheric Environment, 33: 745-757.

Appel, B.R. and Tokiwa, Y., 1981. Atmospheric particulate nitrate sampling errors deu to reactions with particulate and gaseous strong acids. Atmospheric Environment, 15: 1087-1089.

Appel, B.R., Wall, S.M., Halk, M., Kothny, E.L. and Tokiwa, Y., 1980a. Evaluation of techniques for sulfuric acid and particulate strong acidity mesurements in ambient air. Atmospheric Environment, 14: 559-563.

Appel, B.R., Wall, S.M., Tokiwa, Y. and Halk, M., 1980b. Simulaneous nitric acid, particulate nitrate and acidity measurements in ambient air. Atmospheric Environment, 14: 549-554.

Arimoto, R., Duce, R.A., Ray, B.J., Ellis, W.G., Cullen, J.D. and Merill, J.T., 1995. Trace elements in the atmosphere over the North Altantic. Journal of Geophysical Research, D1: 1119-1213.

Bassett, M.E. and Seinfeld, J.H., 1983. Atmospheric equilibrium model of sulfate and nitrate aerosols. Atmospheric Environment, 17(11): 2237-2252.

Bassett, M.E. and Seinfeld, J.H., 1984. Atmospheric equilibrium model of sulfate and nitrate aerosols - II. Particle size analysis. Atmospheric Environment, 18(6): 1163-1170.

Battye, R., Battye, W., Overcash, C. and Fudge, S., 1994. Development and selection of ammonia emission factor. EPA contract number 68-D3-0034, Work assignment 0-3, USEPA.

Berresheim, H., Wine, P.H. and Davis, D.D., 1995. Sulfur in the atmosphere, in Compostion, Chemistry, and Climate of the Atmosphere. Van Nostrand Reinhold, 251-307 pp.

Bouwman, A.F., Van der Hoek, K.W. and Olivier, J.J., 1995. Uncertainties in the global source distribution of nitrous oxide. Journal of Geophysical Research, 100: 2785-2800.

Brauer, M., Koutrakis, P., Keeler, G.J. and Spengler, J.D., 1991. Indoor and outdoor concentration of inorganic acidic aerosols and gases. Journal of Air & Waste Management Association, 41(2): 171-181.

Bromley, L.A., 1973. Thermodynamic properties of strong electrolytes in aqueous solutions. AIChE J., 19: 313-320.

Brown, S.G., 2001. Characterization of carbonaceous aerosol during the Big Bend Regional Aerosol and Visibility Observational Study. M.S. Thesis, Colorado State University.

Carmichael, G.R., Hong, M.-s., Ueda, H., Chen, L.-L., Murano, K., Park, J.K., Lee, H., Kim, Y., Kang, C. and Shim, S., 1997. Aerosol compostion at Cheju Island, Korea. Journal of Geophysical Research, 102(D5): 6047-6061.

Cheng, Z.L., Lam, K.S., Chan, L.Y., Wang, T. and Cheng, K.K., 2000. Chemical characteristics of aerosols at coastal station in Hong Kong. I. Seasonal variation of major ions, halogens and mineral dusts between 1995 and 1996. Atmospheric Environment, 34: 2771-2783.

Choi, J., Lee, M., Chun, Y., Kim, J. and Oh, S., 2001. Chemical composition and source signature of spring aerosol in Seoul, Korea. Journal of Geophysical Research-Atmospheres, 106 (D16): 18067-18074.

Chun, Y., Boo, K., Kim, J., Park, S. and Lee, M., 2001. Synopsis, transport, and physical characteristics of Asian dust in Korea. Journal of Geophysical Research-Atmospheres, 106 (D16): 18461-18469.

Cooke, M.J. and Wadden, R.A., 1981. Atmospheric factors influencing daily sulfate concentrations in Chicago air. Journal of the Air Pollution Control Association, 31(11): 1197-1199.

Currie, L.A., Gelach, C.W., Lewis, W.D., Balfour, J.A., Copper, S.L., Dattner, R.T., De Cesar, G.E., Gordon, S.L., Heiser, P.K., Hopke, J.J., Shah, G.D., Thurston and Williamson, H.J., 1984. Interlaboratory comparison of source apportionment procedures: result for simulated data sets. Atmospheric Environment, 18: 1517-1537.

Dentener, F.J., Carmichael, G.R., Zhang, Y., Lelieveld, J. and Crutzen, P.J., 1996. Role of mineral aerosol as a reactive surface in the global troposphere. Journal of Geophysical Research, 101: 22869 - 22889.

Echalar, F., Gaudichet, A. and Cachier, H., 1995. Aerosol emissions by tropical forest and savanna biomass burnig characteristic trace elements and fluxes. Geophysical research letters, 22: 3039-3042.

EPA, U.S., 1999. Compendium of methods for the determination of inorganic compounds in ambient air. EPA/625/R-96/010a: Method IO-4.2.

Finlayson-Pitts, B.J. and Pitts, J.N.Jr., 2000. Chemistry of the Upper and Lower Atmosphere. Academic Press.

Gebhart, K.A., Kreidenweis, S.M. and Malm, W.C., 2001. Back-trajectory analyses of fine particulate matter measured at Big Bend National Park in the historical database and the 1996 scoping study. The Science of the Total Environment, 276(1-3): 185-204.

Gebhart, K.A., Malm, W.C. and Flores, M., 2000. A preliminary look at source-receptor Relationships in the Texas-Mexico Border Area. Journal of Air & Waste Management Association, 50: 858-868.

Graf, H.F., Feichter, J. and Langmann, B., 1997. Volcanic sulfur emission: Estimates of source strength and its contribution to the global sulfate distribution. Journal of Geophysical Research, 102: 10727-10738.

Hand, J.L., 2001. A new technique for obtaining aerosol size distributions with applications to estimates of aerosol properties. Ph. D. Thesis, Colorado State University.

Herckes, P., Wendling, R., Sauret, N., Mirabel, P. and Wortham, H., 2002. Cloudwater studies at a high elevation site in the Vosges Mountains. Environmental pollution, 117: 169-177.

Hering, S., Eldering, A. and Seinfeld, J.H., 1997. Bimodal character of accumulation mode aerosol mass distributions in Southern California. Atmospheric Environment, 31(1): 1-11.

Hitchcock, D.A., Spiller, L.L. and Wiison, W.E., 1980. Sulfuric acid aerosols and HCl release in coastal atmospheres: Evidence of rapid formation of sulfuric acid particulates. Atmospheric Environment, 14: 165-182.

Hopke, P.K., 1988. Target transformation factor analysis as an aerosol mass apportionment method: a review and sensitivity study. Atmospheric Environment, 22: 1777-1792.

Jacobson, M.Z., 1999. Studying the effects of calcium and magnesium on size-distributed nitrate and ammonium with EQUISOLV II. Atmospheric Environment, 33: 3635-3649.

Jacobson, M.Z., Tabazdeh, A. and Turco, R.P., 1996. Simulating equilibrium within aerosols and noneuqilibrium between gases and aerosols. Journal of Geophysical Research, 101(D4): 9079-9091.

John, W., Wall, S.M., Ondo, J.L. and Winklmayr, W., 1990. Modes in the size distributions of atmospheric inorganic aerosol. Atmospheric Environment, 24A(9): 2349-2359.

Kaiser, H.F., 1958. The Varimax criterion for analytic rotation in factor analysis. Psychometrika, 23: 187-200.

Kerminen, V.-M. and Wexler, A.S., 1995. Growth laws for atmospheric aerosol particles: An examination of the bimodality of the accumulation mode. Atmospheric Environment, 29(22): 3263-3275.

Kim, Y.P. and Seinfeld, J.H., 1993. Atmospheric gas-aerosol Equilibrium I. Thermodynamic model. Aerosol Science and Technology, 19: 157-181.

Kim, Y.P. and Seinfeld, J.H., 1995. Atmospheric gas-aerosol Equilibrium III. Thermodynamics of crustal elements Ca^{2+}, K^{+}, and Mg^{2+}. Aerosol Science and Technology, 22: 93-110.

Kim, Y.P., Seinfeld, J.H. and Saxena, P., 1993. Atmospheric gas-aerosol equilibrium II. Analysis of common approximates and activity coefficent calculation methods. Aerosol Science and Technology, 19: 182-198.

Koutrakis, P., Wolfson, J.M., Slater, J.L., Brauer, M., Spengler, J.D., Stevens, R.K. and Stone, C.L., 1988a. Evaluation of an annular denuder/filter pack system to collect acidic aerosols and gases. Evironmental Science & Technology, 22(12): 1463-1467.

Koutrakis, P., Wolfson, J.M. and Spengler, J.D., 1988b. An improved method of measuring aerosol strong acidity: Results from a nine-month study in St. Louis, Missouri and Kingston, Tennessee. Atmospheric Environment, 22: 157-162.

Koutrakis, P., Wolfson, J.M., Spengler, J.D., Stern, B. and Franklin, C.A., 1989. Equilibrium size of atmospheric aerosol sulfates as a function of the relative humidity. Journal of Geophysical Research, 94(D5): 6442-6448.

Kusik, C.L. and Meissner, H.P., 1978. Electrolyte activity coefficients in inorganic processing. AIChE Symp. Ser., 173: 14-20.

Lee, G., 1992. The variation of nitric acid vapor and nitrate aerosol concentrations near the Island of Hawaii. Ph. D. Thesis, University of Rhode Island.

Lee, H.S., Wadden, R.A. and Scheff, P.A., 1993. Measurement and evaluation of acid air pollutants in Chicago using an annular denuder system. Atmospheric Environment, 27A: 543-553.

Lodge, J., J. P., 1989. Methods of Air Sampling and Analysis, 3rd edn. Lewis, Chelsea, MI.

Marple, V.A., Rubow, K.L. and Behm, S.M., 1991. A Microorifice Uniform Deposit Impactor (MOUDI): Description, Calibration, and Use. Aerosol Science and Technology, 14: 434-446.

Meng, Z. and Seinfeld, J.H., 1994. On the source of the submicrometer droplet mode of urban and regional aerosols. Aerosol Science and Technology, 20: 253-265.

Meng, Z., Seinfeld, J.H., Saxena, P. and Kim, Y.P., 1995a. Atmopheric Gas-aerosol Equilibrium IV. Thermodynamics of carbonates. Aerosol Science and Technology, 23: 131-154.

Meng, Z.Y., Seinfeld, J.H., Saxena, P. and Kim, Y.P., 1995b. Contribution of water to particulate mass in the Southern Coast Air Basin. Aerosol Science and Technology, 22: 111-123.

Meszaros, E., Barcza, T., Gelencser, A., Hlavay, G.K., Krivacsy, Z., Molnar, A. and Polyak, K., 1997. Size distributions of inorganic and organic species in the atmospheric aerosol in Hungary. Journal of Aerosol Science, 28(7): 1163-1175.

Nenes, A., Pandis, S.N. and Pilinis, C., 1998. ISORROPIA : A new Thermodynamic equilibrium model for multiphase multicomponent inorganic aerosols. Aquatic Geochemistry, 4: 123-152.

Nenes, A., Pandis, S.N. and Pilinis, C., 1999. Continued development and testing of a new thermodynamic aerosol module for urban and regional air quality models. Atmospheric Environment, 33: 1553-1560.

Ohta, S. and Okita, T., 1990. A chemical characterization of atmospheric aerosol in SAPPORO. Atmospheric Environment, 24A: 815-822.

Padgett, P.E. and Bytnerowicz, A., 2001. Depostion and adsorption of the air pollutant HNO_3 vapor to soil surfaces. Atmospheric Environment, 35: 2405-2415.

Pakkanen, T.A., 1996. Study of formation of coarse particle nitrate aerosol. Atmospheric Environment, 30(14): 2475-2482.

Pakkanen, T.A., Kerminen, V.-M., Hillamo, R.E., Makinen, M., Makela, T. and Virkkula, A., 1996. Distribution of Nitrate over Sea-salt and Soil derived particles-Implications from a field study. Journal of Atmospheric Chemistry, 24: 189-205.

Perrino, C., Santis, F.D. and Febo, A., 1990. Criteria for the choice of a denuder sampling technique devoted to the measurement of atmospheric nitrous and nitric acids. Atmospheric Environment, 24A: 617-626.

Pilinis, C. and Seinfeld, J.H., 1987. Continued development of a general equilibrium model for inorganic multicomponent atmospheric aerosols. Atmospheric Environment, 21(11): 2453-2466.

Pilinis, C., Seinfeld, J.H. and Grosjean, D., 1989. Water content of atmospehric aerosols. Atmospheric Environment, 23: 1601-1606.

Pitzer, K.S., 1973. Theoretical considerations of solubility with emphasis on mixed aqueous electrolytes. Pure and Applied Chemistry, 58: 1599-1610.

Potukuchi, S. and Wexler, A.S., 1995a. Identifying solid-aqueous phase transitions in atmospheric aerosol I. Neutral-acidity solutions. Atmospheric Environment, 29: 1663-1676.

Potukuchi, S. and Wexler, A.S., 1995b. Identifying solid-aqueous phase transitions in atmospheric aerosol II. acidic solutions. Atmospheric Environment, 29: 3357-3364.

Prospero, J.M. and Savoie, D.L., 1989. Effect of continental sources on nitrate concentration over Pacific Ocean. Nature, 339: 687.

Raes, F., Dingenen, R.V., Vignati, E., Wilson, J., Putaud, J.-P., Seinfeld, J.H. and Adams, P., 2000. Formation and cycling of aerosols in the global troposphere. Atmospheric Environment, 34: 4215-4240.

Saxena, P., Hudischewskyj, A.B., Seigneur, C. and Seinfeld, J.H., 1986. A comparative study of equilibrium approaches to the chemical characterization of secondary aerosols. Atmospheric Environment, 20(7): 1471-1483.

Scheff, P.A., Wadden, R.A. and Allen, R.J., 1984. Quantitative assessment of Chicago air pollution through analysis of covariance. Atmospheric Environment, 18(8): 1623-1631.

Seinfeld, J.H. and Pandis, S.N., 1998. Atmospheric chemistry and physics. John Wiley & Sons.

sickles, J.E., Perrino, C., Allegrini, I., Febo, A. and Possanzini, M., 1988. Sampling and analysis of ambient air near Los Angeles using an annular denuder system. Atmospheric Environment, 22: 1619-1625.

Sloane, C.S., Watson, J., Chow, J., Pritchett, L. and Richards, L.W., 1991. Size segregated fine particle measurements by chemical species and their impact on visibility impairment in Denver. Atmospheric Environment, 25A: 1013-1024.

Spengler, J.D., Brauer, M. and Koutrakis, P., 1990. Acid air and health. Environmental Science & Technology, 24(7): 946-956.

Spengler, J.D., Keeler, G.J., Koutrakis, P., Ryan, P.B., Raizenne, M. and Franklin, C.A., 1989. Exposures to acidic aerosols. Environmental Health Perspectives, 79: 43-51.

Spurny, K.R., 2000. Aerosol chemical processes in the environment. Lewis.

Stokes, R.H. and Robinson, R.A., 1966. Interactions in aqueous nonelectrolyte solutions, I. Solute-solvent equilibria. Journal of Physical Chemistry, 70: 2126-2130.

Tabazadeh, A., Jacobson, M.Z., Singh, H.B., Toon, O.B., Lin, J.S., Chatfield, R.B., Thakur, A.N., Talbot, R.W. and Dibb, J.E., 1998. Nitric acid scavenging by mineral and biomass burning aerosols. Geophysical Research Letters, 25: 4185-4188.

Tsai, C.-J., Perng, S.-B. and Chiou, S.-F., 2000. Use of two different acidic aerosol samplers to measure acidic aerosols in Hsinchu, Taiwan. Journal of Air & Waste Management Association, 50: 2120-2128.

Warneck, P., 1988. Chemistry of the Natural Atmosphere. Academic Press, New York.

Watson, J.G., Chow, J.C., Lurmann, F. and Musarra, S., 1994. Ammonia nitrate, nitric acid, and ammonia equilibrium in winter time Phoenix, Arizona. Journal of air & waste management Association, 44: 405-412.

Wexler, A.S. and Seinfeld, J.H., 1991. Second-generation inorganic aerosol model. Atmospheric Environment, 25A(12): 2731-2748.

Wilson, T.R.S., 1975. Salinity and the major elements of sea water. In:Riley, J. P., Skirrow, G. (Eds),Chemical Oceanography (1, 2 Edition). Academic, Orlando FL.

Winklmayr, W., Wang, H.-C. and John, W., 1990. Adaptation of the Twomey Algorithm to the inversion of cascade impactor data. Aerosol Science and Technology, 13: 322-331.

Wolff, G.T., 1984. On the nature of nitrate in coarse continental aerosols. Atmospheric Environment, 18(5): 977-981.

Yoshizumi, K. and Hoshi, A., 1985. Size distributions of ammonium nitrate and sodium nitrate in atmospheric aerosols. Environmental Science & Technology, 19: 258-261.

Zhuang, H., Chan, C.K., Fang, M. and Wexler, A.S., 1999. Size distributions of particulate sulfate, nitrate, and ammonium at a coatal site in Hong Kong. Atmospheric Environment, 33: 843-853.

Appendix A : Summary of sample validity during BRAVO

Table A1. Summary of CSU BRAVO sample validity (July)

		July																														
Measurement	**Instrument**	**1**	**2**	**3**	**4**	**5**	**6**	**7**	**8**	**9**	**10**	**11**	**12**	**13**	**14**	**15**	**16**	**17**	**18**	**19**	**20**	**21**	**22**	**23**	**24**	**25**	**26**	**27**	**28**	**29**	**30**	**31**
URG PM-2.5 Aerosol	URG Sampler	X	X, B	X	X	C	X, B	C	X	X,B	X	X	X	X, B	X	X	X,B	X	X	X	X,B	X	X	X,B	X	X	X	X,B	X	X	X,B	X
		A	A	A	A	A	A	A	A	A	A	A	A	A	A	A	A	A	A	A	A	A	A	A	A	A	A	A	A	A	A	A
URG HNO3 and NH3 Denuder	URG Denuder	X	X, B	X	X	X	X, B	X	X	X,B	X	X	X	X, B	X	X	X,B	X	X	X	X,B	X	X	X,B	X	X	X	X,B	X	X	X,B	X
		A	A	A	A	A	A	A	A	A	A	A	A	A	A	A	A	A	A	A	A	A	A	A	A	A	A	A	A	A	A	A
MOUDI	Micro Orifice Uniform Deposit Impactor	X	X	X	X	B	**X**	X	X	X	X	X	X	B	X	X	X	X	X	B	X	X	X	X	X	X	B	X	X	X	X	X
			A	A			A		A			A					A		A	A	A			A	A						A	
SEM filter	Open face filter holder	N	N	N	N	N	N	N	N	N	N	N	N	N	N	N	N	X	X	X	X	X	X	X	X	X	X	X	X	X	X	X
Organic Aerosol sample	2 Channel Organic sampler	X	X	X	X	X	X, B	X	X	X	X	X	X	X,B	X	X	X	X	X	X	X,B	X	X	X	X	X	X	X,B	X	X	X	X

Key **X : Valid sample**
B : Blank sample
A : Analyzed
C : Invalid sample (Suspected Contamination)
N : No sample

Table A2. Summary of CSU BRAVO sample validity (August)

		August																														
Measurement	**Instrument**	**1**	**2**	**3**	**4**	**5**	**6**	**7**	**8**	**9**	**10**	**11**	**12**	**13**	**14**	**15**	**16**	**17**	**18**	**19**	**20**	**21**	**22**	**23**	**24**	**25**	**26**	**27**	**28**	**29**	**30**	**31**
URG PM-2.5 Aerosol	URG Sampler	X	X	X,B	X	X	X,B	X	X	X	X,B	X	X	X, B	X	X	X	X,B	X	X	X,B	X	X	X	X,B	X	X	X,B	X	X	X	X,B
		A	A	A	A	A	A	A	A	A	A	A	A	A	A	A	A	A	A	A	A	A	A	A	A	A	A	A	A	A	A	A
URG HNO3 and NH3 Denuder	URG Denuder	X	X	X,B	X	X	X,B	X	X	X	X,B	X	X	X, B	X	X	X	X,B	X	X	X,B	X	X	X	X,B	X	X	X,B	X	X	X	X,B
		A	A	A	A	A	A	A	A	A	A	A	A	A	A	A	A	A	A	A	A	A	A	A	A	A	A	A	A	A	A	A
MOUDI	Micro Orifice Uniform Deposit Impactor	X	B	X	X	X	X	X	X	B	X	X	X	X	X	X	B	X	X	X	X	X	X	B	X	X	X	X	X	X	B	X
			A	A											A	A					A	A			A			A	A			
SEM filter	Open face filter holder	X	X	X	X	X	X	X	X	X	X	X	X	X	X	X	X	X	X	X	X	X	X	X	X	X	X	X	X	X	X	X
Organic Aerosol sample	2 Channel Organic sampler	X	X	X,B	X	X	X	X	X	X	X,B	X	X	X	X	X	X,B	X	X	X	X	X	X	X	X,B	X	X	X	X	X	X	X

Key **X : Valid sample**
B : Blank sample
A : Analyzed
C : Invalid sample (Suspected Contamination)
N: No sample

Table A3. Summary of CSU BRAVO sample validity (September)

		September																												
Measurement	**Instrument**	**1**	**2**	**3**	**4**	**5**	**6**	**7**	**8**	**9**	**10**	**11**	**12**	**13**	**14**	**15**	**16**	**17**	**18**	**19**	**20**	**21**	**22**	**23**	**24**	**25**	**26**	**27**	**28**	**29**	**30**
URG PM-2.5 Aerosol	URG Sampler	X	X	X,B	X	X	X	X	X	X	X,B	X	X	X	X	X	X	X,B	X	X	X	X,B	X	X	X,B	X	X	X	X,B	X	X
		A	A	A	A	A	A	A	A	A	A	A	A	A	A	A	A	A	A	A	A	A	A	A	A	A	A	A	A	A	A
URG HNO3 and NH3 Denuder	URG Denuder	X	X	X,B	X	X	X	X	X	X	X,B	X	X	X	X	X	X	X,B	X	X	X	X,B	X	X	X,B	X	X	X	X,B	X	X
		A	A	A	A	A	A	A	A	A	A	A	A	A	A	A	A	A	A	A	A	A	A	A	A	A	A	A	A	A	A
MOUDI	Micro Orifice Uniform Deposit Impactor	X	X	X		X (48 hr)	B	X	X	X	X	X	X	B	X	X	X	X	X	X	B	X	X	X	X	X	X	B	X	X	X
		A	A				A		A						A	A						A								A	
SEM filter	Open face filter holder	X	X	X	X	X	X	X	X	X	X	X	X	X	X	X	X	X	X	X	X	X	X	X	X	X	X	X	X	X	X
Organic Aerosol sample	2 Channel Organic sampler	X	X	X	X	X	X	X	X	X,B	X	X	X	X	X,B	X	X	X	X	X	X	X,B	X	X	X	X	X	X	X,B	X	X

Key **X : Valid sample**
B : Blank sample
A : Analyzed
C : Invalid sample (Suspected Contamination)
N: No sample

Table A4. Summary of CSU BRAVO sample validity (October)

		October																														
Measurement	**Instrument**	**1**	**2**	**3**	**4**	**5**	**6**	**7**	**8**	**9**	**10**	**11**	**12**	**13**	**14**	**15**	**16**	**17**	**18**	**19**	**20**	**21**	**22**	**23**	**24**	**25**	**26**	**27**	**28**	**29**	**30**	**31**
URG PM-2.5 Aerosol	URG Sampler	X,B	X	X	X	X,B	X	X	X,B	X	X	X	X,B	X	X	X,B	X	X	X	X,B	X	X	X,B	X	X	X	X,B	X	X	X,B	X	X
		A	A	A	A	A	A	A	A	A	A	A	A	A	A	A	A	A	A	A	A	A	A	A	A	A	A	A	A	A	A	A
URG HNO3 and NH3 Denuder	URG Denuder	X	X	X,B	X	X	X,B	X	X	X	X,B	X	X	X, B	X	X	X	X,B	X	X	X,B	X	X	X	X,B	X	X	X,B	X	X	X	X,B
		A	A	A	A	A	A	A	A	A	A	A	A	A	A	A	A	A	A	A	A	A	A	A	A	A	A	A	A	A	A	A
MOUDI	Micro Orifice Uniform Deposit Impactor	X	X	X	B	X	X	X	X	X	X	B	X	X	X	X	X	X	B	X	X	X	X	X	X	B	X	X	X	X	B	X
					A	A		A	A	A	A		A	A	A	A	A	A				A						A	A	A			
SEM filter	Open face filter holder	X	X	X	X	X	X	X	X	X	X	X	X	X	X	X	X	X	X	X	X	X	X	X	X	X	X	X	X	X	X	X
Organic Aerosol sample	2 Channel Organic sampler	X	X	X	X,B	X,B	X	X	X	X	X	X	X,B	X	X	X	X	X	X	X,B	X	X	X	X	X	X	X,B	X	X	X	X	X

Key **X : Valid sample**
B : Blank sample
A : Analyzed
C : Invalid sample (Suspected Contamination)
N: No sample

Appendix B : Standard Operating procedure for URG annular denuder sampler and MOUDI

Collection of Inorganic Aerosol and Trace Gas Samples Using the URG Annular Denuder Sampler

BRAVO Ion Balance Project
Summer/Fall 1999
Big Bend National Park, Texas

Colorado State University

Contents

1. Scope

This Standard Operating Procedure describes a sampling and analytical protocol for the URG annular denuder system (ADS). This system was developed to measure reactive acidic and basic gases and particulate matter. The chemical species to be determined using this Standard Operating Procedure (SOP) are gaseous HNO_3 (Denuder 1) and NH_3 (Denuder 2) and particulate SO_4^{-2}, NO_3^{-2}, Cl^-, NH_4^+, K^+, Ca^{+2}, Na^+, Mg^{+2}, and H^+. Once collected, the species concentrations are quantified by Ion Chromatography (IC, Dionex-500) analysis except that the H^+ concentration of particulate matter is measured using a pH meter (Orion Model-250A and ROSS Sure-flow combination electrode).

2. Summary of method

Ambient air is drawn through a cyclone (D_{50} = 2.5 μm), and along etched glass denuder walls (air passes through two denuders in series) which have been coated with chemicals that absorb the gaseous species of interest. The remaining air stream is then filtered through 47mm Teflon, nylon, and coated glass fiber filters in series. The Teflon filter (Gelman Teflo, 2 μm pore size) is used to collect particulate matter. The nylon membrane filter (Gelman Nylasorb) and coated glass fiber filter are used to capture nitric acid and ammonia, respectively, which may be volatilized from particulate matter on the Teflon filter.

After sampling the annular denuders are extracted with 10mL of deionized water. The extract solution is analyzed for ions corresponding to the collected gaseous species after aliquot. The first denuder is for gaseous HNO_3, and the second denuder for gaseous NH_3. The filters are placed face downward into Nalgene polypropylene bottles (125mL) with 6mL of the extract solution (0.0001N $HClO_4$ and 150 μl ethanol for the Teflon filter, anion IC eluent (a weak solution of carbonate/bicarbonate) for the nylon filter, and deionized water for the glass fiber filter). The filter bottle is capped and put in an ultrasonic bath for 30 minutes. The extract solution from the Teflon filter is analyzed for pH and for major ions (SO_4^{-2}, NO_3^-, Cl^-, NH_4^+, K^+, Ca^{+2}, Na^+, and Mg^{+2}). The extract solution of the nylon and glass fiber filters are analyzed for NO_3^- and NH_4^+, respectively.

The analysis of anion and cation concentration collected by the denuders and filters is performed using standard techniques of ion chromatography on two Dionex model DX-500 ion chromatgoraphs. H^+ is measured using an Orion Model 250A portable pH meter and a Ross Sure-Flow combination pH electrode.

3. Annular denuder sampler set-up and operation

The URG denuder/filter-pack assembly is used to collect daily, 24-hour samples. Samples are run from 0800-0800 local time. Two parallel sampling trains are used to facilitate a rapid change between samples. Air is drawn through the sample train at a nominal value of 10 lpm (actual volumetric flow) in order to provide the desired 2.5 μm aerodynamic diameter size cut in the URG cyclone. Flow is provided by a vacuum pump and controlled by a mass flow controller. A dry gas meter is installed in-line between the filter pack and mass flow controller in order to provide an integrated measure of total sample flow. The sample flow read by the dry gas meter is corrected to ambient conditions by correcting for the pressure drop through the denuders and filters. An inline pressure measurement is used to make this correction.

3.1 Sample train assembly

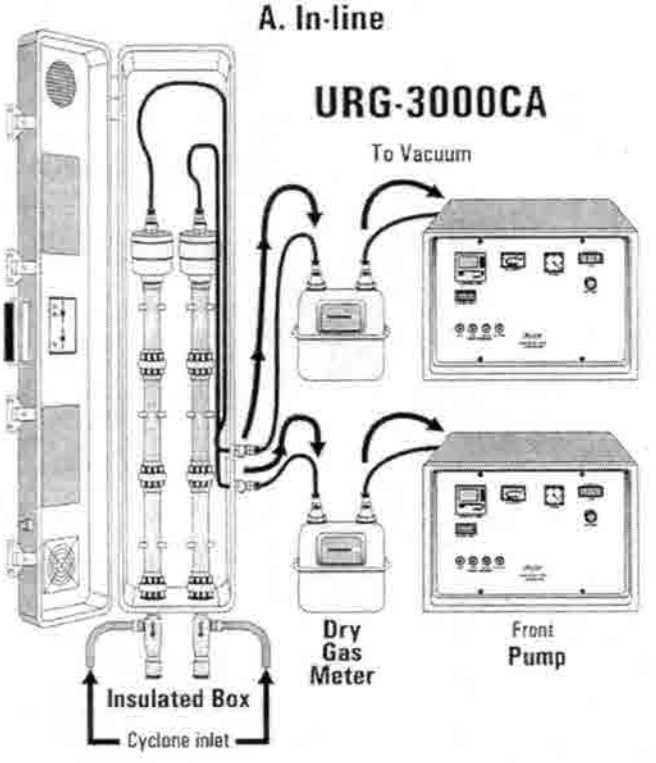

Figure B1 Schematic of the dual channel URG annular denuder system. The system depicted in the figure differs from the system used in this study as follows: the BRAVO project sampler has two denuders (not three) and has a 3-stage (not 2-stage) filter pack.

Air is drawn in series through two a cyclone, two 242 mm annular denuders, a 3-stage filter pack, a dry gas meter, a mass flow controller, and a vacuum pump. Figure B1, taken from the URG sampler manual, illustrates the setup except that the figure depicts three denuders in series and a 2-stage filter pack. The flow is set at 10 actual lpm at ambient conditions using the mass flow controller, with appropriate corrections for atmospheric pressure and temperature deviations from standard conditions.

The sampling train should be assembled as follows. Clean procedures should be followed to avoid contamination of the denuders or filter pack.

- The cyclone, mounted below the sampling box, is attached to the first denuder (coated with a NaCl solution, see below, for collection of HNO_3) using a coupler.
- The 1st denuder is connected to the 2nd denuder (coated with citric acid, see below, for NH_3 collection) using a second coupler.
- The 2nd denuder screws into the bottom of the 3-stage filter pack holder which is loaded with Teflon, nylon, and coated glass fiber filters (in that order, from bottom to top).
- Tubing is connected at the top of the filter pack with a quick connect. The tube passes through the sampling box and the other end connects to the inlet of the dry gas meter.
- The outlet of the dry gas meter connects to the vacuum port on the URG sampling pump assembly.

Assembly of the two denuders with the filter pack should be completed in the laboratory so that only the cyclone and tubing need to be attached outside.

3.2 Setting the flow rate

The flow rate is set by adjusting the setpoint on the mass flow controller. The setpoint control is accessed on the front of the URG pump assembly (see the URG manual for details of how to adjust the setting). An estimate of ambient temperature and pressure at the sampling site is needed to choose the mass flow setpoint.

The following equation is used to determine the "Corrected Flow Rate" that should be set on the pump for atmospheric condition other than 21^0 Celsius (294.18 K) and 760 mm Hg (these are

the standard conditions for which the Sierra mass flow controller in the URG pump assembly is calibrated) in order to achieve an actual volumetric flow rate of 10 lpm.

$$Q_V = Q_S \cdot \left(P_S / P_I \right) \cdot \left(T_I / T_S \right)$$

where

Q_S = the standard flow rate in LPM

Q_V = the desired ambient volumetric flow rate (LPM) at a given temperature, and barometric pressure

P_S = the standard condition barometric pressure (760 mm Hg)

P_I = the indicated (ambient) barometric pressure reading (in mm Hg)

T_S = the standard condition temperature (294.18 K)

T_I = the indicated temperature reading in degree Kelvin at the time of the calibrator flow reading

Table B1 illustrates mass flow setpoints determined for conditions typical of operation at the SimLab and at Big Bend National Park. Pressure differences from standard conditions due to differences in sampling altitude exert the greatest influence on the ratio of standard to actual flow rates.

For the BRAVO experiment at Big Bend National Park the mass flow controller setpoint should be adjusted to 8.71 slpm in order to achieve a nominal actual flow rate of 10 lpm. Actual volumetric flow will vary somewhat with temporal changes in ambient temperature and pressure. The actual sample volume will be determined from readings made with an in-line dry gas meter.

Table B1 Calculation of actual flow for ambient flow of 10 lpm

	Q_V (LPM)	P_S (mm Hg)	P_I (mmHg)	T_S (K)	T_I (K)	Q_S (LPM)
Standard Conditions	10	760	760	294.18	294.18	10
Simlab	10	760	637.7	294.18	300.18	8.22
Big Bend	10	760	675.2	294.18	300.18	8.71

3.2 Sampler operation

- Before the sample begins, record the initial volume from the dry gas meter on the log sheet and reset the elapsed timer.
- Start the pump at 08:00 local time. Reset the elapsed timer on the front of the pump assembly. Record the start time, your initials, and which denuder channel (1 or 2) is used on the log sheet. Also record the denuder and filter pack serial numbers on the log sheet.
- After the pump has run a few (15-30) minutes record the following items on the log sheet
    - initial pressure drop through the sampler assembly (read in inches of Hg from the vacuum gauge on the front of the URG pump assembly)
    - the setpoint and actual flow from the mass flow controller (displayed on the pump assembly panel; use the toggle switch to change between the flow setpoint and the actual flow reading) on the log sheet. If the set and read values for the flow differ by more than 10 % the pump is having trouble achieving the desired flow. Shut the pump off (be sure to record this action and the time it is taken on the log sheet) and check for clogging of the system upstream of the mass flow controller. The most likely source of clogging is the coated glass fiber filter; try replacing it with a fresh one and restarting the pump (record on log sheet). Clogging should also be evidenced by an abnormally high reading on the vacuum gauge.
- The sample is scheduled to end at 08:00, 24 hours after it starts. A few minutes before 08:00 record the following items on the log sheet:
    - Vacuum gauge reading
    - Flow setpoint and reading from mass flow controller
- At 08:00 turn off the pump. Record the following items on the log sheet
    - Operator initials
    - Sample stop time

- Elapsed time
- Final reading on Dry Gas Meter

- The denuder and filter pack assembly should be removed from the sampler as soon as possible. If necessary, however, it may stay up to several hours on the sampler before retrieval. Removal is accomplished by the following steps:
    - Unscrew the coupler at the bottom of the 1st denuder and replace it with a clean cap. Cover the coupler still attached to the cyclone with a piece of clean Parafilm (the side against the paper backing is the clean side).
    - Disconnect the tubing from the filter pack and cap the top of the filter pack or cover with Parafilm.
    - Take the denuder/filter-pack assembly into the lab and place inside the ammonia-free glove box for disassembly and extraction (see section 8 of this SOP).

Note: This procedure may be modified to automate the stop and start of the samples using the programmable capabilities of the URG pump assembly. If automation is employed, the sampler will automatically start and stop at 08:00. In this event

- the operator must be sure to reset the elapsed timer and record the initial volume from the dry gas meter in advance of the automated sample start
- the operator should note on the log sheet that automated operation is being used
- the initial vacuum gauge and flow readings should be taken as soon as possible after 08:30 and the times of these readings recorded
- the final vacuum gauge and flow readings should be taken as close to (but before!) the end of the sample period as possible and the time of the readings recorded
- the final volume should be read from the dry gas meter when the samples are retrieved

4. Preparation of coating and extract solutions, H^+ measurement reagents and IC eluent

Table B2 shows each chemical coating and extract solution used in the study and the volume needed for coating and extracting each denuder and filter.

Table B2 Solutions for Coating, extracting, and H^+ measurement

	Coating solution			Extracting solution				pH
	Denuder 1	Denuder 2	Glass Fiber filter	Teflon filter	Nylon filter	Glass Fiber filter	Denuder 1 and 2	1mL Aliquot (from Teflon)
DI water	90mL						10mL	
Methanol	10mL	50mL	95mL					
Ethanol				150μL				
NaCl	0.1 g							
Citric Acid		0.5 g	25g					
Glycerol			5mL					
$HClO_4$ 0.0001N				5.85mL				
IC Eluent (1.8mM Na_2CO_3/ 1.7mM $NaHCO_3$)					6mL			
KCl 2M (adding solution)								20 μL
Volume of Extracting and Coating	10mL	10mL	650μL	6mL	6mL	6mL	10mL	

5. Sampling and analysis schedule

	Monday		Tuesday		Wednesday		Thursday		Friday		Saturday		Sunday	
Sampler	Channel 1		Channel 2		Channel 1		Channel 1,2		Channel 1		Channel 2		Channel 1 , and 2	
Sampling	Sample(C1)		Sample Blank(C2)		Sample		Sample(C2)		Sample Blank(C1)		Sample		Sample Sample	
Preparation (Sampling)	Assembly (C1,2) Extracting (C1,2) Cleaning (C1,2)	Coating (C2) Setup filter Holder (C2)	Assembly (C2) Extracting (C1,2) Cleaning (C1,2)	Coating (C1) Setup filter Holder (C1)	Assembly (C1) Extracting (C2) Cleaning C2)	Coating (C1,2) Setup filter Holder (C1,2)	Assembly (C1,2) Extracting (C1,2) Cleaning (C1,2)	Coating (C1) Setup filter Holder (C1)	Assembly (C1) Extracting (C1) Cleaning (C1)	Coating (C2) Setup filter Holder (C2)	Assembly (C2) Extracting (C2) Cleaning (C2)	Coating (C1,2) Setup filter Holder (C1,2)	Assembly (C1,2) Extracting (C2) Cleaning (C2)	Coating (C1,2) Setup filter Holder (C1,2)
Preparation (Solution)			Analysis Solution (Cation, pH)						Analysis Solution (Anion, pH)				Coating Glass filter Coating solution Extract solution MOUDI	
Analysis			IC (Cation) pH						IC (Anion) pH					

6. Cleaning procedures

The procedures below outline how to clean the different sampling components used in the URG sampler and in sample handling.

- Whenever cleaning with pure water (DDW) is described, this refers to high purity deionized water taken from the Barnstead EasyPure system. The conductivity of this water should be approximately 18 Megohm-cm. If the water conductivity produced by the system drops below 17.5 Megohm-cm, the system cartridges should be replaced with identical new cartridges following the procedure specified in the Barnstead EasyPure manual.

- Whenever rinsing/washing with DDW is called for in these procedures, rinse with DDW 5-10 times.

- In all cases, **"clean" surfaces of items being cleaned should not come in contact with potential contamination sources**, including fingers, Kimwipes, unclean surfaces, etc....

- If an item must be set down, **create a clean surface by using a piece of fresh aluminum foil. Although EPA procedures call for use of Kimwipes as clean surfaces, do not use them!!!** Kimwipes contain high concentrations of soluble ions, especially sulfate!

- **Do not use Kimwipes to dry "clean" surfaces.** Air dry them. A stream of pure nitrogen is used for denuder drying.

- **Don't assume that new latex gloves are clean – they are not!** Touching of "clean" surfaces with gloves should be avoided. If this is necessary, clean the gloves first by rinsing thoroughly with DDW. After touching a clean surface it should be cleaned by thorough rinsing with DDW and allowed to air dry.

6.1 Denuder cleaning

- Clean insides of denuder caps with DDW. The inside of the cap should be treated as a "clean" surface and should never contact anything but DDW, clean aluminum foil, or a denuder. The outside of the denuder cap does not need to be extremely clean and can be handled with bare hands or gloves; occasional rinsing of the outside of denuder caps is advised, especially if they are dropped.

- Clean denuders with DDW. Denuder ends and interiors should be treated as "clean" surfaces.
    - With both caps removed, allow water to flow through denuder, alternating ends.
    - Replace bottom cap.
    - Partially fill denuder with DDW, cover open end and shake.
    - Repeat 5 times.
    - Remove bottom cap and run DDW through denuder again.
    - Shake off excess DDW and replace caps.

6.2 Cyclone cleaning

Wash cyclone cup every two weeks - more often if residue build-up is noted.

- Pull out bottom cup where large particles accumulate.
- Wash with DDW, tap upside down on clean foil surface to expel water drops, air dry, and replace on cyclone.

Wash entire cyclone once monthly.

- Remove connectors and cup and wash with DDW.
- Shake to remove excess DDW and air dry or dry with clean compressed N_2.

6.3 Coupler cleaning

End/attachment surfaces of couplers are "clean" surfaces; sides of couplers are not. Wash couplers with DDW weekly. Tap on clean foil to expel water drops and air dry. Store cleaned couplers in clean Ziploc bags or assembled with denuders.

6.4 Tweezer (forceps) cleaning

Ends of tweezers are "clean" surfaces. Clean tweezers with DDW prior to each use. Tap tweezers on clean aluminum foil to expel water drops and air dry. Store clean tweezers by wrapping in clean aluminum foil or inside clean Ziploc bags.

7. Coating procedures

7.1 GLASS FIBER FILTER

Coating solution: 25g citric acid
5mL glycerol
95mL methanol

- Glass fiber (GF) filter preparation and coating must be done inside the ammonia-free glove-box.
- Prepare filters by the batch, recording batch number on each petri dish.
- Prepare extra filters to be used for blanks.

1. Place GF filter in 50 mm diameter petri dish.
2. Pipette 650 µl coating solution on filter to wet entire filter.
3. Leave filter in uncovered petri dish inside dessicator within ammonia-free glove-box until dry.
4. Cover with petri dish lid.
5. When filters for batch are done, place all petri dishes with dry filters in zip-lock bag with batch number and store in ammonia-free hood. Can be stored 2-3 weeks.

7. 2 DENUDER COATING

Denuder 1 (for HNO_3)

Coating solution: 0.1g NaCl
90mL DDW
10mL methanol

Denuder 2 (for NH_3)

Coating solution: 0.5 g Citric Acid
50mL Methanol

Denuder top = labeled end, glass close to outside rim.

Denuder bottom = unlabeled end, glass ~1 inch from outside rim.

Each denuder is labeled for NH_3 or HNO_3.

1. Use 5 mL of coating solution to wash denuder.

- Remove top cap of clean denuder (leave bottom capped) and set denuder upright on capped end.
- Slowly pipette 5 mL of appropriate coating solution so that it will cover all surfaces.
- Replace cap.
- Hold denuder horizontally and rotate while lifting one end then the other for 1 minute to distribute the coating solution evenly.
- Remove top cap and decant excess coating solution into chemical waste container.
    - Return denuder to upright position, then decant excess coating solution again; repeat until no solution is decanted.

2. Use 10 mL of coating solution to coat denuder.

- Remove top cap of denuder.
- Pipette 10 mL of coating solution into denuder as described above, then rotate as described above for 1 minute.
- Remove top cap and decant excess solution into chemical waste container.
    - Return denuder to upright position, then decant excess coating solution again; repeat until no solution is decanted.

3. Dry denuders

NOTE: Drying manifold caps are labeled to match denuders. Each denuder must be attached to matching labeled manifold cap.

- Remove top cap of denuder and place on clean aluminum foil.
- Attach top end of each denuder to appropriately labeled drying manifold port.

- Remove bottom cap of denuder and place on clean aluminum foil.
- It is best to dry 4 denuders at once, but if only two, DO NOT cover vacant manifold ports.
- Open valve on nitrogen tank to 6 PSI flow rate. (Indicator needle on regulator is on 2nd red tick)
- Allow flow to continue for 3-4 minutes.
- Remove each denuder from drying manifold and attach opposite end to same drying manifold port.
- Allow flow from nitrogen tank to continue another 3-4 minutes.
- Close valve on nitrogen tank.
- Remove each denuder and replace top and bottom caps, making sure cap numbers match denuder number.
- Place denuders in ammonia-free hood.

8. Extraction procedure

8.1 Denuder extractions

NH_3 extraction must be done in Glove Box; HNO_3 extraction can be done outside of glove box.

1. Place clean aluminum foil on work surface.
2. Remove top cap of denuder and pipette 10mL of DDW over exposed glass surfaces.
3. Replace cap and agitate denuder for 1 minute by rotating denuder while alternately lifting each end to spread DDW evenly over all interior glass surfaces.
4. Decant extraction solution into 5mL cryovial. Label vial appropriately. Decant additional extract solution into waste container.
5. From the 5ml cryovial, pipette 600 µl into IC vial, cap and label appropriately.
6. Place both vials in appropriate racks for refrigeration.

8.2 Filter extractions

After each sampling period, the filter holder is placed in the ammonia-free glove box. Open the holder at each union and, using clean forceps, remove each filter (glass fiber, nylon, and Teflon) individually and place it face down in its own labeled 125 ml Nalgene bottle, then cap. The bottles are placed in freezer until the next anion/cation extraction.

1. Turn on glove box pump and allow to run for ≥ 60 minutes.
2. Remove filters from freezer, let them sit at room temperature for 30-60 minutes.
3. Teflon and glass fiber filter extractions should be performed in the ammonia-free glove box. Nylon filters may be extracted outside the glove box.

Teflon filter extraction - I

1. Teflon filter must be coated with 150 µl of ethanol before perchloric acid extract solution can be added.

- With Teflon filter in bottle, pipette 50 µl of ethanol onto back surface of filter (facing up in bottle) one drop at a time.
- After each drop, angle jar/filter so drop will move across filter to wet as much of surface as possible
- Repeat process two more times, each with another 50 µl of ethanol. Filter should be completely wetted at the end.

NOTE: It is difficult to wet the entire filter with 150 µl of ethanol, because the ethanol does not readily move through the Teflon membrane. Practice may be required to develop a technique that ensures proper wetting of the filter. Also, because ethanol evaporates rapidly, time required to accomplish this step should be kept to a minimum.

2. Add 5.85 ml 0.0001 N perchloric acid ($HClO_4$) by pipette.
   - Pipette 5.0 ml into bottle containing teflon filter, avoiding direct application to the filter.
   - Pipette 850 µL into the bottle, again avoiding direct application to the filter.
   - Replace bottle lid and set aside.

Nylon filter extraction - I

1. Remove bottle lid and pipette 6.0 ml of IC anion eluent ($NaHCO_3/Na_2CO_3$ aqueous solution) over nylon filter.
2. Replace bottle lid and set aside.

Glass fiber filter extraction - I

1. Remove bottle lid and pipette 6.0 ml DDW over filter.
2. Replace bottle lid and set aside.

Ultrasonic bath

1. Fill bath with 1-1.5 inches of water.
2. Place filter bottles into bath and run for 15 minutes.
   - The bath will hold 12 bottles at a time, so start with glass fiber filters since they will have additional step of centrifuging.

Glass fiber filter extraction - II

1. Open each filter bottle and, using a 1 ml pipette, transfer 1.5 ml filter extract into a microcentrifuge tube.
2. Label each tube using a permanent ink pen.
3. Pipette 5 ml of extract solution into cryovial, label, mark with green top, and place in appropriate rack and refrigerate.
4. Place tubes into centrifuge rack so that each tube has another tube in opposite holder to maintain balance.
5. Run centrifuge for 5 minutes at 1000 rpm to separate glass fibers from solution.
6. Pipette 600 µl of extract solution into IC vial, label, and place in appropriate rack and refrigerate.
7. Discard microcentrifuge tubes.

Nylon filter extraction - II

1. Pipette 600 µl into IC vial, label, and place in appropriate rack and refrigerate.
2. Pipette 5 ml into cryovial, label, mark with red top, and place in appropriate rack and refrigerate.

Teflon filter extraction - II

1. Pipette 5 ml into cryovial, label, mark with yellow top, and place in appropriate rack for use in pH measurements (see section 10).
2. Pipette 600 µl into IC vial, label, and place in appropriate rack and refrigerate.

9. Aliquot summary

Figures B2 and B3 shows aliquot for Denuder and filters

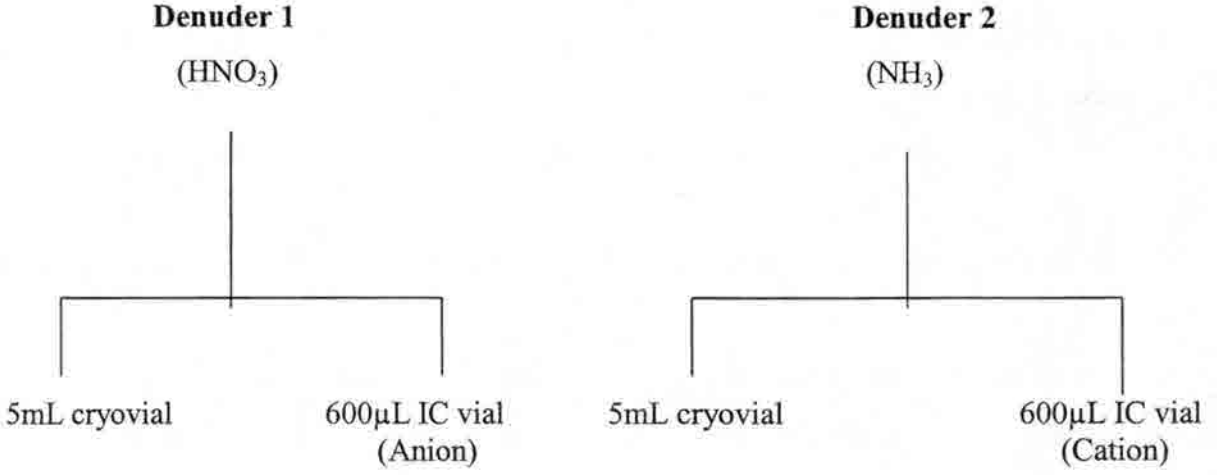

Figure B2 Aliquot for extract solution of Denuder

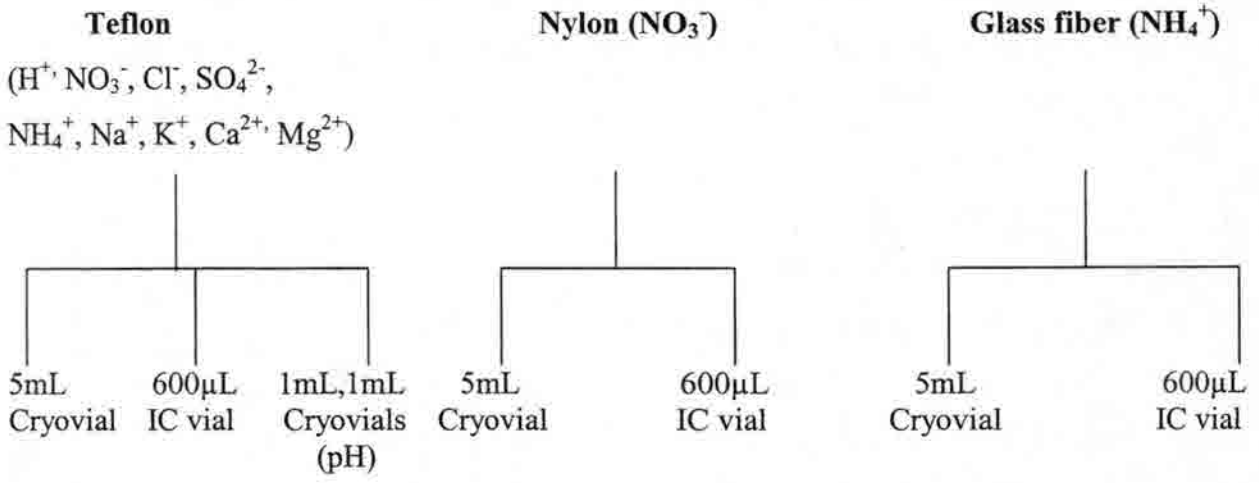

Figure B3 Aliquots for filter extracts

10. pH measurement

10.1 Solutions

Three solutions are needed for pH measurement; these must be made daily. DDW refers to deionized water from the Barnstead EasyPure system (see section 6). In all directions calling for filling a volumetric flask to the fill line, the flask should be filled until the bottom of the meniscus is at the fill line. Adding the last small portion of DDW from a small squirt bottle will enable the line to be matched more easily (thereby avoiding the need to remake solutions in which the flask has been overfilled).

1. Extract solution(ES)
   - Pipette 200µl of 0.1 N $HClO_4$ into a 200ml polypropylene volumetric flask containing 1-2 inches of DDW.
   - Fill volumetric flask to 200 ml line with DDW. Cap flask and mix thoroughly by inversion.
   - Rinse 125 ml Teflon bottle with three small portions of ES solution, fill Teflon bottle with ES solution, and discard remaining ES solution.

2. Working stock solution
   - Using red labeling tape on eight 15 ml Nalgene bottles, number them 1 through 8. These bottles will be referred to below as #_ Red.
   - In a glass volumetric flask (25mL), add the following amounts of 1 N H_2SO_4, then fill with DDW to 25mL fill line. Cap the flask and mix thoroughly by inversion. Transfer each solution to the appropriately labeled 15 ml Nalgene bottle (rinse the bottle a couple times with the solution and discard before filling).

#1	0 µl of 1N H_2SO_4 + DDW to 25 ml
#2	25 µl of 1N H_2SO_4 + DDW to 25 ml
#3	50 µl of 1N H_2SO_4 + DDW to 25 ml
#4	100 µl of 1N H_2SO_4 + DDW to 25 ml
#5	200 µl of 1N H_2SO_4 + DDW to 25 ml

#6 400 µl of 1N H_2SO_4 + DDW to 25 ml

#7 800 µl of 1N H_2SO_4 + DDW to 25 ml

#8 1600 µl of 1N H_2SO_4 + DDW to 25 ml

3. Working solution
   - Label eight 15 ml Nalgene bottles using blue labeling tape, numbers 1 through 8. These bottles will be referred to below as #_ Blue
   - Add 150 µl ethanol, 50 µl working stock, and 5.8mL ES as follows

#1 150 µl ethanol + 50 µl of #1 Red + 5.8 ml ES

#2 150 µl ethanol + 50 µl of #2 Red + 5.8 ml ES

#3 150 µl ethanol + 50 µl of #3 Red + 5.8 ml ES

#4 150 µl ethanol + 50 µl of #4 Red + 5.8 ml ES

#5 150 µl ethanol + 50 µl of #5 Red + 5.8 ml ES

#6 150 µl ethanol + 50 µl of #6 Red + 5.8 ml ES

#7 150 µl ethanol + 50 µl of #7 Red + 5.8 ml ES

#8 150 µl ethanol + 50 µl of #8 Red + 5.8 ml ES

   - Cap each bottle and mix thoroughly by inversion

10.2 pH Meter Calibration

1. Before turning on pH meter, fill electrode with electrode filling solution(ROSS™). If electrode has not been stored in storage solution, let stand for 1 hour in vial containing electrode storage solution before use.
2. Prepare 2 cryovials each with pH 7 solution and 2 with pH 4 buffer solution. One cryovial will be used to wash the electrode, the other to measure pH.
3. After turning pH meter on, set to room temperature by using the ∧ or ∨ keys. Temperature is displayed after model number (250) disappears from screen.
4. Press the '2nd' key then the 'Cal' key. P1 will appear at bottom of screen.
5. Rinse electrode with DDW from a squirt bottle then place in wash vial containing pH 7 buffer solution.
6. Remove electrode from wash vial and place in pH 7 buffer measure vial.

7. When pH meter 'beeps' and displays 'Ready', record pH reading in log book.
8. Press 'Yes' key one time. P2 will appear at bottom of screen.
9. Rinse electrode with DDW then place in wash vial containing pH 4 buffer solution.
10. Remove electrode from wash vial and place in pH 4 buffer measure vial.
11. When meter 'beeps' and displays 'Ready', record pH reading in log book.
12. Press 'Yes' key two times. 'Slp will appear at bottom of screen, followed by a number. That number is the slope of the calibration line and should be ≥ 0.9. Record the value in the log book. If the slope is < 0.9 try repeating the calibration procedure. If this does not resolve the problem, try a different electrode.
13. The pH meter is now calibrated and ready to measure pH of solutions.

10.3 Solution to compute calibration curve.

1. A calibration curve will be plotted from pH measurements taken of solutions of 1 ml '#_ Blue' + 20 µl 2 M KCl.

- Label 20 2 ml cryovials with permanent ink as follows:

  1, 1*, 2, 2*, …, 8, 8*

- For each number 1 through 8 one cryovial (labeled with a *) will be used to wash the pH electrode, the other (without a *) to measure pH.
- Pipette 1 ml of #1 through #8 Blue into appropriately labeled 2 ml cryovial. For example, pipette 1 ml #1 Blue into cryovial 1 and1 ml into cryovial 1*.
- Add 20 µl KCl 2 M to each vial. Cap and mix each vial thoroughly by inversion.
- Place cryovials in numerical order in two columns in a cryovial rack; one column for '*' and one column for other vials.

2. Measure pH of cryovials #1 through #8.

- Allow all solutions to come to room temperature.
- Rinse electrode with DDW.
- Place electrode in #1* (wash), then in #1 (measure). When pH meter 'beeps' with 'Ready' displayed, record pH on log sheet.
- Wash electrode with DDW, then place in #2* to wash, then #2 to measure pH.

- Repeat until pH of each vial number has been recorded.

10.4 pH of samples.

1. Locate 5 ml cryovials containing extracts of Teflon filters which are to be analyzed for pH. For each sample, label one 2 ml cryovial with the sample name and a second with the sample name plus *. Pipette 1 ml of the sample into each vial and cap. Vials labeled with a * will be used for electrode washing, the others for pH measurement.
2. Place 2ml cryovials containing samples from Teflon filter extracts in numerical order in two rows in rack, with vials marked with '*' in one row, vial without '*' in another.
3. Add 20 µl 2 M KCl to each vial. Cap and mix each vial thoroughly by inversion.
4. Allow all sample vials to come to room temperature.
5. Rinse pH electrode with DDW, place in the first sample wash cryovial (labeled with a *), then place in the first sample measurement vial to measure pH.
6. When pH meter 'beeps' and displays the word 'Ready', record pH on log sheet.
7. Repeat until pH has been measured for each sample.

10.5 Checking electrode calibration

1. Using previously prepared wash and measurement buffer vials, measure the pH of the 7 and 4 buffers and record on the log sheet. If these values differ by more than +/- 0.04 from the nominal values, recalibrate the pH electrode and repeat all pH measurements (H_2SO_4 calibration standards and samples). Be sure to note this procedure was followed in the log book, mark the completed log sheet "Invalid due to pH electrode calibration drift" and use a new log sheet for the repeated measurements.
2. When pH measurements are satisfactorily completed, turn off the pH meter, rinse the electrode with DDW, and store it in electrode storage solution.

11. IC Measurement

Extracts from all the denuders and filters described in this SOP will be analyzed by ion chromatography (IC) on a Dionex Model DX500 IC using standard techniques of ion chromatography. A brief summary of methods is presented here, along with a summary of procedures for IC calibration, analysis of quality control samples, and replicate analyses, is presented here. More detailed descriptions of the operation and use of the IC itself and the accompanying PeakNet software can be found in the Dionex product manuals and in the following three CSU IC lab manuals: Practical Overview of the Ion Chromatograph, Step-by-Step IC, and Troubleshooting and Set-Up of the IC.

11.1 Method description

The instrument used for analysis of inorganic ions is a Dionex DX-500 dual channel system. One channel is dedicated to analysis of cations (Sodium, Ammonium, Potassium, Magnesium, Calcium). The other channel is dedicated to anion analysis (Chloride, Nitrate, Sulfate)

The DX-500 ion chromatograph (IC) is attached to an AS3500 autosampler which allows random access to the sampling vials. This allows you to run the same standards at the beginning and end of each run of samples. In addition, the autosampler can be programmed to automatically run duplicate samples.

To make sure that the IC is running properly, periodic duplicates are run as well as standards. At the beginning of each run of samples, regardless of whether they are run for anions or cations a DI water blank and a test standard are run to ensure the method is operating properly. A series of standards are then run from which a calibration curve will be constructed. After the calibration standards are run, samples are run in groups of approximately ten. Within each group of ten, one sample is analyzed in duplicate to gather information about the precision of the measurements. Between sample groups one or more quality control (QC) samples are run to check for drift in instrument response and as independent checks on the instrument calibration. At the end of the run, a series of standards are reanalyzed to ensure significant drift has not occurred over the course of the run. These QC standards and their placement in the analysis sequence are described in more detail in sections below.

Cations are analyzed with a Dionex CS-12 Column preceded by a CG-12 guard column, with a Dionex Cation Self Regenerating Supressor operating in Auto Suppression Recycle Mode. Detection is with a Dionex CD20 conductivity detector. 50 µl sample injections are made by the AS3500 autosampler. The cation eluent is 20 mM Methanesulfonic Acid, prepared from concentrated methanesulfonic acid and DI water. 2.6 ml of concentrated MSA is added to a 2-l plastic eluent reservoir. DI water is added to the 2 l mark, and the eluent is then pressurized with helium. The pump is primed and the system is started with a flow rate of 1 ml/minute and left to equilibrate for at least one hour before starting analyses. Note the time, pressure and total conductivity in the DX-500 logbook now and periodically while the instrument is running. Expected background conductivity for the cation analysis is between 1 and 2 µS.

Anions are analyzed with a Dionex AS4A-SC Column and AG4A-SC guard column. Supression is with a Dionex Anion Self Regenerating Suppressor, and detection is by a Dionex CD20 conductivity detector. An AS3500 autosampler is used to introduce the samples into the column. Sample injection volume is 25 µl. The anion eluent is 1.8 mM Na_2CO_3/1.7 mM $NaHCO_3$. The eluent is prepared from a stock solution of 180 mM Na_2CO_3/170 mM $NaHCO_3$ (prepared by adding 19.08 g of Na_2CO_3 and 14.28 g of $NaHCO_3$ to a clean one-liter glass volumetric flask and adding deionized water to the 1 l mark). 20 ml of stock solution is added to a clean plastic 2 l eluent reservoir which is then filled with deionized water (with a conductivity of at least 18 megohm-cm) to the 2 l mark. The eluent is then pressurized with helium. The pump is primed and the system is started with a flow rate of 2 ml/minute and left to equilibrate for at least one hour before starting analyses. The time, pressure and total conductivity are noted in the DX-500 logbook periodically while the instrument is operating. The expected background conductivity for the anion analysis is ~14 µS.

Previously prepared "IC" vials are loaded into racks of forty for the AS3500 autosampler. If samples have not been previously prepared, 500 µl of each sample is pipetted into a 500 µl sample vial and the top is securely screwed on. Sample vials are polypropylene 500 µL with screw-type polyethylene caps with Teflon/silicon/Teflon septa (supplied by the SUN division of Comar, Inc).

Standards should be loaded in autosampler tray A and samples in tray B. After a run is completed the samples should be refrigerated as soon as possible.

11.2 Calibration Standards

Stock solutions of Anions and Cations and Organic Acids should be prepared for the analyses. The anion and cation stock solutions can be prepared in advance and stored in polyethylene bottles in the refrigerator for several weeks.

The anion stock solution is prepared as follows:

0.005 N Chloride

0.01 N Nitrate

0.01 N Sulfate

NaCl	(Sodium Chloride)	0.292 grams/liter
$NaNO_3$	(Sodium Nitrate)	0.850 grams/liter
Na_2SO_4	(Sodium Sulfate)	0.710 grams/liter

Weigh out the above chemicals and place them in a clean 1 l flask. Fill the flask half-way full with DI water and gently shake the flask to dissolve the crystals. Then fill the flask to the 1 l mark with DI water and mix by inversion.

The cation stock solution is prepared as follows:

0.005 N Calcium

0.005 N Magnesium

0.01 N Ammonium

0.005 N Sodium

0.005 N Potassium

NH_4Cl	(Ammonium Chloride)	0.535 grams/liter
NaCl	(Sodium Chloride)	0.292 grams/liter
KCl	(Potassium Chloride)	0.373 grams/liter
MgCl2 •6H2O	(Magnesium Chloride)	0.508 grams/liter
CaCl2 •2H2O	(Calcium Chloride)	0.368 grams/liter

Weigh out the above chemicals and place them in a clean 1 L flask. Fill the flask half-way full with DI water and gently shake the flask to dissolve the crystals. Then fill the flask to the 1 L mark with DI water and mix by inversion.

Preparation of standards from stock solutions:

All of these dilutions are prepared in the same way. Wear clean (rinsed) latex examination gloves when preparing the standards to prevent contamination.

Use a clean pipette tip and pipette the appropriate of stock solution into a clean volumetric flask of the specified size. Fill the flask with DI water to the fill line. Mix thoroughly.

Transfer the solution to the appropriately labeled standard solution to two or three polyethylene bottles, using a small portion of standard to rinse the bottle prior to filling them. Leave one bottle in the CSU lab and take one or two bottles to the field for on-site use.

Anion Standards

Standard Number	Concentration	Volume of Stock/flask
1	2 μN NO_3^-/ 2 μN $SO4^{2-}$ / 1 μN Cl^-	50 μl/250 ml
2	10/10/5 μN	100 μl/100 ml
3	20/20/10 μN	200 μl/100 ml
4	40/40/20 μN	400 μl/100 ml
5	100/100/50 μN	1000 μl/100 ml
6	200/200/100 μN	2000 μl/100 ml

Cation Standards

Standard Number	Concentration	Volume of Stock/flask
1	2 μN NH_4^+/1 μN Na^+/1 μN K^+/1 μN Ca^{2+}/1 μN Mg^{2+}	50 μl/250 ml
2	4/2/2/2/2 μN	40 μl/100 ml
3	8/4/4/4/4 μN	80 μl/100 ml
4	20/10/10/10/10 μN	200 μl/100 ml
5	30/15/15/15/15 μN	300 μl/100 ml
6	40/20/20/20/20 μN	400 μl/100 ml
7	80/40/40/40/40 μN	800 μl/100 ml
8	120/60/60/60/60 μN	1200 μl/100 ml
9	160/80/80/80/80 μN	1600 μl/100 ml

11.3 QC samples and standards

The following types of QC samples/standards are analyzed as part of each IC run.

- 10% of samples are run in duplicate to establish measurement precision.
- Dilutions of NIST-traceable standards purchased from Dionex are analyzed to establish measurement accuracy for each ion.
- Low level standards and blanks/DI water are analyzed to establish analytical detection limits.
- One calibration standard (anion standard 5, cation standard 7) is run after every 10 samples to measure calibration drift within a run and to establish changes in instrument response between runs.
- Several calibration standards are reanalyzed at the end of each IC run as a second check on calibration drift.

11.4 Sample analysis schedules

For each IC run, the following analysis schedule should be used. Additional test or control samples may be added at the operator's discretion.

Injection 1:	DI water	DI water
Injection 2:	Anion standard 5	cation standard 7
Injection 3:	DI water	DI water
Injections 4 to n	Anion standards 1-6	Cation standards 1-9
Injection n+1	DI water	DI water
Injection n+2 to n+m	Dionex check standards	Dionex check standards
Injection n+m to n+m+11	Samples 1-10 plus 1 replicate	Samples 1-10 plus 1 replicate
Injection n+m+12	Anion standard 5	Cation standard 7
Injection n+m+13	DI water	DI water

After this continue running groups of 10 samples plus 1 replicate followed by a standard (anion standard 5 or cation standard 7) and DI water. At the end of the run, reanalyze all odd numbered calibration standards.

11.5 QC of calibrations and sample chromatograms

This is a brief overview of QC for IC analytical results. The operator should consult the CSU IC lab manuals for further detailed procedures.

- Check all chromatograms to ensure peaks are properly marked and integrated; adjust as needed following procedures in the CSU IC lab manuals.
- Make sure all peaks are identified properly; change component times as needed in the method to correct misidentification problems. See CSU IC lab manuals for details.
- Add the areas marked for all analyses of anion standard 5 or cation standard 7 to a project control chart. Changes in area exceeding 10% warrant further investigation. It is possible they represent a problem with the standard or a change in instrument response. Consult the project PI regarding what action to take.
- Make sure calibration curves for each ion fit closely to the calibration standards. The difference between the nominal and calculated value of each standard's ion concentrations should be less than 10% for concentrations greater than 10 μN.
- Compare the measured and nominal concentrations of the Dionex check standards. They should agree within 10% for concentrations exceeding 10 μN. Consult the project PI if larger discrepancies are observed.
- Make sure all standards > 10 μN analyzed during the run are within 10% of their nominal values. If they are not, response may have drifted warranting reanalysis of the entire run. Consult the project PI for appropriate action.
- Examine concentrations obtained for replicate analyses to ensure they agree within 10% for concentrations > 10 μN. Consult the project PI regarding appropriate action if they do not. Replicate concentrations will be used at the end of the study to establish measurement precision.

12. Additional QA/QC Procedures and comments

- Blanks should be taken for all filters and denuders at least once per week. Blanks are to be taken by loading denuders and filters into the sampler, leaving them there at least 1 hour, then retrieving them and processing them the same way samples are processed.

- When personnel staffing permits, duplicate denuder/filter setups should be run once per week.

- All actions taken should be recorded in the Ion Balance project log book. Entries should include date, time, and operator name.

- All log sheets should be completed fully as actions are taken. Do not wait to make log sheet entries.

- Copies of all log sheets and log book entries should be made on a weekly basis and returned to CSU for safe keeping. All IC data should be backed up weekly to a ZIP disk or CD.

- All IC results and chromatograms and all log sheets should be punched and stored in labeled 3-hole ring binders.

MOUDI Sampler

Colorado State University
Standard Operating Procedure
BRAVO, summer 1999

Overview:

The MOUDI (Micro Orifice Uniform Deposition Impactor) sampler is used to collect size-resolved airborne particulate matter. 24 hour samples will be collected at Big Bend National Park, Texas beginning at approximately 08:00 Central Standard Time. The largest 8 stages of the MOUDI are used, corresponding to the following aerodynamic diameter size ranges: (Stage 1A) 18 – 10 μm, (Stage 2A) 10 – 5.6 μm, (Stage 3A) 5.6 – 3.2 μm, (Stage 4A) 3.2 – 1.8 μm, (Stage 5A) 1.8 – 1.0 μm, (Stage 6A) 1.0 – 0.56 μm, (Stage 7A) 0.56- 0.32 μm, (Stage 8A) 0.32 – 0.176 μm. Additionally, there is an initial stage (we will call it Stage 0) that collects particles with diameter > 18 μm and a filter at the very bottom of the MOUDI (called the after-filter) that collects particles < 0.176 μm. We are not using an after-filter. Analysis of the collected size-resolved PM will focus on quantification of the primary ionic species, e.g., nitrate, sulfate, ammonium, chloride, sodium, etc… MOUDI samples will be analyzed for a subset of periods when $PM_{2.5}$ aerosol chemistry measurements indicate a significant presence of both sodium and sulfate.

How does this sampler work?

The MOUDI sampler is a sequential impaction device. It works as follows:

1. A pump pulls the ambient air through an inlet which is on the roof of the CSU BRAVO chemistry trailer. This inlet is covered with a rain shield and some aluminum bug screen.
2. The air flow is then pulled into the MOUDI sampler housing, where 9 aluminum foil impaction surfaces collect 9 size ranges of PM.
3. There are 2 magnehelics in the MOUDI sampler housing. The upper magnehelic (Magnehelic 1) measures the pressure drop across several stages. The manufacturer prescribes setting Magnehelic 1 to 20.7 inches of water, which should correspond to a 30 l/min flow rate through the MOUDI. The lower magnehelic (Magnehelic 2) measures the difference in pressure between the final stage and the ambient environment. Magnehelic 2 should read 21 inches of water when Magnehelic 1 is set to 20.7 inches of water. Magnehelic 2 is designed to be used to determine if there is a problem (clogging or leaking) inside the MOUDI sampler. If Magnehelic 2 increases from 21, but Magnehelic 1 is still at 20.7, clogging is likely present. A low reading on magnehelic 2 suggests a leak has developed.
4. After air has transited the impaction stages and leaves the MOUDI sampler housing, the air flow is pulled through the "flow determination tubing" that leads to the pump, which is under the trailer. During this stretch, the air flow goes through Magnehelic 3, then a dry gas meter, followed by a flow control valve. Magnehelic 3 and the dry gas meter will be used with an elapsed time meter to determine the total air volume pulled through the MOUDI and to check the manufacturer's 30 l/min flow rate.

****Reminder:** This sampler is used to quantify trace levels of inorganic ionic compounds found in the airborne PM, so it is very important not to contaminate the sampler with inorganic compounds – DO NOT TOUCH the inside of the sampler or the impaction surfaces with your hands! Impaction surfaces need to be handled with clean stainless steel tweezers.

Sampling scheme for BRAVO:

We will be collecting 24 hr samples with the MOUDI, so impaction surfaces will be changed once a day. Impaction surfaces that are sampling the ambient air will be switched at the specified time – approximately 8 am CST every day. We have several extra impaction surface holders, so at 8 am (or as close as possible) we will remove the "used" impaction surface holders from the MOUDI and load the "new" impaction surface holders in the MOUDI. Because we don't have two full sets of good impaction surface holders (some of the rings pop off easily in the MOUDI vacuum), some impaction surface holders will need to be unloaded and reloaded to start the next sample. After the new impaction surfaces are readied, the MOUDI is reassembled and sampling is started. Once the MOUDI is running, remove any remaining "used" impaction surfaces from the impaction surface holders and place them into newly labeled petri dishes. At the same time, load new impaction surfaces onto the available impaction surface holders and put these holders in a clean plastic tupperware container– ready to be loaded onto the MOUDI the following day. One day a week (typically Monday), we will not run the MOUDI, but collect blanks and clean.

How do I operate the MOUDI?

At 8 am every day:

1. Deal with the other samplers (URG, organic aerosol, and SEM denuder/filter samplers) 1st, then go to the MOUDI.
2. Take out the MOUDI log sheet and record the final magnehelic readings for all 3 magnehelics.
3. Record the dry gas meter reading.
4. Close the flow control valve.
5. Unplug the MOUDI pump.
6. Record the stop time.
7. Go to the MOUDI pump box and record the elapsed time meter reading.
8. Zero the elapsed time meter – i.e., press the red button on the elapsed time meter.
9. Go back into the trailer, it is now time to change the impaction surface holders.

10. Tear off a new, big piece of aluminum foil. This will be your work surface, and you should make it as long as the piece of tape on the MOUDI table. Set it out right in front of the piece of tape. This piece of tape is labelled "top", "0", "1", "2", …, "8" so that you can easily keep track of the MOUDI stages.
11. Remove the tubing from the MOUDI sampler housing. Get the yellow handled nut wrench out. Loosen the hose clamps at the top and bottom of the MOUDI sampler housing. Gently pull off these tubes. Also pull off the tubes that go to Magnehelics 1 and 2.
12. Briefly flip down the switch at the lower left hand corner of the MOUDI sampler housing. This will cause the MOUDI stages to rotate out of their snug fit into the housing.
13. Once the MOUDI stages are free, with 2 hands pull the stages out and set them on the aluminum foil work surface.
14. Get out and open the tupperware that contains the clean and "new" impaction surface holders.
15. Pull apart the MOUDI stages. Only touch the outside of the stages. Set each stage on the aluminum foil work surface in front of the corresponding stage number that is on the tape, so you would put the top stage in front of the "0", the next stage in front of the "1" and so on.
16. Get out a pair of clean tweezers.
17. Using the tweezers, pull the impaction surface holders off of each stage and place each directly in front of the corresponding stage.
18. Put a pair of new latex gloves on and rinse with DI water from the Barnstead EasyPure system (new latex gloves are not clean). Air dry.
19. Using the tweezers, load a "new" impaction surface holder from the tupperware onto each stage except the bottom one. Some holders are marked with the position they work well in (the vacuum is higher in the higher numbered stages; some impaction surface holder rings pop up under this higher vacuum and should only be used on lower numbered stages). The bottom impaction surface holder (stage 8) needs to be reused. Unload this surface, place the "used" impaction surface into the appropriate, labeled petri dish, reload the impaction surface holder with a clean impaction surface

and load onto the bottom MOUDI stage. Procedures for loading/unloading impaction surfaces are specified below.

20. Put the stages back together in the correct order. This should be easy since they are sitting in front of you in descending order.
21. Place the stages back into the housing. Try to make the stacked stages sit against the gears.
22. Reconnect all the tubes. Be sure to snug down the hose clamps.
23. Briefly flip up the switch in the lower left hand corner of the housing. This will cause the stages to rotate together and snug in place firmly.
24. Record the new sample name on the log sheet. The sample name = BBMMDDM where BB stands for Big Bend, MM stands for month (e.g., July = 07), DD stands for the day of the month on which the sample is started (e.g., july 4^{th} = 04), M stands for MOUDI. Individual impaction foils will be named in the same way except the impaction stage number (0-8) will be appended to the end.
25. Record the initial dry gas meter reading.
26. Plug the pump back in.
27. SLOWLY open the flow control valve until Magnehelic 1 is reading 20.7 inches of water. (Note: Magnehelic 2 should be reading 21" H_2O when you do this. If it reads higher you have a problem with one of your impaction surfaces and you need to take the MOUDI apart and realign the impaction surfaces. If an impaction surface has "popped up" it needs to be replaced with a new one. If Magnehelic 2 reads less than 20" it is likely a like has developed and you will need to regrease the MOUDI o-rings as outlined in the cleaning section.)
28. Record the start time.
29. Record the initial magnehelic readings for all 3 magnehelics.
30. Good work, now you are 1/2 way done. You must now load/unload the impaction surfaces from the impaction surface holders that you just removed from the MOUDI. Since these are currently sitting out in the open, you must do this right away.

Load/unloading impaction surfaces from the impaction surface holders:

1. Get out the 8 remaining empty petri dishes that used to contain these aluminum foil impaction plates. Label each with the names of the samples that you are about to remove (or just removed) from the sampler. Sample names= BBMMDDMS where BB stands for Big Bend, MM stands for month (e.g., July = 07), DD stands for the day of the month the sample was started (e.g., july 4^{th} = 04), M stands for MOUDI, and S stands for Stage number (which will be 0-8). If you do this early in the morning or the previous day, it is easier.
2. Get 8 new petri dishes with unused impaction sufaces. Each aluminum foil impaction surface has been sprayed with Silicon grease and baked; it is important to make sure that you do not flip the petri dishes over.
3. Put a pair of clean gloves on, rinse with DI water, and air dry.
4. Time to swap out the "used" impaction surfaces for the "new" impaction surfaces. With the tweezers and the dental pick, pull off the ring that holds the impaction surface onto the impaction surface holder. Using the tweezers, take off the "used" impaction surface and place into the corresponding labelled petri dish. Using the tweezers, place a "new" impaction surface into the impaction surface holder. Using the tweezers and dental pick, place the hold down ring over the impaction surface and press down firmly to seal it in place. Close the petri dishes. This is a rather involved step that takes some tweezer and dental pick practice.
5. Repeat step 5 for each impaction surface holder.
6. Using the tweezers, put the impaction surface holders back into the tupperware container and seal it.
7. Place the dental pick and tweezers into the "dirty utensil tupperware".
8. Put the petri dishes with the "used" impaction surfaces into the MOUDI petri dish box in the refrigerator. Be sure they stay upright. Log these into the inventory sheet that is in the box.
9. Record the actions taken, the time, and your name in the BRAVO Ion Balance log book. If you had any problems during your switch, please write them down both in the log book and on the MOUDI log sheets.
10. Crumple up the just-used aluminum foil surface and dispose.

*** If you drop the new aluminum foil impaction surface on anything but the clean aluminum foil surface, you need to throw it away and start over.

*** If you drop a "used" impaction surface, pick it up as fast and as cleanly as possible. Record exactly what happened on the MOUDI log sheet and in the Ion Balance log book.

Every Monday:

Take a blank. You should do the same thing that you do every other day, but do not plug the MOUDI pump in. Come back to the MOUDI a little later (time delay is up to you), and swap the impaction surfaces out again. Label the blanks that you pull out of the MOUDI as "BBMMDDMSBLK", where BB stands for Big Bend, MM stands for the month (06 = June), DD stands for the day of the month, and MS = S^{th} stage of MOUDI, and BLK = blank. You also will be cleaning, so before you install tomorrow's impaction surfaces, take the MOUDI apart.

➔ Clean the utensils, tupperware, impaction surface holders, and the MOUDI stages.

How to clean (i.e., get rid of the inorganic ionic species):

1. Locate the following items: Aluminum foil, latex gloves, DI water from the Barnstead EasyPure system, a plastic wash tub, dilute Triton X-100 solution, Q-tips, and plastic bags which can be used to cover everything while they dry. All of these items should be under the MOUDI table.
2. Spread out a piece of new aluminum foil to use as a work surface.
3. Put on the latex gloves and rinse with DI.
4. You need to determine how dirty the MOUDI is so you will know if you have to scrub the stages with soap and a Q-tip. Look at the underside of the first and last stage (stages 0 and 8). Do you see dirt around the nozzle holes? If you do, then you need to scrub. If you do not, then don't worry about the soap and Q-tips (i.e., skip ahead to step 7)

5. Fill the wash tub with DI and a small amount of Triton soap. Now scrub the underside each stage with a Q-tip in the soapy water.
6. Rinse the soapy water off completely with DI water.
7. Rinse and fill the wash tub and each tupperware container with DI.
8. Soak all the stages in the tub of DI water, and soak all the items contained in the tupperware in their respective tupperware. Rinse the tupperware a few extra times after finishing with everything else.
9. Rinse each piece thoroughly with DI after you have let them soak for at least 1 hr. Only touch the pieces with clean tweezers or tongs.
10. After rinsing, set each piece out on the aluminum foil to air dry. Place a clean plastic bag over the pieces as they dry.
11. Once dry, reassemble the sampler. Again, remember that you must use tweezers. You can't touch impaction surface holders. You can touch the outside of the stages, this will make it easier to reassemble.
12. Following cleaning, the MOUDI o-rings should be regreased with the silicone grease from the MOUDI accessories box. Remove the double O-rings from the side of each MOUDI stage. Apply a small amount of grease to your fingers and grease each O-ring, getting more grease as needed. Put the O-rings back onto the MOUDI. It is best to remove, grease, and replace O-rings one stage at a time. Disassemble the after-filter stage and grease those O-rings as well.
13. Once it is all put back together, load a new set of impaction surfaces and get ready for sampling at 8 am tomorrow.

When to clean:

Blanks should be taken and cleaning performed on a weekly basis. The exact day is unimportant, but Monday generally works best with the rest of the BRAVO activity schedule. This day can be changed if needed.

If you drop or touch the impaction surface holder, an impaction surface hold down ring, or the inside of the stages, then you need to clean them.

Shipping:

Make a copy of the petri dish box inventory sheet and put the copy in the MOUDI Sampler Notebook with the log sheets. Put the original back in to the box and tape the box shut. The petri dish box will be express shipped back to CSU in an insulated container with gel ice packets or dry ice or may be hand carried by BRAVO personnel. The dishes should be loaded with the collection surfaces facing up (so that the grease does not readily contact the petri dish lid) and the shipping box should be labeled "Keep Upright" and the top indicated.

Troubleshooting:

Remember to record any problems and attempts to solve them in both the Ion Balance project log book and on the MOUDI log sheet.

The pump is not working.

Solution: Replace the pump. We brought 1 spare pump. You should be able to unscrew the nuts from underneath the pump box and pull the "dead" pump out of the pump box. The new pump should fit in the pump box as well as the old pump.

The elapsed time meter does not read 24 hrs after the day of sampling (accounting for any difference due to a non-08:00 start or stop time).

Solution: The pump has an automatic thermal shut down – i.e., if the pump gets too hot the pump will automatically shut down until it has cooled down. If this occurs, the elapsed time meter will show an elapsed time less than 24 hrs for the day long sample. Please record this info on the log sheet and in the log book.

The fan is not working.

***Solution*:** Check the wire connections. If they are intact and the fan still isn't working, then you need to replace the fan. Spare fans should be located with the spare pumps.

The elapsed time meter is dead.

Solution: Check the wire connections. If they are intact and the elapsed time meter still isn't working, then you need to replace it. Spare elapsed time meters should be located with the spare pumps.

The magnehelic 2 reading exceeds 21" H_2O when the sample is started.

Solution: It is likely one of the impaction surface holder rings and/or the impaction surface has popped up. Close the flow valve, unplug the pump, and disassemble the MOUDI. Replace any impaction surfaces that have popped up. Reassemble and restart the MOUDI (be sure to SLOWLY open the flow valve when starting), checking to ensure readings are now

OK. Record the new start time and all actions on the log sheet and in the log book.

The magnehelic 2 reading is less than ~20" H_2O when the sample is started.

Solution: It is likely a leak has developed between stages or in the after-filter assembly. Close the flow valve, unplug the pump and disassemble the MOUDI. Remove impaction surface holders, regrease O-rings (as outlined above) and reassemble, making sure the after-filter assembly is tightly attached (the two bottom tube attachment points should be aligned). Restart the MOUDI and record the new start time and all actions on the log sheet and in the log book.

The magnehelic reading increased substantially during sampling.

***Solution*:** It is likely a clog developed during sampling or an impaction surface may have popped off. Please note the problem and any observations of possible causes on the log sheet and in the Ion Balance project log book.

Appendix C : URG sampler and MOUDI logsheet

MOUDI Log Sheet

Sample name :_____ Date :_____

Start time : _____

Initial Dry Gas Meter reading : _____ m^3

Initial Magnehelic 1 reading :_____ inches of H_2O
(Adjust flow valve so that Magnehelic 1 reads 20.7 inches of H_2O)

Initial Magnehelic 2 reading : _____ inches of H_2O
(Magnehelic 2 should read 21 inches of H_2O, if it doesn't you have a leak or a log and you need to reload the impaction surface)

Initial Magnehelic 3 reading : _____ PSI

Note : Remember to zero the elapsed time meter

Stop time : _____

Final Dry Gas Meter reading : _____ m^3

Final Magnehelic 1 reading :_____ inches of H_2O

Final Magnehelic 2 reading : _____ inches of H_2O

Final Magnehelic 3 reading : _____ PSI

Elapsed time meter : _____ Min

Comments

Log sheet (Denuder)

Operator(s):

BLK	Date	Channel	Start Time	Stop time	Initial volume (Dry meter)	Final volume (Dry meter)	Total sampling volume		Sample Name	Serial Num. (Filter Holder, Denuder)	Extract Date/time	Aliquot
								Teflon			Batch:	Anion, Cation
Commets					Initial Vacuum	Final Vacuum	Elapsed Time	Nylon			Batch:	Anion
								Glass fiber		Batch:		Cation
					Set Flow	Reading Flow	Temp AM/PM	Denuder 1 (Nitric Acid)		Batch:	Batch:	Anion
								Denuder 2 (Ammonia)		Batch:	Batch:	Cation
BLK	Date	Channel	Start Time	Stop time	Initial volume (Dry meter)	Final volume (Dry meter)	Total sampling volume		Sample Name	Serial Number	Extract Date/time	Aliquot
								Teflon			Batch:	Anion, Cation
Comments					Initial Vacuum	Final Vacuum	Elapsed Time	Nylon			Batch:	Anion
								Glass fiber		Batch :		Cation
					Set Flow	Reading Flow	Temp AM/PM	Denuder 1 (Nitric Acid)		Batch:	Batch:	Anion
								Denuder 2 (Ammonia)		Batch:	Batch:	Cation

Sample : BB0701T1 -> BB : Project Name, 0701 : Date, T(Teflon), G(Glass), N(Nylon), DA(Denuder for NH_3), and DN(Denuder for NO_3), 1 or 2:Channel 1, 2

Blank : BB0701TB1 -> BB : Project Name, 0701 : Date, T(Teflon), G(Glass), N(Nylon), DA(Denuder for NH_3), and DN(Denuder for NO_3), B: Blank, 1 or 2:Channel 1 or 2

Batch sheet

Operator :

Filter	Batch Num.	Date	Num.	Batch Num.	Date	Num	Batch Num.	Date	Num.	Comments
Glass fiber filter										For 1 week (11 each Sunday)
Coating Solution	Batch Num.	Date	Vol.	Batch Num.	Date	Vol.	Batch Num.	Date	Num.	Comments
Denuder 1										For 2 weeks (200 mL Sunday)
Denuder 2										For 2 weeks (200mL Sunday)
Glass fiber filter (Citric Acid)										For 1 month (100mL Sunday)
NH3 Remover (Cittric Acid))										For 2 months (500mL Sunday)
Extracting Solution	Batch Num.	Date	Vol.	Batch Num.	Date	Vol.	Batch Num.	Date	Num.	Comments
0.1 N HClO4										For 2 months (Transfer into small bottle, Sunday)
0.0001N HClO4										Daily (100mL Tuesday, Friday)
Ethanol										Daily(Transfer into small bottle, Tuesday and Friday)
Nylon filter (IC Eluent)										For 1 month(250mL Sunday)
Glass fiber Filter (DI Water)										Daily (Fresh DI Water)
Analysis Solution	Batch Num.	Date	Vol.	Batch Num.	Date	Vol.	Batch Num.	Date	Num.	Comments
IC Eluent(Anion)										Daily (2L, Friday)
IC Eluent(Cation)										Daily (2L, Tuesday)

BRAVO Ion Balance Project Summer/Fall 1999

Big Bend National Park, Texas

Log sheet (pH measurement)

Sample name	pH of sample	Operator Name	Date of pH measurement	pH meter Calibration Slope	pH of Calibration curve							
					# 1	# 2	# 3	# 4	# 5	# 6	# 7	# 8
					# of Batch (Working H_2SO_4 STD) :							
					# 1	# 2	# 3	# 4	# 5	# 6	# 7	# 8
					# of Batch (Working H_2SO_4 STD) :							
					# 1	# 2	# 3	# 4	# 5	# 6	# 7	# 8
					# of Batch (Working H_2SO_4 STD) :							

Appendix D: URG data tables

Table D1. BRAVO BBNP $PM_{2.5}$ Raw data for Anion and Cation (URG)

Date	Sample Name	Extract Volume (L) For filter	Extract Volume (L) For Denuder	Sampling Gas Vol (m^3)	Cl^- $\mu g/m^3$ Teflon	NO_3^- $\mu g/m^3$ Teflon	$N[NO_3^-]$ $\mu g/m^3$ Nylon	Total NO_3^- $\mu g/m^3$ Teflon+Nylon	SO_4^{2-} $\mu g/m^3$ Teflon	Na^+ $\mu g/m^3$ Teflon	NH_4^+ $\mu g/m^3$ Teflon	K^+ $\mu g/m^3$ Teflon	Mg^{2+} $\mu g/m^3$ Teflon	Ca^{2+} $\mu g/m^3$ Teflon	NH3 ug/m3 Denuder	HNO_3 $\mu g/m^3$ Denuder
7/1	BB0701	0.006	0.01	16.203	0.03465	0.23685	0.03236	0.26921	2.64851	0.17962	0.72112	0.04314	0.04023	0.15226	0.43249	0.63544
7/2	BB0702	0.006	0.01	17.069	0.16437	0.26559	0.06994	0.33553	1.22457	0.23355	0.30316	0.02515	0.04866	0.14736	0.31778	0.32746
7/3	BB0703	0.006	0.01	16.004	0.17676	0.15870	0.08504	0.24375	0.56138	0.15255	0.12348	0.00850	0.02387	0.04222	0.26017	0.11221
7/4	BB0704	0.006	0.01	16.364	0.03548	0.05999	0.04704	0.10704	0.28887	0.04889	0.10225	0.00545	0.00909	0.01337	0.47820	0.10050
7/4	BB0704	0.006	0.01	15.378	0.05111	0.05127	0.06046	0.11172	0.31170	0.05382	0.10811	0.00961	0.00825	0.02088	0.30842	0.08359
7/6	BB0706	0.006	0.01	15.562	0.07627	0.22749	0.12450	0.35200	0.76133	0.14483	0.20524	0.00648	0.03491	0.07286	0.37765	0.15468
7/8	BB0707	0.006	0.01	16.753	0.04456	0.23507	0.11299	0.34806	1.24109	0.11905	0.28212	0.02044	0.02886	0.10241	0.30303	0.21176
7/9	BB0709	0.006	0.01	17.056	0.01297	0.14063	0.12493	0.26557	2.20452	0.08475	0.54356	0.01155	0.01911	0.08769	0.28147	0.42930
7/10	BB0710	0.006	0.01	15.714	0.03736	0.11052	0.17252	0.28304	2.57779	0.09199	0.74855	0.01538	0.02612	0.12525	0.26758	0.20411
7/11	BB0711	0.006	0.01	15.713	0.04860	0.03337	0.07810	0.11147	0.85337	0.03994	0.32759	0.03553	0.00807	0.04790	0.24808	0.12712
7/11	BB0711	0.006	0.01	15.002	0.00638	0.02479	0.07610	0.10089	0.84735	0.01223	0.32645	0.01251	0.00039	0.01274	0.17561	0.15037
7/12	BB0712	0.006	0.01	16.473	0.03370	0.14967	0.11897	0.26865	2.32593	0.10500	0.64303	0.01396	0.02417	0.09343	0.21648	0.26088
7/13	BB0713	0.006	0.01	16.265	0.10043	0.18154	0.16691	0.34845	1.12747	0.14434	0.27709	0.01197	0.02493	0.07481	0.33935	0.20301
7/14	BB0714	0.006	0.01	16.945	0.07720	0.14156	0.12137	0.26292	1.13441	0.10493	0.27734	0.01966	0.02436	0.07486	0.49468	0.14020
7/15	BB0715	0.006	0.01	15.502	0.06627	0.19048	0.16817	0.35864	1.58229	0.11434	0.39929	0.01967	0.02352	0.14426	0.52084	0.17804
7/16	BB0716	0.006	0.01	16.667	0.07325	0.20973	0.16488	0.37462	1.68128	0.12927	0.38091	0.01858	0.02940	0.16274	0.46071	0.24725
7/17	BB0717	0.006	0.01	15.761	0.06046	0.13496	0.12482	0.25978	1.09002	0.09968	0.27695	0.01354	0.01587	0.09139	0.33463	0.18311
7/18	BB0718	0.006	0.01	16.818	0.02605	0.04157	0.06965	0.11122	0.37886	0.03600	0.10760	0.00739	0.00668	0.01501	0.28342	0.17497
7/18	BB0718	0.006	0.01	15.676	0.03216	0.03819	0.08185	0.12004	0.39142	0.03968	0.12235	0.00359	0.00651	0.00575	0.23477	0.17325
7/19	BB0719	0.006	0.01	16.756	0.05966	0.15669	0.05837	0.21506	0.66308	0.08948	0.18861	0.01008	0.01880	0.13088	0.30491	0.13576
7/20	BB0720	0.006	0.01	15.720	0.09499	0.12704	0.15141	0.27844	0.80905	0.09187	0.17929	0.01015	0.02073	0.09897	0.18710	0.14832
7/21	BB0721	0.006	0.01	16.793	0.02749	0.08061	0.07662	0.15723	0.90847	0.06900	0.24775	0.00587	0.00960	0.02742	0.22990	0.19550
7/22	BB0722	0.006	0.01	15.186	0.03992	0.09893	0.10750	0.20643	1.26595	0.06912	0.30631	0.01189	0.01287	0.04901	0.62350	0.12469

7/23	BB0723	0.006	0.01	16.041	0.11642	0.22951	0.15996	0.38947	1.72264	0.17713	0.41730	0.02676	0.04327	0.20589	0.38940	0.16459
7/24	BB0724	0.006	0.01	16.449	0.12439	0.24462	0.17114	0.41576	1.50658	0.18566	0.35952	0.02795	0.04482	0.28017	0.26825	0.15821
7/25	BB0725	0.006	0.01	15.562	0.09403	0.24924	0.11303	0.36227	1.56857	0.16415	0.39030	0.02985	0.05159	0.32890	0.18483	0.18585
7/25	BB0725	0.006	0.01	16.294	0.09595	0.24124	0.10681	0.34805	1.34818	0.16253	0.36586	0.02836	0.05025	0.32859	0.12542	0.16358
7/26	BB0726	0.006	0.01	17.254	0.05227	0.11013	0.11423	0.22436	2.49271	0.09497	0.60776	0.01298	0.02795	0.14647	0.15343	0.23409
7/27	BB0727	0.006	0.01	16.050	0.05089	0.05769	0.08387	0.14156	3.10593	0.07709	0.78167	0.01359	0.01872	0.05221	0.13995	0.26264
7/28	BB0728	0.006	0.01	17.247	0.03083	0.02738	0.07180	0.09919	2.73000	0.05111	0.70643	0.01143	0.00934	0.05103	0.22701	0.31567
7/29	BB0729	0.006	0.01	15.721	0.02097	0.00260	0.04613	0.04873	2.07788	0.03650	0.57582	0.01433	0.00867	0.04444	0.34231	0.35433
7/30	BB0730	0.006	0.01	17.183	0.01263	0.01169	0.04199	0.05367	1.21928	0.00642	0.31544	0.00437	-0.00017	0.03688	0.39833	0.45547
7/31	BB0731	0.006	0.01	16.224	0.01075	0.00550	0.02430	0.02980	1.19365	0.01437	0.31433	0.00217	0.00369	0.02697	0.21402	0.39770
8/1	BB0801	0.006	0.01	16.837	0.03095	0.03799	0.08371	0.12170	3.60844	0.06365	1.06606	0.01143	0.01663	0.07812	0.36039	0.44237
8/1	BB0801	0.006	0.01	15.891	0.03346	0.04914	0.08378	0.13292	3.71381	0.05737	1.08214	0.03100	0.00908	0.07210	0.30981	0.46036
8/2	BB0802	0.006	0.01	16.541	0.07162	0.16232	0.16345	0.32577	2.93721	0.15060	0.70477	0.03723	0.03394	0.15127	0.25924	0.26705
8/3	BB0803	0.006	0.01	15.412	0.08626	0.22633	0.22392	0.45026	4.06395	0.18822	0.81617	0.02938	0.04807	0.22406	0.14210	0.45220
8/4	BB0804	0.006	0.01	15.156	0.05164	0.14452	0.23236	0.37688	4.52899	0.13269	0.69568	0.02802	0.03348	0.12598	0.07045	0.80449
8/5	BB0805	0.006	0.01	15.845	0.02953	0.05046	0.06313	0.11359	2.40320	0.07748	0.76927	0.02369	0.01528	0.08817	0.35801	0.73333
8/6	BB0806	0.006	0.01	17.471	0.02654	0.04172	0.06896	0.11068	2.45039	0.05432	0.69766	0.01450	0.00810	0.05505	0.06950	0.69428
8/7	BB0807	0.006	0.01	16.186	0.02655	0.05836	0.06893	0.12729	3.15900	0.06017	0.88086	0.01638	0.00725	0.08580	0.10679	0.69687
8/8	BB0808	0.006	0.01	17.247	0.02183	0.05843	0.10393	0.16236	4.30770	0.06494	1.11421	0.01986	0.01340	0.12270	0.07830	0.74607
8/8	BB0808	0.006	0.01	16.093	0.02511	0.06817	0.10029	0.16846	4.39712	0.07020	1.13694	0.01997	0.01599	0.12231	0.04995	0.79056
8/9	BB0809	0.006	0.01	17.190	0.03217	0.08285	0.10535	0.18821	3.64264	0.08545	0.81508	0.02122	0.01917	0.11771	0.05543	0.51648
8/10	BB0810	0.006	0.01	16.437	0.03183	0.09072	0.07828	0.16900	1.80280	0.06697	0.45710	0.03825	0.01078	0.08668	0.10910	0.43856
8/11	BB0811	0.006	0.01	14.420	0.04676	0.07737	0.07995	0.15731	1.62748	0.08188	0.50723	0.01155	0.01269	0.10347	0.12436	0.41950
8/12	BB0812	0.006	0.01	16.491	0.03476	0.06574	0.06855	0.13429	1.57483	0.08013	0.46237	0.00711	0.01256	0.16704	0.32592	0.44726
8/13	BB0813	0.006	0.01	16.934	0.05250	0.14077	0.06698	0.20775	1.66421	0.12927	0.42542	0.00887	0.02196	0.11077	0.11515	0.47036
8/14	BB0814	0.006	0.01	16.513	0.06749	0.19795	0.04459	0.24254	1.55968	0.14242	0.44044	0.02472	0.02985	0.20467	0.08653	0.33313
8/15	BB0815	0.006	0.01	17.103	0.04054	0.17329	0.06697	0.24026	1.55489	0.10791	0.46467	0.02510	0.03172	0.25968	0.07936	0.46090
8/15	BB0815	0.006	0.01	16.338	0.04752	0.18608	0.07033	0.25641	1.57923	0.11794	0.47372	0.02757	0.03722	0.28546	0.06202	0.48210
8/16	BB0816	0.006	0.01	17.041	0.02696	0.14076	0.14076	0.28152	4.46351	0.13570	0.98970	0.03338	0.03273	0.19107	0.09479	0.90227
8/17	BB0817	0.006	0.01	16.230	0.01861	0.06301	0.08776	0.15077	4.56028	0.07760	1.01639	0.02154	0.01608	0.09912	0.06086	1.43229
8/18	BB0818	0.006	0.01	16.945	0.01192	0.05157	0.06386	0.11544	2.63297	0.08246	0.69794	0.01329	0.01312	0.06528	0.18191	0.58496
8/19	BB0819	0.006	0.01	16.372	0.03196	0.09676	0.09335	0.19012	2.72457	0.10287	0.53586	0.01089	0.01639	0.07645	0.16768	0.71587

8/20	BB0820	0.006	0.01	17.061	0.00736	0.04294	0.09111	0.13405	5.96522	0.05789	1.08644	0.01458	0.00692	0.06787	0.06558	1.39464
8/21	BB0821	0.006	0.01	16.428	0.02538	0.04075	0.08376	0.12450	6.59521	0.06549	1.76025	0.03113	0.00972	0.10656	0.04126	1.55539
8/22	BB0822	0.006	0.01	17.127	0.03067	0.04191	0.08164	0.12354	5.25029	0.04792	1.50359	0.02397	0.00766	0.06837	0.03291	1.26339
8/22	BB0822	0.006	0.01	16.155	0.03278	0.03890	0.07596	0.11487	5.42427	0.06173	1.55281	0.03064	0.00636	0.19060	0.02488	1.53719
8/23	BB0823	0.006	0.01	16.798	0.04191	0.08501	0.10560	0.19062	2.54130	0.10835	0.71430	0.00475	0.01378	0.03221	0.09768	1.04887
8/24	BB0824	0.006	0.01	15.428	0.01048	0.03350	0.07159	0.10509	1.12137	0.03505	0.41277	0.00335	0.00293	0.00647	0.17440	0.19727
8/25	BB0825	0.006	0.01	16.070	0.01165	0.03309	0.06248	0.09558	1.91466	0.04386	0.53625	0.00818	0.00662	0.00748	0.26017	0.30115
8/26	BB0826	0.006	0.01	16.127	0.03310	0.04866	0.09547	0.14412	2.05378	0.09665	0.62777	0.01658	0.01167	0.00596	0.24615	0.34228
8/27	BB0827	0.006	0.01	16.777	0.03246	0.05630	0.08866	0.14497	1.38992	0.09364	0.42623	0.01580	0.01039	0.01584	0.35335	0.44433
8/28	BB0828	0.006	0.01	16.269	0.03308	0.06377	0.06332	0.12709	0.85855	0.09114	0.29703	0.01211	0.01013	0.02927	0.24944	0.36020
8/29	BB0829	0.006	0.01	16.866	0.02951	0.04035	0.07056	0.11091	1.54928	0.07728	0.49175	0.01460	0.00852	0.02089	0.20972	0.52156
8/29	BB0829	0.006	0.01	16.125	0.02638	0.04197	0.06988	0.11185	1.56206	0.07707	0.50280	0.01455	0.00900	0.01901	0.23520	0.50919
8/30	BB0830	0.006	0.01	16.979	0.01603	0.03110	0.05914	0.09024	2.51263	0.05183	0.74090	0.00988	0.00743	0.01576	0.20913	0.90220
8/31	BB0831	0.006	0.01	16.100	0.02219	0.02356	0.07253	0.09609	4.91725	0.03907	1.35067	0.01428	0.00530	0.05086	0.10292	1.01388
9/1	BB0901	0.006	0.01	16.890	0.01461	0.02268	0.06055	0.08323	8.56818	0.03079	2.03656	0.02167	0.00453	0.06108	0.07179	1.26919
9/2	BB0902	0.006	0.01	16.070	0.02819	0.02661	0.08516	0.11178	6.03330	0.04043	1.61779	0.02219	0.00486	0.05492	0.11668	0.81484
9/3	BB0903	0.006	0.01	17.223	0.02038	0.02872	0.06305	0.09177	5.13420	0.04861	1.46173	0.02220	0.00796	0.05780	0.17244	0.62599
9/4	BB0904	0.006	0.01	15.658	0.00163	0.03515	0.11424	0.14939	3.15418	0.06440	0.98465	0.01453	0.00792	0.09483	0.27484	0.38513
9/5	BB0905	0.006	0.01	16.850	0.04759	0.10704	0.11388	0.22093	1.00233	0.11076	0.29567	0.00724	0.01294	0.02740	0.35415	0.25131
9/6	BB0906	0.006	0.01	16.594	0.03538	0.04774	0.09413	0.14186	0.56592	0.07315	0.19525	0.00530	0.00874	0.01181	0.24415	0.23088
9/7	BB0907	0.006	0.01	16.062	0.01920	0.04816	0.05788	0.10604	0.55310	0.02894	0.16192	0.00979	0.00704	0.02148	0.18104	0.25344
9/8	BB0908	0.006	0.01	16.929	0.01445	0.03822	0.05492	0.09314	1.13749	0.03080	0.30515	0.00776	0.00693	0.01335	0.17524	0.23301
9/9	BB0909	0.006	0.01	15.937	0.02923	0.05273	0.07863	0.13137	1.26286	0.06102	0.36053	0.00707	0.00773	0.00317	0.15633	0.28961
9/10	BB0910	0.006	0.01	16.550	0.02750	0.05955	0.07954	0.13909	1.19488	0.07118	0.37034	0.01120	0.00987	0.02129	0.17596	0.32477
9/11	BB0911	0.006	0.01	8.794	0.01862	0.05794	0.05625	0.11418	1.01680	0.02933	0.29761	0.01974	0.00630	0.00738	0.11988	0.20924
9/12	BB0912	0.006	0.01	16.129	0.00963	0.03712	0.05326	0.09038	1.13176	0.02660	0.36859	0.00945	0.00443	0.01029	0.19713	0.22464
9/12	BB0912	0.006	0.01	15.318	0.01250	0.03277	0.06846	0.10123	1.16703	0.02440	0.36140	0.01378	0.00414	0.01648	0.24036	0.24435
9/13	BB0913	0.006	0.01	15.962	0.00613	0.03169	0.10205	0.13373	4.03553	0.03068	1.18450	0.01389	0.00528	0.01009	0.08386	0.58349
9/14	BB0914	0.006	0.01	15.562	0.00820	0.03106	0.08555	0.11661	7.79636	0.04494	1.50727	0.01929	0.00900	0.08159	0.08831	0.94099
9/15	BB0915	0.006	0.01	16.590	0.03667	0.05357	0.08742	0.14099	7.13240	0.05504	1.56439	0.03266	0.00716	0.05435	0.09464	1.04601
9/16	BB0916	0.006	0.01	15.537	0.03019	0.04655	0.08808	0.13463	5.72173	0.05531	1.41789	0.04605	0.00854	0.04806	0.09240	1.19639
9/17	BB0917	0.006	0.01	16.295	0.01605	0.06413	0.08147	0.14560	2.60955	0.05409	0.66658	0.03527	0.00609	0.03247	0.07159	0.90854

9/18	BB0918	0.006	0.01	17.637	0.03570	0.05714	0.08603	0.14317	3.50210	0.06671	0.96585	0.02567	0.00868	0.04540	0.07570	0.47411
9/19	BB0919	0.006	0.01	16.824	0.03717	0.04421	0.06145	0.10566	3.02798	0.06567	0.77949	0.02231	0.00997	0.04431	0.14647	0.47454
9/19	BB0919	0.006	0.01	15.914	0.02967	0.04533	0.06800	0.11333	3.40442	0.05989	0.83332	0.02167	0.00747	0.05122	0.09503	0.40863
9/20	BB0920	0.006	0.01	16.784	0.01280	0.03257	0.06780	0.10037	4.04996	0.02901	1.14288	0.02348	0.00550	0.05541	0.14916	0.74863
9/21	BB0921	0.006	0.01	15.209	0.01105	0.02543	0.08191	0.10734	3.26546	0.00354	0.94475	0.01589	0.00249	0.04490	0.06371	0.83898
9/22	BB0922	0.006	0.01	15.745	0.01797	0.02811	0.07487	0.10298	2.10265	0.00972	0.59452	0.01117	0.00144	0.05009	0.10340	0.52827
9/23	BB0923	0.006	0.01	15.765	0.00958	0.02666	0.02241	0.04907	1.91635	0.00709	0.56784	0.00491	0.00296	0.06384	0.08307	0.66932
9/24	BB0924	0.006	0.01	17.048	0.01535	0.03381	0.02923	0.06304	2.17905	0.02468	0.64591	0.01280	0.00184	0.07293	0.21238	0.63538
9/25	BB0925	0.006	0.01	16.231	0.00773	0.02658	0.02933	0.05591	1.18946	0.00680	0.35475	0.00520	0.00135	0.03934	0.12098	0.59089
9/26	BB0926	0.006	0.01	16.967	0.01191	0.03178	0.03441	0.06619	2.28329	0.02626	0.66901	0.00871	0.00292	0.08801	0.11703	0.60461
9/26	BB0926	0.006	0.01	16.152	0.01462	0.03361	0.03407	0.06769	2.32607	0.02792	0.68949	0.01002	0.00262	0.08918	0.11334	0.62613
9/27	BB0927	0.006	0.01	17.080	0.02466	0.04224	0.06227	0.10451	4.51374	0.05988	1.22509	0.01538	0.01044	0.07413	0.24259	0.55930
9/28	BB0928	0.006	0.01	15.478	0.02968	0.06006	0.09370	0.15377	3.91045	0.06657	1.09159	0.01576	0.01465	0.09912	0.13984	0.42746
9/29	BB0929	0.006	0.01	15.451	0.01184	0.03875	0.04645	0.08520	0.77258	0.00696	0.25644	0.00501	0.00335	0.02934	0.00000	0.36622
9/30	BB0930	0.006	0.01	15.503	0.01537	0.03154	0.04558	0.07712	1.52606	0.02500	0.46272	0.00424	0.00776	0.04281	0.02417	0.41276
10/1	BB1001	0.006	0.01	16.557	0.01362	0.04514	0.03661	0.08176	1.24812	0.02108	0.42639	0.00694	0.00269	0.05795	0.07745	0.42662
10/2	BB1002	0.006	0.01	15.937	0.01588	0.07327	0.06580	0.13907	1.60772	0.04215	0.52440	0.01178	0.00682	0.06043	0.09970	0.52625
10/3	BB1003	0.006	0.01	16.514	0.03001	0.08017	0.07161	0.15178	1.43823	0.06156	0.44725	0.00852	0.00733	0.03371	0.14995	0.43080
10/3	BB1003	0.006	0.01	15.669	0.03434	0.07832	0.08520	0.16353	1.48912	0.06761	0.45913	0.01033	0.00935	0.04251	0.13738	0.46811
10/4	BB1004	0.006	0.01	16.181	0.04443	0.11078	0.12755	0.23833	2.98491	0.09773	0.88964	0.01044	0.01629	0.05045	0.11309	0.52494
10/5	BB1005	0.006	0.01	15.549	0.02859	0.05859	0.12006	0.17865	5.29277	0.06085	1.32285	0.02504	0.01341	0.06240	0.04151	1.05242
10/6	BB1006	0.006	0.01	16.348	0.01913	0.04163	0.06119	0.10282	3.26656	0.03805	0.92622	0.03257	0.00812	0.05943	0.01844	0.75973
10/7	BB1007	0.006	0.01	16.057	0.03093	0.08002	0.08037	0.16039	3.11830	0.06606	0.91248	0.03214	0.01308	0.24591	0.08347	0.64871
10/8	BB1008	0.006	0.01	16.476	0.01084	0.06184	0.05349	0.11534	0.72539	0.01390	0.22860	0.00925	0.00465	0.12048	0.00910	0.44116
10/9	BB1009	0.006	0.01	15.349	0.00527	0.04313	0.06178	0.10491	0.92410	0.00153	0.28501	0.01024	0.00147	0.02734	0.04172	0.69832
10/10	BB1010	0.006	0.01	16.103	0.00964	0.04088	0.04018	0.08106	1.10841	0.00574	0.34561	0.01063	-0.00118	0.02210	0.02475	0.79164
10/10	BB1010	0.006	0.01	15.436	0.00923	0.04096	0.04553	0.08649	1.13404	0.00375	0.34665	0.00805	0.00137	0.01846	0.00000	0.92378
10/11	BB1011	0.006	0.01	15.948	0.02734	0.04943	0.06809	0.11752	4.68252	0.01397	1.31737	0.02287	0.00373	0.05127	0.05318	1.32717
10/12	BB1012	0.006	0.01	15.324	0.01166	0.03276	0.06528	0.09804	8.05983	0.03339	1.80717	0.01684	0.01285	0.06716	0.00000	1.43387
10/13	BB1013	0.006	0.01	16.232	0.02228	0.03597	0.04948	0.08545	6.03023	0.02974	1.41086	0.01922	0.00912	0.05926	0.01217	0.99532
10/14	BB1014	0.006	0.01	15.563	0.02522	0.04361	0.06476	0.10837	4.16833	0.04095	1.09685	0.01311	0.00951	0.04643	0.03808	1.05677
10/15	BB1015	0.006	0.01	16.696	0.03287	0.05301	0.06036	0.11337	3.94399	0.04627	1.18689	0.01897	0.01162	0.07418	0.02927	0.70351

10/16	BB1016	0.006	0.01	15.475	0.02818	0.08916	0.11295	0.20210	3.58574	0.04270	1.15939	0.02835	0.01112	0.11810	0.07406	0.64377
10/17	BB1017	0.006	0.01	14.159	0.01893	0.13053	0.25423	0.38477	0.82861	0.01120	0.30147	0.04225	0.01287	0.11353	0.00000	0.25411
10/17	BB1017	0.006	0.01	14.247	0.01836	0.12921	0.23284	0.36205	0.87510	0.01762	0.34915	0.04792	0.00773	0.12018	0.00000	0.26272
10/18	BB1018	0.006	0.01	14.831	0.01076	0.06670	0.18129	0.24799	1.22072	0.00902	0.44048	0.02238	0.00651	0.04965	0.00000	0.52811
10/19	BB1019	0.006	0.01	14.673	0.01276	0.03852	0.09529	0.13382	1.48080	0.01325	0.55350	0.01567	0.00293	0.04277	0.00000	0.58790
10/20	BB1020	0.006	0.01	15.151	0.01446	0.03485	0.05891	0.09376	0.95156	0.01903	0.36524	0.00929	0.00111	0.01785	0.00000	0.43502
10/21	BB1021	0.006	0.01	15.252	0.00899	0.03316	0.03011	0.06327	0.82468	0.01167	0.34196	0.00400	0.00263	0.06291	0.00279	0.46231
10/22	BB1022	0.006	0.01	15.859	0.00872	0.02697	0.02251	0.04948	0.85298	0.01131	0.34676	0.00932	0.00023	0.03396	0.00000	0.61746
10/23	BB1023	0.006	0.01	15.094	0.00662	0.02759	0.04435	0.07194	1.67831	0.01416	0.68242	0.01616	0.00304	0.10849	0.00000	1.25577
10/24	BB1024	0.006	0.01	15.717	0.00338	0.04093	0.03384	0.07477	1.21368	0.01940	0.50029	0.03075	0.00329	0.12003	0.00000	0.96182
10/24	BB1024	0.006	0.01	15.111	0.00845	0.05094	0.03544	0.08638	1.25114	0.01652	0.47374	0.02686	0.00082	0.07193	0.00000	1.09049
10/25	BB1025	0.006	0.01	15.745	0.00662	0.04369	0.02858	0.07227	1.48777	0.02164	0.55988	0.03673	0.00273	0.09988	0.00000	0.87685
10/26	BB1026	0.006	0.01	15.587	0.00942	0.04414	0.04390	0.08804	1.35907	0.02841	0.51230	0.03853	0.00617	0.12758	0.00000	0.76689
10/27	BB1027	0.006	0.01	16.031	0.01725	0.05219	0.05614	0.10833	1.56060	0.04121	0.55705	0.04507	0.00764	0.10260	0.02061	0.60572
10/28	BB1028	0.006	0.01	15.439	0.02273	0.05564	0.07322	0.12886	2.43220	0.04637	0.82200	0.04497	0.00557	0.10085	0.08372	0.59792
10/29	BB1029	0.006	0.01	16.257	0.02761	0.07274	0.07160	0.14434	2.47858	0.04056	0.82248	0.05469	0.01067	0.31677	0.08360	0.59072
10/30	BB1030	0.006	0.01	14.949	0.01451	0.02363	0.02637	0.05000	0.30021	0.00830	0.11511	0.01475	0.00107	0.09209	0.00000	0.24194
10/31	BB1031	0.006	0.01	15.155	0.00814	0.01448	0.00172	0.01620	0.32389	0.00601	0.13255	0.00697	0.00000	0.06339	0.00000	0.35009
10/31	BB1031	0.006	0.01	13.975	0.00578	0.01384	0.00120	0.01503	0.35680	0.00128	0.14157	0.00302	0.00000	0.05704	0.00000	0.40107
	Uncertainty, RSD(%)				20.6	-	-	5.2	4.7	11.7	3.3	20.5	18.1	22.9	8.7	8.6

Note : Uncertainty for anion and cation species is one standard deviation based on pooled estimate of the standard deviation, σ_{pooled}, from 17 duplicated samples. RSD = (σ_{pooled} / $\overline{X_{pooled}}$), Uncertainty = RSD × Concentration.

Table D2. BRAVO BBNP $PM_{2.5}$ blank data for anions and cations (URG)

Date	Sample Name	Cl^- (µN) Teflon	NO_3^- (µN) Teflon	NO_3^- of Nylon (µN) Nylon	SO_4^{2-} (µN) Teflon	HNO_3 (µN) Denuder	Na^+ (µN) Teflon	NH_4^+ (µN) Teflon	K^+ (µN) Teflon	Mg^{2+} (µN) Teflon	Ca^{2+} (µN) Teflon	NH_3 (µN) Denuder
7/2	BB0702BLK	0.87	0	0	5.08	0	0	1.8	0.9	4.5	5.9	3.3
7/6	BB0706BLK	0	0	0	5.86	0.99	0.54	0.92	0.57	4	4.38	8.93
7/9	BB0709BLK	0.36	0	0	5.32	0	1.54	1.39	1.01	2.7	4.26	7.41
7/13	BB0713BLK	0.03	0	1.19	5.15	0	0.57	1.1	0.94	3.21	6.64	7.38
7/16	BB0716BLK	0.3	0	0	5.15	0	0.86	0	1.04	2.7	8.83	6.99
7/20	BB0720BLK	0.1	0	0	5.1	0	0.36	0.8	1.08	2.97	6.35	4.59
7/23	BB0723BLK	0	0	0.02	3.73	0	0.34	1.13	0.86	2.67	3.92	4.63
7/27	BB0727BLK	0	0	0.04	3.85	0	0	1.03	0.62	3.46	5.55	4.59
7/30	BB0730BLK	0.24	0	0.01	4.74	0	0.26	1.12	0.69	3.11	6.21	5.64
8/3	BB0803BLK	0.96	0	0	4.95	0	0.35	0.18	0.78	2.73	5.02	5.54
8/6	BB0806BLK	0	0	0	4.97	0	0.13	0	0.41	2.26	4.35	5.3
8/10	BB0810BLK	1.04	0	0	5.67	1.03	0.28	0.39	0.76	3.08	5.32	3.94
8/17	BB0817BLK	0	0	0	5.81	0.15	0	0	0	2.8	4.79	2.14
8/20	BB0820BLK	0	0	0	5.38	0	0	0	0	2.06	4.94	2.08
8/24	BB0824BLK	0.3	0	0	5.7	1.27	0.87	0.21	0.96	3.24	4.74	2.67
8/27	BB0827BLK	1.06	0	0	5.95	0	1.16	0.12	1.14	2.66	4.57	4.45
8/31	BB0831BLK	0.55	0	1.42	6.77	0.99	0.34	0.2	0.73	3.34	5.38	5.55
9/3	BB0903BLK	0	0	1.54	6.25	0	0.52	0.6	0.66	2.59	7.04	4.97
9/10	BB0910BLK	0.52	0	1.09	5.59	0	1.04	1.57	1.23	3.13	4.98	6.48
9/17	BB0917BLK	0.86	0	1	5.62	0	0.68	0.7	0.93	3.01	5.92	4.36
9/21	BB0921BLK	0	0	1.26	5.06	0	0.06	0.06	0.42	3.32	6.12	3.93
9/24	BB0924BLK	0.95	0	0	6.04	0	0.29	0.26	0.46	2.24	10.65	3.1
9/28	BB0928BLK	0	0	0	5.62	0	0.14	0.45	0.42	3.46	7.59	4.88
10/1	BB1001BLK	0	0	0	5.16	0	0.18	0.73	0.47	2.65	4.76	1.7

10/5	BB1005BLK	0.81	0	0	5.36	1.06	0.55	0.82	0.9	3.18	5.09	4.35
10/8	BB1008BLK	0	0	1.17	5.82	0	0.16	0.52	0.47	2.73	4.62	2.17
10/12	BB1012BLK	0	0	0	5.6	1.06	0.45	0.78	0.72	4.32	5.59	2.36
10/15	BB1015BLK	0.97	0	0	5.38	1.43	1.11	1.25	0.88	3.85	5.45	3.05
10/19	BB1019BLK	1.1	0	1.3	5.08	0	1.16	0.38	0.74	3.37	5.47	2.48
10/22	BB1022BLK	0.64	0	0	5.25	0	0.46	0.42	0.5	2.42	9.19	1.86
10/26	BB1026BLK	0.73	0	0	5.67	0	0.78	0.71	0.64	3.29	7.09	2.48
10/29	BB1029BLK	0.67	0	0	5.4	0	0.82	0.75	0.95	2.82	7.38	2.8

Table D3. BRAVO BBNP $PM_{2.5}$ Raw data for acidity (H^+ concentration) (URG)

Date	Sample Name	pH Measured Date	pH	H+ µN	Uncertainty* (RSD(%)=4.8) H+ µeq/m³	H+ µeq/m³	H+ ng/m³	pH meter calibration Slope	H_2SO_4 STD Curve STD1	STD2	STD3	STD4	STD5	STD6	STD7	STD8	Slope A	Intercept B	R2
	BB0702BLK	7/6	4.11	0				97.9	4.12	4.09	4.06	4	3.89	3.75	3.54	3.29	0.3586	1.006	0.9997
7/1	BB0701	7/6	4	22.38	0.0084	0.000403	8.35	97.9	4.12	4.09	4.06	4	3.89	3.75	3.54	3.29	0.3586	1.006	0.9997
7/2	BB0702	7/6	4.07	7.49	0.0027	0.000128	2.65	97.9	4.12	4.09	4.06	4	3.89	3.75	3.54	3.29	0.3586	1.006	0.9997
7/3	BB0703	7/6	4.09	3.66	0.0014	0.000067	1.38	97.9	4.12	4.09	4.06	4	3.89	3.75	3.54	3.29	0.3586	1.006	0.9997
7/4	BB0704	7/6	4.09	3.66	0.0014	0.000065	1.35	97.9	4.12	4.09	4.06	4	3.89	3.75	3.54	3.29	0.3586	1.006	0.9997
7/4	BB0704	7/6	4.09	3.66	0.0014	0.000069	1.44	97.9	4.12	4.09	4.06	4	3.89	3.75	3.54	3.29	0.3586	1.006	0.9997
	BB0706BLK	7/9	4.09	0				98	4.1	4.08	4.05	3.99	3.88	3.74	3.55	3.3	0.3717	1.009	0.9996
7/6	BB0706	7/9	4.1	0.00	0.0000	0.000000	0.00	98	4.1	4.08	4.05	3.99	3.88	3.74	3.55	3.3	0.3717	1.009	0.9996
7/8	BB0708	7/9	3.97	3.83	0.0014	0.000067	1.38	98	4.1	4.08	4.05	3.99	3.88	3.74	3.55	3.3	0.3717	1.009	0.9996
	BB0709BLK	7/13	4.11	0				97.5	4.1	4.07	4.04	3.99	3.88	3.75	3.53	3.28	0.3515	1.450	0.9992
7/9	BB0709	7/13	4	22.38	0.0079	0.000382	7.93	97.5	4.1	4.07	4.04	3.99	3.88	3.75	3.53	3.28	0.3515	1.450	0.9992
7/10	BB0710	7/13	4.01	20.10	0.0077	0.000373	7.74	97.5	4.1	4.07	4.04	3.99	3.88	3.75	3.53	3.28	0.3515	1.450	0.9992
7/11	BB0711	7/13	4.05	11.50	0.0044	0.000213	4.43	97.5	4.1	4.07	4.04	3.99	3.88	3.75	3.53	3.28	0.3515	1.450	0.9992
7/11	BB0711	7/13	4.05	11.50	0.0046	0.000223	4.64	97.5	4.1	4.07	4.04	3.99	3.88	3.75	3.53	3.28	0.3515	1.450	0.9992
7/12	BB0712	7/13	4	22.38	0.0082	0.000396	8.21	97.5	4.1	4.07	4.04	3.99	3.88	3.75	3.53	3.28	0.3515	1.450	0.9992
	BB0713BLK	7/16	4.11	0				98.8	4.1	4.07	4.05	3.99	3.89	3.74	3.54	3.27	0.3435	2.105	0.9982
7/13	BB0713	7/16	4.05	11.50	0.0043	0.000206	4.28	98.8	4.1	4.07	4.05	3.99	3.89	3.74	3.54	3.27	0.3435	2.105	0.9982
7/14	BB0714	7/16	4.04	13.58	0.0048	0.000234	4.85	98.8	4.1	4.07	4.05	3.99	3.89	3.74	3.54	3.27	0.3435	2.105	0.9982
7/15	BB0715	7/16	4.07	7.49	0.0029	0.000141	2.92	98.8	4.1	4.07	4.05	3.99	3.89	3.74	3.54	3.27	0.3435	2.105	0.9982
	BB0716BLK	7/20	4.12	0				97.8	4.12	4.09	4.06	4	3.91	3.76	3.54	3.27	0.3404	2.314	0.9978
7/16	BB0716	7/20	4.06	11.24	0.0041	0.000197	4.08	97.8	4.12	4.09	4.06	4	3.91	3.76	3.54	3.27	0.3404	2.314	0.9978
7/17	BB0717	7/20	4.06	11.24	0.0043	0.000208	4.31	97.8	4.12	4.09	4.06	4	3.91	3.76	3.54	3.27	0.3404	2.314	0.9978
7/18	BB0718	7/20	4.09	5.43	0.0020	0.000094	1.95	97.8	4.12	4.09	4.06	4	3.91	3.76	3.54	3.27	0.3404	2.314	0.9978

7/18	BB0718	7/20	4.08	7.32	0.0028	0.000136	2.82	97.8	4.12	4.09	4.06	4	3.91	3.76	3.54	3.27	0.3404	2.314	0.9978
7/19	BB0719	7/20	4.11	1.77	0.0006	0.000031	0.64	97.8	4.12	4.09	4.06	4	3.91	3.76	3.54	3.27	0.3404	2.314	0.9978
	BB0720BLK	7/23	4.08	0				99.1	4.07	4.04	4.01	3.95	3.86	3.7	3.5	3.24	0.3202	1.485	0.9992
7/20	BB0720	7/23	4.04	8.02	0.0031	0.000149	3.09	99.1	4.07	4.04	4.01	3.95	3.86	3.7	3.5	3.24	0.3202	1.485	0.9992
7/21	BB0721	7/23	4.01	14.55	0.0052	0.000253	5.24	99.1	4.07	4.04	4.01	3.95	3.86	3.7	3.5	3.24	0.3202	1.485	0.9992
7/22	BB0722	7/23	4.01	14.55	0.0058	0.000279	5.79	99.1	4.07	4.04	4.01	3.95	3.86	3.7	3.5	3.24	0.3202	1.485	0.9992
	BB0723BLK	7/27	4.09	0				98.9	4.08	4.05	4.02	3.97	3.87	3.72	3.51	3.26	0.3355	1.425	0.9995
7/23	BB0723	7/27	4.06	5.81	0.0022	0.000106	2.19	98.9	4.08	4.05	4.02	3.97	3.87	3.72	3.51	3.26	0.3355	1.425	0.9995
7/24	BB0724	7/27	4.09	0.00	0.0000	0.000000	0.00	98.9	4.08	4.05	4.02	3.97	3.87	3.72	3.51	3.26	0.3355	1.425	0.9995
7/25	BB0725	7/27	4.15	0.00	0.0000	0.000000	0.00	98.9	4.08	4.05	4.02	3.97	3.87	3.72	3.51	3.26	0.3355	1.425	0.9995
7/25	BB0725	7/27	4.15	0.00	0.0000	0.000000	0.00	98.9	4.08	4.05	4.02	3.97	3.87	3.72	3.51	3.26	0.3355	1.425	0.9995
7/26	BB0726	7/27	3.95	30.92	0.0108	0.000522	10.84	98.9	4.08	4.05	4.02	3.97	3.87	3.72	3.51	3.26	0.3355	1.425	0.9995
	BB0727BLK	7/30	4.1	0				98.9	4.1	4.07	4.04	3.99	3.88	3.74	3.53	3.27	0.3430	1.654	0.9990
7/27	BB0727	7/30	3.92	40.79	0.0154	0.000741	15.37	98.9	4.1	4.07	4.04	3.99	3.88	3.74	3.53	3.27	0.3430	1.654	0.9990
7/28	BB0728	7/30	3.92	40.79	0.0143	0.000689	14.30	98.9	4.1	4.07	4.04	3.99	3.88	3.74	3.53	3.27	0.3430	1.654	0.9990
7/29	BB0729	7/30	3.98	25.28	0.0097	0.000469	9.72	98.9	4.1	4.07	4.04	3.99	3.88	3.74	3.53	3.27	0.3430	1.654	0.9990
	BB0730BLK	8/3	4.1	0				99.5	4.09	4.06	4.03	3.98	3.88	3.74	3.53	3.28	0.3533	1.363	0.9994
7/30	BB0730	8/3	4.03	13.89	0.0049	0.000236	4.89	99.5	4.09	4.06	4.03	3.98	3.88	3.74	3.53	3.28	0.3533	1.363	0.9994
7/31	BB0731	8/3	4.01	18.29	0.0068	0.000329	6.82	99.5	4.09	4.06	4.03	3.98	3.88	3.74	3.53	3.28	0.3533	1.363	0.9994
8/1	BB0801	8/3	3.9	46.46	0.0167	0.000804	16.69	99.5	4.09	4.06	4.03	3.98	3.88	3.74	3.53	3.28	0.3533	1.363	0.9994
8/1	BB0801	8/3	3.91	43.59	0.0166	0.000800	16.59	99.5	4.09	4.06	4.03	3.98	3.88	3.74	3.53	3.28	0.3533	1.363	0.9994
8/2	BB0802	8/3	3.98	25.28	0.0092	0.000446	9.24	99.5	4.09	4.06	4.03	3.98	3.88	3.74	3.53	3.28	0.3533	1.363	0.9994
	BB0803BLK	8/6	4.11	0				99.7	4.09	4.05	4.02	3.98	3.87	3.72	3.51	3.26	0.3347	1.060	0.9995
8/3	BB0803	8/6	3.84	66.92	0.0263	0.001266	26.26	99.7	4.09	4.05	4.02	3.98	3.87	3.72	3.51	3.26	0.3347	1.060	0.9995
8/4	BB0804	8/6	3.8	80.86	0.0323	0.001555	32.27	99.7	4.09	4.05	4.02	3.98	3.87	3.72	3.51	3.26	0.3347	1.060	0.9995
8/5	BB0805	8/6	3.93	39.87	0.0152	0.000733	15.22	99.7	4.09	4.05	4.02	3.98	3.87	3.72	3.51	3.26	0.3347	1.060	0.9995
	BB0806BLK	8/10	4.07	0				99.8	4.1	4.05	4.02	3.95	3.86	3.7	3.5	3.25	0.3264	-0.146	0.9998
8/6	BB0806	8/10	3.89	43.71	0.0151	0.000729	15.13	99.8	4.1	4.05	4.02	3.95	3.86	3.7	3.5	3.25	0.3264	-0.146	0.9998
8/7	BB0807	8/10	3.86	52.92	0.0198	0.000953	19.77	99.8	4.1	4.05	4.02	3.95	3.86	3.7	3.5	3.25	0.3264	-0.146	0.9998
8/8	BB0808	8/10	3.79	77.07	0.0270	0.001303	27.02	99.8	4.1	4.05	4.02	3.95	3.86	3.7	3.5	3.25	0.3264	-0.146	0.9998
8/8	BB0808	8/10	3.8	73.38	0.0276	0.001329	27.57	99.8	4.1	4.05	4.02	3.95	3.86	3.7	3.5	3.25	0.3264	-0.146	0.9998
8/9	BB0809	8/10	3.83	62.80	0.0221	0.001065	22.09	99.8	4.1	4.05	4.02	3.95	3.86	3.7	3.5	3.25	0.3264	-0.146	0.9998

	BB0810BLK	8/13	4.08	0				99.8	4.09	4.05	4.01	3.96	3.86	3.7	3.5	3.24	0.3188	0.766	0.9994
8/10	BB0810	8/13	3.95	29.03	0.0107	0.000515	10.68	99.8	4.09	4.05	4.01	3.96	3.86	3.7	3.5	3.24	0.3188	0.766	0.9994
8/11	BB0811	8/13	3.99	19.15	0.0080	0.000387	8.03	99.8	4.09	4.05	4.01	3.96	3.86	3.7	3.5	3.24	0.3188	0.766	0.9994
8/12	BB0812	8/13	3.95	29.03	0.0106	0.000513	10.64	99.8	4.09	4.05	4.01	3.96	3.86	3.7	3.5	3.24	0.3188	0.766	0.9994
	BB0813BLK	8/17	4.13	0				99.4	4.13	4.05	4.01	3.98	3.87	3.72	3.51	3.29	0.3584	-2.316	0.9988
8/13	BB0813	8/17	4.09	7.15	0.0026	0.000123	2.55	99.4	4.13	4.05	4.01	3.98	3.87	3.72	3.51	3.29	0.3584	-2.316	0.9988
8/14	BB0814	8/17	4.09	7.15	0.0026	0.000126	2.62	99.4	4.13	4.05	4.01	3.98	3.87	3.72	3.51	3.29	0.3584	-2.316	0.9988
8/15	BB0815	8/17	4.15	0.00	0.0000	0.000000	0.00	99.4	4.13	4.05	4.01	3.98	3.87	3.72	3.51	3.29	0.3584	-2.316	0.9988
8/15	BB0815	8/17	4.15	0.00	0.0000	0.000000	0.00	99.4	4.13	4.05	4.01	3.98	3.87	3.72	3.51	3.29	0.3584	-2.316	0.9988
8/16	BB0816	8/17	3.84	70.41	0.0250	0.001204	24.99	99.4	4.13	4.05	4.01	3.98	3.87	3.72	3.51	3.29	0.3584	-2.316	0.9988
	BB0817BLK	8/20	4.1	0				99.2	4.09	4.05	4.03	3.97	3.86	3.73	3.51	3.27	0.3432	0.671	0.9996
8/17	BB0817	8/20	3.77	90.39	0.0337	0.001624	33.68	99.2	4.09	4.05	4.03	3.97	3.86	3.73	3.51	3.27	0.3432	0.671	0.9996
8/18	BB0818	8/20	3.88	52.39	0.0187	0.000901	18.70	99.2	4.09	4.05	4.03	3.97	3.86	3.73	3.5	3.27	0.3432	0.671	0.9996
8/19	BB0819	8/20	3.88	52.39	0.0194	0.000933	19.35	99.2	4.09	4.05	4.03	3.97	3.86	3.73	3.51	3.27	0.3432	0.671	0.9996
	BB0820BLK	8/24	4.13	0				100.4	4.14	4.09	4.05	4	3.9	3.76	3.54	3.31	0.3755	-0.586	0.9996
8/20	BB0820	8/24	3.63	160.29	0.0568	0.002739	56.82	100.4	4.14	4.09	4.05	4	3.9	3.76	3.54	3.31	0.3755	-0.586	0.9996
8/21	BB0821	8/24	3.71	120.85	0.0445	0.002144	44.49	100.4	4.14	4.09	4.05	4	3.9	3.76	3.54	3.31	0.3755	-0.586	0.9996
8/22	BB0822	8/24	3.78	91.83	0.0324	0.001563	32.42	100.4	4.14	4.09	4.05	4	3.9	3.76	3.54	3.31	0.3755	-0.586	0.9996
8/22	BB0822	8/24	3.79	88.05	0.0330	0.001589	32.96	100.4	4.14	4.09	4.05	4	3.9	3.76	3.54	3.31	0.3755	-0.586	0.9996
8/23	BB0823	8/24	3.94	40.68	0.0146	0.000706	14.65	100.4	4.14	4.09	4.05	4	3.9	3.76	3.54	3.31	0.3755	-0.586	0.9996
	BB0824BLK	8/27	4.1	0				98.5	4.14	4.07	4.03	3.96	3.87	3.71	3.5	3.26	0.3310	-1.511	0.9998
8/24	BB0824	8/27	4.08	3.74	0.0015	0.000071	1.47	98.5	4.14	4.07	4.03	3.96	3.87	3.71	3.5	3.26	0.3310	-1.511	0.9998
8/25	BB0825	8/27	3.95	32.77	0.0123	0.000594	12.33	98.5	4.14	4.07	4.03	3.96	3.87	3.71	3.5	3.26	0.3310	-1.511	0.9998
8/26	BB0826	8/27	3.95	32.77	0.0123	0.000592	12.29	98.5	4.14	4.07	4.03	3.96	3.87	3.71	3.5	3.26	0.3310	-1.511	0.9998
	BB0827BLK	8/31	4.07	0				99.2	4.08	4.06	4.03	3.96	3.92	3.71	3.6	3.38	0.4657	-1.340	0.9920
8/27	BB0827	8/31	3.96	24.53	0.0088	0.000426	8.84	99.2	4.08	4.06	4.03	3.96	3.92	3.71	3.6	3.38	0.4657	-1.340	0.9920
8/28	BB0828	8/31	4.01	12.61	0.0047	0.000226	4.69	99.2	4.08	4.06	4.03	3.96	3.92	3.71	3.6	3.38	0.4657	-1.340	0.9920
8/29	BB0829	8/31	3.95	27.09	0.0097	0.000468	9.71	99.2	4.08	4.06	4.03	3.96	3.92	3.71	3.6	3.38	0.4657	-1.340	0.9920
8/29	BB0829	8/31	3.95	27.09	0.0102	0.000490	10.16	99.2	4.08	4.06	4.03	3.96	3.92	3.71	3.6	3.38	0.4657	-1.340	0.9920
8/30	BB0830	8/31	3.87	49.78	0.0177	0.000855	17.73	99.2	4.08	4.06	4.03	3.96	3.92	3.71	3.6	3.38	0.4657	-1.340	0.9920
	BB0831BLK	9/7	4.07	0				99.9	4.08	4.05	4.02	3.95	3.86	3.73	3.52	3.29	0.3639	0.056	0.9997
8/31	BB0831	9/7	3.76	86.68	0.0326	0.001569	32.56	99.9	4.08	4.05	4.02	3.95	3.86	3.73	3.52	3.29	0.3639	0.056	0.9997

9/1	BB0901	9/7	3.61	158.37	0.0567	0.002733	56.71	99.9	4.08	4.05	4.02	3.95	3.86	3.73	3.52	3.29	0.3639	0.056	0.9997
9/2	BB0902	9/7	3.71	107.89	0.0406	0.001957	40.60	99.9	4.08	4.05	4.02	3.95	3.86	3.73	3.52	3.29	0.3639	0.056	0.9997
	BB0903BLK	9/7	4.05	0				99.9	4.08	4.05	4.02	3.95	3.86	3.73	3.52	3.29	0.3639	0.056	0.9997
9/3	BB0903	9/7	3.76	86.68	0.0304	0.001467	30.44	99.9	4.08	4.05	4.02	3.95	3.86	3.73	3.52	3.29	0.3639	0.056	0.9997
9/4	BB0904	9/7	3.87	47.80	0.0185	0.000890	18.46	99.9	4.08	4.05	4.02	3.95	3.86	3.73	3.52	3.29	0.3639	0.056	0.9997
9/5	BB0905	9/7	3.98	17.62	0.0063	0.000305	6.32	99.9	4.08	4.05	4.02	3.95	3.86	3.73	3.52	3.29	0.3639	0.056	0.9997
9/6	BB0906	9/7	4.01	10.63	0.0039	0.000187	3.87	99.9	4.08	4.05	4.02	3.95	3.86	3.73	3.52	3.29	0.3639	0.056	0.9997
9/7	BB0907	9/10	4.05	9.69	0.0036	0.000176	3.65	99.8	4.1	4.05	4.02	3.96	3.86	3.74	3.53	3.3	0.3733	-0.982	0.9996
9/8	BB0908	9/10	3.99	22.90	0.0082	0.000394	8.18	99.8	4.1	4.05	4.02	3.96	3.86	3.74	3.53	3.3	0.3733	-0.982	0.9996
	BB0910BLK	9/14	4.06	0				99.2	4.09	4.05	4.02	3.95	3.85	3.72	3.51	3.27	0.3449	-0.154	0.9998
9/9	BB0909	9/14	3.96	22.55	0.0086	0.000412	8.56	99.2	4.09	4.05	4.02	3.95	3.85	3.72	3.51	3.27	0.3449	-0.154	0.9998
9/10	BB0910	9/14	3.96	22.55	0.0082	0.000397	8.24	99.2	4.09	4.05	4.02	3.95	3.85	3.72	3.51	3.27	0.3449	-0.154	0.9998
9/11	BB0911	9/14	4.01	10.63	0.0073	0.000352	7.31	99.2	4.09	4.05	4.02	3.95	3.85	3.72	3.51	3.27	0.3449	-0.154	0.9998
9/12	BB0912	9/14	3.98	17.62	0.0066	0.000318	6.61	99.2	4.09	4.05	4.02	3.95	3.85	3.72	3.51	3.27	0.3449	-0.154	0.9998
9/12	BB0912	9/14	3.99	15.23	0.0060	0.000290	6.01	99.2	4.09	4.05	4.02	3.95	3.85	3.72	3.51	3.27	0.3449	-0.154	0.9998
9/13	BB0913	9/14	3.81	67.79	0.0257	0.001238	25.68	99.2	4.09	4.05	4.02	3.95	3.85	3.72	3.51	3.27	0.3449	-0.154	0.9998
9/14	BB0914	9/17	3.56	195.99	0.0762	0.003671	76.16	99.1	4.1	4.05	4.02	3.96	3.85	3.73	3.51	3.28	0.3524	-0.731	0.9994
9/15	BB0915	9/17	3.62	160.45	0.0585	0.002819	58.49	99.1	4.1	4.05	4.02	3.96	3.85	3.73	3.51	3.28	0.3524	-0.731	0.9994
9/16	BB0916	9/17	3.71	115.55	0.0450	0.002168	44.98	99.1	4.1	4.05	4.02	3.96	3.85	3.73	3.51	3.28	0.3524	-0.731	0.9994
	BB0917BLK	9/21	4.08	0				100.1	4.1	4.05	4.03	3.97	3.87	3.75	3.54	3.29	0.3644	0.283	0.9991
9/17	BB0917	9/21	3.9	42.72	0.0159	0.000764	15.85	100.1	4.1	4.05	4.03	3.97	3.87	3.75	3.54	3.29	0.3644	0.283	0.9991
9/18	BB0918	9/21	3.85	58.08	0.0199	0.000960	19.91	100.1	4.1	4.05	4.03	3.97	3.87	3.75	3.54	3.29	0.3644	0.283	0.9991
9/19	BB0919	9/21	3.87	51.72	0.0186	0.000896	18.59	100.1	4.1	4.05	4.03	3.97	3.87	3.75	3.54	3.29	0.3644	0.283	0.9991
9/19	BB0919	9/21	3.87	51.72	0.0197	0.000947	19.65	100.1	4.1	4.05	4.03	3.97	3.87	3.75	3.54	3.29	0.3644	0.283	0.9991
9/20	BB0920	9/21	3.86	54.86	0.0198	0.000953	19.77	100.1	4.1	4.05	4.03	3.97	3.87	3.75	3.54	3.29	0.3644	0.283	0.9991
	BB0921BLK	9/24	4.1	0				99.7	4.09	4.06	4.03	3.98	3.87	3.75	3.54	3.29	0.3640	1.123	0.9992
9/21	BB0921	9/24	3.91	43.59	0.0173	0.000836	17.33	99.7	4.09	4.06	4.03	3.98	3.87	3.75	3.54	3.29	0.3640	1.123	0.9992
9/22	BB0922	9/24	3.96	30.21	0.0116	0.000559	11.61	99.7	4.09	4.06	4.03	3.98	3.87	3.75	3.54	3.29	0.3640	1.123	0.9992
9/23	BB0923	9/24	3.98	25.28	0.0097	0.000467	9.70	99.7	4.09	4.06	4.03	3.98	3.87	3.75	3.54	3.29	0.3640	1.123	0.9992
	BB0924BLK	9/28	4.1	0				98.9	4.1	4.06	4.03	3.97	3.86	3.75	3.54	3.29	0.3643	0.245	0.9990
9/24	BB0924	9/28	3.95	32.77	0.0116	0.000560	11.62	98.9	4.1	4.06	4.03	3.97	3.86	3.75	3.54	3.29	0.3643	0.245	0.9990
9/25	BB0925	9/28	4.02	16.07	0.0060	0.000289	5.99	98.9	4.1	4.06	4.03	3.97	3.86	3.75	3.54	3.29	0.3643	0.245	0.9990

9/26	BB0926	9/28	3.98	25.28	0.0090	0.000434	9.01	98.9	4.1	4.06	4.03	3.97	3.86	3.75	3.54	3.29	0.3643	0.245	0.9990
9/26	BB0926	9/28	3.97	27.72	0.0104	0.000500	10.38	98.9	4.1	4.06	4.03	3.97	3.86	3.75	3.54	3.29	0.3643	0.245	0.9990
9/27	BB0927	9/28	3.86	58.61	0.0208	0.001000	20.75	98.9	4.1	4.06	4.03	3.97	3.86	3.75	3.54	3.29	0.3643	0.245	0.9990
	BB0928BLK	10/1	4.13	0				99.1	4.12	4.09	4.06	4.01	3.91	3.78	3.57	3.32	0.3896	1.300	0.9992
9/28	BB0928	10/1	3.92	46.10	0.0180	0.000868	18.01	99.1	4.12	4.09	4.06	4.01	3.91	3.78	3.57	3.32	0.3896	1.300	0.9992
9/29	BB0929	10/1	4.09	7.15	0.0028	0.000135	2.80	99.1	4.12	4.09	4.06	4.01	3.91	3.78	3.57	3.32	0.3896	1.300	0.9992
9/30	BB0930	10/1	4.04	17.07	0.0067	0.000321	6.66	99.1	4.12	4.09	4.06	4.01	3.91	3.78	3.57	3.32	0.3896	1.300	0.9992
	BB1001BLK	10/5	4.2	0				99.4	4.2	4.13	4.07	3.99	3.92	3.78	3.53	3.3	0.3592	-1.624	0.9981
10/1	BB1001	10/5	4.06	24.00	0.0088	0.000423	8.77	99.4	4.2	4.13	4.07	3.99	3.92	3.78	3.53	3.3	0.3592	-1.624	0.9981
10/2	BB1002	10/5	4.05	26.03	0.0099	0.000476	9.88	99.4	4.2	4.13	4.07	3.99	3.92	3.78	3.53	3.3	0.3592	-1.624	0.9981
10/3	BB1003	10/5	4.05	26.03	0.0095	0.000459	9.53	99.4	4.2	4.13	4.07	3.99	3.92	3.78	3.53	3.3	0.3592	-1.624	0.9981
10/3	BB1003	10/5	4.05	26.03	0.0100	0.000484	10.05	99.4	4.2	4.13	4.07	3.99	3.92	3.78	3.53	3.3	0.3592	-1.624	0.9981
10/4	BB1004	10/5	3.99	39.23	0.0147	0.000707	14.66	99.4	4.2	4.13	4.07	3.99	3.92	3.78	3.53	3.3	0.3592	-1.624	0.9981
	BB1005BLK	10/8	4.06	0				98.9	4.1	4.06	4.02	3.97	3.86	3.71	3.51	3.28	0.3512	-0.646	0.9997
10/5	BB1005	10/8	3.73	99.11	0.0385	0.001858	38.55	98.9	4.1	4.06	4.02	3.97	3.86	3.71	3.51	3.28	0.3512	-0.646	0.9997
10/6	BB1006	10/8	3.84	57.45	0.0213	0.001024	21.25	98.9	4.1	4.06	4.02	3.97	3.86	3.71	3.51	3.28	0.3512	-0.646	0.9997
10/7	BB1007	10/8	3.98	17.62	0.0066	0.000320	6.64	98.9	4.1	4.06	4.02	3.97	3.86	3.71	3.51	3.28	0.3512	-0.646	0.9997
	BB1008BLK	10/12	4.07	0				99.5	4.09	4.06	4.02	3.95	3.85	3.71	3.51	3.26	0.3359	0.379	0.9998
10/8	BB1008	10/12	4.06	1.98	0.0007	0.000035	0.73	99.5	4.09	4.06	4.02	3.95	3.86	3.71	3.51	3.26	0.3359	0.379	0.9998
10/9	BB1009	10/12	4	14.89	0.0059	0.000283	5.87	99.5	4.09	4.06	4.02	3.95	3.86	3.71	3.51	3.26	0.3359	0.379	0.9998
10/10	BB1010	10/12	3.99	17.22	0.0065	0.000312	6.47	99.5	4.09	4.06	4.02	3.95	3.86	3.71	3.51	3.26	0.3359	0.379	0.9998
10/10	BB1010	10/12	3.99	17.22	0.0067	0.000325	6.74	99.5	4.09	4.06	4.02	3.95	3.86	3.71	3.51	3.26	0.3359	0.379	0.9998
10/11	BB1011	10/12	3.79	77.07	0.0292	0.001409	29.22	99.5	4.09	4.06	4.02	3.95	3.86	3.71	3.51	3.26	0.3359	0.379	0.9998
	BB1012BLK	10/15	4.09	0				100.9	4.11	4.09	4.05	4	3.87	3.75	3.56	3.32	0.3911	0.089	0.9995
10/12	BB1012	10/15	3.61	164.19	0.0648	0.003123	64.80	100.9	4.11	4.09	4.05	4	3.87	3.75	3.56	3.32	0.3911	0.089	0.9995
10/13	BB1013	10/15	3.68	127.65	0.0476	0.002292	47.56	100.9	4.11	4.09	4.05	4	3.87	3.75	3.56	3.32	0.3911	0.089	0.9995
10/14	BB1014	10/15	3.81	73.60	0.0286	0.001379	28.60	100.9	4.11	4.09	4.05	4	3.87	3.75	3.56	3.32	0.3911	0.089	0.9995
	BB1015BLK	10/19	4.09	0				99.4	4.11	4.07	4.02	3.97	3.87	3.72	3.52	3.28	0.3518	-0.532	0.9999
10/15	BB1015	10/19	3.84	63.26	0.0229	0.001104	22.91	99.4	4.11	4.07	4.02	3.97	3.87	3.72	3.52	3.28	0.3518	-0.532	0.9999
10/16	BB1016	10/19	3.93	36.21	0.0141	0.000682	14.15	99.4	4.11	4.07	4.02	3.97	3.87	3.72	3.52	3.28	0.3518	-0.532	0.9999
10/17	BB1017	10/19	4.07	3.83	0.0016	0.000079	1.64	99.4	4.11	4.07	4.02	3.97	3.87	3.72	3.52	3.28	0.3518	-0.532	0.9999
10/17	BB1017	10/19	4.07	3.83	0.0016	0.000078	1.63	99.4	4.11	4.07	4.02	3.97	3.87	3.72	3.52	3.28	0.3518	-0.532	0.9999

10/18	BB1018	10/19	4.02	14.22	0.0058	0.000279	5.80	99.4	4.11	4.07	4.02	3.97	3.87	3.72	3.52	3.28	0.3518	-0.532	0.9999
	BB1019BLK	10/22	4.11	0				99.3	4.11	4.07	4.03	3.98	3.89	3.73	3.54	3.3	0.3711	-0.273	0.9999
10/19	BB1019	10/22	4.05	11.50	0.0047	0.000228	4.74	99.3	4.11	4.07	4.03	3.98	3.89	3.73	3.54	3.3	0.3711	-0.273	0.9999
10/20	BB1020	10/22	4.07	7.49	0.0030	0.000144	2.99	99.3	4.11	4.07	4.03	3.98	3.89	3.73	3.54	3.3	0.3711	-0.273	0.9999
10/21	BB1021	10/22	4.08	5.55	0.0022	0.000106	2.20	99.3	4.11	4.07	4.03	3.98	3.89	3.73	3.54	3.3	0.3711	-0.273	0.9999
	BB1022BLK	10/26	4.1	0				99.2	4.11	4.07	4.04	3.98	3.89	3.73	3.54	3.3	0.3706	-0.125	0.9999
10/22	BB1022	10/26	4.08	3.74	0.0014	0.000069	1.43	99.2	4.11	4.07	4.04	3.98	3.89	3.73	3.54	3.3	0.3706	-0.125	0.9999
10/23	BB1023	10/26	4.09	1.85	0.0007	0.000036	0.74	99.2	4.11	4.07	4.04	3.98	3.89	3.73	3.54	3.3	0.3706	-0.125	0.9999
10/24	BB1024	10/26	4.07	5.68	0.0022	0.000105	2.19	99.2	4.11	4.07	4.04	3.98	3.89	3.73	3.54	3.3	0.3706	-0.125	0.9999
10/24	BB1024	10/26	4.07	5.68	0.0023	0.000110	2.27	99.2	4.11	4.07	4.04	3.98	3.89	3.73	3.54	3.3	0.3706	-0.125	0.9999
10/25	BB1025	10/26	4.09	1.85	0.0007	0.000034	0.71	99.2	4.11	4.07	4.04	3.98	3.89	3.73	3.54	3.3	0.3706	-0.125	0.9999
	BB1026BLK	10/30	4.09	0				99.1	4.1	4.06	4.03	3.97	3.87	3.72	3.52	3.29	0.3608	-0.426	0.9998
10/26	BB1026	10/30	4.07	3.83	0.0015	0.000072	1.49	99.1	4.1	4.06	4.03	3.97	3.87	3.72	3.52	3.29	0.3608	-0.426	0.9998
10/27	BB1027	10/30	4.05	7.84	0.0030	0.000143	2.96	99.1	4.1	4.06	4.03	3.97	3.87	3.72	3.52	3.29	0.3608	-0.426	0.9998
10/28	BB1028	10/30	4	18.72	0.0073	0.000353	7.33	99.1	4.1	4.06	4.03	3.97	3.87	3.72	3.52	3.29	0.3608	-0.426	0.9998
	BB1029BLK	10/30	4.09	0				99.1	4.1	4.06	4.03	3.97	3.87	3.72	3.52	3.29	0.3608	-0.426	0.9998
10/29	BB1029	10/30	4.08	1.89	0.0007	0.000034	0.70	99.1	4.1	4.06	4.03	3.97	3.87	3.72	3.52	3.29	0.3884	-0.582	0.9997
10/30	BB1030	11/10	4.09	1.85	0.0007	0.000036	0.75	99.1	4.12	4.09	4.05	3.99	3.89	3.74	3.55	3.32	0.3884	-0.582	0.9997
10/31	BB1031	11/10	4.08	3.74	0.0015	0.000072	1.49	99.1	4.12	4.09	4.05	3.99	3.89	3.74	3.55	3.32	0.3884	-0.582	0.9997
10/31	BB1031	11/10	4.09	1.85	0.0008	0.000039	0.80	99.1	4.12	4.09	4.05	3.99	3.89	3.74	3.55	3.32	0.3884	-0.582	0.9997

* : Uncertainty for anion and cation species is one standard deviation based on pooled estimate of the standard deviation, σ_{pooled}, from 17 duplicate samples. $RSD = (\sigma_{pooled} / \overline{X_{pooled}})$, Uncertainty = RSD × Concentration.

Appendix E : MOUDI data tables and figures

Table E1. Size range for stages of MOUDI

Stage	Stage0 (Inlet)	Stage1	Stage2	Stage3	Stage4	Stage5	Stage6	Stage7	Stage8
Size Range	>18 μm	10.0 – 18.0 μm	5.6 – 10.0 μm	3.2 – 5.6 μm	1.8 – 3.2 μm	1.0 – 1.8 μm	0.56 – 1.0 μm	0.32 –0.56 μm	0.18 –0.32 μm

Table E2. BRAVO MOUDI raw data for anion and cation

Date	Sample Name	Extract Volume	Sampling volume	Elapsed Time	Cl^-	NO_3^-	SO_4^{2-}	Na^+	NH_4^+	K^+	Mg^{2+}	Ca^{2+}	Cl^-	NO_3^-	SO_4^{2-}	Na^+	NH_4^+	K^+	Mg^{2+}	Ca^{2+}
					Stage0								Stage1							
		L	m^3	Min	ng/m^3	ng/m^3	ng/m^3	ng/m^3	ng/m^3	ng/m^3	ng/m^3	ng/m^3	ng/m^3	ng/m^3	ng/m^3	ng/m^3	ng/m^3	ng/m^3	ng/m^3	ng/m^3
7/2	BB0702M	0.06	41.70	1416.5	3.44	10.87	63.85	3.71	1.44	4.02	0.10	28.67	6.96	8.82	13.46	4.42	0.59	0.14	0.00	31.06
7/3	BB0703M	0.06	41.27	1402.0	3.16	5.87	9.82	0.63	0.77	0.00	0.38	42.48	3.02	7.83	0.00	0.33	0.00	0.00	0.16	12.39
7/6	BB0706M	0.06	42.66	1435.1	1.89	5.58	12.40	0.06	0.08	0.00	0.00	15.30	0.76	7.95	0.00	0.03	0.00	0.00	0.00	0.00
7/8	BB0708M	0.06	41.16	1422.4	1.11	23.19	14.45	0.00	0.89	2.79	0.48	9.37	2.36	13.45	3.68	2.31	0.65	1.66	0.00	12.91
7/11	BB0711M	0.06	42.37	1425.5	0.00	2.83	14.21	0.00	0.00	0.00	0.00	0.00	0.00	3.89	0.00	0.00	0.00	0.00	0.00	0.00
7/16	BB0716M	0.06	41.72	1432.4	1.17	13.22	7.66	0.06	0.72	0.94	0.04	5.55	2.04	11.28	6.51	0.83	0.74	1.17	0.00	6.09
7/18	BB0718M	0.06	41.91	1429.5	0.00	3.74	2.53	0.00	0.35	0.56	0.04	3.71	0.00	0.20	0.00	0.00	1.52	0.00	0.00	0.00
7/20	BB0720M	0.06	41.71	1424.6	0.00	1.46	3.71	0.00	0.00	0.00	0.00	2.69	1.32	4.46	2.22	2.99	0.00	0.00	0.00	0.00
7/23	BB0723M	0.06	39.96	1366.1	0.00	3.37	6.60	0.00	0.00	0.00	0.00	0.00	2.07	6.98	4.59	1.34	0.00	0.00	0.00	0.00
7/24	BB0724M	0.06	39.24	1400.4	2.81	8.83	5.03	0.73	0.66	1.40	0.00	3.13	4.70	13.19	5.45	2.22	0.90	1.42	0.10	30.24
7/30	BB0730M	0.06	42.81	1438.4	0.00	6.91	39.77	0.00	0.00	0.00	0.00	14.09	0.00	14.73	2.06	0.00	0.00	0.19	0.00	4.29
8/3	BB0803M	0.06	43.10	1442.0	0.00	12.47	0.00	0.36	0.00	0.26	0.00	0.00	7.01	30.38	9.55	6.59	0.00	2.98	0.00	2.13
8/14	BB0814M	0.06	41.81	1416.2	0.00	12.51	5.81	0.00	0.00	0.00	0.00	9.49	0.00	6.56	4.44	0.00	0.00	0.00	0.00	10.34
8/15	BB0815M	0.06	40.92	1419.0	0.33	8.84	0.00	0.00	0.00	0.00	0.00	5.76	0.00	14.02	7.76	0.00	0.00	0.00	0.00	12.80
8/20	BB0820M	0.06	42.20	1424.0	0.00	17.38	5.92	0.00	0.00	0.00	0.00	8.46	0.00	26.32	6.15	0.00	0.00	0.00	0.00	9.87

8/21	BB0821M	0.06	41.11	1420.0	0.67	17.00	7.87	1.19	0.31	0.75	0.11	11.17	0.09	50.52	10.31	0.50	0.52	1.08	0.36	20.19
8/24	BB0824M	0.06	41.05	1450.0	0.00	0.46	30.09	0.00	0.00	0.00	0.00	0.00	0.00	0.84	0.65	0.00	0.00	0.00	0.00	0.00
8/27	BB0827M	0.06	28.96	1405.0	0.28	16.33	5.20	0.00	0.00	0.00	0.00	1.32	0.00	24.38	0.00	0.00	0.00	0.00	0.00	8.68
8/28	BB0828M	0.06	40.02	1416.0	0.00	5.74	5.05	0.00	0.00	0.00	0.00	1.54	0.07	13.62	0.00	0.00	0.00	0.00	0.30	2.19
9/1	BB0901M	0.06	40.29	1427.0	1.93	13.22	30.50	1.48	2.12	1.99	0.93	10.85	3.81	32.24	0.00	1.93	2.52	3.16	1.76	25.71
9/2	BB0902M	0.06	38.87	1420.0	0.00	11.62	10.59	0.46	0.38	0.00	0.00	3.97	0.26	29.44	9.92	1.24	0.23	1.23	0.00	8.59
9/8	BB0908M	0.06	29.66	1374.0	0.00	2.60	0.00	0.00	0.00	0.00	0.00	0.00	0.00	2.50	0.00	0.00	0.00	0.00	0.00	0.00
9/14	BB0914M	0.06	37.22	1429.0	0.00	13.27	28.56	0.00	1.88	1.66	0.77	9.07	3.74	24.07	6.15	2.06	2.08	2.47	0.15	6.73
9/15	BB0915M	0.06	37.86	1426.2	0.00	13.40	6.50	0.00	0.00	0.00	0.00	10.37	0.00	29.11	7.39	0.24	0.00	0.00	0.00	3.53
9/21	BB0921M	0.06	38.19	1434.4	0.00	21.91	0.00	0.00	0.00	0.00	0.00	3.73	0.00	22.62	9.44	0.00	0.49	1.73	0.00	7.46
9/29	BB0929M	0.06	38.57	1427.4	1.94	13.08	7.13	1.15	0.09	23.50	0.06	13.91	0.00	13.02	5.32	0.00	0.28	0.00	0.00	7.06
10/5	BB1005M	0.06	36.45	1428.4	3.70	18.22	0.00	2.49	2.16	2.12	0.17	12.78	3.15	34.03	6.73	2.37	2.16	2.57	0.53	36.10
10/7	BB1007M	0.06	37.61	1431.4	0.00	21.62	41.76	2.12	1.01	1.54	0.00	29.49	0.00	22.29	9.28	0.13	0.48	0.57	0.07	16.91
10/8	BB1008M	0.06	36.67	1430.1	0.00	13.93	14.35	0.69	2.52	2.69	0.48	28.00	3.19	19.40	4.64	1.53	2.34	4.09	0.54	42.29
10/9	BB1009M	0.06	37.89	1424.5	0.00	7.77	0.00	0.00	0.60	0.00	0.00	1.17	0.00	9.18	0.00	0.00	0.49	0.00	0.00	0.00
10/10	BB1010M	0.06	37.41	1433.6	0.38	11.85	14.79	0.11	1.25	0.97	0.00	13.36	0.00	16.22	3.59	0.00	1.24	0.09	0.00	0.00
10/12	BB1012M	0.06	38.05	1426.4	2.42	22.78	6.52	0.00	0.63	0.00	0.16	3.13	1.52	55.27	6.39	0.00	1.76	0.00	0.50	10.00
10/13	BB1013M	0.06	38.01	1427.5	0.00	15.51	60.83	0.00	0.55	0.00	0.00	17.23	0.00	34.44	6.05	0.00	1.04	0.12	0.00	5.77
10/14	BB1014M	0.06	36.42	1429.3	0.00	16.69	2.58	0.00	0.88	0.16	0.00	1.90	0.00	33.55	0.00	0.00	1.63	0.00	1.85	8.29
10/15	BB1015M	0.06	37.93	1432.0	1.05	14.32	0.71	11.97	1.67	9.11	0.52	14.80	0.00	28.69	0.00	0.00	1.90	0.96	1.85	15.87
10/16	BB1016M	0.06	37.91	1434.3	0.00	17.88	15.90	0.00	3.98	0.95	0.00	7.30	0.00	22.98	6.38	0.40	2.04	1.06	0.00	6.21
10/17	BB1017M	0.06	37.51	1421.3	0.03	15.56	14.32	0.00	2.20	0.48	0.21	7.02	0.31	24.27	14.20	0.00	4.65	0.53	1.02	11.53
10/21	BB1021M	0.06	37.40	1406.4	1.89	9.17	3.47	0.00	0.00	0.00	0.00	1.19	0.17	10.14	0.00	0.00	0.00	0.00	0.00	1.64
10/27	BB1027M	0.06	35.38	1424.5	0.00	3.70	0.00	0.00	0.00	0.00	0.00	2.40	5.42	13.94	2.89	2.65	0.00	0.60	0.55	11.83
10/28	BB1028M	0.06	34.36	1424.0	1.37	5.54	0.93	0.84	0.00	0.00	0.00	7.03	0.00	9.32	1.79	0.00	0.66	0.00	0.86	12.83
10/29	BB1029M	0.06	35.18	1428.4	1.52	21.28	24.21	1.04	3.49	4.80	0.04	34.44	0.00	21.36	14.09	0.00	2.98	2.94	0.86	43.12

Date	Sample Name	Extract Volume	Sampling Gas volume	Elapsed Time	Cl^-	NO_3^-	SO_4^{2-}	Na^+	NH_4^+	K^+	Mg^{2+}	Ca^{2+}	Cl^-	NO_3^-	SO_4^{2-}	Na^+	NH_4^+	K^+	Mg^{2+}	Ca^{2+}
					Stage2								Stage3							
7/2	BB0702M	0.06	41.70	1416.5	48.88	30.27	19.94	33.98	2.94	2.64	4.16	92.45	230.47	168.00	90.48	175.69	4.75	10.62	17.35	111.89

7/3	BB0703M	0.06	41.27	1402.0	17.13	9.95	7.90	16.48	0.98	0.78	0.00	16.56	135.10	79.76	49.78	99.74	2.00	4.80	9.00	88.51
7/6	BB0706M	0.06	42.66	1435.1	26.54	38.49	16.81	21.32	0.71	0.58	1.63	14.80	73.97	195.32	58.30	103.14	2.53	7.09	8.35	28.72
7/8	BB0708M	0.06	41.16	1422.4	7.60	65.32	15.82	11.70	2.11	2.90	1.33	32.15	6.58	183.74	48.69	44.34	3.88	5.68	4.25	23.19
7/11	BB0711M	0.06	42.37	1425.5	2.60	12.40	16.26	1.07	3.95	0.87	0.44	26.21	2.69	36.65	23.59	3.99	7.48	3.76	1.38	34.04
7/16	BB0716M	0.06	41.72	1432.4	20.31	57.26	20.27	13.85	1.81	3.00	0.62	27.92	63.00	304.43	99.76	87.20	2.97	9.81	10.94	83.23
7/18	BB0718M	0.06	41.91	1429.5	0.24	6.75	2.88	3.16	0.52	0.00	0.11	5.47	8.39	56.19	21.40	21.92	2.47	2.51	1.14	13.02
7/20	BB0720M	0.06	41.71	1424.6	15.86	43.58	14.73	16.24	0.26	0.74	0.21	20.34	60.39	185.57	63.36	86.40	3.41	13.27	7.57	55.44
7/23	BB0723M	0.06	39.96	1366.1	55.42	78.66	36.07	43.39	1.74	2.47	2.72	44.70	157.05	360.08	121.51	168.97	6.66	34.05	21.18	121.81
7/24	BB0724M	0.06	39.24	1400.4	40.50	81.96	31.71	27.80	3.62	5.89	4.29	55.28	102.46	302.33	114.13	113.72	5.49	14.72	15.22	120.19
7/30	BB0730M	0.06	42.81	1438.4	0.00	25.38	13.01	0.00	0.00	0.00	0.00	13.79	0.00	63.72	26.61	1.39	0.53	1.00	0.18	35.47
8/3	BB0803M	0.06	43.10	1442.0	120.21	193.79	36.22	126.71	2.02	76.94	3.73	42.64	46.54	548.65	137.82	143.43	3.32	14.25	21.63	116.21
8/14	BB0814M	0.06	41.81	1416.2	21.60	45.62	17.03	20.46	2.21	1.99	4.34	112.22	66.91	164.46	72.19	93.01	9.79	8.64	10.52	115.20
8/15	BB0815M	0.06	40.92	1419.0	12.62	55.33	22.84	16.82	2.69	2.12	0.78	50.27	39.24	217.49	93.91	81.72	8.97	11.22	13.10	124.76
8/20	BB0820M	0.06	42.20	1424.0	0.34	131.70	25.22	17.02	0.10	0.98	2.31	71.72	0.41	213.88	54.70	55.74	1.17	4.19	5.74	79.99
8/21	BB0821M	0.06	41.11	1420.0	0.00	174.78	27.19	9.76	2.63	3.43	4.64	73.43	0.17	235.04	62.14	38.09	3.37	6.13	7.67	108.00
8/24	BB0824M	0.06	41.05	1450.0	0.00	6.39	4.57	1.38	0.22	1.53	0.26	0.00	0.00	35.88	11.29	14.81	1.07	4.83	1.20	0.00
8/27	BB0827M	0.06	28.96	1405.0	8.68	94.82	17.69	34.24	0.63	4.77	1.06	18.90	6.14	247.74	56.16	85.52	2.80	7.26	4.86	21.69
8/28	BB0828M	0.06	40.02	1416.0	5.55	62.82	15.35	17.76	0.13	1.20	0.83	12.17	7.00	183.98	40.11	68.26	1.10	4.20	5.09	36.14
9/1	BB0901M	0.06	40.29	1427.0	3.25	100.67	26.71	4.46	4.33	4.22	1.72	34.94	1.49	141.47	38.39	13.46	5.96	6.99	3.44	45.88
9/2	BB0902M	0.06	38.87	1420.0	0.92	116.61	19.43	5.80	1.75	0.78	1.38	39.85	0.00	171.04	42.87	26.49	2.70	3.83	5.13	64.32
9/8	BB0908M	0.06	29.66	1374.0	0.19	8.89	0.00	0.60	0.00	0.00	0.00	1.23	2.42	35.49	14.18	11.62	1.32	0.00	0.00	7.03
9/14	BB0914M	0.06	37.22	1429.0	2.32	103.43	21.89	12.94	3.43	3.74	2.63	17.39	1.28	157.69	46.19	32.95	5.84	6.30	4.92	26.25
9/15	BB0915M	0.06	37.86	1426.2	0.57	124.61	23.47	14.02	2.01	1.90	1.87	32.02	0.00	192.90	48.49	41.23	3.11	4.44	4.75	44.26
9/21	BB0921M	0.06	38.19	1434.4	0.00	57.57	27.63	0.00	5.99	0.60	0.40	23.21	0.00	127.30	104.41	1.50	28.59	3.17	3.58	58.98
9/29	BB0929M	0.06	38.57	1427.4	0.00	30.07	18.88	0.76	3.26	0.50	0.24	53.42	0.00	63.59	25.28	1.45	6.91	1.88	2.07	37.94
10/5	BB1005M	0.06	36.45	1428.4	2.54	133.96	16.86	15.24	4.07	4.88	2.39	44.23	4.14	287.85	54.33	57.50	5.13	7.23	8.14	80.62
10/7	BB1007M	0.06	37.61	1431.4	0.00	93.13	21.32	10.65	2.53	4.04	3.44	76.39	4.22	246.44	55.65	52.71	4.43	7.77	10.10	136.33
10/8	BB1008M	0.06	36.67	1430.1	0.00	34.06	16.58	1.89	5.16	4.31	1.55	48.17	3.47	83.25	30.58	10.10	7.98	8.53	5.81	101.34
10/9	BB1009M	0.06	37.89	1424.5	0.00	19.09	3.28	0.00	2.60	0.95	0.00	8.80	0.00	54.55	14.35	2.41	5.95	2.98	2.50	43.14
10/10	BB1010M	0.06	37.41	1433.6	0.00	36.11	4.05	0.00	2.59	0.60	0.00	11.70	0.00	65.08	13.50	0.40	4.86	1.52	0.00	18.29
10/12	BB1012M	0.06	38.05	1426.4	1.07	154.61	20.97	2.55	3.32	0.00	1.90	28.86	1.98	199.75	42.88	12.45	4.98	2.01	2.83	48.96

10/13	BB1013M	0.06	38.01	1427.5	0.00	135.60	17.29	1.75	3.08	0.96	0.00	39.61	0.00	184.14	39.50	9.42	4.63	7.18	4.21	68.16
10/14	BB1014M	0.06	36.42	1429.3	0.00	96.25	8.14	2.86	2.56	1.28	0.01	20.34	0.00	175.23	29.96	17.50	4.15	3.02	2.15	41.21
10/15	BB1015M	0.06	37.93	1432.0	0.00	103.12	19.08	3.59	4.30	2.57	1.21	51.88	1.37	140.92	31.52	22.04	5.66	6.23	4.43	97.66
10/16	BB1016M	0.06	37.91	1434.3	0.00	66.50	13.72	2.19	4.83	2.70	1.86	46.15	0.27	191.76	40.26	14.58	8.01	6.82	7.33	97.41
10/17	BB1017M	0.06	37.51	1421.3	3.18	79.84	49.99	0.36	22.10	5.02	4.07	44.13	6.58	222.89	136.95	4.86	61.46	12.70	9.36	139.34
10/21	BB1021M	0.06	37.40	1406.4	0.11	26.33	8.67	0.00	1.94	0.16	0.00	18.63	0.51	50.59	21.63	0.30	5.90	1.26	0.14	30.53
10/27	BB1027M	0.06	35.38	1424.5	0.32	66.57	11.51	10.22	2.21	2.35	1.26	50.73	1.69	156.36	27.64	27.07	3.37	4.06	4.40	90.71
10/28	BB1028M	0.06	34.36	1424.0	1.58	85.18	11.02	8.82	2.52	0.96	1.33	55.00	2.80	230.79	31.45	39.60	5.09	4.83	6.66	102.87
10/29	BB1029M	0.06	35.18	1428.4	2.02	74.23	34.17	6.96	8.43	8.22	3.06	119.52	4.54	229.50	66.67	27.38	16.12	17.68	16.06	197.33

Date	Sample Name	Extract Volume	Sampling Gas volume	Elapsed Time	Cl^-	NO_3^-	SO_4^{2-}	Na^+	NH_4^+	K^+	Mg^{2+}	Ca^{2+}	Cl^-	NO_3^-	SO_4^{2-}	Na^+	NH_4^+	K^+	Mg^{2+}	Ca^{2+}
					Stage4								Stage5							
7/2	BB0702M	0.06	41.70	1416.5	153.55	208.84	94.28	172.82	3.10	8.91	15.93	53.28	53.23	144.25	118.26	115.39	5.74	10.43	14.10	63.67
7/3	BB0703M	0.06	41.27	1402.0	101.86	120.80	47.68	113.62	1.01	4.81	8.61	20.76	44.94	112.75	79.22	85.19	3.59	3.10	5.85	30.14
7/6	BB0706M	0.06	42.66	1435.1	29.75	155.54	45.34	97.54	2.27	5.41	7.67	17.84	10.79	113.02	68.44	65.48	5.68	3.63	4.70	8.32
7/8	BB0708M	0.06	41.16	1422.4	4.21	138.34	63.75	51.49	3.05	5.25	4.37	27.10	0.37	45.26	83.45	36.52	7.93	4.72	3.06	9.22
7/11	BB0711M	0.06	42.37	1425.5	3.06	24.12	23.41	6.71	3.18	1.06	0.68	33.40	0.00	11.78	39.30	2.45	8.38	0.65	0.76	2.33
7/16	BB0716M	0.06	41.72	1432.4	23.43	284.71	111.03	93.01	2.49	9.05	11.23	45.39	4.42	124.69	163.64	63.46	9.79	7.54	7.18	19.73
7/18	BB0718M	0.06	41.91	1429.5	1.38	57.14	24.64	25.16	1.32	1.74	0.94	4.50	0.00	21.28	18.38	17.08	1.66	0.00	0.61	0.00
7/20	BB0720M	0.06	41.71	1424.6	24.83	189.85	69.61	72.35	2.69	5.55	6.62	29.60	1.01	77.35	69.67	44.28	5.59	2.46	3.00	16.01
7/23	BB0723M	0.06	39.96	1366.1	45.81	269.13	111.49	114.03	5.84	9.37	14.62	62.36	8.56	129.25	173.07	47.71	12.57	3.94	3.94	12.39
7/24	BB0724M	0.06	39.24	1400.4	44.03	319.35	135.75	107.60	4.72	12.46	14.54	83.42	12.02	162.60	173.91	80.79	9.81	12.35	10.46	46.01
7/30	BB0730M	0.06	42.81	1438.4	27.06	37.24	28.49	31.42	0.00	9.73	0.00	17.47	0.00	2.52	43.62	4.91	5.59	0.00	0.00	0.73
8/3	BB0803M	0.06	43.10	1442.0	12.46	322.34	141.04	104.78	2.98	10.63	14.09	53.46	0.00	101.38	268.23	55.07	29.30	7.94	10.14	29.00
8/14	BB0814M	0.06	41.81	1416.2	51.15	146.54	72.24	85.50	5.06	9.74	7.90	88.25	11.79	94.91	105.05	61.22	11.07	4.39	6.50	48.29
8/15	BB0815M	0.06	40.92	1419.0	16.11	172.80	86.47	65.74	5.82	8.84	8.06	65.01	7.48	95.92	133.26	48.09	12.89	8.40	6.07	41.09
8/20	BB0820M	0.06	42.20	1424.0	0.00	87.83	46.88	42.30	0.04	0.81	1.63	14.23	0.00	5.30	172.02	19.14	32.26	0.00	0.72	4.80
8/21	BB0821M	0.06	41.11	1420.0	0.00	70.89	52.42	30.89	1.95	3.09	4.27	25.00	0.00	4.33	213.73	20.03	52.27	2.18	2.10	26.47
8/24	BB0824M	0.06	41.05	1450.0	0.00	37.01	15.53	17.97	1.48	2.52	0.35	0.00	0.00	30.54	87.62	36.19	24.89	25.02	0.62	0.00
8/27	BB0827M	0.06	28.96	1405.0	1.83	127.70	52.24	68.91	1.00	5.53	3.88	4.79	0.00	30.34	135.04	42.48	31.05	1.55	1.81	3.72

8/28	BB0828M	0.06	40.02	1416.0	3.40	110.13	34.56	55.17	0.27	7.53	3.81	5.99	0.00	30.78	42.40	28.98	1.92	0.69	1.31	3.06
9/1	BB0901M	0.06	40.29	1427.0	0.74	34.28	32.56	12.18	5.00	3.92	2.13	10.45	1.74	0.12	481.76	8.50	119.99	3.21	3.52	18.70
9/2	BB0902M	0.06	38.87	1420.0	0.97	47.88	34.64	19.43	1.55	1.83	2.09	14.51	0.00	5.98	384.78	12.30	101.88	0.59	2.24	15.05
9/8	BB0908M	0.06	29.66	1374.0	0.00	24.82	9.15	11.90	0.89	0.00	0.70	16.96	0.00	5.65	10.77	7.46	0.55	0.00	1.31	0.00
9/14	BB0914M	0.06	37.22	1429.0	0.00	48.95	43.42	19.62	4.82	4.01	1.93	8.31	0.00	3.96	248.75	12.64	53.25	3.18	2.47	7.23
9/15	BB0915M	0.06	37.86	1426.2	0.00	60.87	34.77	24.44	2.99	1.53	1.52	10.89	0.00	8.32	178.87	13.99	38.54	0.00	2.70	28.38
9/21	BB0921M	0.06	38.19	1434.4	0.00	32.34	115.58	0.32	31.25	1.12	1.48	16.43	0.00	8.04	297.85	0.66	102.67	0.66	0.00	8.80
9/29	BB0929M	0.06	38.57	1427.4	0.00	43.62	22.42	1.24	4.91	1.94	1.81	14.67	0.00	15.79	25.31	2.51	6.14	0.00	0.00	25.26
10/5	BB1005M	0.06	36.45	1428.4	3.23	117.25	49.91	43.49	4.93	5.52	4.05	17.02	4.13	13.74	142.58	25.49	30.65	3.87	1.57	14.44
10/7	BB1007M	0.06	37.61	1431.4	0.00	132.70	46.45	36.43	1.98	7.24	5.88	53.84	0.00	27.47	107.00	25.63	18.57	1.44	1.18	17.03
10/8	BB1008M	0.06	36.67	1430.1	0.00	46.36	17.26	7.28	4.51	2.54	0.61	33.00	0.00	24.39	15.06	6.32	4.42	0.91	0.00	14.05
10/9	BB1009M	0.06	37.89	1424.5	0.00	26.10	9.59	1.82	3.92	1.39	1.26	16.74	0.00	4.70	8.95	0.00	3.99	0.00	0.00	0.00
10/10	BB1010M	0.06	37.41	1433.6	0.00	20.13	11.30	1.75	3.64	18.73	1.04	7.47	0.00	7.51	28.79	0.73	9.10	12.13	0.00	0.55
10/12	BB1012M	0.06	38.05	1426.4	1.10	61.36	42.34	9.36	4.33	0.00	0.57	13.71	0.91	11.16	266.26	7.54	62.32	0.00	2.31	10.09
10/13	BB1013M	0.06	38.01	1427.5	0.00	52.07	33.19	6.63	3.09	2.81	0.91	11.88	0.00	9.19	148.81	5.43	34.95	1.09	0.44	7.21
10/14	BB1014M	0.06	36.42	1429.3	0.00	70.94	27.07	16.04	2.66	1.72	0.81	8.30	0.00	13.89	67.70	8.02	11.43	0.54	0.00	0.00
10/15	BB1015M	0.06	37.93	1432.0	0.00	64.02	27.19	16.11	2.62	1.86	1.81	12.82	0.00	14.55	88.96	12.59	21.37	1.07	1.88	5.63
10/16	BB1016M	0.06	37.91	1434.3	0.67	120.16	34.58	19.28	5.20	10.46	5.44	75.68	0.03	23.81	97.86	12.45	20.73	1.96	0.08	8.78
10/17	BB1017M	0.06	37.51	1421.3	3.68	123.02	71.81	3.03	28.56	4.73	4.50	74.04	0.09	43.05	52.25	0.58	14.63	0.81	0.71	8.76
10/21	BB1021M	0.06	37.40	1406.4	1.17	21.47	15.40	0.51	3.98	0.00	0.00	28.56	0.71	9.23	15.10	0.00	4.03	0.00	0.00	3.54
10/27	BB1027M	0.06	35.38	1424.5	0.00	66.55	18.76	11.92	1.37	0.79	1.06	28.97	0.00	13.03	20.79	5.29	1.83	0.18	0.86	2.36
10/28	BB1028M	0.06	34.36	1424.0	0.00	88.08	21.74	20.38	1.39	1.30	2.37	32.67	0.00	16.75	32.33	7.92	4.77	1.02	0.75	0.69
10/29	BB1029M	0.06	35.18	1428.4	0.90	102.36	34.89	14.38	8.73	7.62	4.25	88.66	3.69	28.96	38.79	7.54	7.72	3.32	0.62	24.48

Date	Sample Name	Extract Volume	Sampling Gas volume	Elapsed Time	Cl^-	NO_3^-	SO_4^{2-}	Na^+	NH_4^+	K^+	Mg^{2+}	Ca^{2+}	Cl^-	NO_3^-	SO_4^{2-}	Na^+	NH_4^+	K^+	Mg^{2+}	Ca^{2+}
					Stage6								Stage7							
7/2	BB0702M	0.06	41.70	1416.5	0.00	7.41	188.08	9.93	60.74	1.04	1.68	7.49	0.38	4.21	533.46	1.48	187.79	0.53	0.29	8.30
7/3	BB0703M	0.06	41.27	1402.0	0.00	7.68	63.45	6.72	14.72	0.11	0.00	1.10	2.86	4.27	313.97	6.61	81.19	0.00	0.73	53.10
7/6	BB0706M	0.06	42.66	1435.1	0.00	3.67	100.74	3.49	25.20	0.00	0.00	0.00	0.00	3.65	350.41	0.00	120.45	0.23	0.15	0.00

7/8	BB0708M	0.06	41.16	1422.4	1.03	4.91	272.39	2.89	68.48	2.52	0.57	4.90	0.90	5.57	826.10	1.75	243.85	5.04	1.30	11.50
7/11	BB0711M	0.06	42.37	1425.5	0.00	3.88	262.21	0.00	49.88	0.58	1.47	29.91	0.76	5.71	399.46	0.00	135.33	3.56	0.00	15.39
7/16	BB0716M	0.06	41.72	1432.4	0.00	4.40	328.26	6.32	87.49	3.25	0.91	3.97	1.65	5.97	774.90	1.80	261.77	4.32	0.08	5.05
7/18	BB0718M	0.06	41.91	1429.5	0.00	0.00	27.03	1.24	5.35	0.00	0.00	0.00	0.00	0.00	150.34	0.22	56.02	0.54	0.00	0.00
7/20	BB0720M	0.06	41.71	1424.6	0.00	7.34	99.36	1.48	28.91	0.00	0.00	3.54	0.00	2.94	355.92	0.00	138.73	0.00	0.00	0.00
7/23	BB0723M	0.06	39.96	1366.1	0.00	1.30	387.71	4.40	103.72	1.20	3.21	3.10	0.00	0.00	800.88	0.74	241.75	3.84	0.00	24.15
7/24	BB0724M	0.06	39.24	1400.4	0.59	6.82	276.43	8.14	63.52	3.90	1.14	9.96	0.95	0.00	649.36	2.92	199.39	6.06	0.31	2.18
7/30	BB0730M	0.06	42.81	1438.4	0.00	0.30	176.02	0.00	56.73	0.00	0.00	0.00	0.00	0.00	476.17	0.00	175.21	0.00	0.00	0.29
8/3	BB0803M	0.06	43.10	1442.0	0.00	6.18	974.01	42.12	203.55	12.19	3.38	16.79	0.00	4.21	1596.81	1.45	354.03	7.10	0.50	0.00
8/14	BB0814M	0.06	41.81	1416.2	0.00	5.67	282.71	10.32	96.65	0.00	0.01	2.23	0.00	3.01	654.07	0.18	197.51	1.71	0.00	3.05
8/15	BB0815M	0.06	40.92	1419.0	2.34	4.28	197.44	2.04	73.97	0.00	0.03	23.14	0.77	4.25	704.24	1.93	230.16	5.97	0.52	10.61
8/20	BB0820M	0.06	42.20	1424.0	0.11	3.56	1567.45	6.90	294.05	3.94	4.12	37.61	0.00	1.08	2943.24	0.00	535.55	9.02	3.67	34.57
8/21	BB0821M	0.06	41.11	1420.0	4.41	3.46	2012.64	5.34	482.60	9.20	4.60	30.54	1.84	5.79	3416.81	2.94	834.01	27.34	1.59	23.20
8/24	BB0824M	0.06	41.05	1450.0	0.00	2.41	326.09	9.13	103.34	3.93	0.00	0.00	0.00	5.69	530.10	0.00	186.34	3.26	0.00	0.00
8/27	BB0827M	0.06	28.96	1405.0	0.00	4.76	423.38	0.71	138.42	2.77	0.85	2.51	3.53	15.19	829.70	10.25	318.84	11.22	1.26	21.51
8/28	BB0828M	0.06	40.02	1416.0	1.58	6.29	141.70	4.26	45.53	1.21	0.00	0.03	2.49	3.41	471.55	0.00	176.07	2.99	0.06	3.50
9/1	BB0901M	0.06	40.29	1427.0	4.32	3.25	3761.64	5.80	968.48	11.76	5.03	34.41	1.66	0.00	3548.23	4.12	919.82	14.21	3.35	31.13
9/2	BB0902M	0.06	38.87	1420.0	3.44	4.47	2608.93	3.24	741.55	5.95	5.84	43.61	0.00	11.29	2771.99	3.30	791.29	14.49	5.04	30.83
9/8	BB0908M	0.06	29.66	1374.0	0.00	0.00	57.02	0.00	7.78	0.00	0.01	0.45	0.00	0.00	175.17	0.00	60.00	0.00	0.00	0.00
9/14	BB0914M	0.06	37.22	1429.0	0.00	3.56	2833.11	2.97	616.01	6.95	4.91	22.12	0.00	2.96	5402.57	3.22	1279.19	9.99	3.30	18.51
9/15	BB0915M	0.06	37.86	1426.2	0.00	6.50	2120.42	4.14	532.01	4.95	3.28	54.01	0.00	14.72	3881.01	7.52	988.70	17.78	7.82	94.40
9/21	BB0921M	0.06	38.19	1434.4	0.00	9.80	799.93	0.00	276.91	4.67	1.32	6.80	0.00	9.70	1529.06	0.00	574.15	7.53	3.40	14.33
9/29	BB0929M	0.06	38.57	1427.4	0.00	5.19	44.64	0.00	16.11	0.00	0.00	0.00	0.00	8.84	310.24	0.00	123.66	1.28	0.00	7.70
10/5	BB1005M	0.06	36.45	1428.4	2.58	8.88	1162.12	6.16	322.56	6.23	4.99	21.25	2.67	10.76	3136.59	5.71	850.62	14.92	5.58	40.34
10/7	BB1007M	0.06	37.61	1431.4	0.00	7.65	561.28	4.67	194.23	4.45	0.09	7.59	0.00	5.56	1490.47	3.24	480.69	15.50	2.19	13.60
10/8	BB1008M	0.06	36.67	1430.1	0.00	5.44	43.43	0.00	19.56	1.49	0.81	1.51	2.51	3.35	307.43	4.28	126.71	5.49	0.56	27.71
10/9	BB1009M	0.06	37.89	1424.5	0.00	0.00	55.38	0.00	17.63	0.00	0.00	0.00	0.00	2.01	437.09	0.00	164.32	2.65	0.00	3.13
10/10	BB1010M	0.06	37.41	1433.6	0.00	4.89	99.63	0.00	41.75	15.11	0.00	0.00	0.00	3.97	349.34	0.06	173.91	13.35	0.00	7.24
10/12	BB1012M	0.06	38.05	1426.4	1.17	8.00	1966.07	4.60	448.90	5.11	3.14	27.88	1.05	7.78	4911.74	4.36	1137.84	11.52	6.48	40.65
10/13	BB1013M	0.06	38.01	1427.5	0.00	6.65	1152.43	2.70	255.91	3.07	2.05	63.82	0.00	11.44	4020.69	3.83	965.59	10.81	2.69	32.74
10/14	BB1014M	0.06	36.42	1429.3	0.00	8.24	536.33	2.37	180.40	3.59	3.32	30.61	0.00	6.60	2411.31	1.06	638.10	8.17	2.78	27.52

10/15	BB1015M	0.06	37.93	1432.0	0.47	8.69	670.43	3.58	240.78	5.08	3.43	18.58	4.70	10.93	2187.12	2.52	617.17	10.87	7.17	33.23
10/16	BB1016M	0.06	37.91	1434.3	0.13	11.54	600.90	1.71	225.36	4.79	1.24	5.91	1.87	8.74	1682.32	2.21	573.68	15.75	1.75	8.43
10/17	BB1017M	0.06	37.51	1421.3	1.49	12.75	62.30	0.00	23.37	1.47	0.00	15.27	0.00	42.12	430.36	0.00	175.50	18.84	0.79	5.69
10/21	BB1021M	0.06	37.40	1406.4	0.51	4.95	32.05	0.00	12.33	0.65	0.00	0.00	0.67	6.23	406.05	0.00	155.69	3.14	0.00	2.04
10/27	BB1027M	0.06	35.38	1424.5	0.00	0.00	59.06	0.00	22.28	1.99	0.00	0.98	0.00	1.68	835.52	5.56	306.56	27.73	0.83	8.92
10/28	BB1028M	0.06	34.36	1424.0	0.61	0.00	179.23	1.24	63.72	3.11	0.00	0.00	7.66	0.00	1372.06	5.26	531.50	26.32	0.64	8.21
10/29	BB1029M	0.06	35.18	1428.4	0.00	0.00	128.68	0.66	53.89	3.00	0.00	1.24	3.20	3.48	1219.54	6.12	470.17	26.50	0.00	1.73

Date	Sample Name	Extract Volume	Sampling Gas volume	Elapsed Time	Cl^-	NO_3^-	SO_4^{2-}	Na^+	NH_4^+	K^+	Mg^{2+}	Ca^{2+}
					Stage8							
7/2	BB0702M	0.06	41.70	1416.5	0.00	0.00	199.55	0.00	89.85	0.98	0.00	0.00
7/3	BB0703M	0.06	41.27	1402.0	0.00	2.51	117.49	0.00	50.19	0.00	0.00	0.68
7/6	BB0706M	0.06	42.66	1435.1	0.00	0.00	153.13	0.00	58.45	0.01	0.00	0.00
7/8	BB0708M	0.06	41.16	1422.4	2.27	0.00	473.42	1.57	147.59	1.72	1.52	27.87
7/11	BB0711M	0.06	42.37	1425.5	0.04	5.26	208.67	0.00	81.31	2.73	0.45	1.00
7/16	BB0716M	0.06	41.72	1432.4	0.27	4.58	348.41	0.00	127.02	2.73	0.00	0.21
7/18	BB0718M	0.06	41.91	1429.5	0.04	0.00	109.59	2.17	48.03	3.00	0.00	1.88
7/20	BB0720M	0.06	41.71	1424.6	0.00	0.00	210.59	0.00	84.37	0.00	0.00	0.00
7/23	BB0723M	0.06	39.96	1366.1	0.00	0.00	308.43	0.00	104.11	0.00	0.00	0.00
7/24	BB0724M	0.06	39.24	1400.4	3.59	4.75	248.87	1.46	91.35	3.00	0.00	0.00
7/30	BB0730M	0.06	42.81	1438.4	0.00	9.76	397.12	0.00	153.43	1.11	0.00	2.99
8/3	BB0803M	0.06	43.10	1442.0	0.00	2.64	1005.93	1.00	254.04	4.49	0.00	2.27
8/14	BB0814M	0.06	41.81	1416.2	0.00	2.75	233.29	0.00	84.65	0.88	0.00	0.00
8/15	BB0815M	0.06	40.92	1419.0	0.00	11.73	262.01	0.00	94.61	1.44	0.00	2.97
8/20	BB0820M	0.06	42.20	1424.0	0.00	3.03	1365.96	0.00	220.60	1.26	3.97	120.59
8/21	BB0821M	0.06	41.11	1420.0	61.98	14.23	1302.68	58.09	327.61	52.01	0.40	3.58
8/24	BB0824M	0.06	41.05	1450.0	0.00	0.28	120.15	0.00	37.57	0.00	0.13	0.82
8/27	BB0827M	0.06	28.96	1405.0	0.00	17.28	291.17	0.00	113.35	5.82	1.28	0.71
8/28	BB0828M	0.06	40.02	1416.0	1.71	12.30	196.95	0.67	75.94	2.16	0.00	40.89

9/1	BB0901M	0.06	40.29	1427.0	0.00	3.60	561.57	0.49	158.27	5.06	2.30	10.89
9/2	BB0902M	0.06	38.87	1420.0	0.00	9.66	489.70	0.00	167.46	8.03	0.00	10.94
9/8	BB0908M	0.06	29.66	1374.0	0.00	0.00	107.63	0.00	42.29	0.00	0.00	0.00
9/14	BB0914M	0.06	37.22	1429.0	1.40	0.00	607.82	1.86	169.69	4.59	1.77	11.72
9/15	BB0915M	0.06	37.86	1426.2	0.00	6.04	632.81	0.00	171.43	3.39	0.00	9.05
9/21	BB0921M	0.06	38.19	1434.4	0.00	6.34	355.28	0.00	139.92	1.49	0.00	4.47
9/29	BB0929M	0.06	38.57	1427.4	0.00	9.63	127.64	0.00	55.28	1.55	0.00	0.00
10/5	BB1005M	0.06	36.45	1428.4	3.71	4.46	581.63	2.85	170.44	4.43	2.64	14.80
10/7	BB1007M	0.06	37.61	1431.4	0.00	5.48	351.24	0.00	125.28	3.22	0.00	0.55
10/8	BB1008M	0.06	36.67	1430.1	0.00	2.07	111.82	0.00	54.40	0.14	0.40	1.79
10/9	BB1009M	0.06	37.89	1424.5	0.00	2.87	138.64	0.00	60.21	0.00	0.00	0.00
10/10	BB1010M	0.06	37.41	1433.6	0.00	6.56	101.89	0.00	50.76	14.93	0.00	11.49
10/12	BB1012M	0.06	38.05	1426.4	7.46	4.93	767.11	5.21	212.79	3.69	1.72	19.61
10/13	BB1013M	0.06	38.01	1427.5	0.00	8.72	676.11	0.00	181.09	2.80	3.00	17.99
10/14	BB1014M	0.06	36.42	1429.3	0.00	8.10	402.89	0.00	143.70	2.31	0.60	25.77
10/15	BB1015M	0.06	37.93	1432.0	0.49	6.81	316.85	0.45	109.21	3.01	0.00	6.20
10/16	BB1016M	0.06	37.91	1434.3	0.00	4.48	259.54	0.00	98.21	2.27	0.00	0.00
10/17	BB1017M	0.06	37.51	1421.3	2.05	15.78	132.53	0.00	52.52	4.23	0.59	21.07
10/21	BB1021M	0.06	37.40	1406.4	0.18	5.11	166.27	0.00	65.31	1.13	0.00	0.26
10/27	BB1027M	0.06	35.38	1424.5	0.00	0.00	366.31	0.42	150.76	5.87	0.00	0.00
10/28	BB1028M	0.06	34.36	1424.0	0.00	0.00	374.54	0.00	130.74	4.36	0.84	0.00
10/29	BB1029M	0.06	35.18	1428.4	0.00	0.00	349.58	0.00	124.34	4.66	0.00	0.00
	Uncertainty, RSD(%)				4.4	5.9	5.5	3.2	4.8	4.4	5.3	3.4

Note : Uncertainty for anion and cation species is one standard deviation based on pooled estimate of the standard deviation, σ_{pooled}, from replicate sample analysis. RSD = (σ_{pooled} / $\overline{X_{pooled}}$), Uncertainty = RSD × Concentration.

Table E3. BRAVO MOUDI blank data of anions and cations

Date	Sample Name	Extract Volume (L)	Sampling Gas volume (m^3)	Elapsed Time (Min)	Cl^- Stage0 (μN)	Stage1 (μN)	Stage2 (μN)	Stage3 (μN)	Stage4 (μN)	Stage5 (μN)	Stage6 (μN)	Stage7 (μN)	Stage8 (μN)
7/5	BB0705M BLK	0.06	0	0	0.38	1.49	0.868	0.509	0.409	0.796	0.782	0.401	0.695
7/19	BB0719M BLK	0.06	0	0	0	0	0.459	0	0.1575	0.251	0	0	0
8/2	BB0802M BLK	0.06	0	0	0.409	4.869	0.282	0	0.065	0.21	4.51	0.257	0
9/6	BB0906M BLK	0.06	0	0	0.221	0.177	0.163	0.15	0.2775	0	0.109	0.419	0.516
10/4	BB1004M BLk	0.06	0	0	0.672	0.287	0.47	0.593	0.367	0.5705	1.532	1.013	0.598
					NO_3^- Stage0	Stage1	Stage2	Stage3	Stage4	Stage5	Stage6	Stage7	Stage8
7/5	BB0705M BLK	0.06	0	0	0	1.024	1.323	0	0	2.86	0.942	1.046	1.067
7/19	BB0719M BLK	0.06	0	0	0	0	0.687	0	0.3575	0	0	0	0
8/2	BB0802M BLK	0.06	0	0	0	0.702	0.671	0.72	0.326	0.627	1.717	1.187	0.766
9/6	BB0906M BLK	0.06	0	0	0.847	0	0.85	0	0	0.646	0.773	0.648	0.782
10/4	BB1004M BLk	0.06	0	0	0.777	0.642	0.72	0	0	0	0	0.71	0.769
					SO_4^{2-} Stage0	Stage1	Stage2	Stage3	Stage4	Stage5	Stage6	Stage7	Stage8
7/5	BB0705M BLK	0.06	0	0	0.822	0.97	0	0	1.4	0	0	0.792	0
7/19	BB0719M BLK	0.06	0	0	0	0	0	0	0.365	0	0	0	0
8/2	BB0802M BLK	0.06	0	0	0	0	0	0	0	0	0	0	0
9/6	BB0906M BLK	0.06	0	0	0	0	0.704	0	0	0	0.955	1.198	0
10/4	BB1004M BLk	0.06	0	0	0	0	0	0	0	0	0	0	0
					Na^+ Stage0	Stage1	Stage2	Stage3	Stage4	Stage5	Stage6	Stage7	Stage8
7/5	BB0705M BLK	0.06	0	0	0.344	2.879	0.693	0.37	0.3895	0.306	0.721	0.384	0.666
7/19	BB0719M BLK	0.06	0	0	0	0	0.195	0	0	0	0	0	0

8/2	BB0802M BLK	0.06	0	0	0.379	5.06	0.283	0.194	0.294	0.327	4.98	0.249	0.358
9/6	BB0906M BLK	0.06	0	0	0	0	0	0	0	0.3665	0.062	0.448	0.067
10/4	BB1004M BLk	0.06	0	0	0.709	0.411	0.419	0.838	0.475	0.827	1.528	1.024	0.644
					NH_4^+								
					Stage0	**Stage1**	**Stage2**	**Stage3**	**Stage4**	**Stage5**	**Stage6**	**Stage7**	**Stage8**
7/5	BB0705M BLK	0.06	0	0	0.221	0.348	0.282	0.437	0.206	0.221	0.281	0.219	0.276
7/19	BB0719M BLK	0.06	0	0	0	0	0	0	0	0	0	0.017	0
8/2	BB0802M BLK	0.06	0	0	0	0	0	0	0	0	0	0	0
9/6	BB0906M BLK	0.06	0	0	0.493	0.477	0.626	0.398	0.213	0.225	0.193	0.2	0.24
10/4	BB1004M BLk	0.06	0	0	0.584	0.577	0.568	0.584	0.59	0.589	0.573	0.617	0.62
					K^+								
					Stage0	**Stage1**	**Stage2**	**Stage3**	**Stage4**	**Stage5**	**Stage6**	**Stage7**	**Stage8**
7/5	BB0705M BLK	0.06	0	0	0.215	1.114	0.34	0.269	0.2665	0.501	0.287	0.242	0.251
7/19	BB0719M BLK	0.06	0	0	0	0	0	0	0	0	0	0	0
8/2	BB0802M BLK	0.06	0	0	0.007	0.192	0.008	0	0.055	0.044	0.113	0.084	0.066
9/6	BB0906M BLK	0.06	0	0	0	0	0	0	0	0	0	0	0
10/4	BB1004M BLk	0.06	0	0	0.482	0.314	0.322	0.362	0.305	0.478	0.522	0.402	0.359
					Mg^{2+}								
					Stage0	**Stage1**	**Stage2**	**Stage3**	**Stage4**	**Stage5**	**Stage6**	**Stage7**	**Stage8**
7/5	BB0705M BLK	0.06	0	0	2.457	3.1	2.457	2.069	2.331	3.006	2.323	2.062	2.376
7/19	BB0719M BLK	0.06	0	0	1.984	2.063	2.054	1.98	1.796	1.935	1.938	1.975	1.936
8/2	BB0802M BLK	0.06	0	0	2.375	2.378	2.203	2.206	2.223	2.171	2.291	2.256	2.177
9/6	BB0906M BLK	0.06	0	0	4.549	4.418	6.85	4.446	2.239	2.2105	2.517	2.273	2.206
10/4	BB1004M BLk	0.06	0	0	2.497	2.566	2.475	2.613	2.522	2.659	2.452	2.466	2.505
					Ca^{2+}								
					Stage0	**Stage1**	**Stage2**	**Stage3**	**Stage4**	**Stage5**	**Stage6**	**Stage7**	**Stage8**
7/5	BB0705M BLK	0.06	0	0	3.676	10.255	10.273	3.211	4.8205	5.599	6.194	3.289	7.802

7/19	BB0719M BLK	0.06	0	0	3.33	3.296	3.338	3.54	2.646	3.0865	2.818	3.259	2.974
8/2	BB0802M BLK	0.06	0	0	6.152	3.946	3.512	3.436	3.643	3.424	3.508	3.772	2.519
9/6	BB0906M BLK	0.06	0	0	7.184	7.301	11.09	8.555	3.858	3.4975	3.588	3.991	3.742
10/4	BB1004M BLk	0.06	0	0	3.945	4.258	4.797	4.549	5.351	3.96	3.564	3.893	5.806

Figure E1. BRAVO MOUDI (anion and cation) daily plots

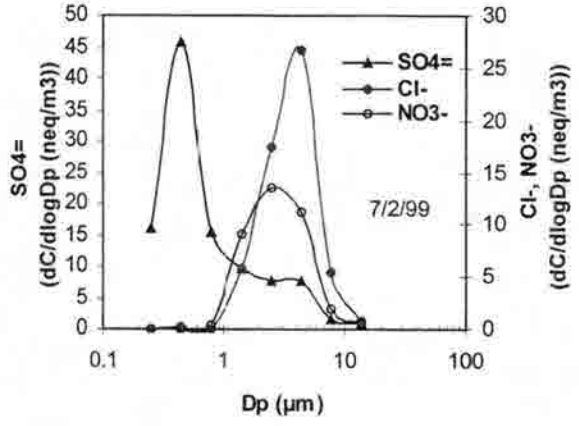

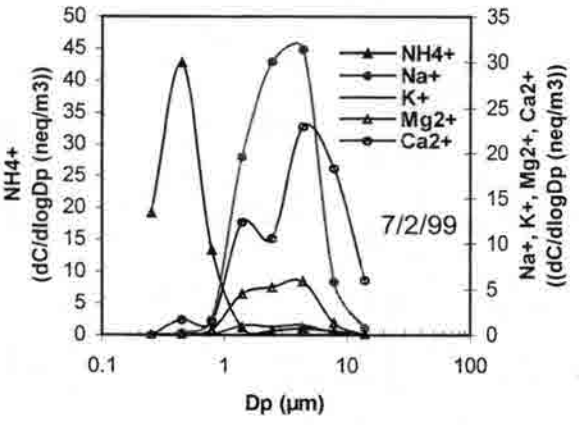

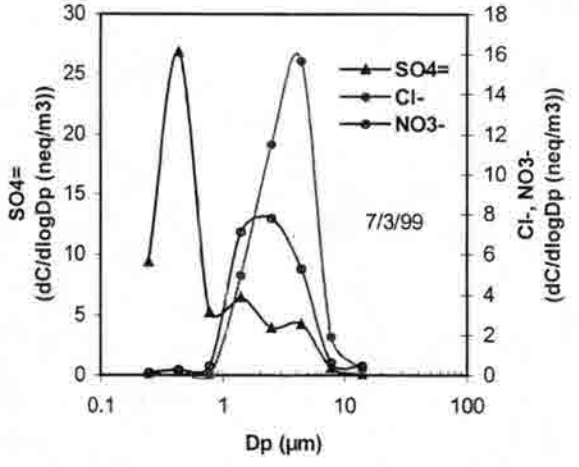

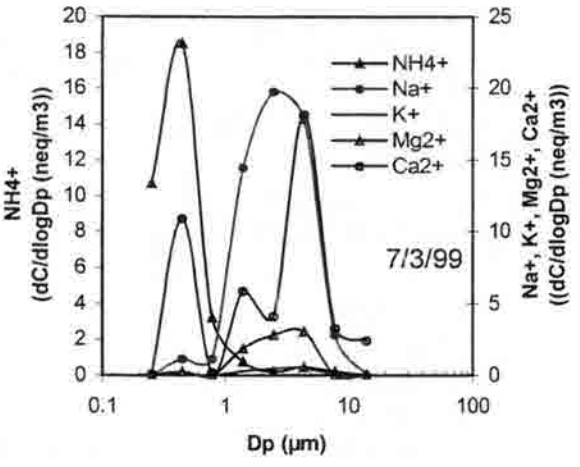

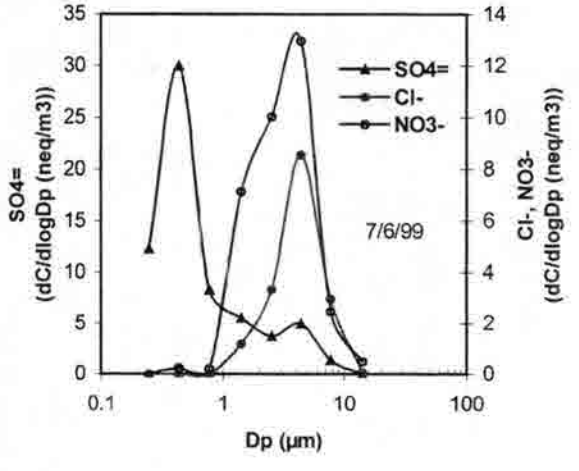

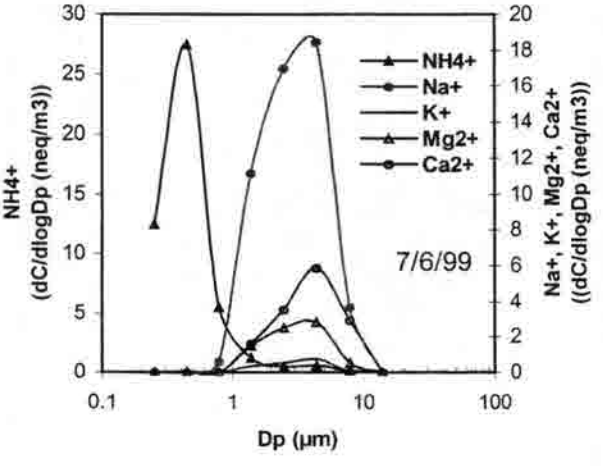

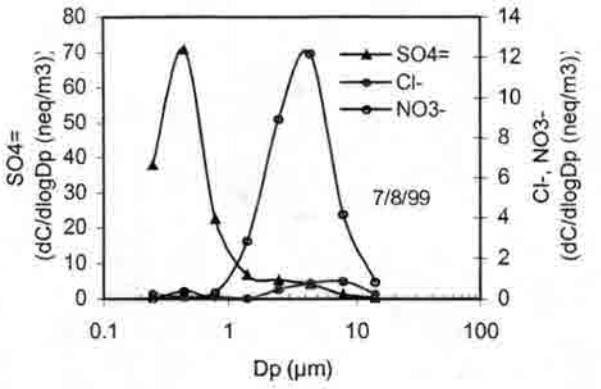
SO4=
(dC/dlogDp (neq/m3))
Cl-, NO3-
(dC/dlogDp (neq/m3))
SO4=
Cl-
NO3-
7/8/99
Dp (µm)

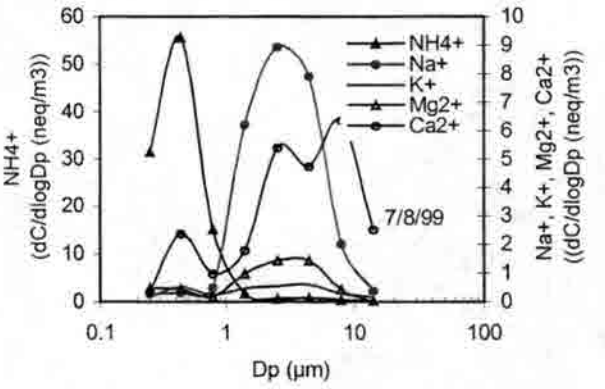
NH4+
(dC/dlogDp (neq/m3))
Na+, K+, Mg2+, Ca2+
((dC/dlogDp (neq/m3))
NH4+
Na+
K+
Mg2+
Ca2+
7/8/99
Dp (µm)

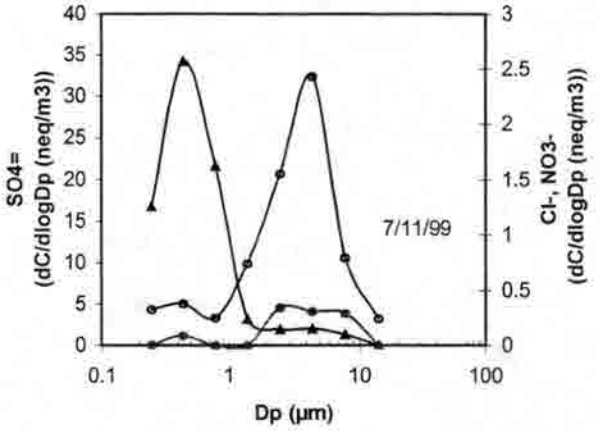
SO4=
(dC/dlogDp (neq/m3))
Cl-, NO3-
(dC/dlogDp (neq/m3))
7/11/99
Dp (µm)

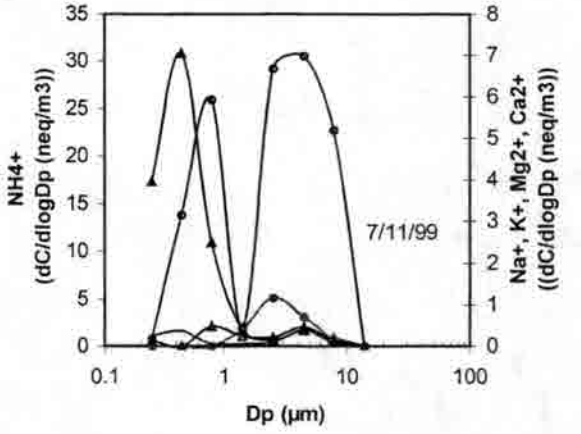
NH4+
(dC/dlogDp (neq/m3))
Na+, K+, Mg2+, Ca2+
((dC/dlogDp (neq/m3))
7/11/99
Dp (µm)

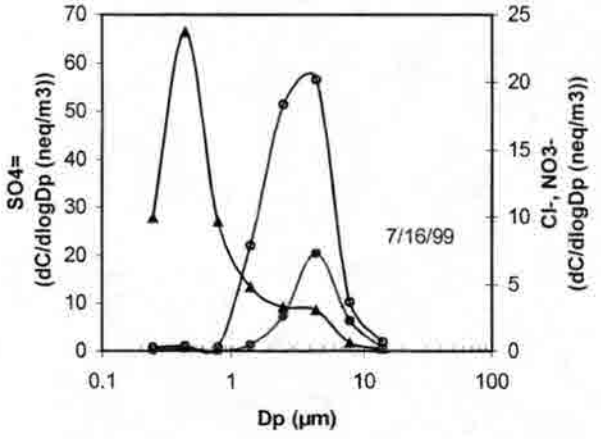
SO4=
(dC/dlogDp (neq/m3))
Cl-, NO3-
(dC/dlogDp (neq/m3))
7/16/99
Dp (µm)

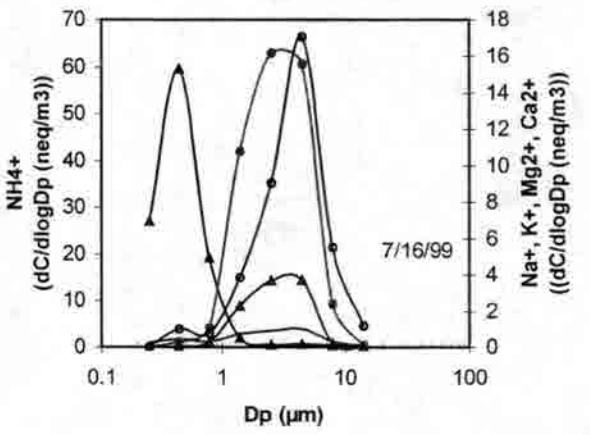
NH4+
(dC/dlogDp (neq/m3))
Na+, K+, Mg2+, Ca2+
((dC/dlogDp (neq/m3))
7/16/99
Dp (µm)

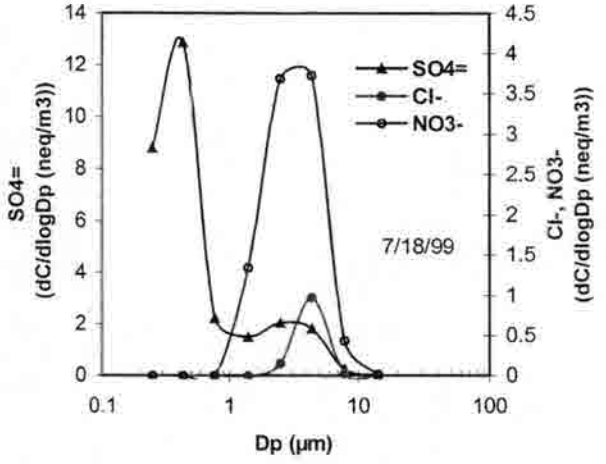
SO4=
Cl-
NO3-
7/18/99
SO4= (dC/dlogDp (neq/m3))
Cl-, NO3- (dC/dlogDp (neq/m3))
Dp (µm)

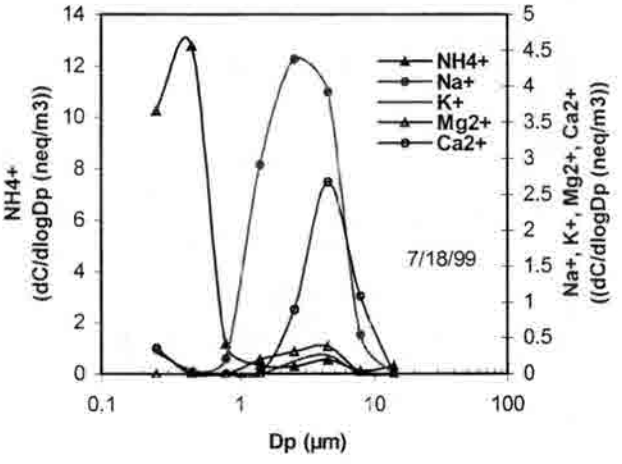
NH4+
Na+
K+
Mg2+
Ca2+
7/18/99
NH4+ (dC/dlogDp (neq/m3))
Na+, K+, Mg2+, Ca2+ ((dC/dlogDp (neq/m3))
Dp (µm)

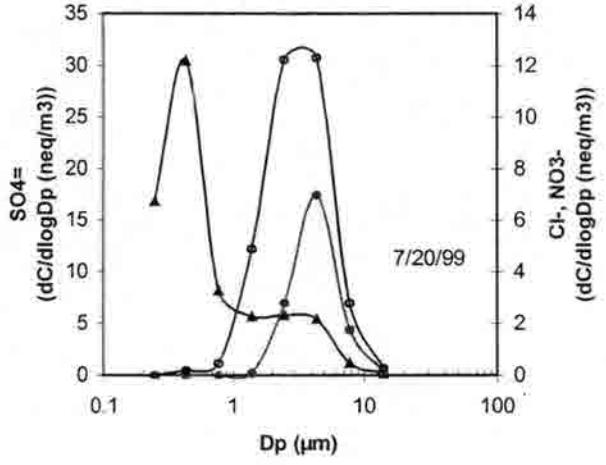
7/20/99
SO4= (dC/dlogDp (neq/m3))
Cl-, NO3- (dC/dlogDp (neq/m3))
Dp (µm)

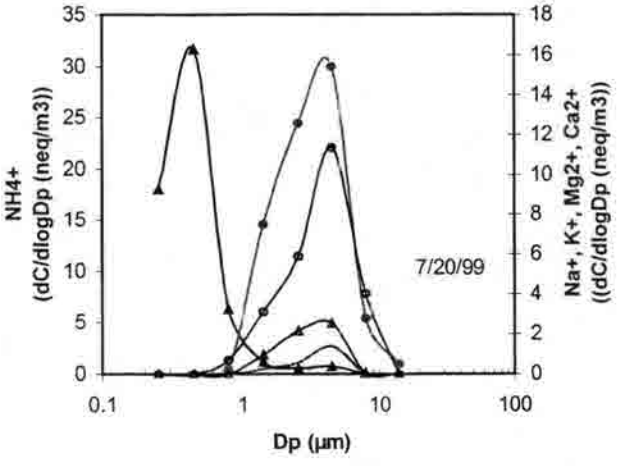
7/20/99
NH4+ (dC/dlogDp (neq/m3))
Na+, K+, Mg2+, Ca2+ ((dC/dlogDp (neq/m3))
Dp (µm)

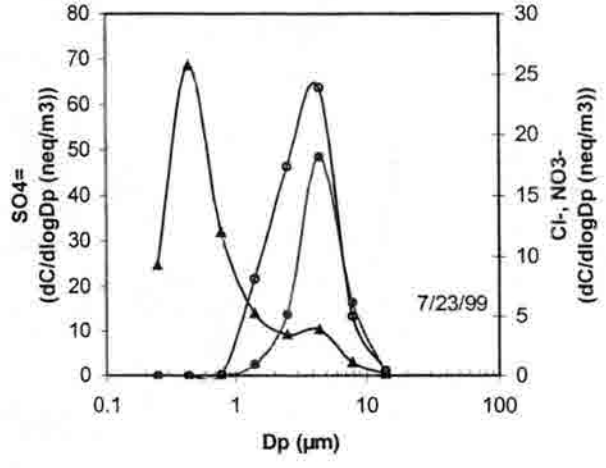
7/23/99
SO4= (dC/dlogDp (neq/m3))
Cl-, NO3- (dC/dlogDp (neq/m3))
Dp (µm)

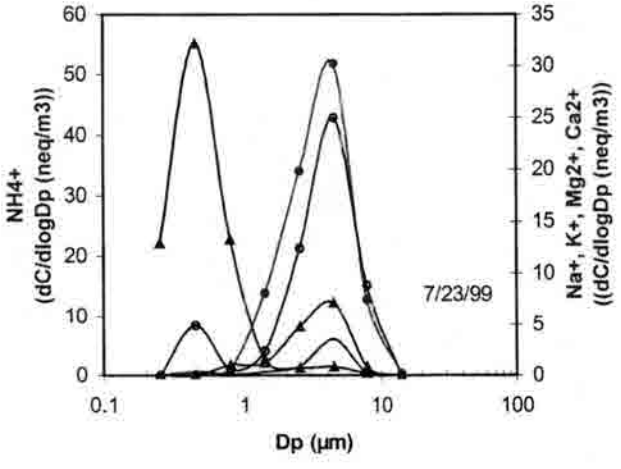
7/23/99
NH4+ (dC/dlogDp (neq/m3))
Na+, K+, Mg2+, Ca2+ ((dC/dlogDp (neq/m3))
Dp (µm)

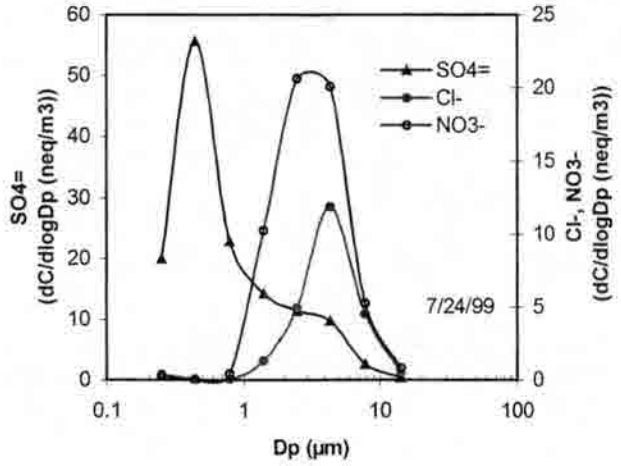
SO4=
Cl-
NO3-
7/24/99
SO4= (dC/dlogDp (neq/m3))
Cl-, NO3- (dC/dlogDp (neq/m3))
Dp (µm)

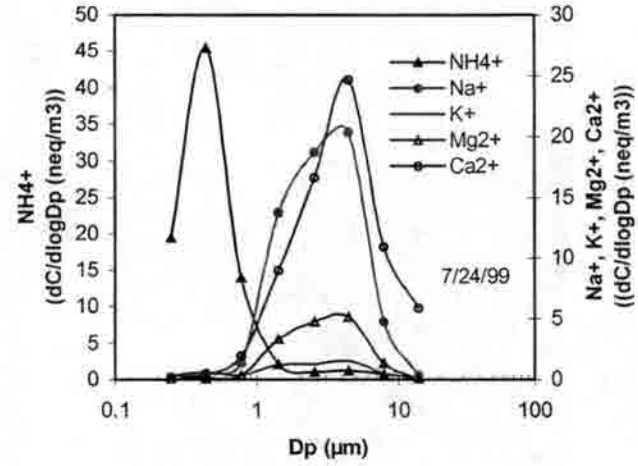
NH4+
Na+
K+
Mg2+
Ca2+
7/24/99
NH4+ (dC/dlogDp (neq/m3))
Na+, K+, Mg2+, Ca2+ ((dC/dlogDp (neq/m3))
Dp (µm)

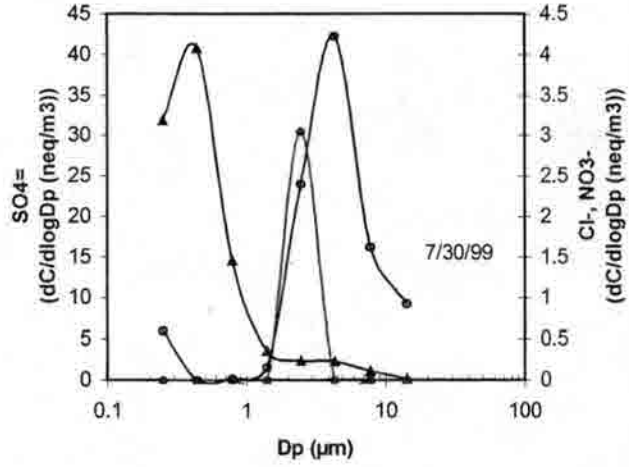
7/30/99
SO4= (dC/dlogDp (neq/m3))
Cl-, NO3- (dC/dlogDp (neq/m3))
Dp (µm)

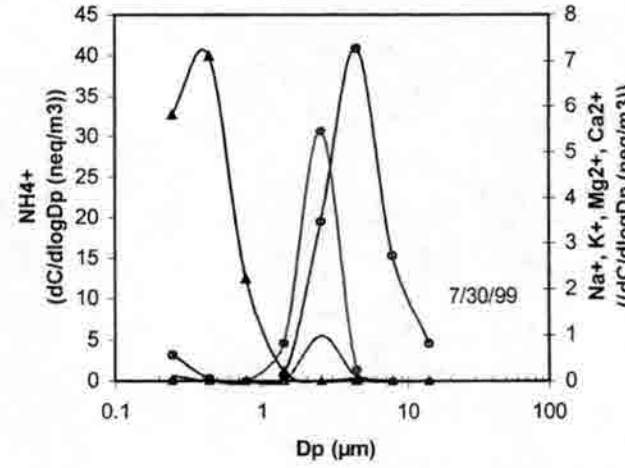
7/30/99
NH4+ (dC/dlogDp (neq/m3))
Na+, K+, Mg2+, Ca2+ ((dC/dlogDp (neq/m3))
Dp (µm)

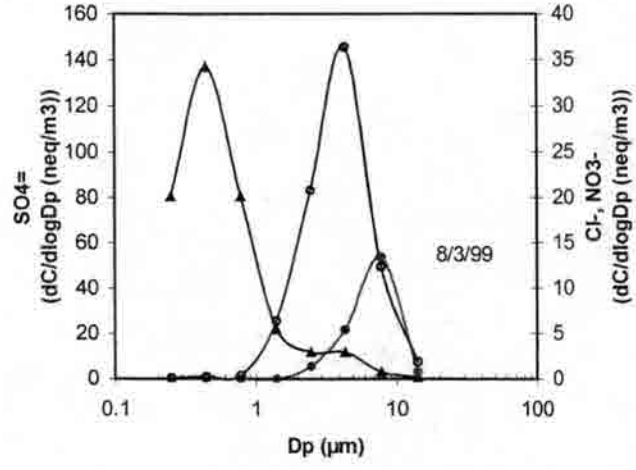
8/3/99
SO4= (dC/dlogDp (neq/m3))
Cl-, NO3- (dC/dlogDp (neq/m3))
Dp (µm)

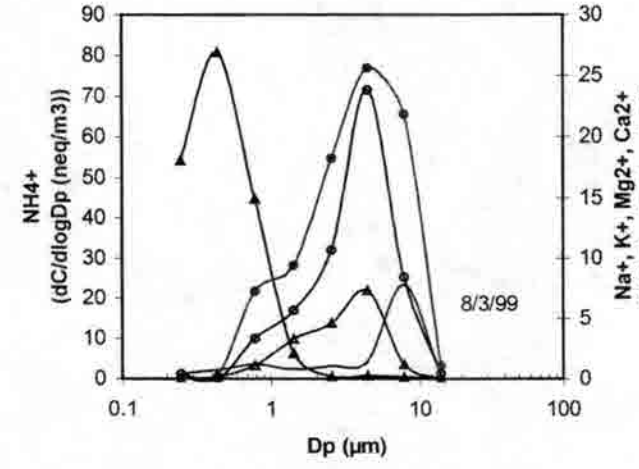
8/3/99
NH4+ (dC/dlogDp (neq/m3))
Na+, K+, Mg2+, Ca2+ ((dC/dlogDp (neq/m3))
Dp (µm)

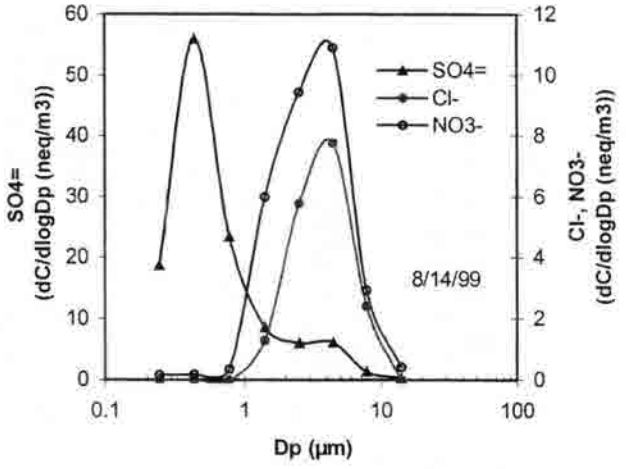
SO4=
(dC/dlogDp (neq/m3))
Cl-, NO3-
(dC/dlogDp (neq/m3))
SO4=
Cl-
NO3-
8/14/99
Dp (µm)

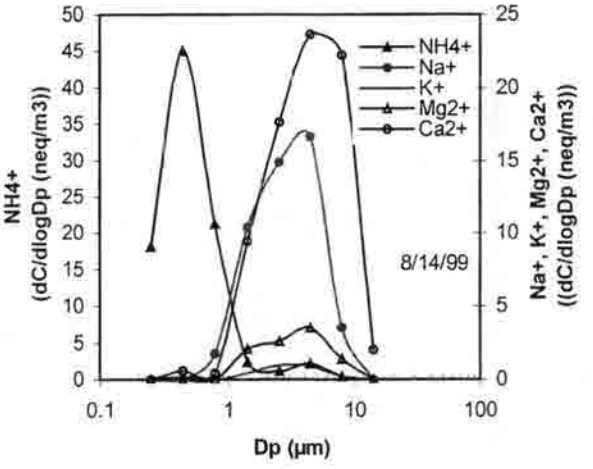
NH4+
(dC/dlogDp (neq/m3))
Na+, K+, Mg2+, Ca2+
((dC/dlogDp (neq/m3))
NH4+
Na+
K+
Mg2+
Ca2+
8/14/99
Dp (µm)

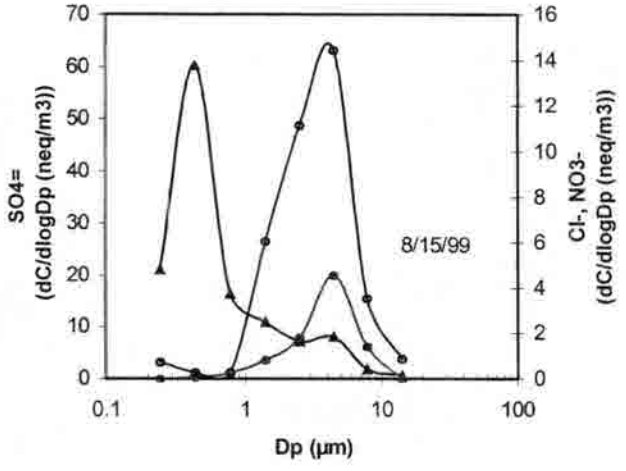
SO4=
(dC/dlogDp (neq/m3))
Cl-, NO3-
(dC/dlogDp (neq/m3))
8/15/99
Dp (µm)

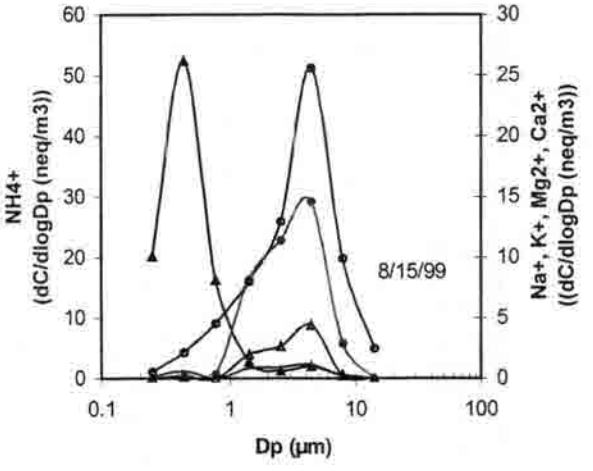
NH4+
(dC/dlogDp (neq/m3))
Na+, K+, Mg2+, Ca2+
((dC/dlogDp (neq/m3))
8/15/99
Dp (µm)

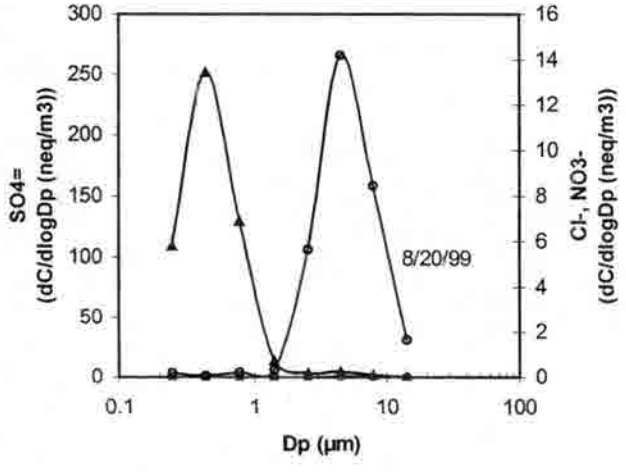
SO4=
(dC/dlogDp (neq/m3))
Cl-, NO3-
(dC/dlogDp (neq/m3))
8/20/99
Dp (µm)

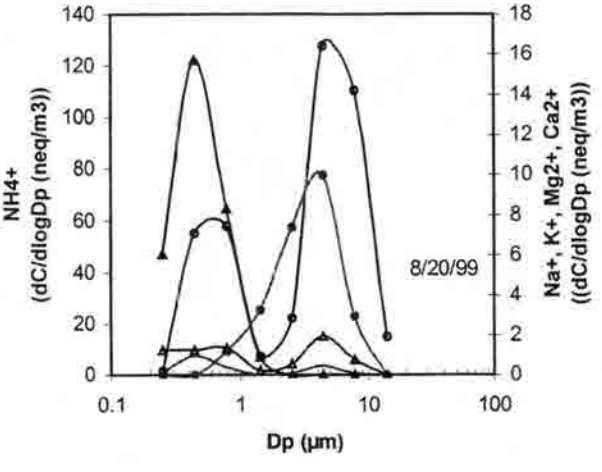
NH4+
(dC/dlogDp (neq/m3))
Na+, K+, Mg2+, Ca2+
((dC/dlogDp (neq/m3))
8/20/99
Dp (µm)

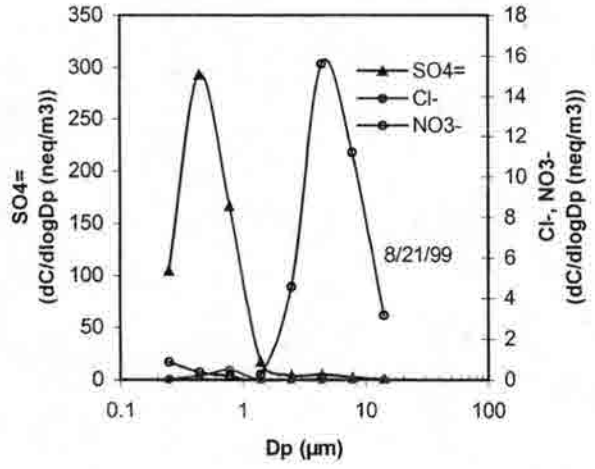
SO4=
(dC/dlogDp (neq/m3))
Cl-, NO3-
(dC/dlogDp (neq/m3))
SO4=
Cl-
NO3-
8/21/99
Dp (µm)

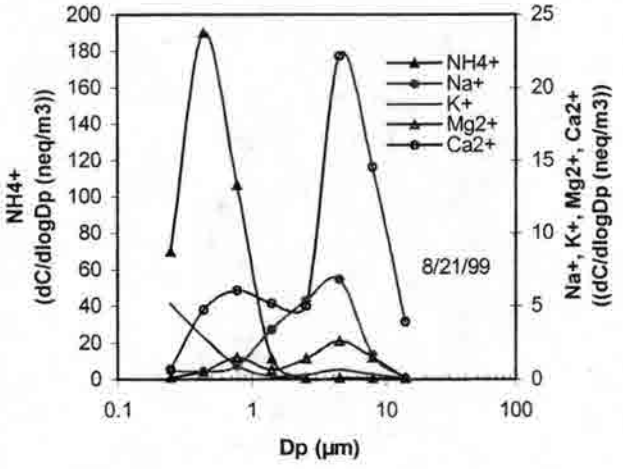
NH4+
(dC/dlogDp (neq/m3))
Na+, K+, Mg2+, Ca2+
((dC/dlogDp (neq/m3))
NH4+
Na+
K+
Mg2+
Ca2+
8/21/99
Dp (µm)

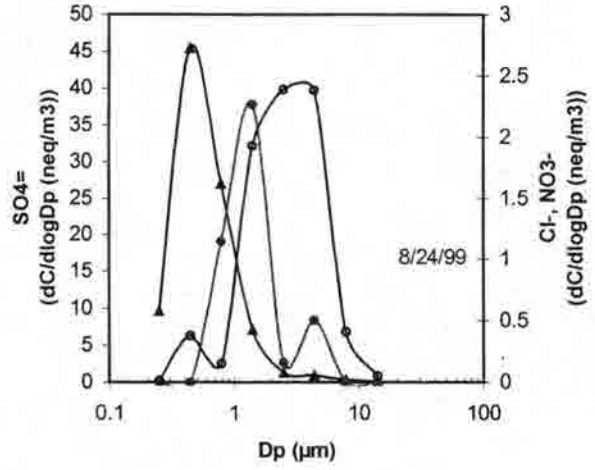
SO4=
(dC/dlogDp (neq/m3))
Cl-, NO3-
(dC/dlogDp (neq/m3))
8/24/99
Dp (µm)

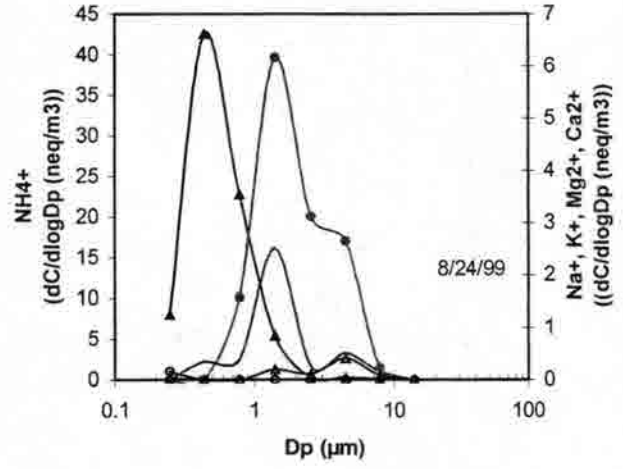
NH4+
(dC/dlogDp (neq/m3))
Na+, K+, Mg2+, Ca2+
((dC/dlogDp (neq/m3))
8/24/99
Dp (µm)

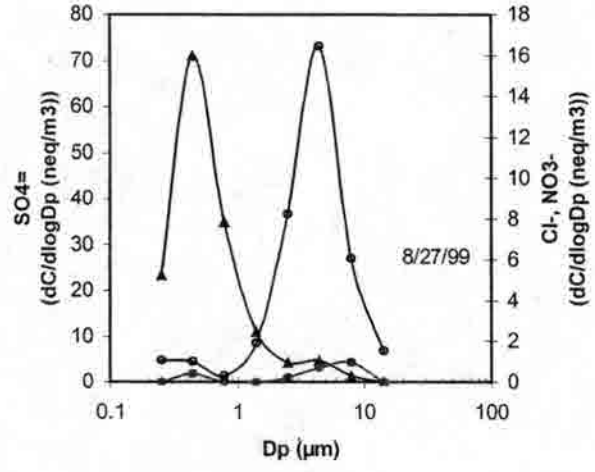
SO4=
(dC/dlogDp (neq/m3))
Cl-, NO3-
(dC/dlogDp (neq/m3))
8/27/99
Dp (µm)

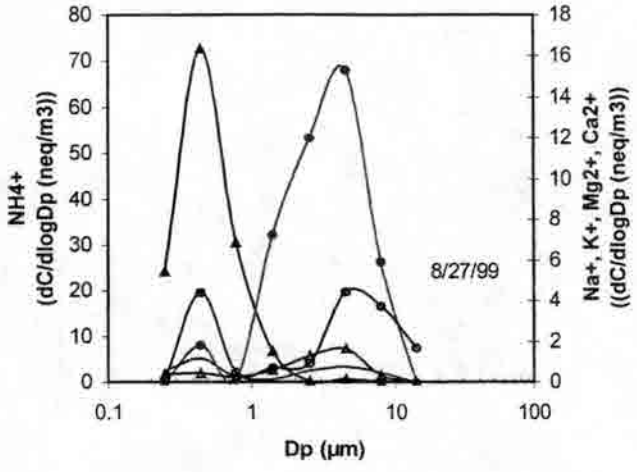
NH4+
(dC/dlogDp (neq/m3))
Na+, K+, Mg2+, Ca2+
((dC/dlogDp (neq/m3))
8/27/99
Dp (µm)

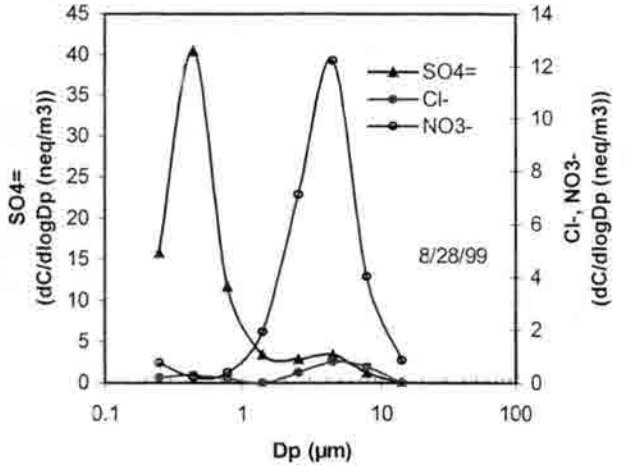
SO4=
Cl-
NO3-
8/28/99
SO4= (dC/dlogDp (neq/m3))
Cl-, NO3- (dC/dlogDp (neq/m3))
Dp (µm)

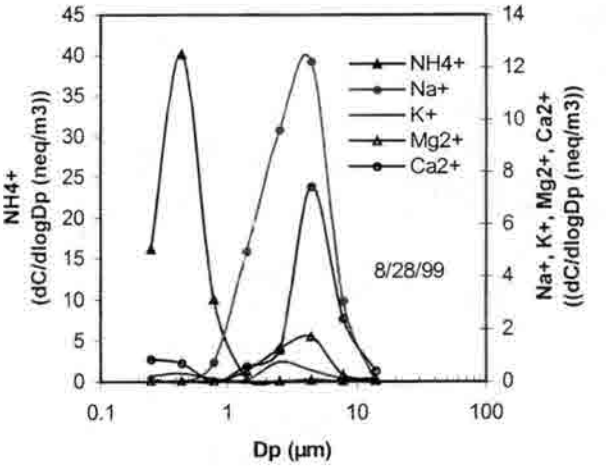
NH4+
Na+
K+
Mg2+
Ca2+
8/28/99
NH4+ (dC/dlogDp (neq/m3))
Na+, K+, Mg2+, Ca2+ ((dC/dlogDp (neq/m3))
Dp (µm)

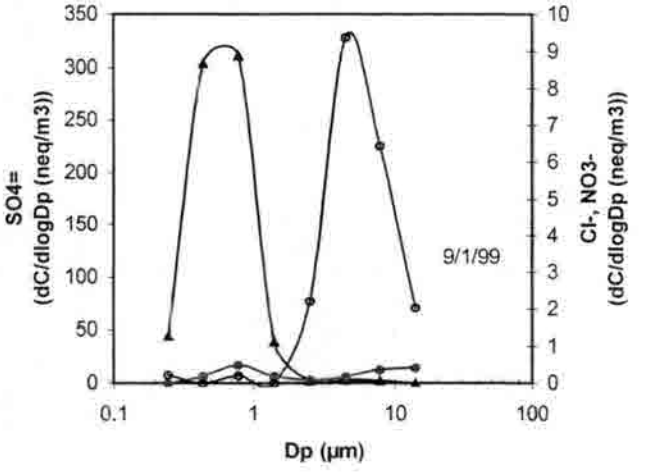
9/1/99
SO4= (dC/dlogDp (neq/m3))
Cl-, NO3- (dC/dlogDp (neq/m3))
Dp (µm)

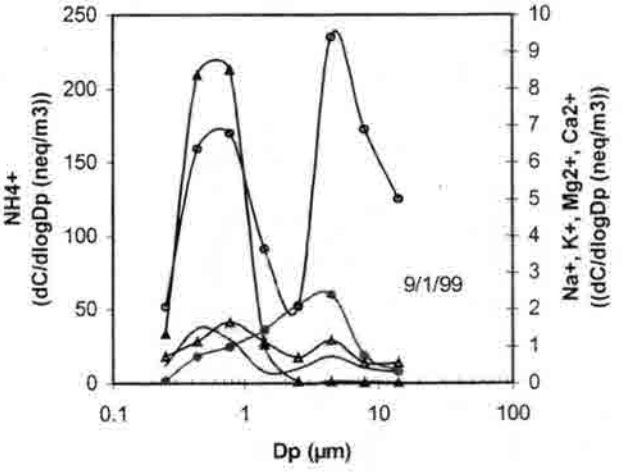
9/1/99
NH4+ (dC/dlogDp (neq/m3))
Na+, K+, Mg2+, Ca2+ ((dC/dlogDp (neq/m3))
Dp (µm)

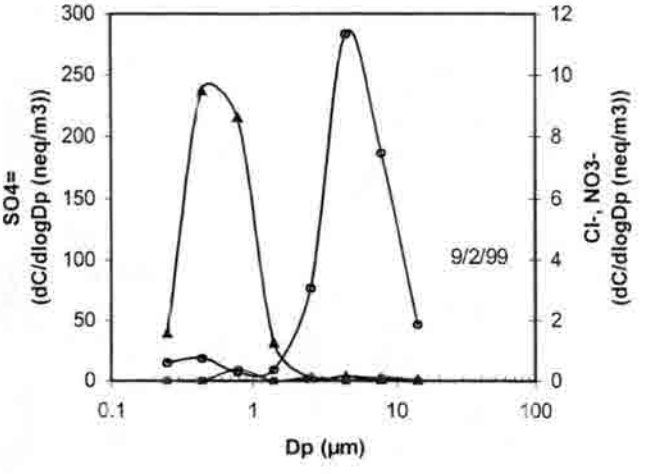
9/2/99
SO4= (dC/dlogDp (neq/m3))
Cl-, NO3- (dC/dlogDp (neq/m3))
Dp (µm)

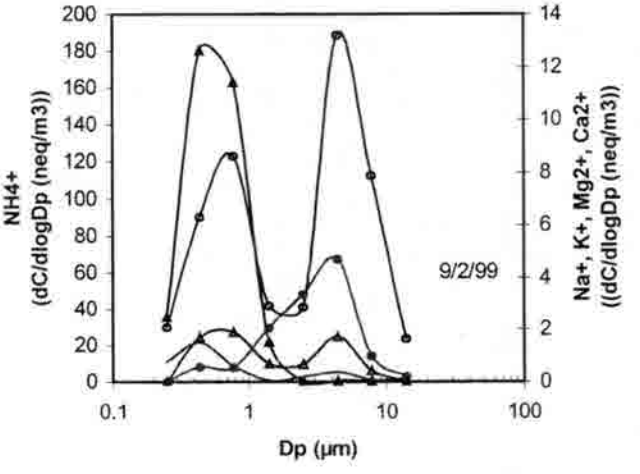
9/2/99
NH4+ (dC/dlogDp (neq/m3))
Na+, K+, Mg2+, Ca2+ ((dC/dlogDp (neq/m3))
Dp (µm)

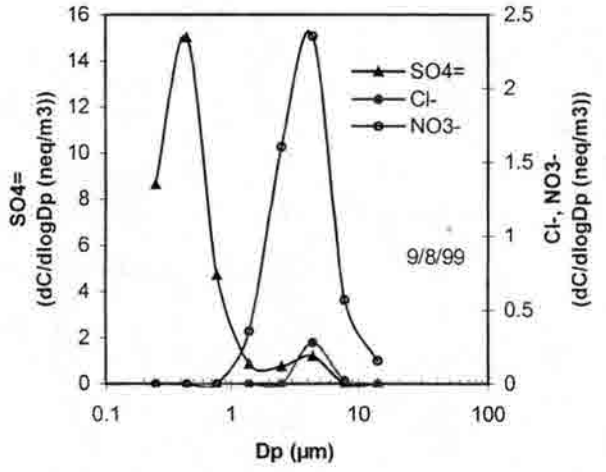
SO4=
Cl-
NO3-
9/8/99
SO4= (dC/dlogDp (neq/m3))
Cl-, NO3- (dC/dlogDp (neq/m3))
Dp (µm)

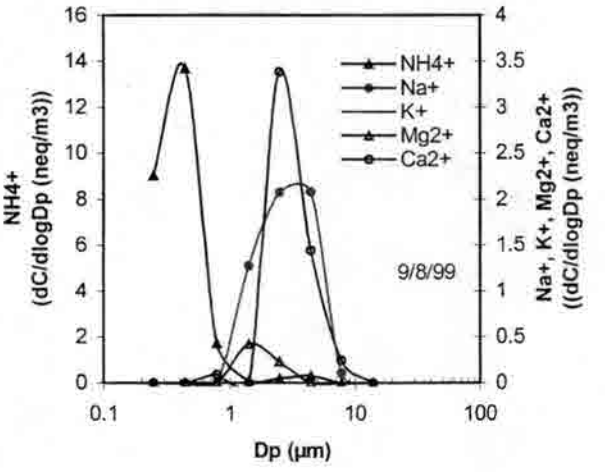
NH4+
Na+
K+
Mg2+
Ca2+
9/8/99
NH4+ (dC/dlogDp (neq/m3))
Na+, K+, Mg2+, Ca2+ ((dC/dlogDp (neq/m3))
Dp (µm)

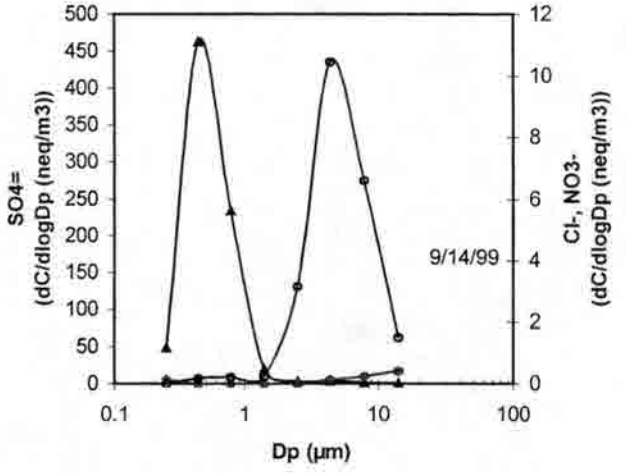
9/14/99
SO4= (dC/dlogDp (neq/m3))
Cl-, NO3- (dC/dlogDp (neq/m3))
Dp (µm)

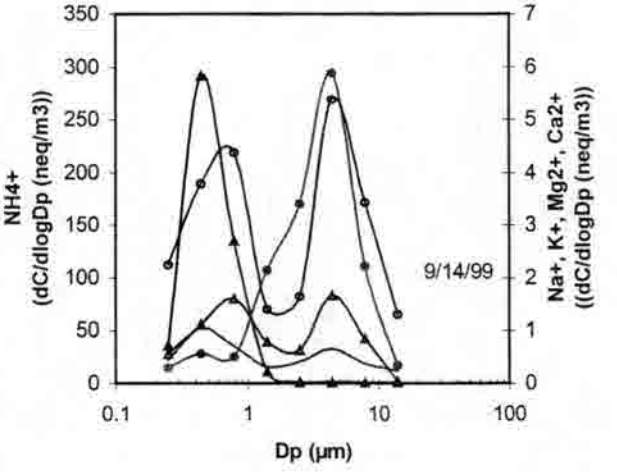
9/14/99
NH4+ (dC/dlogDp (neq/m3))
Na+, K+, Mg2+, Ca2+ ((dC/dlogDp (neq/m3))
Dp (µm)

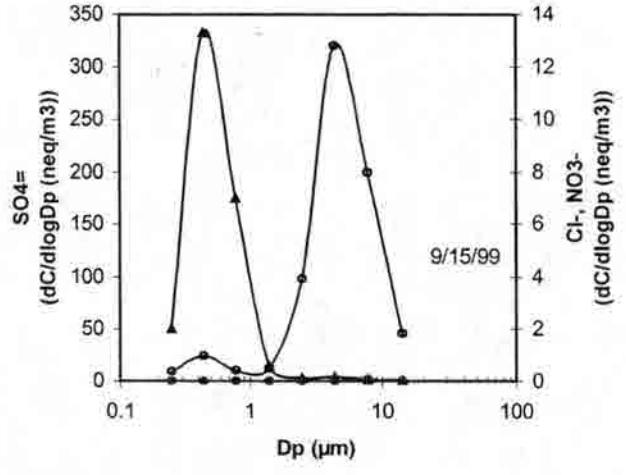
9/15/99
SO4= (dC/dlogDp (neq/m3))
Cl-, NO3- (dC/dlogDp (neq/m3))
Dp (µm)

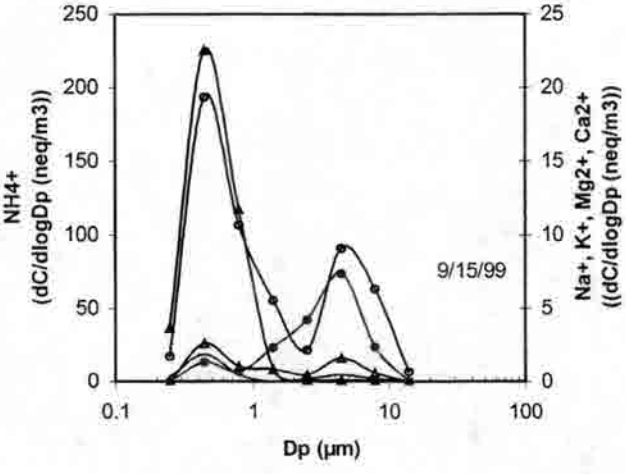
9/15/99
NH4+ (dC/dlogDp (neq/m3))
Na+, K+, Mg2+, Ca2+ ((dC/dlogDp (neq/m3))
Dp (µm)

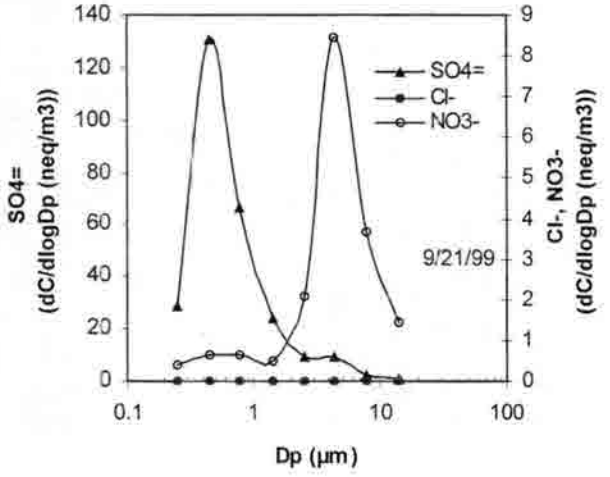
SO4=
Cl-
NO3-
9/21/99
SO4= (dC/dlogDp (neq/m3))
Cl-, NO3- (dC/dlogDp (neq/m3))
Dp (µm)

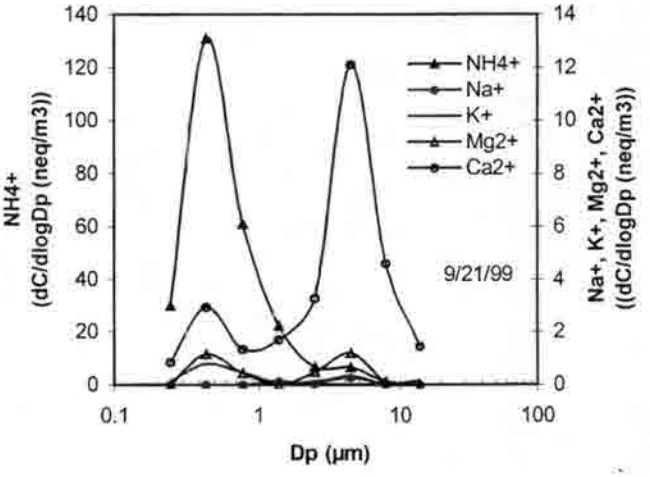
NH4+
Na+
K+
Mg2+
Ca2+
9/21/99
NH4+ (dC/dlogDp (neq/m3))
Na+, K+, Mg2+, Ca2+ ((dC/dlogDp (neq/m3))
Dp (µm)

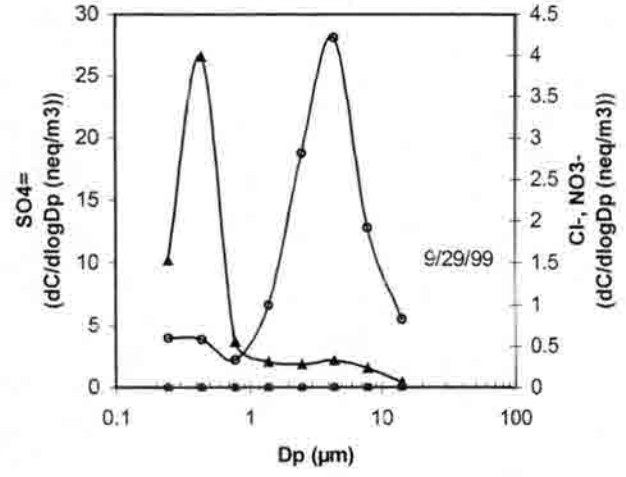
9/29/99
SO4= (dC/dlogDp (neq/m3))
Cl-, NO3- (dC/dlogDp (neq/m3))
Dp (µm)

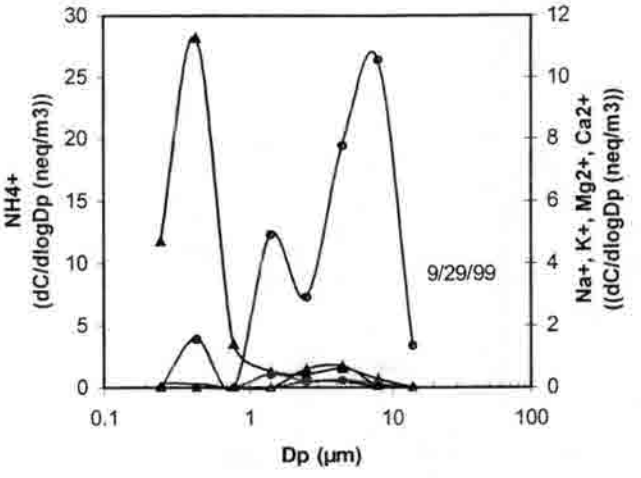
9/29/99
NH4+ (dC/dlogDp (neq/m3))
Na+, K+, Mg2+, Ca2+ ((dC/dlogDp (neq/m3))
Dp (µm)

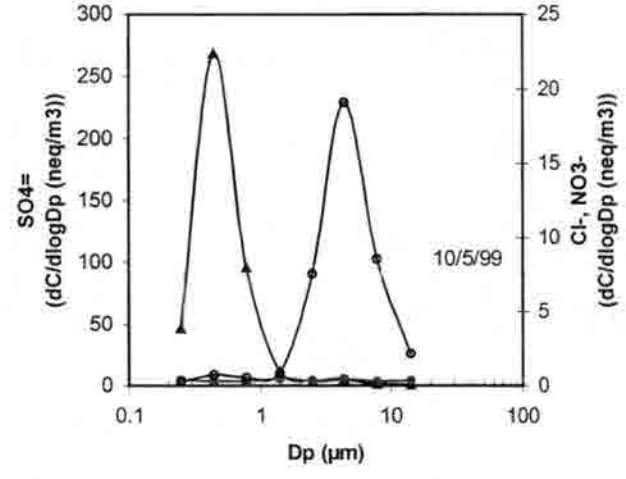
10/5/99
SO4= (dC/dlogDp (neq/m3))
Cl-, NO3- (dC/dlogDp (neq/m3))
Dp (µm)

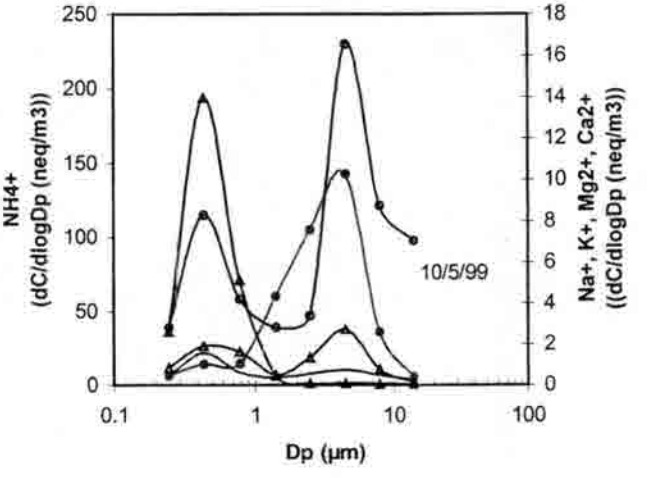
10/5/99
NH4+ (dC/dlogDp (neq/m3))
Na+, K+, Mg2+, Ca2+ ((dC/dlogDp (neq/m3))
Dp (µm)

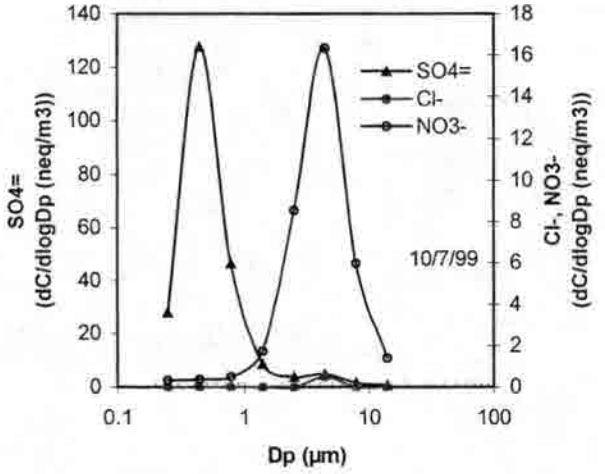
SO4=
Cl-
NO3-
10/7/99
SO4= (dC/dlogDp (neq/m3))
Cl-, NO3- (dC/dlogDp (neq/m3))
Dp (µm)

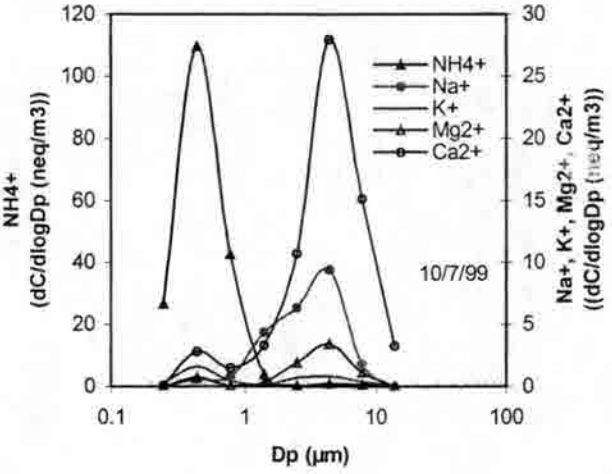
NH4+
Na+
K+
Mg2+
Ca2+
10/7/99
NH4+ (dC/dlogDp (neq/m3))
Na+, K+, Mg2+, Ca2+ ((dC/dlogDp (neq/m3))
Dp (µm)

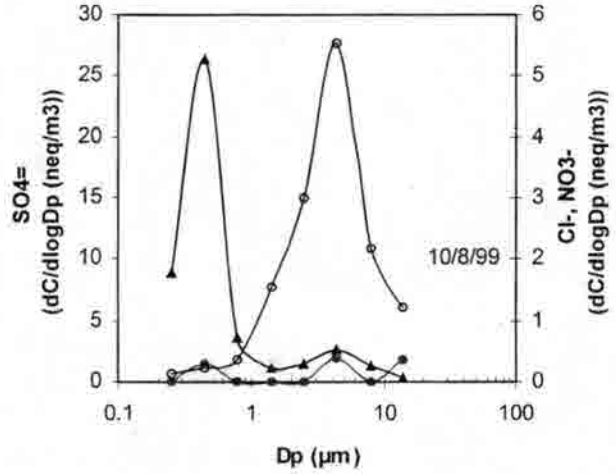
10/8/99
SO4= (dC/dlogDp (neq/m3))
Cl-, NO3- (dC/dlogDp (neq/m3))
Dp (µm)

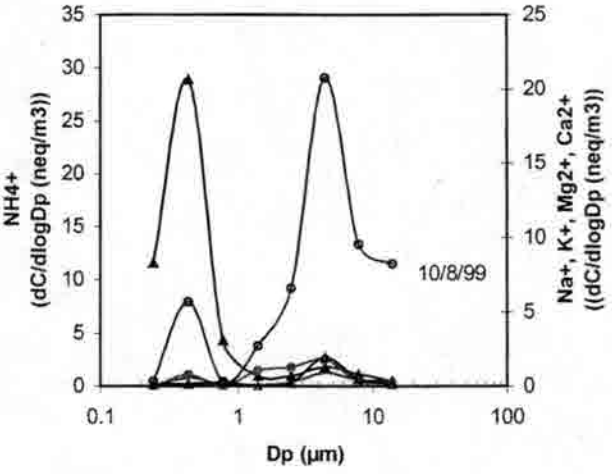
10/8/99
NH4+ (dC/dlogDp (neq/m3))
Na+, K+, Mg2+, Ca2+ ((dC/dlogDp (neq/m3))
Dp (µm)

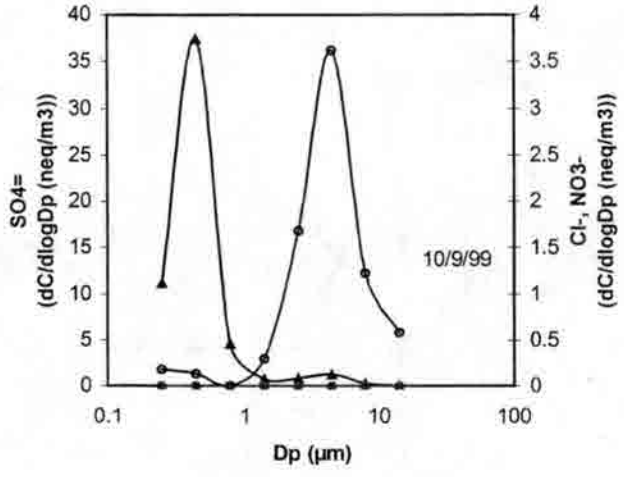
10/9/99
SO4= (dC/dlogDp (neq/m3))
Cl-, NO3- (dC/dlogDp (neq/m3))
Dp (µm)

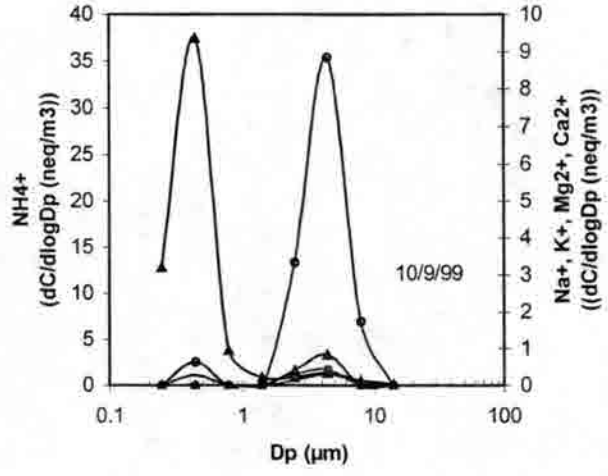
10/9/99
NH4+ (dC/dlogDp (neq/m3))
Na+, K+, Mg2+, Ca2+ ((dC/dlogDp (neq/m3))
Dp (µm)

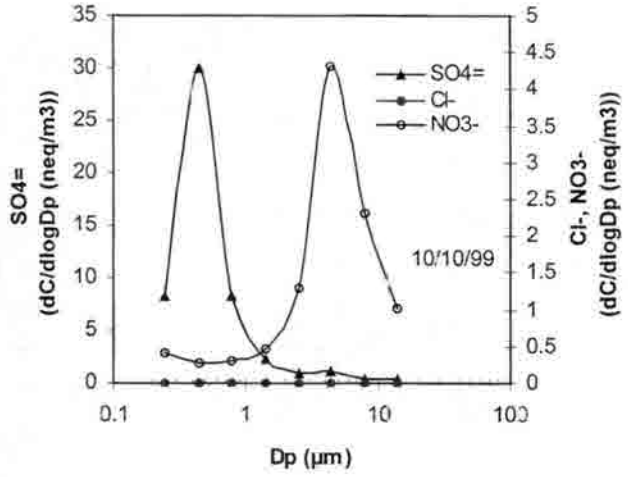
SO4=
Cl-
NO3-
10/10/99
SO4= (dC/dlogDp (neq/m3))
Cl-, NO3- (dC/dlogDp (neq/m3))
Dp (µm)

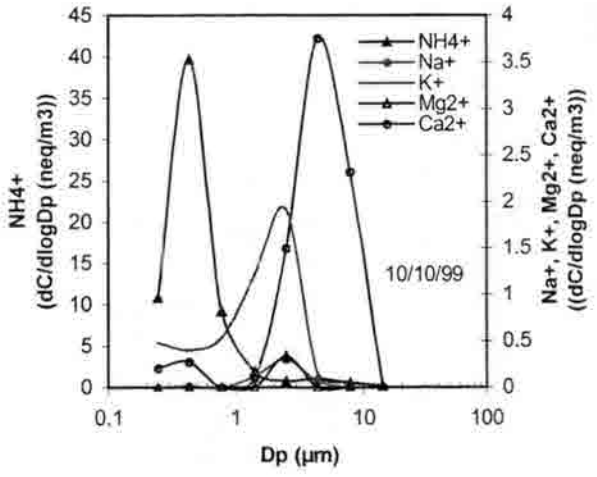
NH4+
Na+
K+
Mg2+
Ca2+
10/10/99
NH4+ (dC/dlogDp (neq/m3))
Na+, K+, Mg2+, Ca2+ ((dC/dlogDp (neq/m3))
Dp (µm)

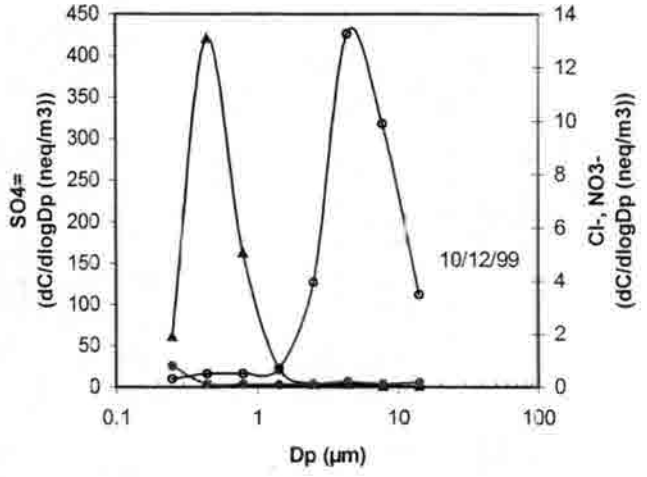
10/12/99
SO4= (dC/dlogDp (neq/m3))
Cl-, NO3- (dC/dlogDp (neq/m3))
Dp (µm)

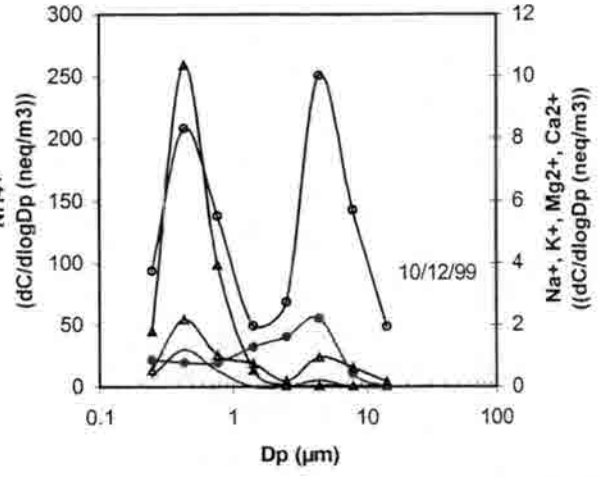
10/12/99
NH4+ (dC/dlogDp (neq/m3))
Na+, K+, Mg2+, Ca2+ ((dC/dlogDp (neq/m3))
Dp (µm)

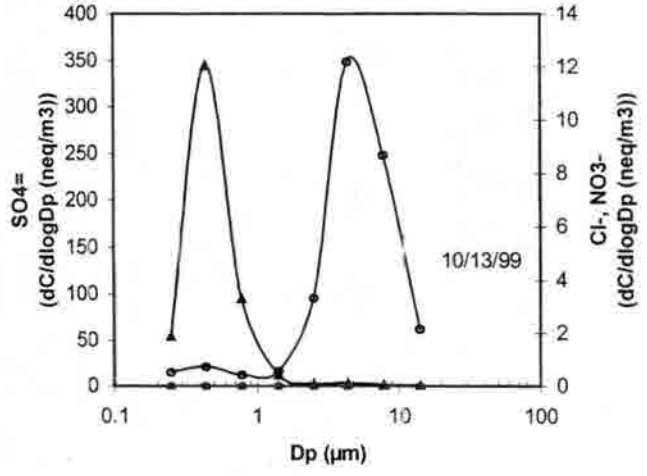
10/13/99
SO4= (dC/dlogDp (neq/m3))
Cl-, NO3- (dC/dlogDp (neq/m3))
Dp (µm)

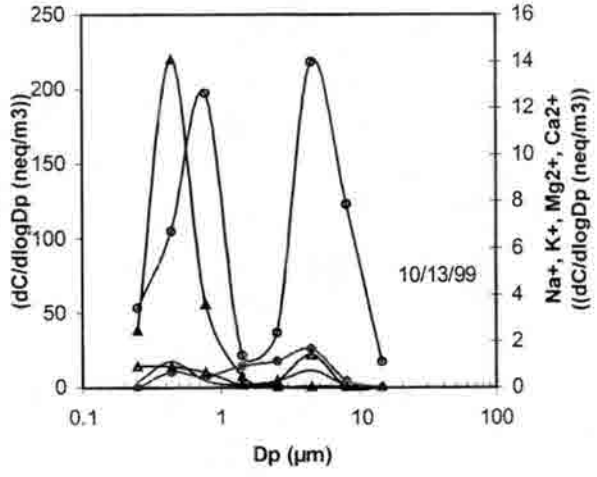
10/13/99
NH4+ (dC/dlogDp (neq/m3))
Na+, K+, Mg2+, Ca2+ ((dC/dlogDp (neq/m3))
Dp (µm)

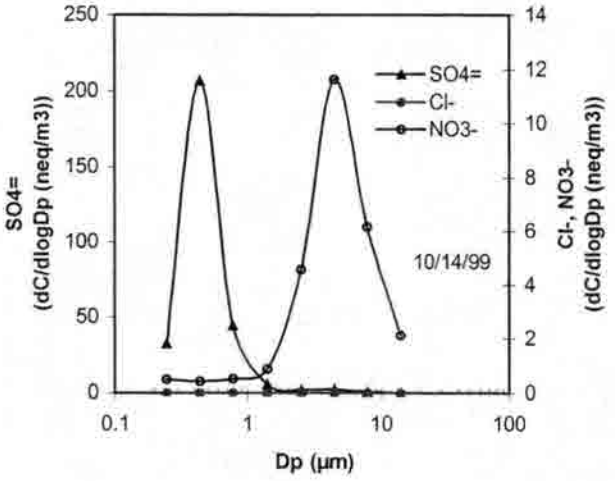
SO4=
(dC/dlogDp (neq/m3))
Cl-, NO3-
(dC/dlogDp (neq/m3))
SO4=
Cl-
NO3-
10/14/99
Dp (µm)

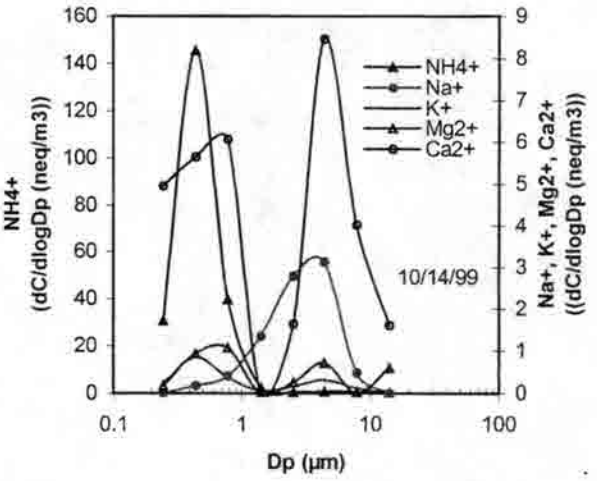
NH4+
(dC/dlogDp (neq/m3))
Na+, K+, Mg2+, Ca2+
((dC/dlogDp (neq/m3))
NH4+
Na+
K+
Mg2+
Ca2+
10/14/99
Dp (µm)

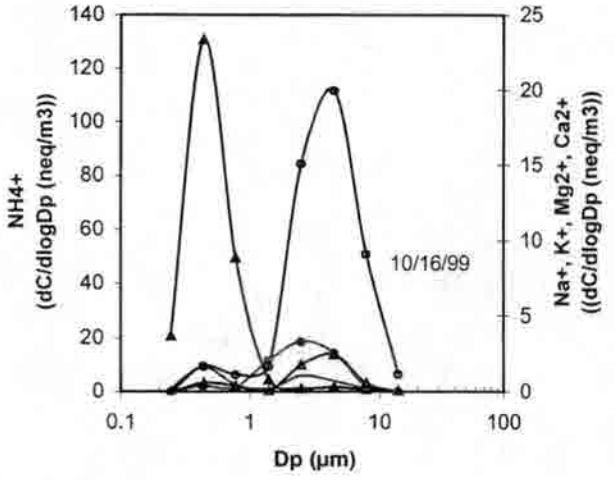
NH4+
(dC/dlogDp (neq/m3))
Na+, K+, Mg2+, Ca2+
((dC/dlogDp (neq/m3))
10/16/99
Dp (µm)

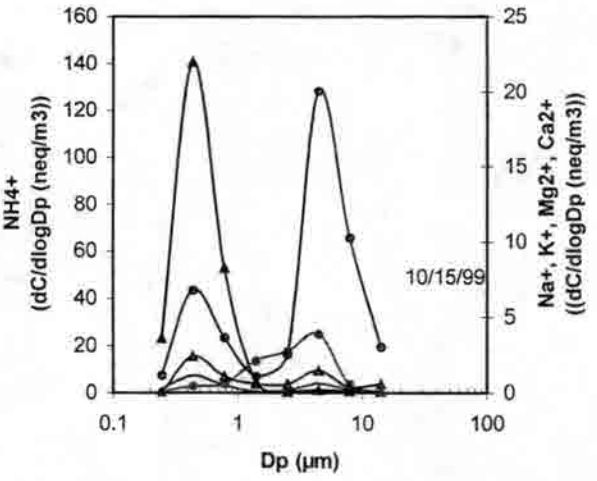
NH4+
(dC/dlogDp (neq/m3))
Na+, K+, Mg2+, Ca2+
((dC/dlogDp (neq/m3))
10/15/99
Dp (µm)

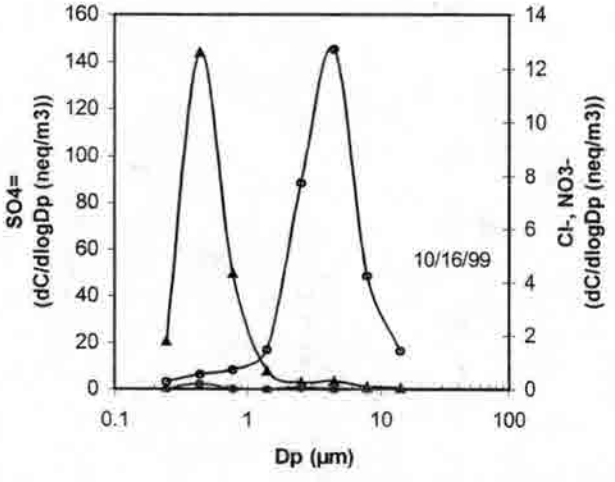
SO4=
(dC/dlogDp (neq/m3))
Cl-, NO3-
(dC/dlogDp (neq/m3))
10/16/99
Dp (µm)

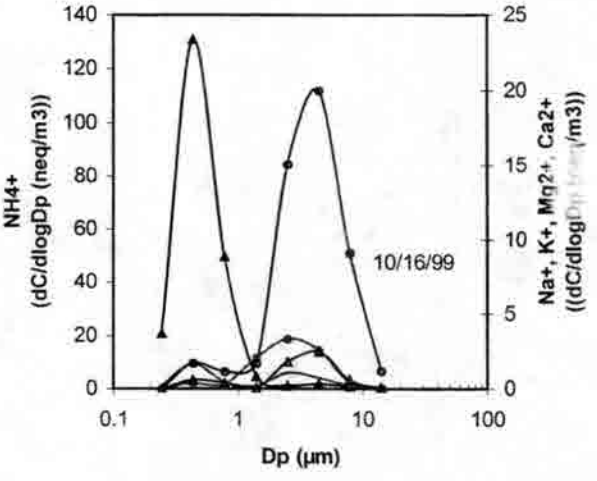
NH4+
(dC/dlogDp (neq/m3))
Na+, K+, Mg2+, Ca2+
((dC/dlogDp (neq/m3))
10/16/99
Dp (µm)

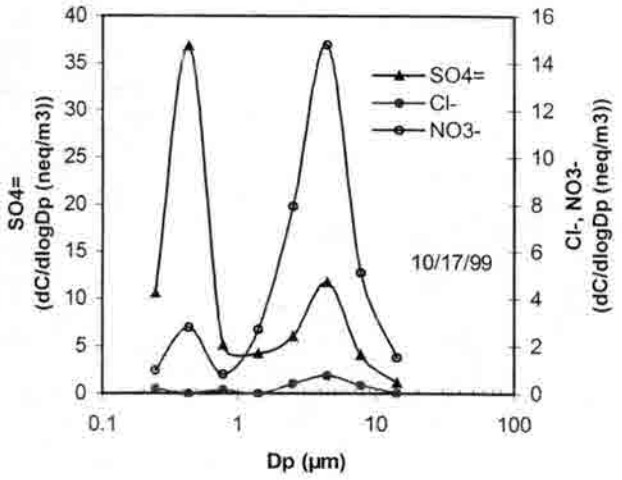
SO4=
(dC/dlogDp (neq/m3))
Cl-, NO3-
(dC/dlogDp (neq/m3))
SO4=
Cl-
NO3-
10/17/99
Dp (µm)

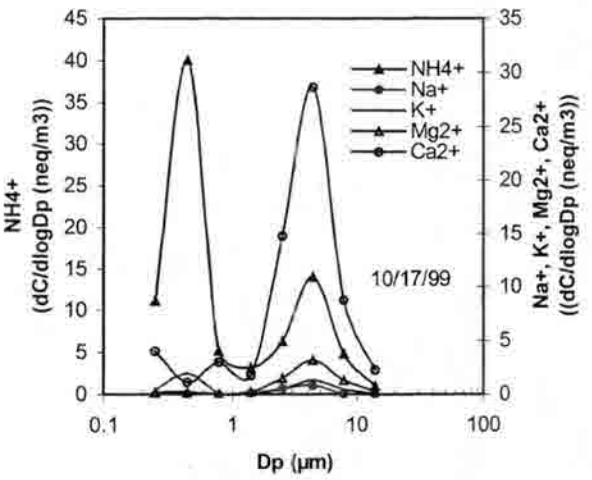
NH4+
(dC/dlogDp (neq/m3))
Na+, K+, Mg2+, Ca2+
((dC/dlogDp (neq/m3))
NH4+
Na+
K+
Mg2+
Ca2+
10/17/99
Dp (µm)

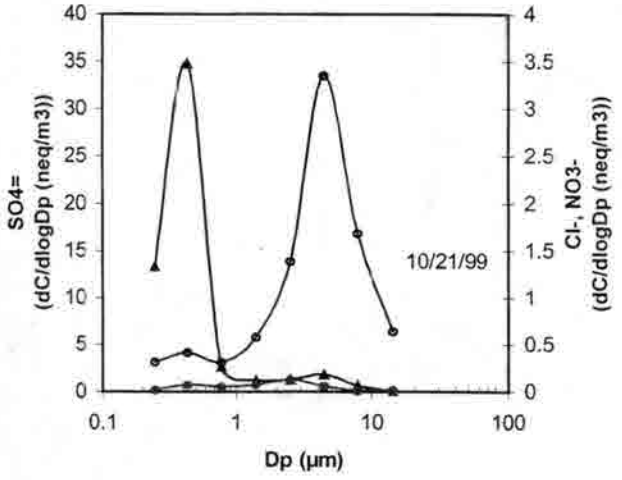
SO4=
(dC/dlogDp (neq/m3))
Cl-, NO3-
(dC/dlogDp (neq/m3))
10/21/99
Dp (µm)

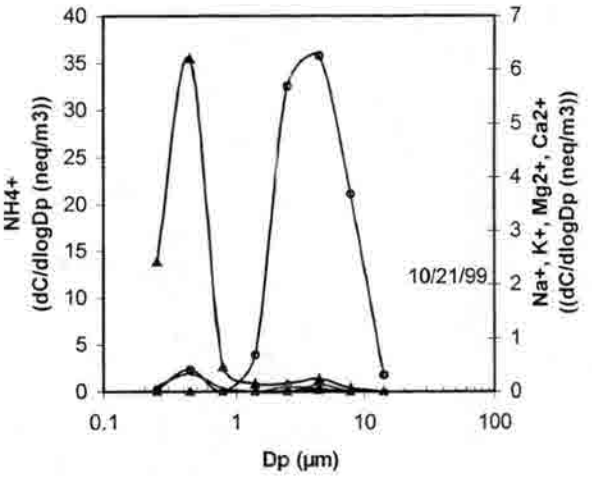
NH4+
(dC/dlogDp (neq/m3))
Na+, K+, Mg2+, Ca2+
((dC/dlogDp (neq/m3))
10/21/99
Dp (µm)

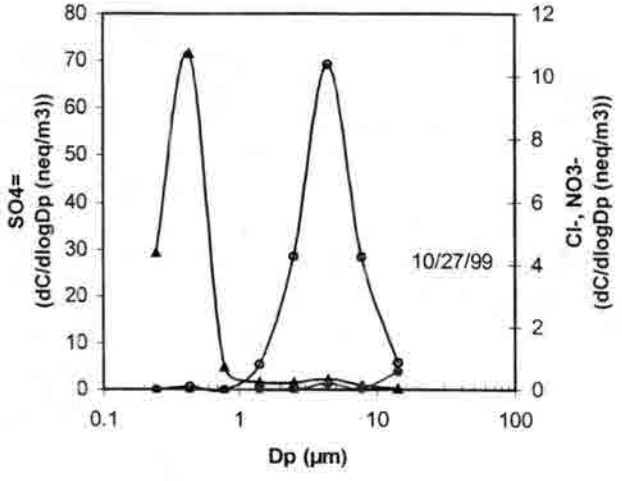
SO4=
(dC/dlogDp (neq/m3))
Cl-, NO3-
(dC/dlogDp (neq/m3))
10/27/99
Dp (µm)

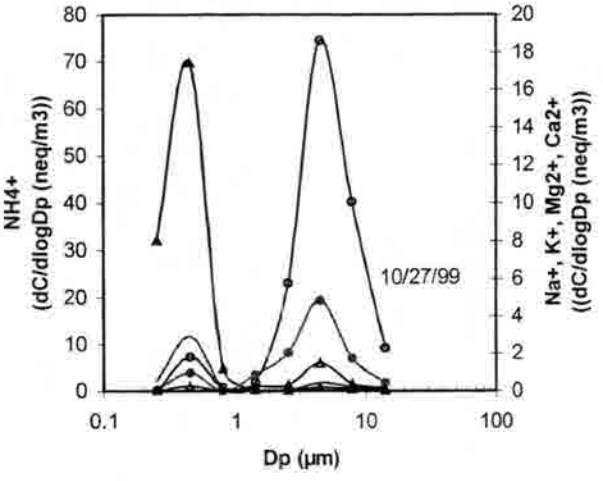
NH4+
(dC/dlogDp (neq/m3))
Na+, K+, Mg2+, Ca2+
((dC/dlogDp (neq/m3))
10/27/99
Dp (µm)

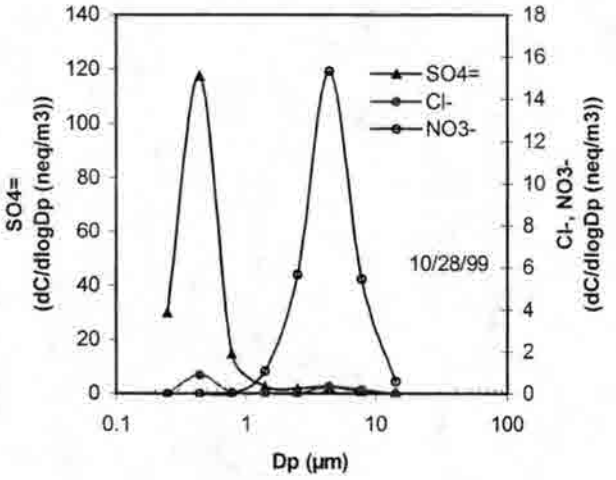
SO4=
(dC/dlogDp (neq/m3))
Cl-, NO3-
(dC/dlogDp (neq/m3))
SO4=
Cl-
NO3-
10/28/99
Dp (µm)

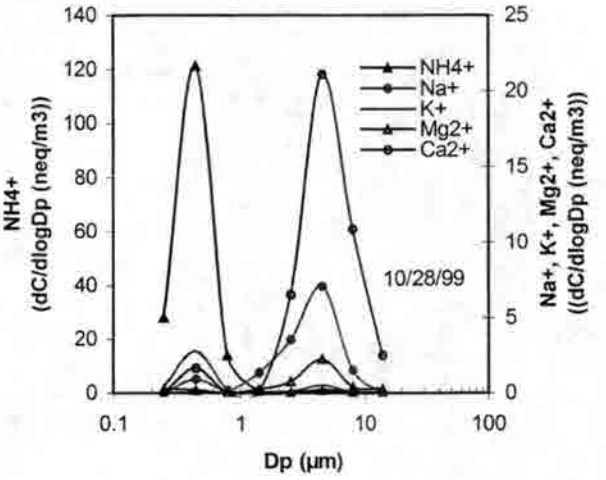
NH4+
(dC/dlogDp (neq/m3))
Na+, K+, Mg2+, Ca2+
((dC/dlogDp (neq/m3))
NH4+
Na+
K+
Mg2+
Ca2+
10/28/99
Dp (µm)

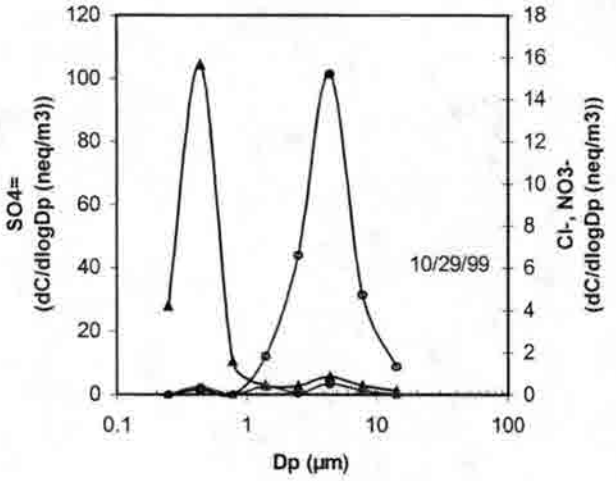
SO4=
(dC/dlogDp (neq/m3))
Cl-, NO3-
(dC/dlogDp (neq/m3))
10/29/99
Dp (µm)

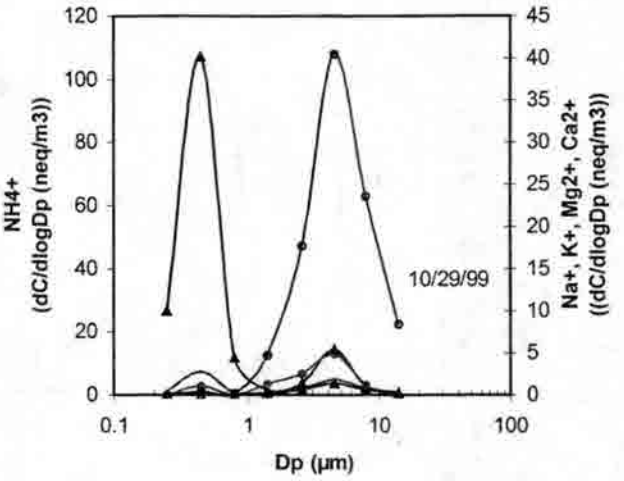
NH4+
(dC/dlogDp (neq/m3))
Na+, K+, Mg2+, Ca2+
((dC/dlogDp (neq/m3))
10/29/99
Dp (µm)

Appendix F : Comparison of the sensitivity of N(-III) and N(V) phase partitioning to humidity (24-hr average, 5th percentile, and 95th percentile of relative humidity)

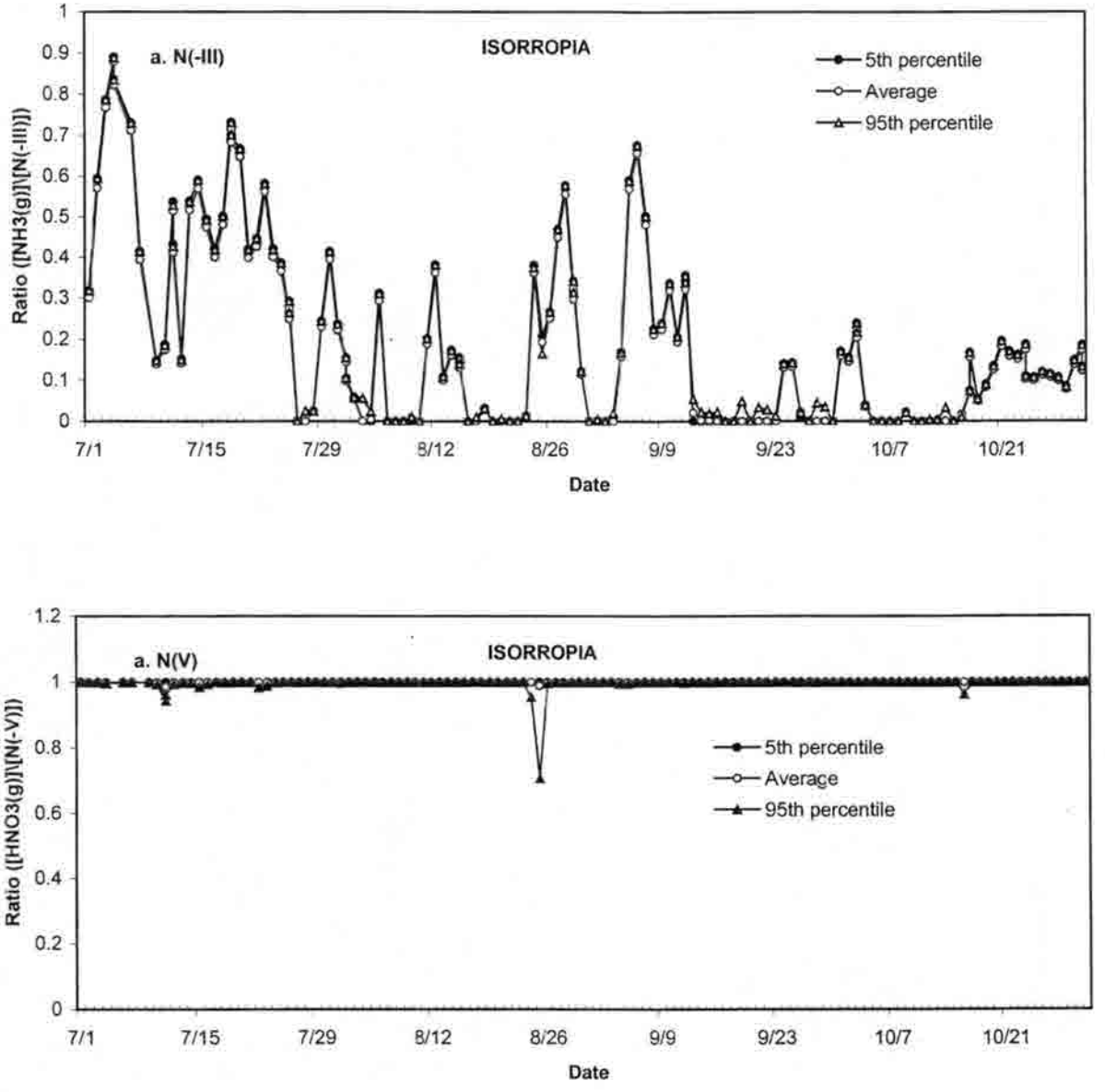

Figure F1 Comparison of the sensitivity of N(-III) and N(V) phase partitioning to different humidities (24-hr average, 5th percentile and 95th percentile of relative humidities) using ISORROPIA